universität wien

DISSERTATION

Titel der Dissertation

„Roles of SUN-1 phosphorylations during *C. elegans* meiosis“

Verfasser

Mag.rer.nat. Alexander Woglar

angestrebter akademischer Grad

Doktor der Naturwissenschaften (Dr.rer.nat.)

Wien, 2013

Studienkennzahl lt. Studienblatt:	A 091 441
Dissertationsgebiet lt. Studienblatt:	Genetik-Mikrobiologie
Betreuerin:	Univ.-Prof. Mag. Dr. Verena Jantsch-Plunger

Contents

Acknowledgement

Ich möchte mich bei meiner Familie, vor allem meinen Eltern, Robert und Helga, und meinen Freunden bedanken die mich über die Jahre meines Doktorats unermüdlich unterstützt haben.

I want thank my supervisor, Verena Jantsch, for an interesting time with a lot of exiting questions raised and some of them even answered.

I want to thank Alexandra Penkner, Antoine Baudrimont and Thomas Machacek for teaching me how to deal with worms. Also I want to thank the rest of the Jantsch and Loidl group for the amazing atmosphere, fruitful discussions and the countless occasions they helped me out over the past years.

I would not be able to assemble a complete list of people (in collaborations, in the Department of Chromosome Biology, the Campus and in the community) who contributed one or the other way to my work during the time of my PhD. Nevertheless I want to cordially thank all of them.

Thank you!

Abstract

Sexual reproducing organisms have to halve their genomes prior to gamete formation to preserve genome size over generations. During meiosis, a diploid cell undergoes two rounds of succeeding chromosome segregation to give rise to four haploid products that can develop into sperms and oocytes. Therefore, prior to the first meiotic division, homologous chromosomes have to be paired and connected to each other by a crossover to be subsequently separated in meiotic anaphase I. Besides pairing of chromosomes, crossover formation requires the introduction of DNA double strand breaks (DSBs) and repair of them by use of the homologous chromosome as a repair template. The therefore required proximity between the homologous chromosomes is established by the synaptonemal complex (SC), a proteinacious structure established between them. The *C. elegans* inner nuclear membrane protein Matefin/SUN-1 transmits cytoplasm-generated kinetic forces onto chromosomes at the onset of leptotene/zygotene. This leads to individualized movement of chromosomes and eventual paring of homologous chromosomes with subsequent formation of the SC between them. Meiotic progression and sequential achievement of these meiotic tasks (pairing, SC formation, DSB repair and recombination) have to be tightly coordinated.

We have found that meiotic chromosome movement is accompanied by formation of SUN-1 aggregates at the putative chromosomal attachment sites at the nuclear envelope and phosphorylation of SUN-1 at multiple residues. The phosphorylations depend on CHK-2 and PLK-2. PLK-2 colocalizes with the SUN-1 aggregates during the time of homology search and interacts physically with SUN-1. Failures in recombination and synapsis lead to the persistence of mobile and phosphorylated SUN-1 aggregates and to persisting recruitment of PLK-2 to chromosome ends. SUN-1 phosphorylations are required for the continuous localization of PLK-2 to chromosome ends and persistent chromosome mobility, characteristic for a zygotene arrest. Furthermore SUN-1 phosphorylation enables the formation of the SC with wild-type kinetics.

In our data we present evidence for a checkpoint that monitors the presence of the obligate crossover mediated by SUN-1 phosphorylation. We propose that signals emanating from failures to successfully finish meiotic tasks are integrated at the

nuclear periphery to regulate chromosome end-led movement and meiotic progression.

Zusammenfassung

Vor der Gamtenfusion müssen sexuell reproduzierende Organismen ihre Genome halbieren, um die Chromosomenanzahl über Generationen konstant zu halten. Dafür durchläuft eine diploide Gametenvorläuferzelle zwei unmittelbar aufeinanderfolgend Chromosomenteilungen während der Meiose. Dies führt zu vier haploiden Tochterzellkernen die sich prinzipiell in Spermien oder Eizellen entwickeln können.

Damit homologe Chromosomen während der ersten meiotischen Teilung voneinander seggregieren können müssen sie gepaart und durch ein Crossover verbunden werden. Für die Etablierung eines meiotischen Crossovers werden, abgesehen von Chromosomenpaarung, auch DNS Doppelstrangbrüche (DSB) und Reperatur der Selbigen unter Verwendung des homologen Chromosomes als Reperturvorlage für homologe Rekombination, benötigt. Die hierfür erforderliche Nähe von homologen Chromosomen wird durch den Synaptonemalen Komplex (SC), einer Proteinstruktur, die zwischen den homologen Partnern aufgebaut wird, hergestellt. Am Beginn der meiotischen Prophase überträgt SUN-1, ein Transmembranprotein in der inneren nukleären Membrane, kinetische Kräfte aus dem Zytoplasma in den Kern. Dies führt zur individuellen Bewegung von Chromosomen, die zu dieser Zeit mit einem Ende an der Kernmembran verankert sind. Die Bewegung der einzellnen Chromosomen wird benötigt um die homologen Chromosomen zu paaren und um ungewollter, nicht homologer SC Formierung entgegenzuwirken. Der koordiniert Ablauf dieser einzellnen Funktionen (homologe Paarung, Aufbau des SC, DSB Generierung und Reperatur) während der Meiose bedarf einem hohen Ausmass and Regulation.

Wir haben herausgefunden, dass SUN-1 Aggregate an diesen Chromosomenbindungsstellen an der Kernmembran formt um die Chromosomenbewegung zu gewährleisten. Gleichzeitig mit dem Beginn seiner Aggregation wird SUN-1 an mehreren Aminosäuren an seinem nukleären N-terminus phosphoryliert. Diese Phosphorylierungen sind von CHK-2 und PLK-2 abhängig. PLK-2 lokalisiert an den SUN-1 Aggregaten und co-prezipitiert mit SUN-1. SUN-1 Aggregate und Phosphorylierung persistieren wenn Synapsis oder Rekombination inhibiert sind und Chromosomenmobiltät wird unter diesen Umstände aufrechterhalten. Für diesen Arrest in der frühen meiotischen Prophase wird die Phosphorylierung von SUN-1 benötigt, um PLK-2 stabil and den mobilen Chromosomenenden zu halten um die damit einhergehende persistierende

Chromosomenmobilität zu gewährleisten. Weiters ist die Phosphorylierung von SUN-1 von Nöten, um den SC mit wildtypischer Kinetik aufzubauen.

Unsere Beobachtungen lassen den Schluss zu, dass SUN-1 Phosphorylierung einen Zellzyklusprogressions Checkpunkt mediert, der das ‚obligate Crossover' gewährleistet.

Introduction

Meiosis – an overview

To maintain the genome size over generations sexually reproducing organism have to halve their number of chromosomes before gamete formation. For this purpose most organisms make use of a specialized form of cell division: meiosis. Fusion of the resulting haploid cells (e.g.: fertilization of an egg by a sperm) yields a diploid zygote with the same number of chromosomes as the parental generation. Over the course of meiosis genetic diversity is generated by random segregation of homologous chromosomes and by reciprocal exchange of genetic information among them.

Mechanistically the halving of the chromosomal number is achieved by one cycle of pre-meiotic DNA replication followed by two successive rounds of cell or nuclear divisions resulting in four haploid nuclei. During the first, or reductional meiotic division, the homologous chromosomes, or more correct, centromeres, are moved to opposite poles of the cell (nucleus). In most sexually reproducing organisms, like yeast, human, mouse or *C. elegans*, a physical link between the homologous chromosomes has to be established to ensure their correct segregation during the first meiotic division by the cellular spindle apparatus. This linkage is formed by crossovers, which are manifestation of physical recombination events between homologous chromosomes during the extended meiotic prophase I. Requirements for crossover formation are sister chromatid cohesion, homolog juxtaposition, formation of DNA double strand breaks (DSBs) and their repair via the homologous chromosome.

The second or equational meiotic division resembles a mitotic division by separating the sister chromatids giving raise to for haploid gametes or gamete-precursors (reviewed in: (Petronczki, Siomos et al. 2003; Gerton and Hawley 2005))

Why using *C. elegans* as a meiotic model system?

The roundworm represents an easily tractable genetic system for both forward and reverse genetic approaches to identify and analysis meiotic mutants. *C. elegans* offers the possibility to isolate mutants that are defective in homologous pairing, synapsis and/or crossover formation by following increased spontaneous occurrence of males (5A; XO) among the self-progeny of hermaphroditic worms (5A; XX). Males arise due to X chromosome non-disjunction in meiosis I; only 0,02% of the progeny of a self-fertilized wild-type are males; mutations that result in more males are referred to as *him* (*h*igh *i*ncidence of *m*ales) (Hodgkin, Horvitz et al. 1979).
RNA-mediated interference (RNAi) was not only discovered in worms (Fire, Xu et al. 1998), but is easy to apply by soaking (Tabara, Grishok et al. 1998), feeding (Timmons and Fire 1998) or injecting (Fire, Xu et al. 1998) dsRNA. Recently techniques for targeted genomic deletions (Frokjaer-Jensen, Davis et al. 2010; Wood, Lo et al. 2011) and single copy insertion transgenes (Frokjaer-Jensen, Davis et al. 2008) were developed and made available.
The body wall and also the gonad of *C. elegans* are transparent. This fact makes this model highly suitable for immunofluorescence on whole fixed tissues and also for live imaging of meiocytes progressing through the gonad. Further advantages of *C. elegans* as a meiotic model are the short generation time (2.5 days on 25°C), the appearance as self-fertile hermaphrodites or males respectively and the ability to be frozen for permanent storage.

Meiosis I in the *C. elegans* gonad – A cytological overview

In the two gonad tubes of *C. elegans* hermaphrodites (one in the males) nuclei undergo the complete meiotic prophase I in a timely and spatially organized manner. In the adult worm meiocytes progress through the meiotic cell cycle as they move down the gonad tube from the distal tip to the spermatheca. By that, at a given position of the syncytial gonad the nuclei have spent the same time in meiosis (Hirsh, Oppenheim et al. 1976; Crittenden, Troemel et al. 1994). Therefore the gonad represents a highly synchronous meiotic time course. The germline comprises half of

the total number of nuclei in an adult hermaphrodite worm (Hirsh, Oppenheim et al. 1976).

The distal end of the gonad contains germ cell nuclei undergoing mitotic divisions and pre-meiotic S-phase (Crittenden, Leonhard et al. 2006). Further done the gonad, about 20 cell rows from the distal tip cell, a meiotic stem cell niche is induced by the distal tip cell causing rows of meiotic cells to form and move down to the proximal end, while they undergo the differed stages of prophase (Kimble and White 1981; Watt and Hogan 2000).

Meiosis is entered in leptotene/zygotene. In contrast to other organisms studied these first two stages of meiotic prophase I cannot be readily distinguished cytologically in *C. elegans*. Leptotene/zygotene in worms corresponds to the transition zone in the gonad, in which chromatin adapts a half moon shaped configuration (Hirsh, Oppenheim et al. 1976). In the transition zone homologous chromosomes pair and synapse (Dernburg, McDonald et al. 1998; MacQueen, Colaiacovo et al. 2002; Colaiacovo, MacQueen et al. 2003). Also meiotic DSBs start to be induced in this stage (Alpi, Pasierbek et al. 2003; Colaiacovo, MacQueen et al. 2003; Mets and Meyer 2009).

Meiocytes move down the gonad with an approximate speed of one cell row per hour (Crittenden, Leonhard et al. 2006). After 7 to 12 cell rows synapsis between homologous chromosomes is completed and cells enter pachytene. With beginning of pachytene chromosomes start to redistribute throughout the nuclear volume. In this meiotic stage DSB repair and recombination take place along fully synapsed chromosomes (MacQueen, Colaiacovo et al. 2002; Alpi, Pasierbek et al. 2003; Colaiacovo, MacQueen et al. 2003).

Diplotene starts with the disassembly of the SC (Martinez-Perez and Villeneuve 2005). Indicative for diplotene chiasmata, the cytological manifestations of crossovers, become apparent.

In the stage of diakinesis meiocytes leave the syncytium and cellularize. Due to further chromosome condensation, six DAPI positive structures become visible, which correspond to the six bivalents. These pairs of homologs are held together only by one chiasma per chromosome (Villeneuve 1994).

The following sections summarize insights gained into the function and orchestration of meiosis I in *C. elegans* and highlight conserved features, but also underline the differences among model organisms studied.

Meiotic sister chromatid cohesion and cohesins

During mitotic divisions duplicated sister chromatids are held together by the proteinacious cohesin complex until anaphase. Thereby cohesins enable sister kinetochore bi-orientation in metaphase and sister chromatid segregation into two daughter cells by the mitotic spindles (for review see: (Nasmyth and Haering 2009)). The cohesin complex is build up by four highly conserved subunits: two SMC subunits (SMC-1 and SMC-3), SCC-3, and a kleisin subunit (Losada, Hirano et al. 1998; Hagstrom and Meyer 2003). Cohesins mediate sister chromatid cohesion most likely by forming a ring which entraps both sisters upon replication and thereby holding them together (Ivanov and Nasmyth 2007). SMC proteins bear two ATP binding motifs separated by two coiled-coil domains that are interrupted by a hinge region (Melby, Ciampaglio et al. 1998). By folding back at the hinge region each SMC protein forms intra-molecular coiled-coils and generates at the opposite site an ATPase activity containing head domain (Haering, Lowe et al. 2002). Smc1p and Smc3p hetero-dimerize at their hinge region. Finally the ring structure of cohesins is established by interaction of the ATPase-containing head domain regions of the two SMC proteins with the kleisin subunit and Scc3p (Haering, Schoffnegger et al. 2004). Besides the components of the cohesin complex, cohesin loading upon pre-meiotic DNA replication requires two highly conserved proteins: Scc2p and Scc4p (SCC-2 and MAU-2 in worms) (Ciosk, Shirayama et al. 2000; Gillespie and Hirano 2004; Rollins, Korom et al. 2004; Tonkin, Wang et al. 2004; Seitan, Banks et al. 2006; Watrin, Schleiffer et al. 2006; Lightfoot, Testori et al. 2011). After establishment cohesion requires also PDS-5 to prevent premature sister chromatid separation during the meiotic prophase in *C. elegans* (Wang, Yoder et al. 2003).

Following bi-oriented attachment of all kinetochores to the mitotic spindle in metaphase, the kleisin subunit is cleaved which allows for sister chromatids to segregate to opposite poles of the newly formed daughter cell (Uhlmann, Lottspeich et al. 1999). However in meiosis I, cohesion must be maintained at centromeres to allow co-segregation of sister chromatids. At the same time cohesion distal to a chiasma must be lost to allow the exchange of recombined chromosomal arms. In meiotic anaphase II cohesins have to be released from centromeric regions of the chromosome to allow segregation of the two sister chromatids to opposite cell poles.

The different requirements between meiosis and mitosis are met in part by expression of meiotic-specific kleisin subunits. These meiotic specific kleisin were shown to be protected around centromeres during meiosis I (for review see: (Bardhan 2010))**.** During mitotic divisions SCC-1 is the only kleisin expressed in *C. elegans*. In contrast to only Rec8p in budding yeast (Klein, Mahr et al. 1999) higher organisms express more than one meiotic specific kleisin subunit (Bai, Peirson et al. 1999; Parisi, McKay et al. 1999; Lee, Iwai et al. 2003; Jiang, Xia et al. 2007; Lee and Hirano 2011). During *C. elegans* meiosis three different kleisin subunits are expressed: REC-8, COH-3, and COH-4 (Pasierbek, Jantsch et al. 2001; Severson, Ling et al. 2009). Also during anaphase I of *C. elegans* meiosis REC-8 is protected from removal at certain region between sister chromatids to prevent their opposite segregation (Rogers, Bishop et al. 2002) (see below). For meiotic cohesion REC-8, COH-3, and COH-4 are redundant, but not so for assembly of the SC, which is independent of REC-8 but dependents on COH-3/4 (Severson, Ling et al. 2009). In addition REC-8 might serve a conserved function as a sister barrier during meiotic recombination. In several organisms, including *C. elegans*, meiotic DSBs are repaired rather via the sister then via the homologous partner in respective *rec-8* mutant backgrounds (Pasierbek, Jantsch et al. 2001; Webber, Howard et al. 2004; Heidinger-Pauli, Unal et al. 2008; Severson, Ling et al. 2009; Kim, Weiner et al. 2010). Generally cohesins are required for meiotic repair (via the homologous partner or the sister) and therefore also for homologous recombination in worms (Pasierbek, Jantsch et al. 2001; Pasierbek, Fodermayr et al. 2003; Smolikov, Eizinger et al. 2007; Severson, Ling et al. 2009; Baudrimont, Penkner et al. 2011; Lightfoot, Testori et al. 2011). Also nuclei in the pre-meiotic zone of the gonad exhibit higher number of DNA lesions in cohesin mutants (Hayashi, Chin et al. 2007; Baudrimont, Penkner et al. 2011). Strikingly cohesins are also required for activating damage induced apoptosis during *C. elegans* meiosis (Lightfoot, Testori et al. 2011).

High resolution ChIP-chip analysis in budding yeast revealed that cohesion is established at certain position of the chromosome, mainly between convergent open reading frames (Lengronne, Katou et al. 2004). Furthermore upon entry into meiosis cohesin is visible as distinct stretches along the sister chromatids (Klein, Mahr et al. 1999; Pasierbek, Jantsch et al. 2001). Therefore the cohesin complex mediates the adaptation of the chromosome in a loop and axis conformation (Blat, Protacio et al. 2002). HTP-3 and Red1p two orthologous proteins from worm and yeast, which are

part of the meiotic axes and later on the lateral elements of the SC, colocalize with cohesins. Also stable localization of these two factors show interdependence with cohesins and cohesion can be impaired by the lack of axial element proteins (Goodyer, Kaitna et al. 2008; Severson, Ling et al. 2009; Kim, Weiner et al. 2010).

Meiotic chromosome axes

After or concomitant to pre-meiotic S-phase and establishment of sister chromatid cohesion a substantial structural reorganization of chromosome takes place. The first step is the establishment of chromosome axes or so called axial elements between sister chromatids. Later on axial elements are termed lateral elements of the SC, once transversal filaments of the SC are established between them. Chromosome axes play an essential role in homologous pairing, synapsis and meiotic recombination.

Chromosomal axis proteins and cohesins components colocalize and it has been proposed that cohesins are either part of the axes or even their foundation (Klein, Mahr et al. 1999; Eijpe, Offenberg et al. 2003). In budding yeast axes formation is dependent on Rec8p (Klein, Mahr et al. 1999) and also in worms loading/stabilization of axial element proteins is, at least partially, dependent on cohesins (Goodyer, Kaitna et al. 2008; Severson, Ling et al. 2009; Baudrimont, Penkner et al. 2011).

Besides the cohesin complex the axial elements are build up by HORMA domain proteins. In *C. elegans* HTP-1/2/3 and HIM-3 were identified as HORMA domain containing paralogs localizing to the chromosomal axes (Aravind and Koonin 1998; Zetka, Kawasaki et al. 1999; Couteau, Nabeshima et al. 2004; Martinez-Perez and Villeneuve 2005; Goodyer, Kaitna et al. 2008; Martinez-Perez, Schvarzstein et al. 2008). Several studies from budding yeast suggest that the functions of the meiotic axes in pairing, DSB formation and recombination are similar or conserved between worm and yeast (e.g.: (Klein, Mahr et al. 1999; Trelles-Sticken, Adelfalk et al. 2005; Panizza, Mendoza et al. 2011)). The four HORMA domain proteins have evolved partially different function in *C. elegans,* allowing the dissection of distinct roles for the chromosome axes in meiosis. HTP-3 is required for localization of the other HORMA domain proteins (Goodyer, Kaitna et al. 2008; Severson, Ling et al. 2009). Homologous pairing and synapsis depend on HTP-3 (Goodyer, Kaitna et al. 2008).

Interestingly HTP-3 is required for meiotic DSB formation and associated with MRE-11 and RAD-50 (Goodyer, Kaitna et al. 2008). RAD-50 and MRE-11 are presumably required for meiotic DSB resection in worms, but not break formation *per se* (Chin and Villeneuve 2001; Hayashi, Chin et al. 2007). This suggests that DSB formation and procession might be similarly coupled to the meiotic axes as it was demonstrated for yeast (Panizza, Mendoza et al. 2011). Pairing is also defective in *htp-1* mutants, but DSBs form in this background. HIM-3 loading partially depends on HTP-1 and similar to HTP-3, HTP-1 prevents premature loss of cohesion (Martinez-Perez, Schvarzstein et al. 2008). A prolonged transition zone is a general feature of synapsis mutants (e.g. *syp-2*) (MacQueen, Colaiacovo et al. 2002; Colaiacovo, MacQueen et al. 2003). When combined with *htp-1* mutation the prolonged transition zone of synapsis mutants is suppressed (Martinez-Perez and Villeneuve 2005). Further the usage of the sister chromatid as a repair template is initially blocked by HTP-1 and additionally HTP-1 inhibits the loading of central element proteins onto non-homologously paired chromosomes and thereby couples successful pairing to synapsis. In contrast HTP-2 is necessary for wild type level loading of central element proteins (Couteau and Zetka 2005). HIM-3 displays the strongest pairing phenotype of all HORMA domain proteins. This might be due to the fact that in HIM-3 autosomes fail to connect to the nuclear envelope and are not mobile during leptotene zygotene (Baudrimont, Penkner et al. 2010). Analogous to HTP-1, HIM-3 serves as a sister barrier during the time window of meiotic recombination (Couteau, Nabeshima et al. 2004).

Homologous pairing and meiotic chromosome movement

Pairing and synapsis between homologous chromosomes occurs after pre-meiotic DNA replication, establishment of cohesion and meiotic axes when nuclei enter the transition zone (Dernburg, McDonald et al. 1998). The transition zone is marked by crescent shaped chromatin and is classically referred to as the leptotene/zygotene stage in worm. More correctly the transition zone represents only the zygotene stage of meiosis, since hardly any nucleus can be found in that region with not yet initialized synapsis. Unlike in other organisms in *C. elegans*, pairing and SC formation are independent of meiotic DSBs and recombination (Dernburg, McDonald

et al. 1998). Also homolog recognition can be genetically separated from synapsis and recombination (MacQueen, Colaiacovo et al. 2002; Alpi, Pasierbek et al. 2003; Colaiacovo, MacQueen et al. 2003), but repair of DSBs must take place in the context of the SC to give rise to the crucial crossover between the homologous chromosome in *C. elegans* (Colaiacovo, MacQueen et al. 2003). Accountable for this DSB independent pairing in *C. elegans* are so called homologous recognition regions or pairing centers (Rosenbluth and Baillie 1981; Herman, Kari et al. 1982; Rose, Baillie et al. 1984; McKim, Howell et al. 1988; Herman and Kari 1989; Villeneuve 1994). These pairing centers are localized on one sub-telomeric region of each chromosome (McKim, Howell et al. 1988). The use of chromosomal pairing centers and independency of DSBs in meiosis for pairing is not unique to *C. elegans*. In *Drosophila* males the rDNA region serves as a pairing center for the sex chromosome (McKee 1996). In budding yeast pairing of non-homologous centromeres is dependent on cohesins and Zip1p, the central element component of the SC in yeast, but independent of Spo11p (Tsubouchi and Roeder 2005; Bardhan, Chuong et al. 2010; Obeso and Dawson 2010). In fission yeast the sme2 meiosis-specific noncoding RNAs accumulates at their respective gene locus and greatly enhance pairing of this locus, independent of DSBs, upon ignition of homology search (Ding, Okamasa et al. 2012). Nevertheless *C. elegans* represents the only system described to date in which pairing and SC formation is globally independent of DSBs.

C. elegans expresses four C2H2 zinc finger proteins (HIM-8, ZIM-1-3, referred to as ZIMs) that bind specifically to the highly repetitive sequences of the pairing center of one or two of the six chromosomes (ZIM-1-3 bind to the autosomes and HIM-8 to the X chromosome) (Sanford and Perry 2001; Phillips, Wong et al. 2005; Phillips and Dernburg 2006; Phillips, Meng et al. 2009). These proteins are required for homologous recognition and homologous synapsis of the specific chromosomes they are associated with (Phillips, Wong et al. 2005; Phillips and Dernburg 2006; Phillips, Meng et al. 2009). Nevertheless they cannot be the only factor by which chromosomes identify each other as “self”, since two of the ZIMs bind two different chromosomes.

In the transition zone, when pairing and SC formation take place the pairing centers and the ZIMs are tether to the nuclear envelope as distinct foci, which is required, but not sufficient for homologous pairing (Phillips, Wong et al. 2005; Penkner, Tang et al.

2007). CHK-2 kinase appears to be a master regulator of early prophase events. *chk-2* mutants lack clustered chromatin (MacQueen and Villeneuve 2001) and binding of ZIMs to the pairing centers of autosomes is dependent on CHK-2 (Phillips and Dernburg 2006) In turn ZIM localization to the pairing center is required to recruit the polo-kinase PLK-2 to the sites of chromosome ends tethered to the nuclear envelope (Harper, Rillo et al. 2011; Labella, Woglar et al. 2011). At the same time SUN-1, the inner nuclear membrane component of the meiotic SUN-KASH bridge in *C. elegans*, is phosphorylated in a *chk-2* dependent manner on several nucleoplasmic residues (Penkner, Fridkin et al. 2009). Recruitment of PLK-2 induces aggregation of SUN-1 and its KASH counterpart at the outer nuclear membrane ZYG-12 at sites of ZIM localization. SUN-1 is phosphorylated on S12 in a Polo kinase dependent manner in the population found in chromosome end aggregates (in *plk-2* deletion mutants, PLK-1 can partially substitute PLK-2) (Harper, Rillo et al. 2011; Labella, Woglar et al. 2011). SUN-1 aggregates are highly dynamic and co-localize with ZIMs/PLK-2 throughout the transition zone (Penkner, Fridkin et al. 2009; Sato, Isaac et al. 2009; Baudrimont, Penkner et al. 2010; Harper, Rillo et al. 2011; Labella, Woglar et al. 2011). Consistently PLK-2 can be co-purified with SUN-1 (Labella, Woglar et al. 2011) and HIM-8 interacts with PLK-2 in a Y2H (Harper, Rillo et al. 2011). Evidence for a physical interaction between SUN-1 and the autosomal ZIMs was not yet reported. Abrogation of the SUN/KASH bridge inhibits chromosome movement and chromatin clustering (Penkner, Tang et al. 2007; Penkner, Fridkin et al. 2009). Nevertheless in this situation chromosome still tether to the nuclear envelope, recruit PLK-2 and aggregate SUN-1 (Penkner, Fridkin et al. 2009). Therefore the clustered chromatin in the transition zone is not a consequence of tethering but rather of movement. Also deletion/depletion of all ZIMs, dynein or *plk-2* leads to a failure in chromatin clustering and pairing and chromosomes engaging in non-homologous synapsis (Harper, Rillo et al. 2011; Labella, Woglar et al. 2011; Martinez-Perez, personal communication)). Absence of either a single pairing center or deletion of one specific ZIM induces pairing defects for the respective chromosome, but it does not affect synapsis of the other chromosomes. Nevertheless a single unpaired/unsynapsed chromosome elicits a nucleus wide response. Unaffected and correctly paired/synapsed chromosomes in such a situation display delayed DSB repair and chromatin persist in the TZ-like clustered configuration (Phillips, Wong et al. 2005; Phillips and Dernburg 2006). PLK-2 similar to HTP-1 is required for

prolonging the transition zone in synapsis or pairing defective mutants (Harper, Rillo et al. 2011). Thus HTP-1 and PLK-2 could have checkpoint functions to coordinate pairing, synapsis and meiotic progression (Martinez-Perez and Villeneuve 2005; Harper, Rillo et al. 2011; Labella, Woglar et al. 2011).

The X chromosome exhibits a more robust pairing in different mutant background but also in the wild type than observed for the autosomes (Couteau, Nabeshima et al. 2004; Nabeshima, Villeneuve et al. 2004; Martinez-Perez and Villeneuve 2005; Penkner, Tang et al. 2007; Smolikov, Schild-Prufert et al. 2008; Penkner, Fridkin et al. 2009). The molecular base for this is not yet known. HIM-8 is expressed and binds to the X chromosomal pairing center much earlier than the other ZIMs (Phillips, Wong et al. 2005) and could therefore enhance the pairing efficiency. Alternatively since the X chromosome is heterochromatic during *C. elegans* meiotic prophase (Kelly, Schaner et al. 2002) compartmentalization of silenced chromatin within the nucleus, as shown in other circumstances, could aid pairing of the X chromosome (Cremer, Cremer et al. 2006).

In all organisms studied so far, genetic and cytological evidence suggest that early events of the meiotic prophase are genetically or physically linked to the nuclear envelope. Most prominently in many organisms physical attachment of chromosomes to the nuclear envelope leads to transient steric reorganization of the chromatin (as the crescent shaped nuclei observed in *C. elegans*). This reorganization is a consequence of actively moved chromosomes. The exact mechanistic prerequisites differ from organism to organism, but it is widely conserved that chromosome ends are associated with the nuclear envelope and are moved by force generated in the cytoplasm and transmitted through the nuclear envelope onto chromosomes. This results in rapid movement of single chromosomes. The exact contribution to the process of meiotic recombination and pairing of these movements slightly differs in organisms studied so far. Movement might facilitate pairing of homologous chromosomes by bringing them into closer proximity or by counteracting unwanted non-homologous interaction. Also movement could be required for resolving chromosomal entanglements that arise during synapsing chromosomes in some organisms (for review see: (Koszul and Kleckner 2009)). Alongside telomeric attachment to the nuclear envelope, chromatin of meiotic prophase I nuclei in yeasts and mammals transiently undergoes polarization towards one site of the nucleus. This configuration is termed the “chromosomal bouquet” (for review see: (Scherthan

2001)). This rearrangement of chromatin timely correlates with homologous chromosome pairing, synapsis, and recombination and is required for completing these processes with wild-type kinetics (Chua and Roeder 1997; Conrad, Dominguez et al. 1997; Cooper, Watanabe et al. 1998; Nimmo, Pidoux et al. 1998; Trelles-Sticken, Dresser et al. 2000; Conrad, Lee et al. 2007; Ding, Xu et al. 2007). In all organisms investigated so far SUN domain proteins and their interactors are required for bouquet formation (Chua and Roeder 1997; Chikashige, Tsutsumi et al. 2006; Ding, Xu et al. 2007). Actin-based motors in budding yeast and tubulin based motors in fission yeast drive meiotic prophase chromosome motility (Ding, Chikashige et al. 1998; Koszul, Kim et al. 2008). In *C. elegans* chromosome movement is dependent on dynein and tubulin, since a dynein knock-down and Nacodazol tretment result in unmobile, non-paired and non-homologously synapsed chromosmes (Sato, Isaac et al. 2009; Martinez-Perez, personal communication). A “bouquet” in classical terms, as defined by the local clustering of telomeres has not been observed in *C. elegans*, since only one side of the chromosome is tethered to the nuclear envelop. Nevertheless the formation of crescent shaped chromatin in the leptotene/zygotene stage of meiotic prophase I might be functionally analogues to the bouquet-in addition it has been shown that chromosome ends in worms have a strong tendency to locally cluster in groups. Chromatin clustering and movement in worms not only correlate with successful pairing, homologous synapsis and recombination but chromosome movement is crucial for homolog association and prevention of nonhomologous synapsis (Dernburg, McDonald et al. 1998; Penkner, Tang et al. 2007; Penkner, Fridkin et al. 2009; Sato, Isaac et al. 2009). By reducing the volume of searchable space in a nucleus the crescent shape, analogously to the bouquet, might assist the homology search (Loidl 1990). Furthermore establishment of this clustered form of chromatin depends on the same SUN/KASH nuclear envelope bridge as the bouquet (Penkner, Tang et al. 2007). SUN-1 is expressed in the *C. elegans* germline and in embryos until mid-embryogenesis, where it is maternally deposited (Fridkin, Mills et al. 2004). Its N-terminus reaches into the nuclear lumen, followed by the trans-membrane domain that spans the inner nuclear membrane. On the C terminal end *sun-1* encodes for a SUN (Sad1/UNC-84 homology) domain that localizes to the perinuclear space. Here the SUN domain interacts with the KASH (Klarsicht/ANC-1/Syne homology) domain of the outer nuclear envelope protein ZYG-12. For the human SUN2-KASH1/2 complex the crystal structure was resolved.

Three SUN domains form a trimer via their SUN domains and a part of their coiled-coil domains. This predisposes the SUN domains to bind three KASH domains. The KASH domains bind in three grooves formed between adjacent SUN domains. This interaction provides a stable linkage of the complex. Furthermore conserved cysteines on SUN and KASH domains covalently link both proteins by a covalent disulfide bound (Sosa, Rothballer et al. 2012). In *C.elegans,* the SUN domain is sufficient to for the ZYG-12-SUN-1 interaction (Tzur, Margalit et al. 2006; Minn, Rolls et al. 2009). Also SUN-1 self-interaction was described in the worm. The two coiled coil domains that are located in the perinuclear space are sufficient and required for SUN-1 self-interaction in a yeast-two-hybrid assay (Tzur, Margalit et al. 2006; Minn, Rolls et al. 2009).

In general the SUN-KASH interaction bridges the nuclear envelope and enables the connection of cytoplasmic components, such as the cytoskeleton, to nuclear factors, such as chromosomes or the nuclear lamina (Tzur, Margalit et al. 2006; Minn, Rolls et al. 2009). The interaction between SUN-1 and ZYG-12 for example anchors the centrosome to the nucleus in early embryos (Malone, Misner et al. 2003; Minn, Rolls et al. 2009). A single amino acid change in the SUN domain of SUN-1 (*sun-1(jf18)*) abrogates not only clustering of chromatin and pairing in the transition zone, but also retention of ZYG-12 at the nuclear membrane is disturbed in this mutant (Penkner, Tang et al. 2007). Deletion of *sun-1* results in an unorganized germline with strongly reduced numbers of germ cells and animals are sterile (Fridkin, Mills et al. 2004). Further embryos depleted of SUN-1 are not developing to larvae due to strong defects in nuclear structure, aberrant DNA content and chromatin morphology (Fridkin, Mills et al. 2004). SUN-1 protein further is required for the translocation and local maintenance of the pro-apoptotic protein CED-4 at the nuclear envelope, during ongoing program cell death (Tzur, Margalit et al. 2006). Embryos depleted for SUN-1 therefore show decreased numbers of apoptotic nuclei in embryos (Tzur, Margalit et al. 2006).

Meiotic chromosome synapsis

Pairing centers are sufficient for the initial pairing of chromosomes, but this pairing is

only transient. For stable pairing of homologous chromosomes throughout the gonad of *C. elegans* the formation of the SC between them is required (MacQueen, Colaiacovo et al. 2002). The SC is a proteinacious structured between homologous chromosomes that align them with a distance of about 100nm along their length (Smolikov, Schild-Prufert et al. 2008). The four central element proteins of the SC, SYP-1/2/3/4 localize between the two chromosome axes of homologs, that now build the lateral elements of the SC (MacQueen, Colaiacovo et al. 2002; Colaiacovo, MacQueen et al. 2003; Smolikov, Eizinger et al. 2007; Smolikov, Schild-Prufert et al. 2009). SYP-1 dimerizes and interacts with SYP-2 and SYP-3. SYP-3 interacts with SYP-4 and is the SC central element protein closest to the meiotic axes (Schild-Prufert, Saito et al. 2011). All central element proteins are interdependent of each other for building up a wild-type central element structure (Colaiacovo, MacQueen et al. 2003; Smolikov, Eizinger et al. 2007; Smolikov, Schild-Prufert et al. 2009).

Whereas the lateral element forming HORMA domain proteins are conserved across species, the central element forming proteins are not conserved with respect to their primary structure. Also the numbers of different central elements components in different organisms diverge. Budding yeast only expresses one central element component (Zip1p), higher organisms in general more than one (Sym, Engebrecht et al. 1993; MacQueen, Colaiacovo et al. 2002; Colaiacovo, MacQueen et al. 2003; Costa, Speed et al. 2005; de Vries, de Boer et al. 2005; Hamer, Gell et al. 2006; Bolcun-Filas, Costa et al. 2007; Smolikov, Eizinger et al. 2007; Smolikov, Schild-Prufert et al. 2009; Schramm, Fraune et al. 2011). Some organisms studied, such as *T. thermophilia* and *S. pombe*, which display many conserved meiotic features, lost the SC over the course of evolution and use, if at all, only reminiscences of it (Bahler, Wyler et al. 1993; Loidl and Scherthan 2004; Lorenz, Wells et al. 2004). Despite the diversity at the primary amino acid sequence levels of central element components, on ultra-structural level the SC displays striking similarities and conservations among species. Under EM resolution the SC is an electron-dense tripartite structure that resembles a railroad track or a zipper (Moses 1958). Also the distance of the lateral elements of roughly 100nm is conserved among species.

Assembly of the SC is highly progressive and formation of the SC between non-homologous chromosomes must be prevented. Several factors were identified that are involved in connecting successful pairing with SC formation. Besides HTP-1 and PLK-2 (Couteau and Zetka 2005; Harper, Rillo et al. 2011; Labella, Woglar et al.

2011) also HAL-2 is required to inhibit SC polymerization until a corresponding pair of homologous is found. In *hal-2* mutants homologous pairing is defective and chromosomes engaging in non-homologous synapsis. When combined with synapsis mutants pairing significantly improves (Zhang, Miley et al. 2012).

Once the SC is fully formed between homologous chromosomes meiocytes exit the zygotene stage and enter early pachytene. Chromosome movement of autosomes, which leads to tight chromatin clustering, ceases (Penkner, Fridkin et al. 2009; Sato, Isaac et al. 2009). The lack of central element proteins leads to an arrest in leptotene/ zygotene and nuclei are found in tightly clustered configuration throughout the gonad (MacQueen, Colaiacovo et al. 2002). Additionally, independent of the DNA damage checkpoint, unsynapsed pairing centers can trigger apoptosis in the germline as well (Bhalla and Dernburg 2005). This is dependent on the core apoptotic machinery, the ZIMs and the pachytene checkpoint gene *pch-2* (Bhalla and Dernburg 2005; Harper, Rillo et al. 2011).

Unlike in mammals, plants and budding yeast, in *C. elegans* SC formation is independent of meiotic DSBs and recombination (Giroux, Dresser et al. 1989; Dernburg, McDonald et al. 1998; McKim, Green-Marroquin et al. 1998; Baudat, Manova et al. 2000; Grelon, Vezon et al. 2001; Zhang, Miley et al. 2012). In *C. elegans* synapsis is initiated at the pairing centers and progresses downwards along the chromosomal axes, whereas in yeast synapsis is believed to be initiated at recombination sites (Agarwal and Roeder 2000; MacQueen, Phillips et al. 2005). Two taxon-specific proteins were identified that allowed the evolution of recombination independent SC polymerization in *C. elegans*: HIM-19 and CRA-1. Deletion of *him-19* or *cra-1* results in initiation of synapsis but polymerization is dependent on DSBs in these backgrounds (Smolikov, Schild-Prufert et al. 2008; Tang, Machacek et al. 2010). Although synapsis is independent of DSBs, recombination must take place in the context of the SC to give rise to the crucial crossover between the homologous chromosomes in *C. elegans* (Colaiacovo, MacQueen et al. 2003). In the absence of synapsis, RAD-51 foci accumulate until late into prophase I, afterwards the persisting DSBs are presumably repaired using the sister chromatid as a repair template (MacQueen, Colaiacovo et al. 2002; Colaiacovo, MacQueen et al. 2003). Budding yeast synapsis mutants also display a reduction of crossovers in the absence of synapsis, nevertheless the dependency on synapsis for crossover formation is most pronounced in *C. elegans*, were cross-over formation completely depends on the

presence of the SC (Colaiacovo, MacQueen et al. 2003; de Vries, de Boer et al. 2005). How the SC fulfills its role in crossover formation is not yet clear. The budding yeast SUMO E3 ligase Zip3 is required to form the SC and is found at late recombination nodules which were first identified in multiple organisms as silver stained bodies on pachytene chromosomes under the EM (Maguire 1966; Carpenter 1975; Zickler 1977; Rasmussen and Holm 1984; Agarwal and Roeder 2000; Borner, Kleckner et al. 2004). The *C. elegans* paralog ZHP-3 is not required for SC formation. Nevertheless it localizes initially to the synapsed axes before it retracts to multiple distinct foci and finally to one focus per chromosome which is positioned at the crossover site (Jantsch, Pasierbek et al. 2004; Bhalla, Wynne et al. 2008). In the absence of ZHP-3 cross-over formation is abolished. Furthermore correct localization of ZHP-3 depends on a fully established SC (Jantsch, Pasierbek et al. 2004).

In the early 20th century already it was observed in *D. melanogaster* that the formation of a crossover in a given locus on the chromosome inhibits the formation of crossover in the vicinity (Sturtevant 1913). This phenomenon was termed crossover interference and is conserved among most species. Crossover interference spaces crossovers further apart from each other than expected if they were randomly positioned. In *C. elegans* only one crossover per bivalent is formed, therefore the worm exhibit the strongest crossover interference possible. Crossover interference is conserved among animals that have an SC, and was not found in *S. pombe*, which does not build up an SC. Ensuring crossover interference therefore might be one of the conserved key functions of the SC. Indeed, when the integrity of the SC is weakened or its continuity along the chromosome is interrupted, crossover interference is strongly reduced or abolished in *C. elegans* (Hillers and Villeneuve 2003; Nabeshima, Villeneuve et al. 2004; Hayashi, Mlynarczyk-Evans et al. 2010)}. Organisms other than *C. elegans* that build up an SC form two types of crossovers, interfering and non-interfering ones. In general, crossovers that are interfering are dependent on the synaptonemal complex and associated proteins, the so-called ZMM pathway. In budding yeast this pathway beside the SC proteins requires Msh4 and Msh5, on which all crossovers depend in worms (Zalevsky, MacQueen et al. 1999; Kelly, Dernburg et al. 2000; Borner, Kleckner et al. 2004; Chen, Tsubouchi et al. 2008). The non-interfering crossovers are independent on the ZMM proteins but dependent on the MUS-81 nuclease (de los Santos, Hunter et al. 2003). MUS-81

was shown to play a redundant or backup role in *C. elegans* crossover formation and is only required for crossover formation upon irradiation induced DSB formation or in the absence of the helicase RTEL-1 (Youds, Mets et al. 2010).
Evidently the SC plays an important role in executing crossover interferences. Nevertheless the electron dense structure of the SC along bivalents is not required to establish interference. In wild-type budding yeast pachytene chromosome spreads Zip2p foci display interfering, nonrandom localization. In *zip1* mutants (lacking the central element of the SC) this localization is not abrogated (Fung, Rockmill et al. 2004), nevertheless crossovers do not interfere genetically. Furthermore in flies a central element mutant still exhibits CO interference (Page and Hawley 2001).
Therefore the molecular mechanism of how interference is communicated and established and what final purpose it serves are exiting and open question for future research.

Meiotic recombination

The main task during meiotic prophase is to establish the obligatory crossover to provide sufficient tension to withstand the spindle forces in anaphase I. Crossover formation starts with the introduction of DSBs in a controlled manner by the topoisomerase II-like protein SPO-11 (Keeney, Giroux et al. 1997; Dernburg, McDonald et al. 1998). DSBs in other organism do not occur randomly but on defined positions, so-called DSB hotspots. These DSB hotspots build the underlying fundament for the recombination map. Also in *C. elegans* recombination events are non-randomly distributed on chromosomes and occur five times more likely in regions with low gene density on chromosome arms than in the middle of the chromosome (Hillers and Villeneuve 2003). Since DSB sites have not been mapped yet, the existence of DSB hot spots remains enigmatic in *C. elegans.* Besides SPO-11, the histone methyl transferase HIM-17, responsible for the H3K9me mark, is required for formation of meiotic breaks (Reddy and Villeneuve 2004). Also in the absence of CHK-2, no breaks are formed (MacQueen and Villeneuve 2001). After break formation long overhanging 3’ tails are generated by removal of SPO-11 and resection of the 5’ end by COM-1, MRE-11 and RAD-50 (Sun, Treco et al. 1991; Chin and Villeneuve 2001; Hayashi, Chin et al. 2007; Penkner, Portik-Dobos et al. 2007).

Stabilized by the BRAC2 homolog, BRC-2, the RecA homolog RAD-51 binds to these overhangs (Petalcorin, Galkin et al. 2007; Jensen, Carreira et al. 2010). Binding of RAD-51 to the ssDNA results in a nucleoprotein filament that is able to search and invade homologous DNA sequences. This leads to the formation of a DNA triple helix in which strand exchange takes place. Finally the formation of a D-loop is the outcome of a successful strand exchange reaction (reviewed in: (Krejci, Altmannova et al. 2012)). Besides Rad51p, in other organisms meiotic recombination depends on another recA like recombinase, Dmc1p (Bishop 1994). Dmc1p, together with the regulatory proteins Hed1p and Mek1p, was shown to ensure the usage of the homologous chromosome as a repair template (Sheridan and Bishop 2006; Tsubouchi and Roeder 2006; Niu, Wan et al. 2009). The *C. elegans* genome does not encode for this factors supporting the idea that the meiotic axes are sufficient to ensure the homolog bias (Couteau, Nabeshima et al. 2004; Couteau and Zetka 2005; Martinez-Perez and Villeneuve 2005; Hayashi, Chin et al. 2007; Goodyer, Kaitna et al. 2008). Alternatively one of the two isoforms of *rad-51* expressed in *C. elegans* could have taken over the meiotic specific function of Dmc1p.

After strand exchange the DSB can be further processed into a Holliday junction by second end capture or can be subjected to strand displacement and produces a non-crossover (Holliday 1964; Szostak, Orr-Weaver et al. 1983; Sun, Treco et al. 1991). RTEL-1, the ortholog of Srs2p, promotes the ejection of the single-stranded DNA (Barber, Youds et al. 2008; Youds, Mets et al. 2010). BRC-2 in worms the functional equivalent of yeast Rad52p, mediates second end capture by promoting single strand annealing (Sugiyama, New et al. 1998; Krejci, Song et al. 2002; Petalcorin, Sandall et al. 2006; Lao, Oh et al. 2008). Holliday junction formation and strand displacement are mostly completed in yeast before the onset of full pachytene (Allers and Lichten 2001; Hunter and Kleckner 2001). Early recombination intermediates resolve in zygotene as non-crossovers by strand displacement and could primarily serve for homology check to assure pairing; those are not subjected to crossover formation in yeast (Giroux, Dresser et al. 1989; Weiner and Kleckner 1994; Peoples, Dean et al. 2002).

Since early meiotic tasks, as homolog searching, seem to be taken over by the pairing centers in *C. elegans,* recombination can be initiated and carried out later (Dernburg, McDonald et al. 1998). Rad-51 foci appear in late zygotene, peak in mid- and disappear in late pachytene (Alpi, Pasierbek et al. 2003; Colaiacovo, MacQueen

et al. 2003). In yeast most double Holliday junctions are resolved as crossovers. The exact nature of crossover precursors in *C. elegans* is not known yet, but, as in other organisms, DSB are produced in excess over crossovers (Mets and Meyer 2009). The residual DSBs are repaired as non-crossover or they are repaired using the sister as a repair template (Adamo, Montemauri et al. 2008; Bickel, Chen et al. 2010). Non-homologous end joining plays only a very minor role in meiotic DSB repair or might act as last backup mechanism usually not applied under wild-type conditions (Martin, Winkelmann et al. 2005; Clejan, Boerckel et al. 2006; Smolikov, Eizinger et al. 2007).

In yeast it is decided very early whether a DSB becomes either a crossover or a non-crossover (Allers and Lichten 2001). In contrast, in *C. elegans* this decision is probably made after completion of SC formation since DSBs introduced randomly in pachytene are sufficient for formation of interfering crossovers (Yokoo, Zawadzki et al. 2012). When as single break is introduced in addition to the SPO-11 generated DSBs in pachytene this break can either become a crossover or a non-crossover (Rosu, Libuda et al. 2011). When a single break is introduced in a *spo-11* deficient meiosis this break always is repaired as a crossover (Rosu, Libuda et al. 2011; Yokoo, Zawadzki et al. 2012). Finally the number of one crossover per chromosome cannot be altered by increasing levels of DSBs by irradiation to at least a 100-fold excess of DSBs of the wild type (Yokoo, Zawadzki et al. 2012). These results demonstrate that *C. elegans* exhibits very robust crossover assurance, interference and homoeostasis, which are most probably not executed at the level of DSB formation, as it is also the case in budding yeast (Martini, Diaz et al. 2006). Most recent evidence suggests that in *C. elegans* roughly 10 DSBs are formed per bivalent over the course of meiosis (Saito, Mohideen et al. 2012). Only a single one of these DSB sites is designated as a future crossover site by MSH-5 ZHP-3 and COSA-1, from late pachytene on (Jantsch, Pasierbek et al. 2004; Bhalla, Wynne et al. 2008; Yokoo, Zawadzki et al. 2012). COSA-1, a cyclin-related protein that is conserved in metazoan localizes exclusively to the crossover site. It is also required for the localization of the ZMM orthologs MSH-4/5 and ZHP-3 into several foci along chromosomes and their consecutive retractions to the single crossover side in late pachytene. Like MSH-4/5 and ZHP-3, COSA-1 is required for crossover formation. Strikingly, COSA-1 fails to detect the additional crossovers generated in an *rtel-1*

mutant (Zalevsky, MacQueen et al. 1999; Jantsch, Pasierbek et al. 2004; Bhalla, Wynne et al. 2008; Yokoo, Zawadzki et al. 2012).

Holliday junctions a cruciform four-way DNA intermediated. Resolution of a Holliday junction can lead to crossover formation accompanied by the exchange of chromosome arms or non-crossover formation and gene conversion, undistinguishable from strand displacement events (Holliday 1964; Szostak, Orr-Weaver et al. 1983; Sun, Treco et al. 1991). In the consensus model of meiotic recombination double Holliday junctions are the canonical intermediates for meiotic crossover repair. Indeed in budding yeast these structures have been observed by electron microscopy and 2D gel analysis (Bell and Byers 1983; Bell and Byers 1983; Schwacha and Kleckner 1995). In contrast in *S. pombe* the meiotic DSB repair intermediate that is required to form crossovers is a single Holiday junction (Cromie, Hyppa et al. 2006). The molecular nature of the DSB repair intermediates in *C. elegans* has not been determined yet.

Bacteria resolve Holliday junctions by usage of RuvC, an endonuclease that cuts Holliday junctions symmetrically, which allows ligation immediately after cleavage without any further processing of the ends (Benson and West 1994). In the ZMM-independent meiosis of fission yeast all Holiday junction are cleaved by Mus81 (Whitby, Osman et al. 2003; Cromie, Hyppa et al. 2006). To data *S. pombe* represents the only eukaryote examined where resolution of meiotic Holiday junctions exclusively depends on one nuclease and the key resolvases for other organisms, excepted for *D. melanogaster* has not yet been identified. MUS81 alone does not play a role in crossover formation in the meiosis of *D. Melanogaster* (Trowbridge, McKim et al. 2007). In flies crossovers are largely generated by the MEI-9 nuclease and MUS312, the XPF-1 nuclease and SLX-4 orthologs (Yildiz, Majumder et al. 2002). SLX-4 is a non-catalytic subunit of endonuclease complexes that is thought to provide a scaffold for SLX-1 and XPF-1 function in human and worm (Fekairi, Scaglione et al. 2009; Saito, Youds et al. 2009). Most of our understanding how resolution works comes from budding yeast. Studies in budding yeast allowed the delineation of two pathways that process Holiday junctions to form crossover. The predominant pathway utilizes the ZMM machinery (*Z*ip1/2/3/4, Msh4/5 and Mer3) presumably to protect recombination intermediates from resolution as non-crossovers (for review see: (Heyer, Ehmsen et al. 2010)). Holiday junction resolved by the ZMM induced pathway give rise to almost exclusively crossovers (Allers and

Lichten 2001). The second pathway is independent of ZMM proteins but dependent on Mus81p that resolves Holiday junctions, as in *S. pombe*, to either crossovers or non-crossovers (Jessop and Lichten 2008; Oh, Lao et al. 2008). When Sgs1p, the ortholog of the BLM-helicases, is absent crossover intermediates accumulate and Mus81p is required for full resolution (Dernburg, Zalevsky et al. 2000; Ketting and Plasterk 2000). Therefore Sgs1p ensures the predominant usage of the ZMM pathway to generate Holiday junction for crossover resolution (Jessop and Lichten 2008; Oh, Lao et al. 2008; De Muyt, Jessop et al. 2012). When the nucleases Mus81p, Slx1-Slx4p, Yen1p (the human GEN1 ortholog) or the MutLγ complex, Mlh1–Mlh3p are depleted simultaneously, crossover formation is decreased to almost zero. Nevertheless although crossover could not been resolved anymore, due to the absence of nuclease activity Holiday junctions accumulate only mildly, because recombination intermediates are resolved/displaced to non-crossovers in an Sgs1p dependent manner. In line with this model, when all four nuclease are depleted in an *sgs1* deficient background, Holiday junctions finally accumulated severely and not only crossover but also non-crossovers are reduced to almost zero (Zakharyevich, Tang et al. 2012).

All crossovers in *C. elegans* are dependent on the ZMM pathway (Zalevsky, MacQueen et al. 1999). Nevertheless in the absence of the helicase RTEL-1, MUS-81 is required to resolve a subset of Holiday junctions that would normally be RTEL-1 dependently dissolved/displaced (Youds, Mets et al. 2010). Also, the double mutants *mus-81*, *him-6*, the Sgs1 ortholog in worm, are synthetic lethal (Saito, Youds et al. 2009). Single knock downs of either MUS-81, SLX-1, XPF-1 or GEN-1 do not reduce offspring viability strongly (Saito, Youds et al. 2009; Bailly, Freeman et al. 2010; Saito, Mohideen et al. 2012). Also mutation in the scaffold protein for SLX-1 and XPF-1, SLX-4 reduces crossovers only slightly and only few unresolved recombination intermediates persist (Saito, Youds et al. 2009). Therefore the activity for HJ resolution is most likely also redundant in *C. elegans* and the key resolution enzymes remain to be determined.

Establishment of bivalent asymmetry in *C. elegans* prior to anaphase I

HJ resolution in *C. elegans* takes place in late pachytene. This is derived from the observation that SLX-4 expression starts in late pachytene and in diplotene chiasmata, the cytological manifestation of crossovers, are visible (Saito, Youds et al. 2009). After diplotene, prior to fertilization, which induces anaphase I, meiotic bivalents undergo dramatic structural rearrangements until diakinesis. These rearrangements set the stage for the meiotic divisions.

In the first division cohesin at the spindle attachment site has to be protected against cleavage by seperase to ensure co-segregation of sister centromeres. In yeasts Sgo1p binds specifically to centromeres during the first division and recruits a PP2A phosphatase to centromeric cohesion (Kitajima, Kawashima et al. 2004; Kitajima, Sakuno et al. 2006; Riedel, Katis et al. 2006). Thereby Rec8p is protected from phosphorylation at centromeres. In yeasts Rec8p hast to be phosphorylated to present a substrate for seperase and non-phosphorylatable Rec8p rescues the premature Rec8p loss when Sgo1p is absent (Katis, Lipp et al. 2010). This mechanism seems to be conserved in many organisms (Kerrebrock, Moore et al. 1995; Mailhes, Hilliard et al. 2003). However the holocentric nature of *C. elegans* chromosomes required an evolutionary adaptation to protect centromeric cohesion. This requirement is met in diakinesis when a long and a short chromosome arm are defined by the position of the single crossover event along the chromosome. Chromatin condensation starting in diplotene gives rise to a cruciform structure with two long and two short arms and the crossover in the middle (Nabeshima, Villeneuve et al. 2005). In *C. elegans* SGO-1 is not required for REC-8 protection during the first division, but it plays a yet enigmatic role in the second division (de Carvalho, Zaaijer et al. 2008). Instead cohesin is dephosphorylated and thereby protected on the long arm by GSP-1 and GSP-2 the PP1 phosphatase in worms (Rogers, Bishop et al. 2002; de Carvalho, Zaaijer et al. 2008). GSP-1/2 are recruited to the long arm by LAB-1. Therefore LAB-1 has overtaken the function of Sgo1p in *C. elegans* (de Carvalho, Zaaijer et al. 2008; Llano, Gomez et al. 2008). The exclusive localization of LAB-1 to the long arm also inhibits the binding of AIR-2, the Auora B kinase in worms, to the long arm, and therefore stays restricted to the short arm (de Carvalho, Zaaijer et al. 2008). AIR-2 dependent phosphorylation of REC-8 allows its cleavage on the short arm, at the metaphase-anaphase transition (Rogers, Bishop et al. 2002).

Also Histone H3 is phosphorylated by AIR-2 exclusively on the short arm (Hsu, Sun et al. 2000; Llano, Gomez et al. 2008). Prior to these events the SC begins to disassembly in late pachytene and it is completely absent from the long arms of the bivalent by diakinesis (MacQueen, Colaiacovo et al. 2002; Nabeshima, Villeneuve et al. 2005; Martinez-Perez, Schvarzstein et al. 2008). HTP-3 and HIM-3 stay along the axes of chromosomes, whereas HTP1/2 are only present on the long arm in diakinesis (Zetka, Kawasaki et al. 1999; Goodyer, Kaitna et al. 2008; Martinez-Perez, Schvarzstein et al. 2008). These asymmetric features resulting from bivalent restructuring require a recombination event (Nabeshima, Villeneuve et al. 2005). But how asymmetry is established and what stage of recombination triggers the restructuring is not yet worked out and will be a subject to exciting future research.

Meiotic coordination and quality control

Different checkpoint mechanisms coordinated the consecutive order of the key meiotic events (replication, pairing, SC formation, recombination, repair and resolution) and ensures that they take place before chromosomes are segregated in anaphase I. Checkpoints are defined to survey and communicated the progression state of cell cycle events to other metabolically/mechanistically independent processes. By this a checkpoint establishes dependencies between two mechanistically independent events and thereby allows timely coordination of them. Such coordination is required for a faithful progression through the cell cycle and different checkpoint deficiencies can result in inviability of respective mutants. Also when things go wrong the checkpoint mechanisms are responsible to halt the cell cycle progression until repair of the damage is completed or the faulty cell is removed by apoptosis. Since DSB formation and repair are central components of meiosis the evolutionary usage of the DNA damage checkpoint machinery to coordinate meiosis is not surprising. In many organisms DSBs are initially detected by ATM1 kinase which leads to the recruitment of the MRN complex and resection of the DSB. The resected single strand is covered by RPA, which in turn recruits ATR kinase. This leads to the activation of CHK1 and CHK2 and the phosphorylation of downstream target. In parallel RAD9, RAD1 and HUS1 (9-1-1 complex) are activated (reviewed in: (Harrison and Haber 2006)). Although these checkpoint functions are similar in

mitosis and meiosis, meiotic specialties of this checkpoint were evolved. For instance in yeast Spo11p induced breaks differ from breaks artificially introduced during meiosis by HO-nuclease or irradiation. Rad53p, the CHK-2 ortholog in yeast, is not activated upon Spo11p induced breaks however irradiation in meiosis elicits the accumulation of phosphorylated Rad53p (Cartagena-Lirola, Guerini et al. 2008).

ATM/ATR dependent damage signaling is required for efficient repair of breaks in budding yeast, mouse and plants (Barlow, Hirotsune et al. 1996; Garcia, Bruchet et al. 2003; Barchi, Roig et al. 2008). In *C. elegans* DSB are repaired in the absence of ATL-1, the ATR ortholog in worms, but crossover formation is abolished (Garcia-Muse and Boulton 2005). ATM-1 seems not to play an important role in *C. elegans* or its functions are partially redundant with ATR-1 in meiosis, since viability is not affected in the deletion mutant. Activation of the meiotic DNA damage checkpoint results in a meiotic progression arrest in many organisms (reviewed in (Longhese, Bonetti et al. 2009)}). In worm hermaphrodite meiosis an arrest upon unrepaired DNA damage was not yet reported, but meiocytes with persistent DNA damage are culled from the germline by apoptosis. This is a highly conserved feature of gametogenesis in higher eukaryotes. In *C. elegans* oogenesis 30 to 50% of the meiocytes undergo apoptosis in the apoptotic zone of the gonads beginning at late pachytene in adult animals (Gumienny, Lambie et al. 1999). Occurrence of this “physiological apoptosis” does not depended on any known stress factor or checkpoint gene and employs the same core apoptotic machinery (*ced-3*, *ced-4* and *ced-9*), as used in apoptosis during development, (Gumienny, Lambie et al. 1999). Although under standard laboratory conditions animals lacking the apoptotic execution machinery do not display strongly decreased offspring quality, they show slightly elevated levels of aneuploid offspring and smaller oocytes in older animals (Gumienny, Lambie et al. 1999; Gartner, Milstein et al. 2000). Therefore physiological levels of apoptosis do not cull exclusively defective meiocytes from the germline. More likely one can speculate that some meiocytes are stochastically subjected to apoptosis in late pachytene, when they begin to enlarge and further on cellularize; this might provide more cytoplasm for meiocytes developing into oocytes (Gumienny, Lambie et al. 1999). DNA damage introduced by irradiation and sensed by the meiotic DNA damage checkpoint machinery leads to elevated apoptosis in the gonad (Gartner, Milstein et al. 2000). Checkpoint factors (such as the worm 9-1-1 complex, atl-1 and CEP-1, the worm p53 ortholog) are required for sensing and transmitting DNA

damage are therefore necessary for elevated steady state numbers of apoptotic nuclei (Gartner, Milstein et al. 2000; Schumacher, Hofmann et al. 2001; Boulton, Gartner et al. 2002; Hofmann, Milstein et al. 2002; Garcia-Muse and Boulton 2005; Derry, Bierings et al. 2007; Stergiou, Doukoumetzidis et al. 2007). Unrepaired meiotic DSBs are sensed by the same machinery and therefore lead to elevated numbers of apoptotic corpses in the germline (Gartner, Milstein et al. 2000). On the other hand, when meiotic DNA DSBs are not produced (e.g. *spo-11*), apoptotic corpses are decreased in numbers, and presumably only physiological apoptosis is left in the germline (MacQueen, Colaiacovo et al. 2002).

Not only signals from unrepaired DNA damage leads to checkpoint activation in *C. elegans*. Nevertheless components of the consensus DNA integrity checkpoint machinery are used to orchestrate and survey DSB independent steps in meiosis. For example *chk-2* mutants, despite initializing and progressing through meiosis, fail to load ZIMs onto the autosomes and do not form DSBs or the SC (MacQueen and Villeneuve 2001). CHK-2 activation does not depend on DSBs or ATM/ATR function in *C. elegans* (MacQueen and Villeneuve 2001; Penkner, Fridkin et al. 2009). *him-19* mutants phenocopy the *chk-2* mutant in aged hermaphrodites. In contrast to *chk-2* mutants, exogenous introduction of DSB restores SC polimerization and loading of ZIMs and chromosome mobility. This is dependent on the presents of CHK-2, which indicates that CHK-2 is also required to detect DSBs in *C. elegans* (Tang, Machacek et al. 2010).

Defects in SC formation can trigger a delay in meiotic progression or apoptosis independently of DSB formation in worms and flies (MacQueen, Colaiacovo et al. 2002; Colaiacovo, MacQueen et al. 2003; Bhalla and Dernburg 2005; MacQueen, Phillips et al. 2005; Joyce and McKim 2009). For the apoptotic response to asynapsis in worms the core apoptotic machinery, the pairing center binding proteins, PLK-2 and the pachytene checkpoint gene *pch-2* are required (Bhalla and Dernburg 2005; Harper, Rillo et al. 2011). The PCH-2 ortholog is also required for the synapsis checkpoint in *D. melanogaster* (Joyce and McKim 2009). Also yeast lacking Pch2p fails to arrest the meiotic cell cycle if SC assembly and recombination are defective (San-Segundo and Roeder 1999; Wu and Burgess 2006).

In mouse and yeast it was shown that PCH-2, an AAA-ATPase, regulates HORMAD-protein localization on meiotic chromosome axes in response to synapsis (Borner, Barot et al. 2008; Wojtasz, Daniel et al. 2009). Also crossover interference requires

Pch2p in yeast (Zanders and Alani 2009). Homologous pairing, SC formation, meiotic cohesion, DSB initiation, crossover formation and the homologous repair bias are all dependent on HORMA proteins that localize at the meiotic axis (Xu, Weiner et al. 1997; Zetka, Kawasaki et al. 1999; Couteau and Zetka 2005; Martinez-Perez and Villeneuve 2005; Goodyer, Kaitna et al. 2008; Severson, Ling et al. 2009; Shin, Choi et al. 2010). Due to their simultaneous involvement in so many processes HORMA domain proteins represent the mechanistic lynchpin in meiosis. Therefore they are good candidates to take over meiotic coordination and surveillance. In mice lacking meiotic DSBs and therefore the synaptonemal complex DSB independent apoptosis is triggered and checkpoint proteins like ATR and BRCA1 accumulate on asynapsed chromosomes (Barchi, Mahadevaiah et al. 2005; Di Giacomo, Barchi et al. 2005; Kouznetsova, Wang et al. 2009). Also HORMAD1 and HORMAD2 localizes specifically to unsynapsed chromosome axes (Wojtasz, Daniel et al. 2009). Most importantly for this checkpoint response the axes components SYCP3, and HORMAD1 are required (Kouznetsova, Wang et al. 2009; Shin, Choi et al. 2010). The synapsis checkpoint dependent cell cycle arrest in *C. elegans* also largely depends on HORMA domain proteins. *htp-1* mutants are able to suppress the prolonged leptotene/zygotene stage induced by synapsis mutants (Martinez-Perez and Villeneuve 2005). The coordination of pairing and synapsis in *C. elgans* requires also HTP-1, which prevents the loading of the SC on unpaired chromosomes (Couteau and Zetka 2005). Whether HORMA domain proteins play a role in synapsis checkpoint induced apoptosis in worms is not established yet. Also whether the establishment of a crossover is monitored or just ensured is in open question for future research.

Proposed aims of this thesis

Aims initially proposed for this thesis are listed in *italic*. References to the Chapters presenting data to the proposed specific questions are added beneath each point.
Data acquired outside of the proposed topic are listed in this section following the proposed questions.

- *Is SUN-1 modified during the time period of homology search?*

Sun-1 is phosphorylated on multiple N-terminal residues at the onset of meiosis (Chapter 1.1 and Chapter 2.6).

- *If so, what is the nature of the modification? What are the molecules that are responsible for the modification?*

The kinases responsible for the phosphorylation are CHK-2 and PLK-2 (Chapter 1.1 and Chapter 2.9).

- *What are the biological consequences of the modification?*

SUN-1 phosphorylation is required to sustain the leptotene/zygotene specific chromatin movement, by keeping PLK-2 stably localized at chromosomal attachment sites under challenged conditions and to establish the SC with wild-type kinetics (Chapter 2.7, Chapter 2.8 and Chapter 2.10).

- *What is regulating SUN-1 aggregate induction?*

CHK-2 dependent recruitment of pairing center proteins to the nuclear envelope and subsequent kinase activity of polo kinase at these sites induce SUN-1 aggregates (Chapter 1.1 and Chapter 2.9).

- *What is regulating SUN-1 aggregate disassembly?*

Polymerization of the SC along chromosomal axes leads to the disassembly of SUN-1 aggregates at the autosomal attachment sites. Achievement of a crossover or a certain crossover intermediate finally leads to the disassembly of the last remaining

SUN-1 aggregate at the sex chromosome in mid pachytene and to de-phosphorylation of SUN-1 (Chapter 2.2 - Chapter 2.5).

Additionally during the time of my thesis I could contribute to a detailed description of SUN-1 aggregate mobility (Chapter 1.2). I contributed to the discovery of two new mechanisms to ensure genomic germline integrity (Chapter 2.5, Chapter 2.7 and Appendix V). Furthermore I could support the characterization of the role of the cohesion complex in mitotic and meiotic DNA DSBs repair in *C. elegans* (Appendix IV) and could contribute to elucidating the highly redundant process of meiotic crossover resolution (Agostinho, et al., under revision).

Chapter 1.0 Contribution to the initial description of SUN-1 phosphorylation, aggregate formation and mobility

Prof. Jantsch and Dr. Penkner initially characterized the inner nuclear envelope protein SUN-1 as a mechanistic key component in the process of meiotic chromosome homology search (Penkner, Tang et al. 2007). The time I started my thesis, they had evidence that the SUN-1 protein was post-translationally modified at the onset of meiosis concomitant with the homology search. Initially I was trained by Alexandra Penkner and got introduced to the SUN-1 project. I participated in the work resulting in the initial description of SUN-1 post-translational modification and aggregate formation and mobility at the onset of meiotic prophase (Penkner, Fridkin et al. 2009; Baudrimont, Penkner et al. 2010). These two publications are attached as Appendix 1&2. In Chapter 1.1&1.2 the most significant findings of these two publications are briefly summarized.

My personal contribution to (Penkner, Fridkin et al. 2009) was to generate strains and their cytological characterization. I found that phosphorylation of SUN-1 was independent of CDK-2, ATM-1 and ATL-1 (the ATR homolog in *C. elegans*). I also established phospho-specific antibodies against serines that were found in mass spectrometry to be phosphorylated (S12pi and S24pi) and tested the specific genetic requirements for the phosphorylation of the different serines. I found that all of them were CHK-2 dependent and independent of meiotic DSB induction. Further I found that there exist two different phosphorylation patterns on specific serines. SUN-1 S12 was only phosphorylated in the moving competent SUN-1 aggregates. In contrast SUN-1 S8pi and S24pi were phosphorylated in the entire population of SUN-1 at nuclear envelope at the onset of the TZ. We could strengthen these results by analysis of mass spectrometry data, where we found that in SUN-1 S12 phosphorylation never occured without simultaneous SUN-1 S8 phosphorylation, however SUN-1 S8 phosphorylation could be detected on peptides with unphosphorylated S12.

I also could show that mimicking phosphorylation was not sufficient to rescue the *chk-2* phenotype with respect to pairing and meiotic progression, leading to the conclusion that CHK-2 was not the direct kinase for SUN-1, or that other targets were

required to be phosphorylated by CHK-2 for meiotic progression. Additionally I expressed recombinant CHK-2 and different forms of SUN-1 as a target for *in vitro* kinase assays, which aimed to test, whether SUN-1 was a direct target of CHK-2. Although I succeeded in expressing and purifying the kinase and its putative target I was not able to show that SUN-1 was the direct target of CHK-2 in *in vitro* kinase assays. Also the attempt to generate a GFP tagged version of CHK-2 to study its localization and interaction partners failed, since the tagged version of CHK-2 was not to functionally expressing *in vivo*.
Contribution to figures in (Penkner, Fridkin et al. 2009) (figure numbers of the publication): Figure 4F, Figure 7ABC, Figure S4, Figure S7, Figure S8 and Table S1

For (Baudrimont, Penkner et al. 2010) I contributed to the design of the study, generated strains, and purified antibodies for this study.
Contribution to figures in Chapter (Baudrimont, Penkner et al. 2010) (figure numbers of the publication): Figure 1DEF, Figure 2, Figure 7C, Figure 8 and Figure S4.

Chapter 1.1 SUN-1 forms mobile aggregates at chromosome ends and is phosphorylated at the onset of leptotene

In brief, in this publication we were able to demonstrate that SUN-1 was organized into rapidly moving aggregates at putative chromosomal attachment site during the time window of chromosome homology search. A functional GFP tagged SUN-1 line was created and it was possible to detect phosphorylation of SUN-1 at multiple residues at the nuclear N-terminus (S8, S12, S24, S35 or T36, S43, S58 and S62). By raising phospho-specific antibodies against some of the serines it could be shown that these phosphorylations were CHK-2 dependent and independent of SPO-11 and ATM/ATR and occured during the time window of SUN-1 aggregation and diminished again during pachytene. It was shown that the absence of synapsis, which prolongs the time window for homology search, also prolongs SUN-1 phosphorylations. Mimicking phosphorylation at certain positions (S12E and S62E) causes a prolongation of the time window of the homology search (prolonged appearance of SUN-1 aggregates), failures in DSB repair via the homolog and the occurrence of univalents at diakinesis (*these observations about the substitution lines, most likely resulted from artifacts generated by the biolistic transformation technology and which led to insufficient expression of the transgenes, see Discussion and Chapter 2.6. During the course of my thesis I regenerated phospho-mutant lines with the mos transformation technology, which allows insertion of the transgenes as a single copy into a defined locus that expresses well during meiosis*) (Frokjaer-Jensen, Davis et al. 2008).

Please find (Penkner, Fridkin et al. 2009) in the Appendix (Appendix I)

Chapter 1.2 Mobile SUN-1 aggregates mediate homologous chromosome pairing by shuffling chromosome ends

Antoine Baudrimont, was able to establish live imaging time lapse microscopy in the *C. elegans* germline by filming the GFP tagged SUN-1 protein. In brief, he could show that ongoing pairing in the TZ did not have an impact on SUN-1 aggregate dynamics. We also found that chromosome axes were required to produce wild-type numbers of SUN-1 aggregates. Also we could show that synapsis and recombination influenced different aspects of aggregate dynamics to various extents.

Please find (Baudrimont, Penkner et al. 2010) in the Appendix (Appendix II)

Chapter 2.1 The SUN-1 phosphorylation patterns correlate with hallmarks of meiotic progression

In Chapter 1.1 (Penkner, Fridkin et al. 2009) we could show that SUN-1 was phosphorylated on seven nucleoplasmic, N-terminal residues: S8, S12, S24, S43, S58, S62, and S35 or T36. Three cytologically active antibodies against phosphorylated S8, S12 and S24 (all raised in guinea pig) were presented in this study. Additionally we generated an antibody in rat against phosphorylated S43 of SUN-1. This newly developed antibody allowed us to co-stain with the other phosphorylations and (indirectly) compare and correlate their subcellular localization. Meiotic SUN-1 phosphorylations on S8, S12, S24, and S43 appeared synchronously with entry to leptotene/zygotene (Figure 1A-D, left panel). S8, S24, and S43 were phosphorylated on the entire population of SUN-1, whereas S12 was exclusively phosphorylated on the population of SUN-1 found in aggregates at the nuclear envelope–attached chromosome ends (highlighted by the pairing center binding proteins HIM-8 and ZIM-2 in Figure 1E&F, left panel). All phosphorylations were dependent on *chk-2*; however in the wild type, they were independent of *spo-11* and *atm-1/atr-1* (Penkner, Fridkin et al. 2009).

In early pachytene, when all chromosome axes are synapsed (MacQueen, Colaiacovo et al. 2002) and chromatin is found more loosely clustered than in leptotene/zygotene (Figure 1, middle panel) SUN-1 stayed phosphorylated on residues 8, 24, and 43. These phospho-modifications were found on the entire population of SUN-1; they can be considered equal (for overlap of localization, see Figure 1C&D, left and middle panel). Therefore the choice of antibodies to detect them in co-stainings for this study was dictated by the compatibility of the established staining protocol with other antibodies. SUN-1 phosphorylated on S12 was now limited to the last persisting SUN-1 aggregate that colocalizes with HIM-8 (Figure 1A&F, middle panel).

In late pachytene, when chromatin is fully dispersed throughout the nuclear volume (Figure 1, right panel), SUN-1 was neither found phosphorylated nor aggregated any longer, but evenly distributed throughout the nuclear envelope (Figure 1A-D, right panel). The ZIMs,I refer to the autosomal pairing center proteins as such, were not colocalizing with SUN-1aggregates anymore and were only found as week foci (or completely absent) at this stage of meiotic prophase ((Phillips, Wong et al. 2005; Phillips and Dernburg 2006) and Figure 1E&F, right panel).

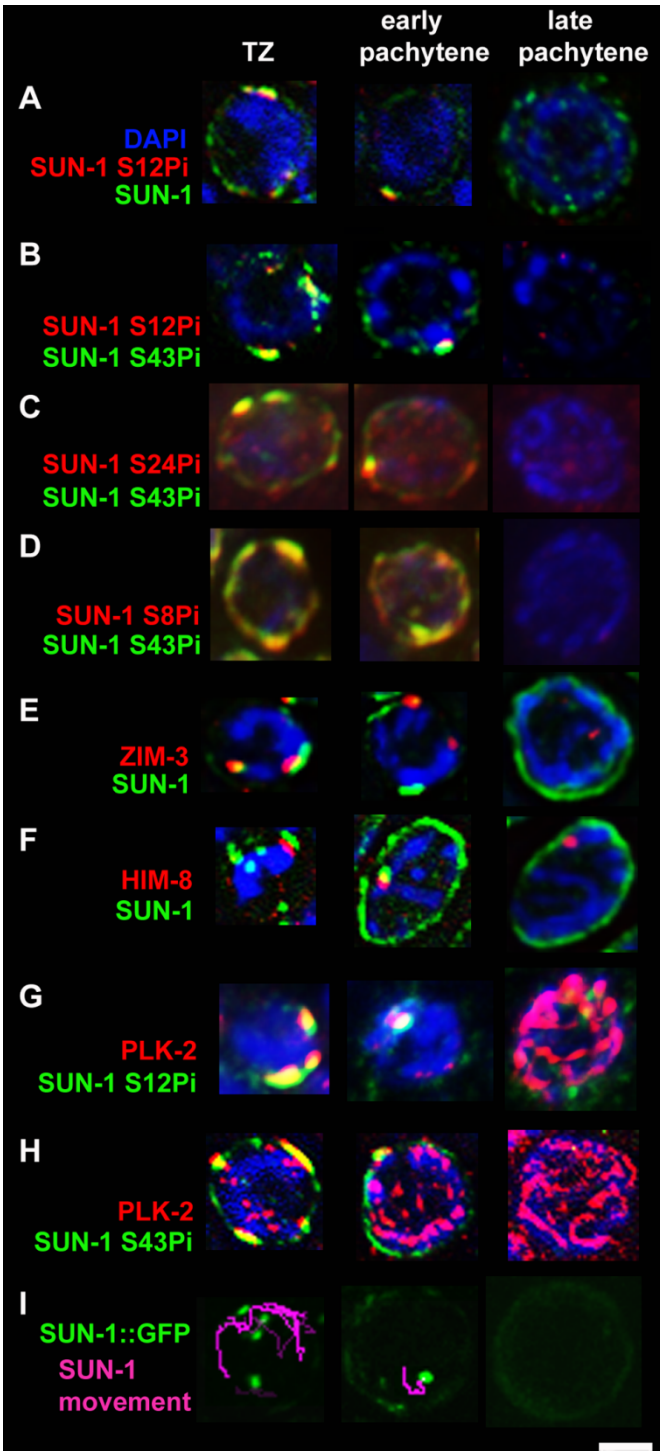

Figure 1. Localization study of SUN-1, SUN1 phosphorylation, ZIMs and PLK-2. Representative wild-type hermaphrodite nuclei from TZ (left), early pachytene (middle), and late pachytene (right). All nuclei were stained with DAPI (blue). (A) SUN-1 (green) forms aggregates in the TZ; these aggregates are phosphorylated on SUN-1 S12 (red). SUN-1 not within aggregates is not phosphorylated on S12. In early pachytene, only one aggregate remains, and it is phosphorylated on S12. In late pachytene, aggregates and SUN-1 phosphorylation on S12 are gone. (B) Phosphorylation of SUN-1 S12 (red) and S43 (green) are seen at the same time. S43 phosphorylation pattern highlights the entire nuclear envelope, including the SUN-1 aggregates at chromosome ends. In early pachytene, SUN-1 S43 remains phosphorylated on the last aggregate (where it overlaps with S12 phosphorylation) and on the entire nuclear envelope. In late pachytene, S43 and S12 phosphorylation is gone. S43 phosphorylation pattern (green) overlaps with S24 (C, red) and S8 (D, red). (E) Autosomal pairing-center binding protein ZIM-3 (red) always colocalizes with SUN-1 (green) aggregates in the TZ. In early pachytene, ZIM-3 does not colocalize with the last remaining prominent SUN-1 aggregate. (F) HIM-8 (red), in contrast, remains colocalized with SUN-1 (green) aggregates in early pachytene. (G) PLK-2 (red) shares the localization pattern with its target phosphorylation site SUN-1 S12 (green) at SUN-1 aggregate(s) in the TZ and early pachytene. PLK-2 starts to localize to synapsing chromosomes from the TZ onwards and is found on all synapsed axes by late pachytene. (H) PLK-2 (red) and S43 phosphorylation (green) only overlap at SUN-1 aggregates. (I) Displacement tracks of SUN-1 aggregates represent 2D plotted chromosome end movements over 3 min. Scale bar, 2 µm.

Given this observations, one can summarize that, when, in a given nucleus in the gonad, SUN-1 is phosphorylated on S8, S24, and S43, the nucleus always displays one (and loosely cluster chromatin, as found in early pachytene) or more (and tightly clustered chromatin, as found in leptotene/zygotene) SUN-1 aggregates colocalizing with one or more ZIMs foci. These aggregates are phosphorylated on S12. This is the case for the wild type and for most of the mutants presented in this study. Therefore, when the term “SUN-1 phosphorylation” is used I refer to all phosphorylation events in one given nucleus, else the phosphorylation site is specified.

Sara LaBella and Monique Zetka from McGill University in Montreal established and published in collaboration with us (Labella, Woglar et al. 2011)* an antibody against PLK-2. PLK-2 localized to the movement-competent and phosphorylated SUN-1 aggregate(s) in leptotene/zygotene and early pachytene (Figure 1G&H and Figure 1I, left and middle panel). PLK-2 stayed localized to these aggregates and also started to relocate to stretches on synapsed chromosomes. Increasing amounts of PLK-2 relocating from pairing center sites to synapsed chromosomes was accompanied by release from the tight chromatin clustering in mid pachytene (Figure 1G&H, middle panel). In late pachytene, when no SUN-1 aggregates are detectable anymore, PLK-2 stretches were fully elongated along synapsed chromosomes and enriched PKL-2 localization on pairing centers can no longer be resolved (Figure 1G&H, right panel).

* The Zetka lab isolated *plk-2(vv44)* in a screen for meiotic pairing mutants. Our collaboration resulted in the publication (Labella, Woglar et al. 2011), attached as Appendix III). My personal contribution to this publication is presented in this chapter and co-cited with (Labella, Woglar et al. 2011). In order to achieve a monographic form for this thesis, findings from this publication are presented alongside with data of another publication Woglar, A., A. Daryabeigi, et al. (2013). "Matefin/SUN-1 Phosphorylation Is Part of a Surveillance Mechanism to Coordinate Chromosome Synapsis and Recombination with Meiotic Progression and Chromosome Movement." PLoS genetics **9**(3): e1003335. in this chapter.

Chapter 2.2 Persistent SUN-1 phosphorylation correlates with synaptic and recombinational errors in the wild type

Nuclei enter leptotene/zygotene and SUN-1 is phosphorylated very synchronously at that stage (Figure 2A). Nevertheless we observed the occasional appearance of single nuclei that showed persistent phosphorylation of SUN-1 in the mid/late pachytene zone in the gonad, where most other nuclei seem synchronously dephosphorylated (Figure 2A, arrow). On average, I counted 2.6 (standard deviation [SD] 2.2) such nuclei in the mid/late pachytene region of wild-type gonads (n = 46). In contrast to the pachytene nuclei surrounding them, these nuclei had a tightly clustered, leptotene/zygotene-like chromatin configuration, were positive for SUN-1 phosphorylation, and had one or more SUN-1 aggregates (positive for S12 phosphorylation). Furthermore, these nuclei also showed high numbers of RAD-51 foci (Figure 2B, blow up), consistent with the presence of unrepaired DSBs. Also occasional synaptic failures could be detected in these “asynchronous” nuclei (Figure 2C, arrow). This cytological appearance could be triggered by apoptosis, which culls half the nuclei in the late pachytene/diplotene zone of the gonad (Gumienny, Lambie et al. 1999). Nevertheless, these nuclei were also present in *ced-3(n717)* apoptosis-defective mutants (Figure 2D, arrow), indicating that they do not represent nuclei with an activated apoptotic machinery.

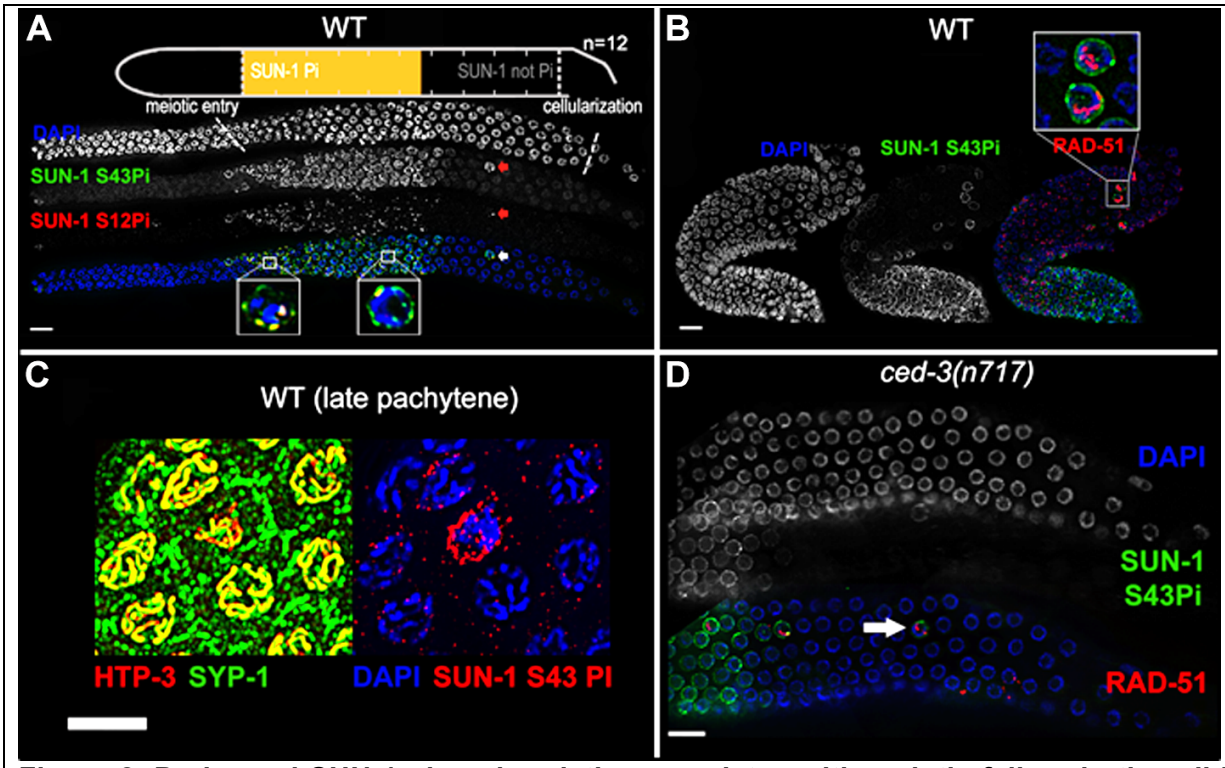

Figure 2. Prolonged SUN-1 phosphorylation correlates with meiotic failure in the wild type. (A) Wild-type (WT) hermaphrodite gonad stained with DAPI (top and blue in merge), anti-SUN-1 S43Pi (middle and green in merge), and anti-SUN-1 S12Pi (bottom and red in merge). Arrow highlights a nucleus in mid/late pachytene zone with clustered chromatin and phosphorylated SUN-1. Magnifications at the bottom of representative TZ or early pachytene nuclei to highlight differences in SUN-1 phosphorylation patterns. Schematics on top delineate quantifications of nuclei with and without phosphorylation of SUN-1 (S8, S12, S24, and S43) in the meiotic part of the gonad (quantified from meiotic prophase entry to beginning of cellularization/diplotene in WT, marked with dotted lines in DAPI channels). Orange represents cell rows with ≥50% of nuclei with SUN-1 phosphorylation. *n*, number of gonads scored for each genotype. Scale bar, 10 μm. (B) Wild-type hermaphrodite gonad stained with DAPI (left and blue in merge), anti-SUN-1 S43Pi (middle and green in merge), and anti-RAD-51 (red in merge). Box, upper right: magnification of representative nuclei in late pachytene with clustered chromatin, phosphorylated SUN-1, and numerous RAD-51signals. Red channel boosted in merge picture to better visualize RAD-51 foci in all nuclei. Scale bar, 10 μm. (C) Mid/late pachytene nuclei of a wild-type hermaphrodite gonad stained with anti-SYP-1 (left, green), anti-HTP-3 (left, red), anti-SUN1 S43Pi (right, red), and DAPI (right, blue). Nucleus in the middle with SUN1 phosphorylation has clustered chromatin and partly unsynapsed chromatin, in contrast to the surrounding nuclei with pachytene characteristics. Scale bar, 5 μm. (D) Nuclei with high numbers of RAD-51 foci, phosphorylated SUN-1, and clustered chromatin are also present in mid/late pachytene in apoptosis-deficient mutants. *ced-3(n717)* mutant hermaphrodite gonad stained with DAPI (top, blue in merged), anti-SUN-1 S43Pi (middle, green in merged), and anti-RAD-51 (bottom, red in merged). Arrow indicates nucleus in late pachytene zone with clustered chromatin, phosphorylated SUN-1, and abundant RAD-51 signal. Scale bar, 10 μm.

These occasional SUN-1 phosphorylation-positive nuclei seemed to be nuclei that were arrested in their meiotic progression due to synaptic or recombination failures.

This was described previously only for synapsis mutants in *C. elegans* (MacQueen, Colaiacovo et al. 2002). To gain further support for this hypothesis, we tested for the presence of phosphorylated CHK-1, an indicator of checkpoint activation as described by Jaramillo-Lambert et al. (Jaramillo-Lambert, Harigaya et al. 2010). The stray leptotene/zygotene-characteristic nuclei in mid/late pachytene displayed the highest levels of CHK-1 phosphorylation in the gonad (Figure 3A, WT panel). We therefore hypothesize that SUN-1 phosphorylation, aggregate persistence, and associated chromosome mobility is sustained in inappropriate late stages in response to the presence of unfinished meiotic tasks.

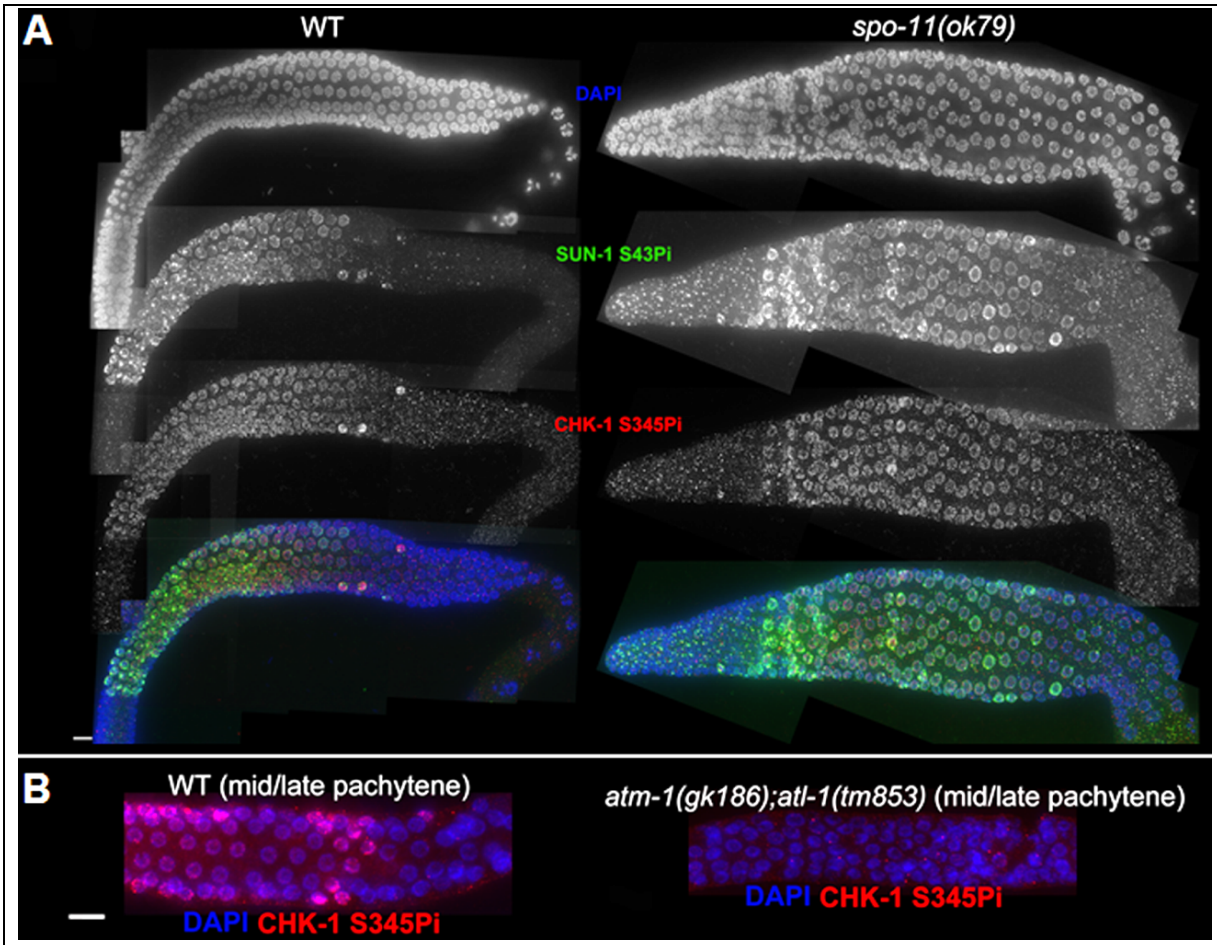

Figure 3. CHK-1 phosphorylation correlates with SUN-1 phosphorylation. (A) SUN-1 phosphorylation correlates with phosphorylated CHK-1 in wild type and mutants. WT (left) and *spo-11(ok79)* mutant (right) hermaphrodite gonad stained with DAPI (top, blue in merged), anti-SUN-1 S43Pi (middle, green in merged), and anti-CHK-1 S345Pi (bottom, red in merged). (B) CHK-1 phosphorylation depends on ATM/ATL. WT (top) and *atm-1(gk186); atl-1(tm853)* mid/late pachytene section; DAPI (blue) and antiCHK-1 S345Pi (red). Scale bars, 10 μm.

Phosphorylated CHK-1 signals overlapped strikingly with phosphorylated SUN-1 from meiotic entry onwards (Figure 3A). The signal intensity we observed was stronger than described previously (Jaramillo-Lambert, Harigaya et al. 2010). CHK-1 is phosphorylated and thereby activated by the damage signal kinases ATM and ATR (*atl-1* in worms) (Zhao and Piwnica-Worms 2001). Consistently, *atm-1; atl-1* double mutants were devoid of phosphorylated CHK-1 signals (Figure 3B). Because SUN-1 phosphorylation still occurred in *atm-1*; *atl-1* (Penkner, Fridkin et al. 2009), we reasoned that signals from meiotic damage must be transmitted through multiple parallel pathways to CHK-1, CHK-2 and SUN-1.

Chapter 2.3 Synaptic and recombination failure independently prolong phosphorylation of SUN-1

To understand the nature of the "meiotic failures" leading to prolonged SUN-1 phosphorylation in the stray leptotene/zygotene-like nuclei late in the gonad, I compared SUN-1 phosphorylation, SUN-1 aggregate persistence, and chromatin morphology between wild-type and mutant worms that were blocked in different steps of meiotic recombination.

I defined and measured the meiotic region of the germline between meiotic entry (marked by chromatin clustering) and diplotene (marked by cellularization of the oocytes; dotted lines in Figure 2A and Figure 4A&B). In the wild type, the distal 56.3 ± 3.8% of the meiotic region was populated by TZ or early pachytene nuclei displaying fully phosphorylated SUN-1 (S8, S12, S24, and S43), one or more SUN-1 aggregates, and clustered chromatin. The proximal 43.8 ± 3.8% of the gonad showed mainly mid/late pachytene nuclei without SUN-1 phosphorylation or aggregates (Figure 2A and Table 1).

Genotype	% of cell rows with SUN-1 aggregates (normalized to gonad length)	*p* values (wild type as reference)	*n*
WT	56.25 ± 3.8	—	12
syp-2(ok307)	85 ± 4.8	9.45E-15	14
rad-51(ok2218)	82.2 ± 6.1	3.55E-11	11
spo-11(ok79)	77.5 ± 5.6	4.75E-10	11
spo-11(ok79); syp-2(ok307)	87.3 ± 4.7	4.75E-14	11
WT 2 h post-70 Gy	57.7 ± 4.1	0.4	9
WT 8 h post-70 Gy	65.6 ± 5.3	1.46E-5	9
WT 24–27 h post-70 Gy	78.3 ± 6.6	8.54E-09	9

Table 1. Length of SUN-1 phosphorylation in wild-type and mutant backgrounds. Dissected gonads were measured from meiotic entry (TZ) to beginning of cellularization. Relative percentage of cell rows with SUN-1 phosphorylation was assessed and normalized to the length of the meiotic gonad from meiotic entry to cellularization. When >50% of nuclei in a cell row were phosphorylated on SUN-1, it was counted as phosphorylated. Variations correspond to the standard deviation. *p* values indicate comparison of percentage of cell rows with SUN-1 phosphorylation between wild type and the respective mutant in a two-tailed *t*-test. *n,* number of hermaphrodites scored.

I first examined the effect of loss of synapsis on SUN-1 phosphorylation. *syp-2* mutants are unable to form an SC due to loss of the central element component. In *syp-2* mutants, repair of DSBs is strongly delayed and never gives rise to a crossover. Leptotene/zygotene-like clustered chromatin persists (Colaiacovo, MacQueen et al. 2003). Both SUN-1 aggregates (surrounding autosomes and the X chromosome) and phosphorylation persisted until late in the gonad in *syp-2(ok307)* mutants and comprised 85 ± 4.8% of the "meiotic gonad" (Figure 4A, Table 1). These features of a progression delay were not abrogated in *syp-2; spo-11* double mutants, which do not form meiotic DSBs (Table 1). This result shows that synapsis defects are sufficient to prolong early prophase SUN-1 phosphorylation and other leptotene/zygotene-like characteristics.

To investigate whether unrepaired DSBs, independent of synaptic failures, can also trigger prolonged SUN-1 phosphorylation, I examined *rad-51(ok2281)* mutants. In this background, the SC assembles normally, but unrepaired DSBs persist (Rinaldo, Bazzicalupo et al. 2002; Alpi, Pasierbek et al. 2003). In *rad-51(ok2218)* germlines, the SUN-1 aggregates that colocalized with autosomal pairing centers disappeared with wild-type kinetics upon exit from the TZ. In contrast, the zone of nuclei showing one SUN-1 aggregate colocalizing with the X-chromosomal pairing center (Figure 4C) was prolonged over almost the entire meiotic gonad (Figure 4B and Table 1). Furthermore, early pachytene-like chromatin clustering persisted in *rad-51(ok2218)* germlines (Figure 4B&C).

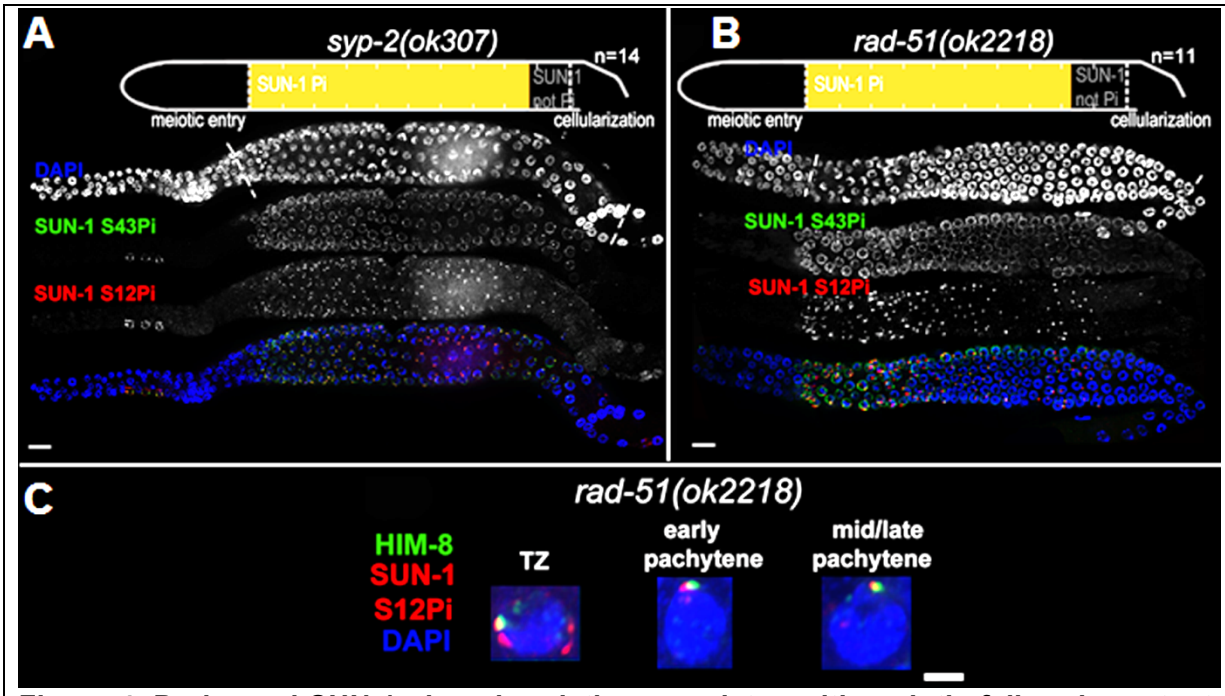

Figure 4. Prolonged SUN-1 phosphorylation correlates with meiotic failure in mutants situation. (A and B) *syp-2(ok307)* (A) and *rad-51(ok2218)* (B) mutant hermaphrodite gonad stained with DAPI (top and blue in merge), anti-SUN-1 S43Pi (middle and green in merge), and anti-SUN-1 S12Pi (bottom and red in merge). Scale bars, 2 μm. (C) Representative nuclei from TZ (left) early pachytene (middle) and mid/late pachytene (right) in *rad-51(ok2218)*. SUN-1 aggregates phosphorylated on S12 (red) colocalize with the HIM-8 signals (green) in all three zones. Scale bars, 2 μm.

Chapter 2.4 SUN-1 cannot be rephosphorylated in pachytene

Since the presence of unrepaired DSBs in *rad-51* and *syp-2* mutants resulted in persistent SUN-1 phosphomodifications, I tested whether the zone in the gonad that displayed SUN-1 phosphorylation and aggregate(s) could be prolonged by introduction of excess exogenous DSBs. In wild-type gonads subjected to a high dosage of ionizing radiation (70 Gy), the zone of nuclei with SUN-1 phosphorylation was not prolonged 20–180 minutes post-irradiation (Figure 5A and Table1). When gonads were dissected 8 h post-irradiation, the zone of nuclei with phosphorylated SUN-1 was prolonged to 65.6 ± 5.3% (compare to the nonirradated reference, 56.3 ± 3.8%; Table 1). Finally, gonads dissected 27 h post-irradiation revealed nuclei with clustered chromatin and phosphorylated and aggregated SUN-1 throughout 78.3 ± 6.6% of the meiotic gonad (Figure 5B and Table 1). Also at 27 h post-irradiation, there was a strong correlation between SUN-1 phosphorylation and abundant RAD-51 signals late in the gonad; the few nuclei without phosphorylation signals also lacked detectable RAD-51 (Figure 5C, arrowheads). Cells migrate with an approximate speed of one cell row per hour (Crittenden, Leonhard et al. 2006); introduction of DNA lesions in TZ/early pachytene nuclei appears to have led to their inability to exit the stage of SUN-1 phosphorylation and chromatin clusters, despite their migration through the gonad. In contrast, when DSBs were introduced in mid/late pachytene nuclei, SUN-1 was not rephosphorylated and TZ/early pachytene characteristics could not be reestablished.

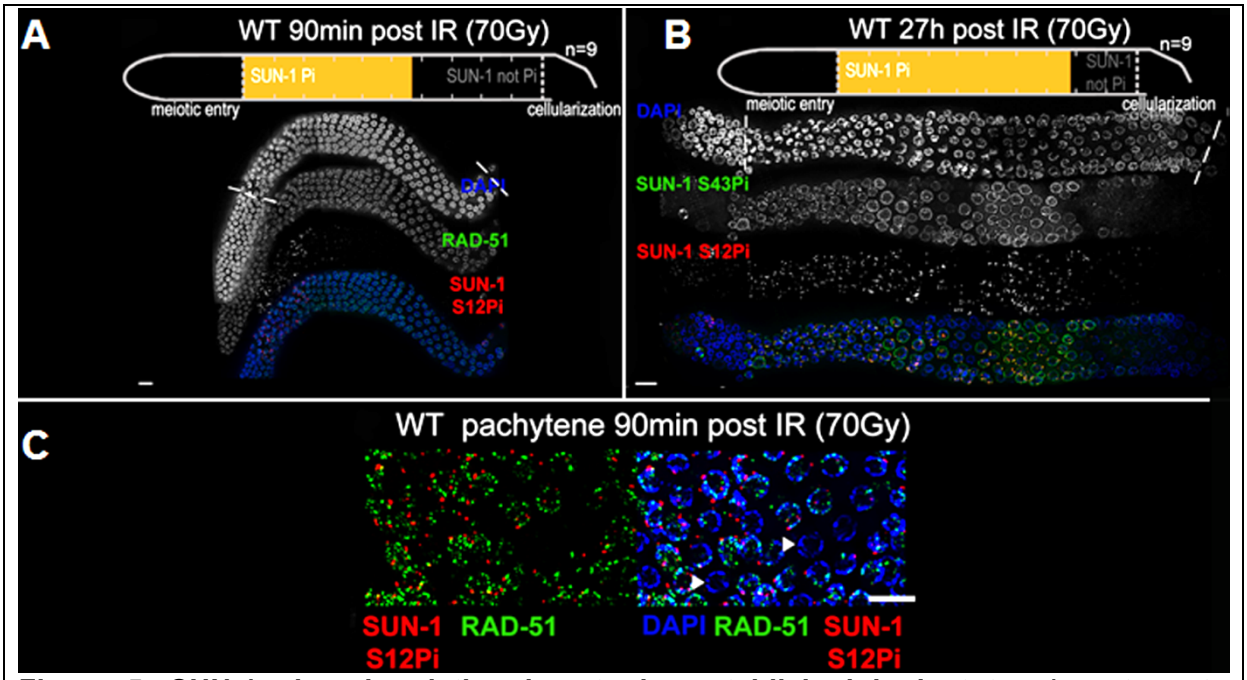

Figure 5. SUN-1 phosphorylation has to be established in leptotene/zygotene to persist late in the gonad. (A) Wild-type hermaphrodite gonad dissected 90 min after 90 Gy gamma irradiation stained with DAPI (top and blue in merge), anti-RAD-51 (middle and green in merge), and anti-SUN-1 S12Pi (bottom and red in merge). (B) Wild-type hermaphrodite gonad dissected 27 h after 70 Gy gamma irradiation; anti-SUN-1 S12Pi (red), anti-SUN-1 S43Pi (green), and DAPI (blue). (C) Irradiation-induced damage correlates with persistent SUN-1 phosphorylation. Pachytene WT hermaphrodite gonad dissected 27 h after 70 Gy gamma irradiation; anti-SUN-1 S12Pi (red), anti-RAD-51 (green), and DAPI (blue, right). Cells devoid of RAD-51 signal are also devoid of SUN-1 S12Pi signal (arrowheads). Scale bars, 10 μm.

Chapter 2.5 A recombination intermediate is required for dephosphorylation of SUN-1 in late pachytene

Pairing and formation of the SC between homologous chromosomes occurs independent of SPO-11-generated meiotic DSBs in *C. elegans* (Dernburg, McDonald et al. 1998). Surprisingly, I observed that *spo-11(ok79)* mutants with fully elongated SCs and no DSBs showed an extended zone with phosphorylated SUN-1 compared to wild-type germlines (Figure 6 and Table 1). In addition, phosphorylated CHK-1 was detectable longer in *spo-11(ok79)* than in wild-type gonads, and the phosphorylated CHK-1 signal overlapped with phosphorylated SUN-1 (Figure 3A). Overall, however, the phosphorylated CHK-1 signals appeared weaker in *spo-11(ok79)* than in wild-type germlines. By subjecting *spo-11(ok79*) mutants to low doses of ionizing radiation (7.5 Gy), the zone with phosphorylated nuclei could be reduced to wild-type length; only one-third of the nuclei were phosphorylated and two-thirds were nonphosphorylated from mid-pachytene onwards (Figure 6). In contrast, in unirradiated *spo-11* control animals, SUN-1 was phosphorylated in almost all nuclei until cellularization (Figure 6). We chose this irradiation dosage because it was too low to generate a massive damage response. Nevertheless, the dosage was high enough to generate sufficient DSBs as substrates for crossover recombination, since 24 h after 7.5 Gy of ionizing radiation, bivalent formation was fully restored in *spo-11(ok79)* mutants to wild-type levels (DAPI signals in diakinesis: wild type/N2: 5.9, *n* = 18; *spo-11(ok79):* 11.6, *n* = 17; and *spo-11(ok79)* irradiated with 7.5 Gy: 6.0, *n* = 21).

Remarkably, even in the absence of DSBs, SUN-1 phosphorylation paralleled by CHK-1 activation was not only initiated but also prolonged. The persistence of nuclei in an early pachytene-like stage could be abrogated by artificially generating a substrate for crossover recombination. Therefore, a yet-unidentified crossover intermediate is required to terminate the signaling that leads to prolongation of early pachytene characteristics, including SUN-1 phosphorylation.

These results collectively suggest that prolonged phosphorylation of SUN-1, the presence of SUN-1 aggregates, and chromosome mobility (leading to chromatin clustering) correlate with a broad range of unfinished meiotic tasks. First, full synapsis and repair of DSBs were required for SUN-1 dephosphorylation in mid-pachytene. Second, the establishment of a crossover or crossover intermediate was necessary to exit from the early pachytene stage in which phosphorylated SUN-1

was observed (see Discussion). Therefore, SUN-1 phosphorylation could be a component of a meiotic surveillance system that monitors the progression or completion of these meiotic tasks.

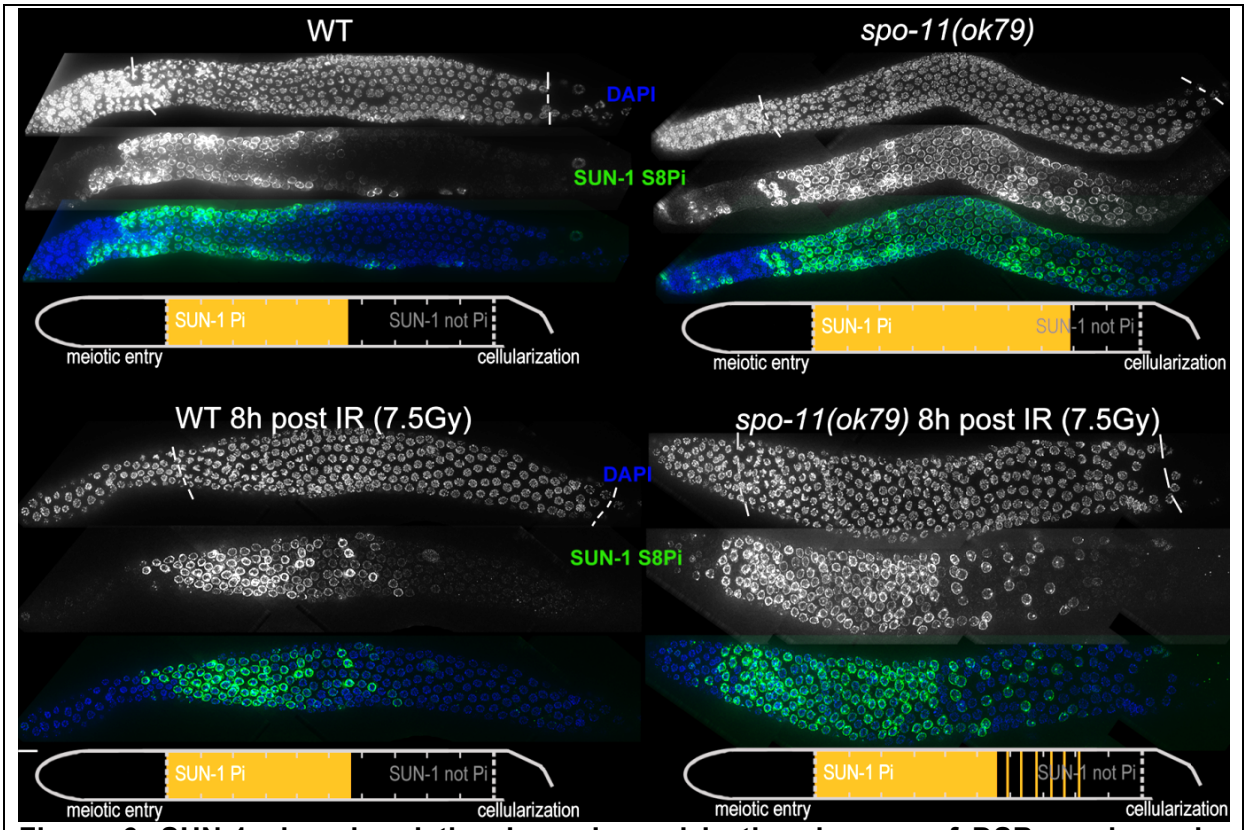

Figure 6. SUN-1 phosphorylation is prolonged in the absence of DSBs and can be decreased to wild-type length by low-dosage irradiation. WT (left) and *spo-11(ok79)* (right) hermaphrodite gonad, not irradiated (top) or irradiated with 7.5 Gy (bottom) dissected 8 h post-irradiation and stained with DAPI (top, blue in merge) and anti-SUN-1 S8Pi (bottom, green in merge). Schematics on the bottom of each gonad represent nuclei with and without phosphorylation of SUN-1 (S8, S12, S24, and S43) in the meiotic part of the gonad (from meiotic prophase entry to beginning of cellularization/diplotene in WT, marked with dotted lines in DAPI channels). Orange represents cell rows with ≥50% of nuclei with SUN-1 phosphorylation. Scale bars, 10 µm.

Chapter 2.6 Analysis of SUN-1 phosphosite mutants in meiosis

Given the broad range of unfinished meiotic tasks SUN-1 phosphorylation correlates with, we wanted to learn more about the role of SUN-1 phosphorylation in the fulfillment of these meiotic tasks. For this purpose we wished to extend our SUN-1 phosphosite mutant analysis. For the previous studies (Penkner, Fridkin et al. 2009; Baudrimont, Penkner et al. 2010) we had to rely on transgenic lines produced by random genomic integration triggered by biolistic transformation. These lines were tedious to produce. Additionally the biolistic transformation methods yielded in multiple copy integration or high copy extra-chromosomal arrays. These multi copy arrays of germline expressed genes can lead to silencing of the corresponding endogenous gene in the gonad (Dernburg, Zalevsky et al. 2000). This silencing can be worsened or weakened over generations and revered by loss of the high copy array. This process is called co-suppression and shares the same enzymatic machinery as RNA inference mediated gene silencing processes (Ketting and Plasterk 2000). It is speculated that this process protects the organism from genomic intruders (e.g.: RNA based viruses and transposons) and ensure genomic integrity.
For this reasons we made use of the more recently developed MosSCI system, which allows integration of a transgene at a defined locus in the genome as a single copy (Frokjaer-Jensen, Davis et al. 2008). We generated five different mutant transgenic *sun-1* lines, all C-terminally tagged with GFP and crossed them into the *sun-1(ok1282)* deletion background. The wild type control (referred to as *sun-1(wt)*) was compared to two different glutamic acid substitution lines, referred to as *sun-1(S12E)* and *sun-1(6E)*, in which all six serines doubtlessly identified as target sites were exchanged to glutamic acid (mass spec analysis could not differentiate between S35 and T36). In addition the wild-type control was compared to two non-phosphorylatable lines (referred to as *sun-1(S12A)* and *sun-1(allA)*, in which all residues found to be phosphorylated, including T36, were replaced by alanine). Subjecting this latter line to mass spectrometry analysis did not detect residual SUN-1 phospho-signals (data not shown; experiments performed by Sonja Frosch).
Mutation of specific residues to alanine generated nonphosphorylatable mutants. Mutations to glutamic acid attempted to mimic constitutively phosphorylated forms of SUN-1. When tested for embryonic viability and occurrence of males due to X-

chromosomal nondisjunction, all *sun-1* phosphosite substitution lines exhibited no or only very subtle defects under standard laboratory conditions (Table 2)

.

	Brood size	Hatch rate (%)	Males (%)	*n*
sun-1(wt)	211.2 ± 24.9	99.2 ± 0.8	0.04 ± 0.12	15
sun-1(S12E)	187.6 ± 35.4	94.1 ± 9.8	0.23 ± 0.24	15
sun-1(6E)	134.3 ± 54.0*	91.5 ± 4.1*	0.33 ± 0.49	15
sun-1(S12A)	245.2 ± 34.9*	98.0 ± 1.6	0.12 ± 0.16	15
sun-1(allA)	207.4 ± 42.7	97.4 ± 2.5	0.25 ± 0.16	15

Table 2. Brood size, hatch rate, and X chromosome nondisjunction of *sun-1* phosphosite mutants. **p* < 0.001 between wild type and the respective mutant in two-tailed *t*-test. Variations correspond to the standard deviation. Data were assessed over the complete self-fertile period of hermaphrodites at 20°C. *n*, number of hermaphrodites scored.

We next asked whether SUN-1 phosphorylation was required to induce movement-competent aggregates at meiotic entry. All *sun-1* phosphosite substitution lines displayed chromatin clustering and were able to form SUN-1 aggregates (data not shown). Moreover, in the completely nonphosphorylatable mutant *sun-1(allA),* SUN-1 aggregate formation was not abrogated. Nevertheless, SUN-1 aggregates in a *sun-1(allA)* background were visibly smaller, and less SUN-1 protein was organized in movement-competent aggregates compared to the wild type (Figure 7A). However, *in vivo* time-lapse imaging of *sun-1(allA)* aggregates showed that they remained mobile and had wild-type movement characteristics (similar velocities in the TZ, movement along similar distances, and the ability to fuse, coalesce, and separate, Figure 7B). These aggregates also colocalized with ZIMs, as seen in the wild type (data not shown).

To address the question of whether SUN-1 phosphorylation influenced meiotic progression, I measured the duration of leptotene/zygotene (TZ), early pachytene, and mid/late pachytene in the different *sun-1* phosphosite mutants. The durations of these three meiotic stages were measured by regarding SUN-1 aggregates and chromatin clustering as a read-out for chromosome movement (see Material and Methods and Figure 7C). In the wild-type reference, the *sun-1(wt)*-expressing transgenic line, the TZ length comprised 21.4 ± 5.0% of the meiotic part of the gonad. The TZ combined with the early pachytene zone was equally as long as the zone that comprised mainly nuclei in the mid/late pachytene stage (Figure 7D, exact quantifications in Table 3). Germlines expressing *sun-1* phosphosite mutants

(glutamic acid and alanine substitutions) exhibited only moderately altered ratios between the TZ and early pachytene. Mutants expressing the multiple glutamic acid–substitution line *sun-1(6E),* which mimics constitutive SUN-1 phosphorylation, showed the most pronounced prolongation of the TZ (Figure 7D and Table 3). Thus, glutamic acid substitutions on SUN-1 elicited only a mild meiotic delay at the stage of chromosome movement. These data were surprising, since we previously observed stronger phenotypes in *sun-1* phosphosite substitution lines (Penkner, Fridkin et al. 2009; Baudrimont, Penkner et al. 2010) generated by particle bombardment; the phenotypes observed in these lines were mainly caused by *sun-1* dosage reduction due to limitations of the bombardment transformation technique (see Discussion and Figure 15).

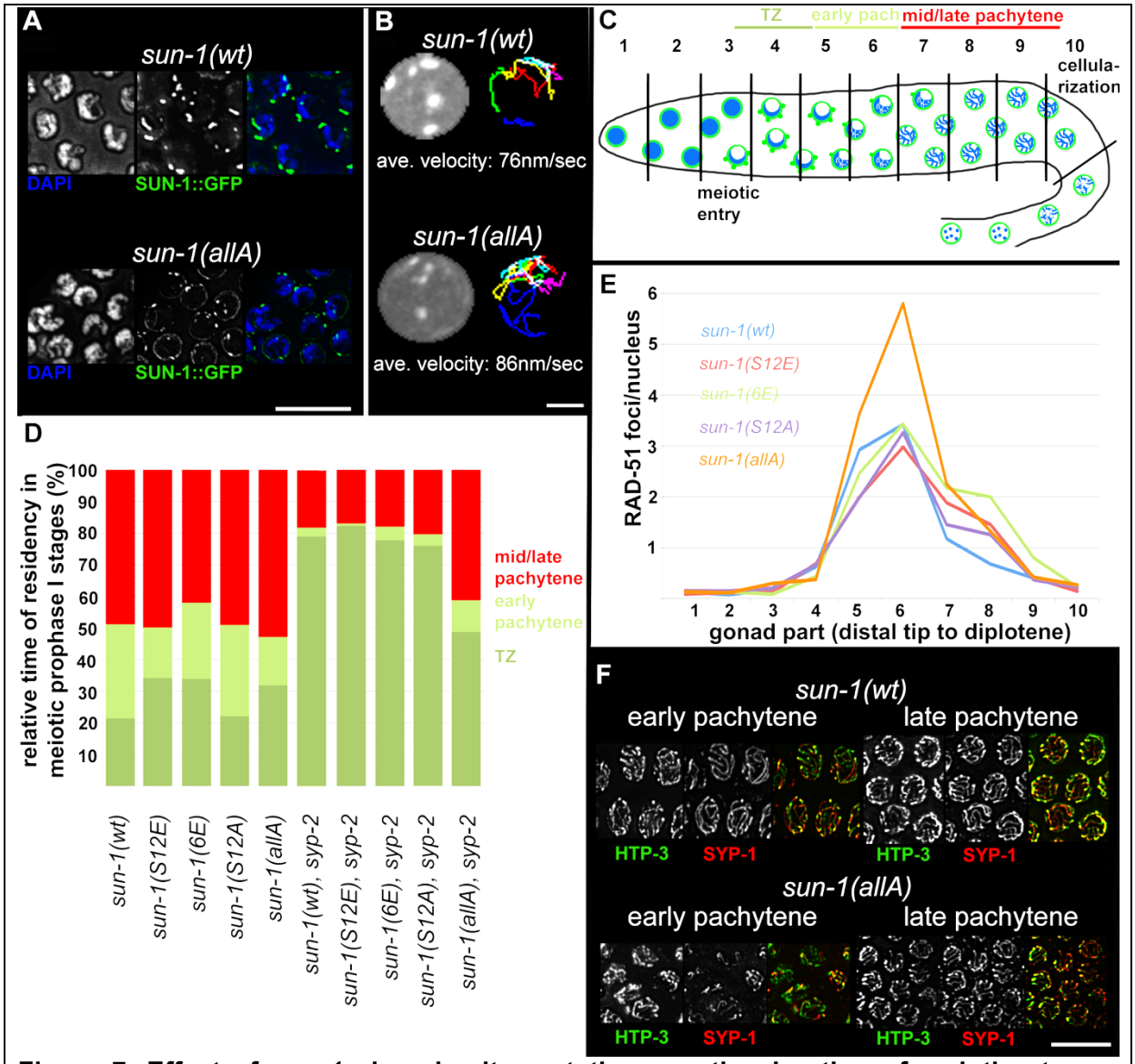

Figure 7. Effect of *sun-1* phosphosite mutations on the duration of meiotic stages, DSB turnover, SUN-1 aggregates, chromosome movement, and synapsis. (A) TZ nuclei of *sun-1(wt); sun-1(ok1282)* (top), and *sun-1(allA); sun-1(ok1282)* (bottom) hermaphrodite gonads stained with DAPI (left; blue in merged picture) and anti-GFP (middle; green in merged picture). Scale bars, 10 µm. (B) First frame of *in vivo* time-lapse GFP-recorded TZ nuclei of *sun-1(wt); sun-1(ok1282)* (top, left) and *sun-1(allA); sun-1(ok1282)* (bottom, left) hermaphrodite gonads. Displacement tracks of SUN-1 aggregates represent 2D plotted chromosome end movements over 3 min (right). Average speed of SUN-1 aggregates in TZ (*n* = 9 nuclei, followed over 3 mins). Scale bar, 2 µm. (C) Schematic of a wild-type hermaphrodite gonad with nuclei in the corresponding zones, as used in the quantifications in Figure 3D: chromatin (blue) and SUN-1 morphology (green). Gonad is subdivided into ten zones, as used for the RAD-51 foci quantification in Figure 3E. Meiotic entry and beginning of cellularization are indicated. (D) Representation of relative time of residency in different meiotic stages, as assessed by presence of SUN-1 aggregates in different mutant backgrounds, normalized to the length of the gonad (from meiotic entry [0%] to start of meiocyte cellularization at diplotene [100%]). Nuclei were sorted into three categories: “TZ” (dark green, more than one SUN-1 aggregate), “early pachytene” (light green, one SUN-1 aggregate), and “late pachytene” (red, no SUN-1 aggregate). Categories were assigned once ≥50% of nuclei in a cell row fulfilled one of these criteria. At least eight gonads were counted

per genotype. (E) Average numbers of RAD-51 foci per nucleus in the hermaphrodite gonad of different *sun-1* phosphosite mutants. Gonads were divided into ten zones, as schematically indicated in (B). Three gonads per genotype were counted. (F) Nuclei from early and late pachytene zones of *sun-1(wt); sun-1(ok1282)* (top) and *sun-1(allA); sun-1(ok1282)* (bottom) hermaphrodite gonads stained with anti-HTP-3 (left, green in merged) and anti-SPY-1 (middle, red in merged). Scale bars, 10 µm.

	TZ (%)	Aggregate zone (%) (TZ + early pachytene)	Zone w/o aggregates (%) (mid/late pachytene)	*n*
sun-1(wt)	21.4 ± 5.0	51.1 ± 6.4	48.9 ± 6.4	8
sun-1(S12E)	31.8 ± 4.0*	47.1 ± 4.1	52.9 ± 4.1	10
sun-1(6E)	33.9 ± 10.6*	58.0 ± 4.5	42.0 ± 4.5	8
sun-1(S12A)	22.0 ± 3.6	50.9 ± 6.1	49.1 ± 6.1	10
sun-1(allA)	34.2 ± 5.5*	50.1 ± 4.3	49.9 ± 4.3	8
syp-2; sun-1(wt)	79.1 ± 2.1	81.9 ± 3.8	18.1 ± 3.8	8
syp-2; sun-1(S12E)	82.3 ± 6.4	83.1 ± 4.8	16.9 ± 4.8	8
syp2; sun-1(6E)	77.7 ± 10.8	82.0 ± 2.9	18.0 ± 2.9	8
syp2; sun1(S12A)	76.0 ± 6.0	79.6 ± 6.1	20.4 ± 6.1	10
syp-2; sun-1(allA)	48.7 ± 5.3*	58.7 ± 5.9*	41.3 ± 5.9*	8

Table 3. Relative duration of leptotene/zygotene, early pachytene, and middle/late pachytene in *sun-1* phosphosite mutants during oogenesis. This table shows the quantifications of the data in Figure 7D. Relative duration of meiotic stages were assessed by quantifying cell rows in the meiotic part of the gonad according to the following criteria: more than one SUN-1 aggregate ("TZ"), one or more SUN-1 aggregates ("aggregate zone", TZ plus early pachytene), or no aggregates ("zone without aggregates"). When >50% of nuclei in a cell row met one of the three criteria, the cell row was scored as such. Percentages ± standard deviation shown represent numbers normalized to gonad length from meiotic entry to beginning of cellularization (diplotene stage in the wild type). *$p < 0.01$ between the reference lines *sun-1(wt)* and *syp-2; sun-1(wt)* and the respective mutant lines in two-tailed *t*-test. n, number of gonads counted.

Chapter 2.7 SUN-1 phosphorylation is required for wild-type kinetics of synaptonemal complex formation and genomic integrity under challenged conditions

Formation of the synaptonemal complex (unpublished data) and meiotic DSB repair kinetics, followed by RAD-51 foci quantification (Alpi, Pasierbek et al. 2003; Colaiacovo, MacQueen et al. 2003) (Figure 7E), were not substantially altered in the SUN-1 phopspho-site mutated lines compared to the wild type, except for one *sun-1* phosphosite mutant. In *sun-1(allA)*-expressing germlines, in which all of the phosphosites were replaced with unphosphorylatable alanine, full elongation of the SC was strongly delayed, but ultimately achieved, since all chromosomal axes colocalized with SYP-1 in late pachytene. In early pachytene, *sun-1(allA)* displayed strongly reduced synapsis (Figure 7F). This delay in SC formation may also explain the accumulation of RAD-51-marked recombination intermediates in the mid-pachytene region that we observed in *sun-1(allA)*-expressing germlines (Figure 7E). A delay in homologous pairing does not account for the delay in synapsis, since the kinetics of homologous pairing were not affected, as assessed by fluorescence in situ hybridization (FISH) (data not shown; the FISH analysis was performed by Cornelia Habacher).

Since SUN-1 phosphorylation was prolonged upon irradiation (Figure 3B&C), I tested whether offspring quality was impaired in *sun-1(allA)* mutants after exposure to 90 Gy of ionizing radiation (Figure 8A). *sun-1(allA)* mutants displayed decreased offspring viability after ionizing radiation compared to the wild type. Embryonic lethality in *sun-1(wt)* was most pronounced 0–24 h post-irradiation when the meiocytes giving rise to the dead embryos were in pachytene or later stages at the time of irradiation. By comparison, 24–48 h post-irradiation, the number of viable offspring was increased in the wild type. The meiocytes giving rise to these embryos were in the TZ or early pachytene stage at the time of irradiation. As shown above, these are the nuclei that were able to maintain SUN-1 phosphorylation in response to massive DNA damage while migrating down the gonadal tube (the rate of nuclei migrating through the gonadal tube is not altered dramatically by ionizing irradiation Table 4). In contrast, offspring quality was not increased at this later time point post-irradiation in *sun-1(allA)* mutants (Figure 8A). These results suggest that SUN-1 phosphorylation contributes to tolerance against ionizing radiation.

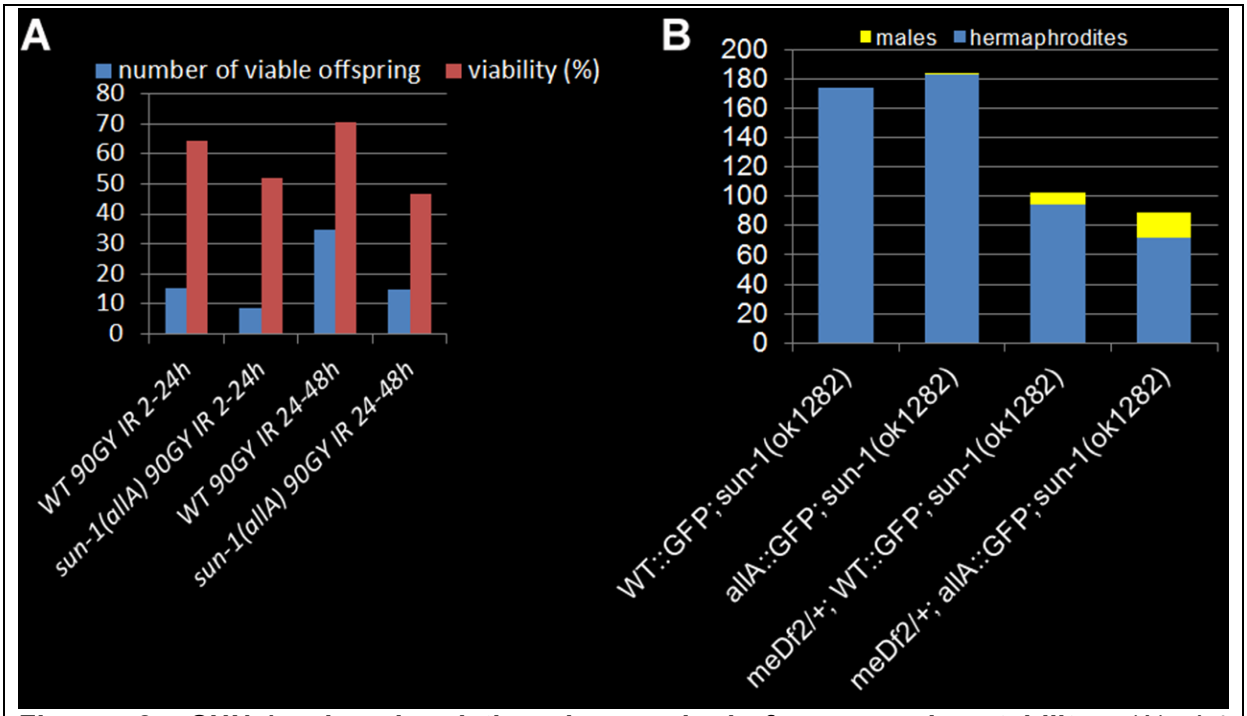

Figure 8. SUN-1 phosphorylation is required for genomic stability. (A) L4 hermaphrodites were irradiated (90 Gy), or not irradiated, and the viability and development of eggs between 2 and 48 h after irradiation was assessed at 20°C. Differences between *sun-1(wt)* and *sun-1(allA)* are significant in a two-tailed t-test ($p < 0.001$). (B) X chromosome non-disjunction of a heterozygous X-chromosomal pairing center deletion in *sun-1(wt)* and *sun-1(allA)* was assessed by quantifying male (X0) offspring (yellow) among the progeny from hermaphrodites over 3 days from L4 onwards (hermaphrodites (XX) are depicted as blue in the graph). ($p < 0.0001$ for average number of males in *meDf2/+*).

	eggs total	eggs/hour	n
irradiated	73.2±17.1	3.7±0.9	20
non-irradiated	56.6±15.7	2.8±0.8	20

Table 4. The progression rate through the gonadal tube is not altered dramatically by ionizing irradiation. L4 worms (*sun-1(wt)*) were selected and grown for 24 h at 20°C to adulthood. Worms were irradiated (50Gy) and allowed to lay eggs for 24 h. The number of eggs laid 4-24 h post irradiation was compared to non-irradiated control animals. Post irradiation fecundity drops only by 22,6% ($p = 0.0028$). n, hermaphrodites quantified. This slight reduction is not exclusively caused by a delay of meiocytes progressing through the gonadal tube. Apoptosis sets in 12 h after irradiation and reaches its peak 24 h post irradiation (Schumacher, Schertel et al. 2005). Therefore some of the reduction of eggs laid after irradiation is due to initiated apoptosis.

I also wanted to test how the non-phosphorylatable *sun-1* mutants behaved when synapsis was challenged. One of the genetically stable synapsis challenge backgrounds in *C. elegans* is a mutant that carries an X-chromosomal pairing center translocation. If this translocation, *meDf2*, is kept heterozygous, still a major fraction

of X chromosomes can undergo synapsis and crossovers can form (Bhalla and Dernburg 2005). This fraction of correctly segregated X chromosome is larger than expected from random segregation, even after the removal of the apoptotic machinery, which culls the compromised meiocytes in this situation (Bhalla and Dernburg 2005). *meDF2/+* leads to an arrest in leptotene/zygotene with phosphorylated SUN-1 (Lamelza and Bhalla 2012). To address whether SUN-1 phosphorylation contributes to the correction of synaptic mistakes, we analyzed the number of males that were produced by non-disjunction from *sun-1(wt)* and *sun-1(allA)* self-fertile hermaphrodites in the *meDf2* heterozygous background. SUN-1 phosphorylation was required to keep X-chromosomal non-disjunction at wild-type levels (Figure 8B). The strong drop in offspring number, also in *meDf2/+; sun-1(allA)*, indicate that SUN-1 phosphorylation is not required for asynapsis induced apoptosis (also see Table 5 in Chapter 2.10).

Overall, the *sun-1* phosphosite mutants displayed only subtle meiotic defects under standard laboratory growth conditions. Glutamic acid substitution attempting to mimic constitutive phosphorylation of SUN-1 was neither capable of delaying the onset of mid/late pachytene, nor was it capable of prolonging the persistence of SUN-1 aggregate(s) to an extent similar to that observed in meiotic mutants (synapsis- or recombination-defective mutants). Defects in SUN-1 aggregate morphology became apparent only when SUN-1 was rendered entirely unphosphorylatable. Strikingly, the ability of SUN-1 to undergo phosphomodification increased the tolerance for ionizing radiation (this was most effective for nuclei that were in TZ/early pachytene when exposed to the damage). Furthermore, phosphomodifications were required for SC formation with wild-type kinetics and also for correct disjunction under challenged conditions in leptotene/zygotene arrested nuclei.

Chapter 2.8 SUN-1 phosphorylation is required for aggregate persistence and chromosome mobility beyond the TZ

Given the fact that *sun-1(allA)* mutants showed a severe delay in SC completion, we expected a greater extension of TZ-like chromosome movement and clustered chromatin. However the delayed synapsis in *sun-1(allA)* prolonged the TZ characteristics only slightly. We therefore crossed the *sun-1(allA)* mutation into a synapsis mutant to assess whether the meiotic progression delay normally observed in the synapsis mutants was influenced by the SUN-1 phosphorylation status. In *sun-1(wt); syp-2(ok307)* mutant germlines, the TZ length comprised 79.1 ± 2.1% of the meiotic part of the gonad, and the mid/late pachytene zone was reduced to 18.1 ± 3.8%. By comparison, in wild-type worms, this region would account for 48.9 ± 6.4% of the meiotic gonad (Figure 7D and Table 3). I found that that *sun-1(allA)* expression in *syp-2* mutants restored the length of the shortened pachytene observed in *sun-1(wt); syp-2* mutants to 41.3 ± 5.9% of the meiotic gonad (Figure 7D and Table 3). SUN-1 aggregates dissolved prematurely and chromatin appeared to be relaxed earlier than in the *sun-1(wt); syp-2* reference strain (Figure 9). No other phosphosite mutant was able to reduce the TZ length in *syp-2* mutants (Figure 7D and Table 3).

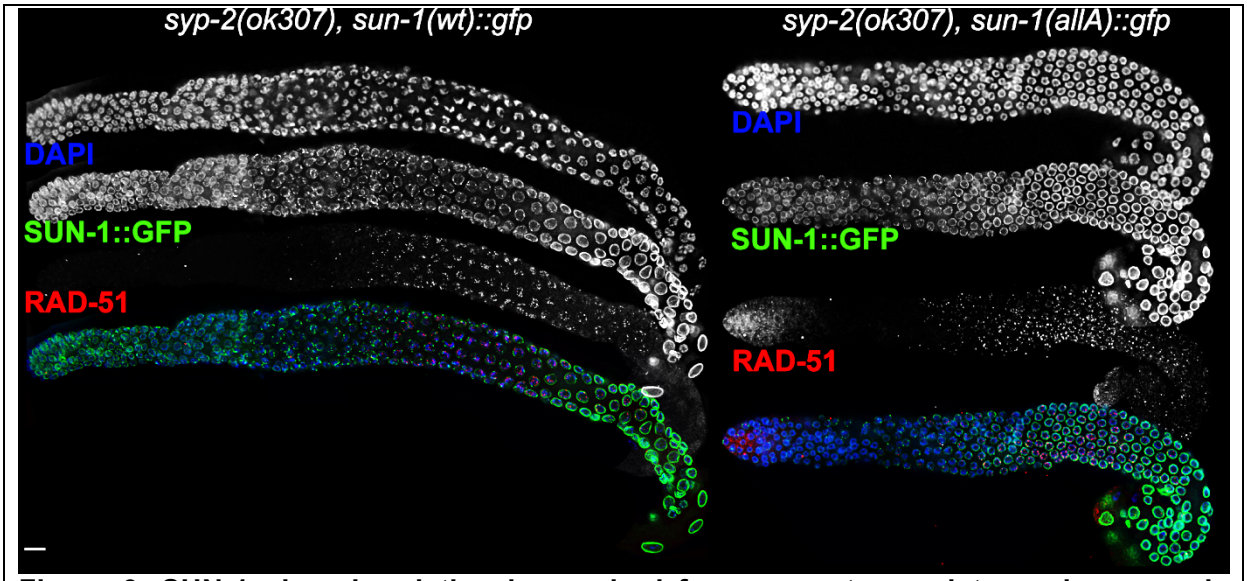

Figure 9. SUN-1 phosphorylation is required for aggregate persistence in synapsis deficient backgrounds, however RAD-51 foci persist. *sun-1(wt); sun-1(ok1282); syp-2(ok307)* (left) and *sun-1(allA); sun-1(ok1282); syp-2(ok307)* (right) hermaphrodite gonads stained with DAPI (top, blue in merge), anti-GFP (middle, green in merge), and anti-RAD-51 (bottom, red in merge). Scale bar, 10 µm.

DSB turnover, as judged by staining for RAD-51, did not differ between *syp-2; sun-1(wt)* and *syp-2* combined with any SUN-1 phosphosite mutant. RAD-51 foci accumulated in late pachytene and disappeared before the diakinesis stage (Figure 9). These results support the idea that the observed accumulation of RAD-51 foci in *sun-1(allA)* mutants (Figure 7E) was due to a delay in repair and not due to an increase in DSB formation. Most likely, this delay in repair is a consequence of the delayed SC formation in *sun-1(allA)* mutants (Figure 7F).

sun-1(allA) decreased the length of the zone displaying more than one SUN-1 aggregate in *syp*-2 mutants to 48.7 ± 5.3% of the meiotic gonad (Table 3). Chromatin also appeared to be more relaxed in early pachytene in *sun-1(allA) syp-2* mutants. *In vivo* time lapse imaging and 2D plotting of aggregate movement in *syp-2; sun-1(wt)* showed that over almost the entire gonad, aggregates displayed similar relative movement towards each other and similar numbers of splitting and fusion events (Figure 10). The movements of chromosome ends towards each other and splitting and fusion events were strongly reduced only in the last 3–5 cell rows, before the SUN-1 aggregates disappeared (the region where nuclei start to leave the syncytium). Long, directional displacement tracks were strongly diminished. Aggregates in this region of the *syp-2* gonad did not move over longer distances, but were rather pushed and pulled on the spot; aggregate velocity by itself was not reduced in these nuclei (Figure 10). In contrast, aggregate dynamics in *syp-2; sun-1(allA)* were markedly different from those in *syp-2; sun-1(wt)*. Most of the aggregates from nuclei in the region corresponding to pachytene displayed restricted movement. Splitting/fusion events and long displacement tracks were absent. The properties of movement resembled those of aggregates in *syp-2; sun-1(wt)* at the very end of the prolonged TZ (Figure 10). Only aggregates at the beginning of the meiotic gonad, corresponding to early TZ in the wild type, displayed the highly dynamic wild-type aggregate behavior, with characteristic long displacement tracks and splitting and fusion events (Figure 10). We therefore conclude that the SUN-1 phosphomodifications are required to keep chromosomes moving continuously until full synapsis is reached.

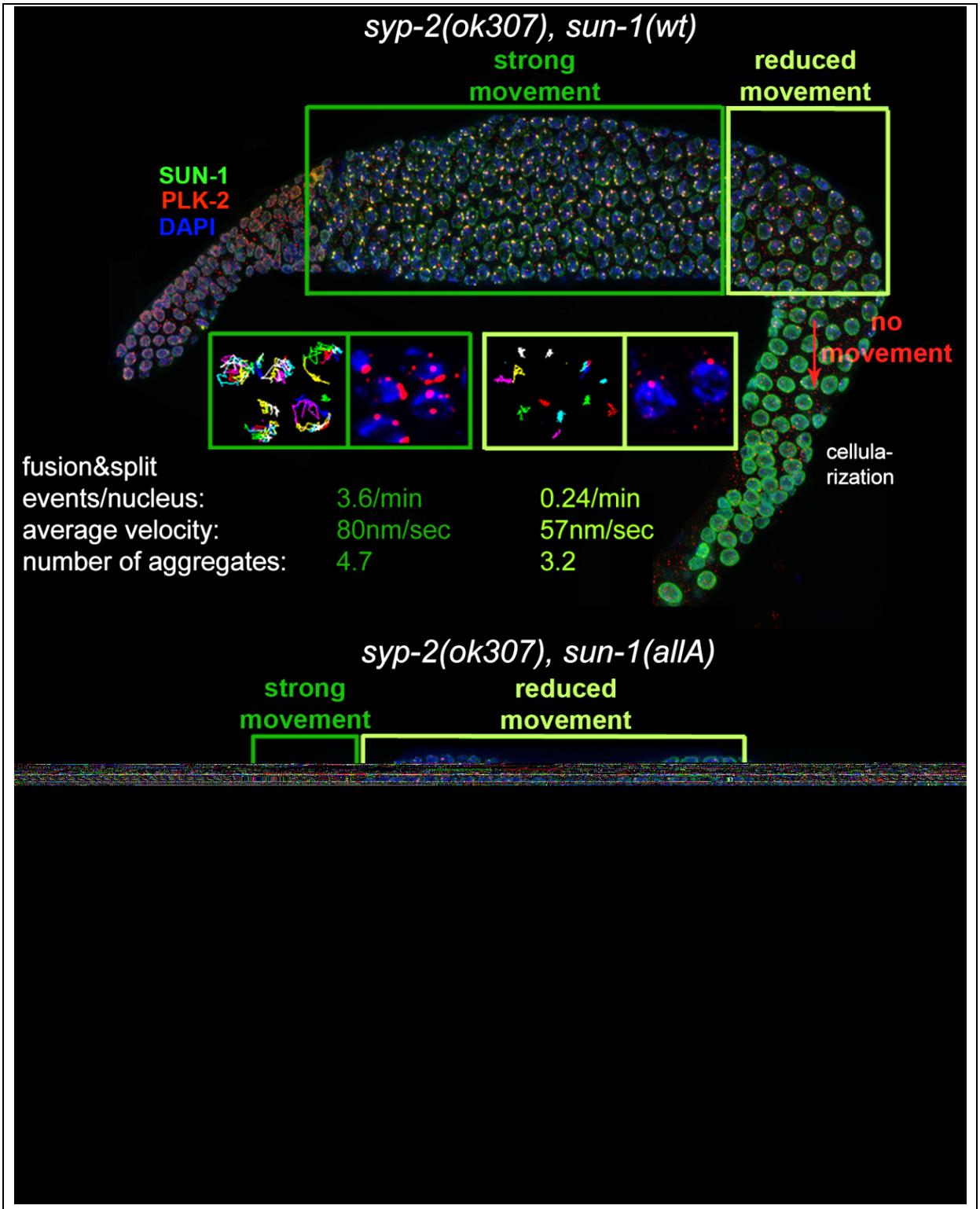

Figure 10. Effect of nonphosphorylatable SUN-1 on aggregate persistence, PLK-2 localization, and chromosome mobility beyond TZ. Hermaphrodite gonad of *sun-1(wt); sun-1(ok1282), syp-2(ok307)* (top) and *sun-1(allA); sun-1(ok1282); syp-2(ok307)* (bottom) stained with DAPI (blue), anti-GFP to highlight SUN-1 (green), and anti-PLK-2 (red). Dark green and light green frames highlight zones with distinct chromosome movement patterns: magnifications of nuclei in the corresponding zones below, showing displacement tracks of 2D plotted chromosome end movements over 3 min (left) and PLK-2 (red) and DAPI (blue). Bottom: average number of aggregates, aggregate velocity (in nm/sec), and fusion/split events (per nucleus/min) for nuclei from corresponding zones. Scale bar, 10 µm.

Chapter 2.9 SUN-1 phosphorylation and aggregate formation is dependent on Polo kinases, PLk-2 (and PLK-1)

Features of *sun-1(allA); syp-2* are to some extent analogous to the *plk-2(ok1936); syp-1* phenotype (Harper, Rillo et al. 2011), in which SUN-1 aggregates form and chromosomes initially move. Despite the synapsis deficiency in both *sun-1(allA); syp-2* and *plk-2(ok1936); syp-1* mutants, chromosome movement stops prematurely (Harper, Rillo et al. 2011). In co-submission with the study from the Dernburg lab (Harper, Rillo et al. 2011) we could show that PLK-2 and SUN-1 aggregates not only colocalize (Figure 1G&H and (Labella, Woglar et al. 2011)), but also that SUN-1 and PLK-2 can be found in a complex upon immunoprecipitation. I could demonstrate this by purifying SUN-1::GFP and detecting PLK-2 with this fraction. The control fraction of solely expressed GFP protein, driven by a pharyngeal mysin promoter in contrast did not co-purify PLK-2 (Figure 11 and (Labella, Woglar et al. 2011)).

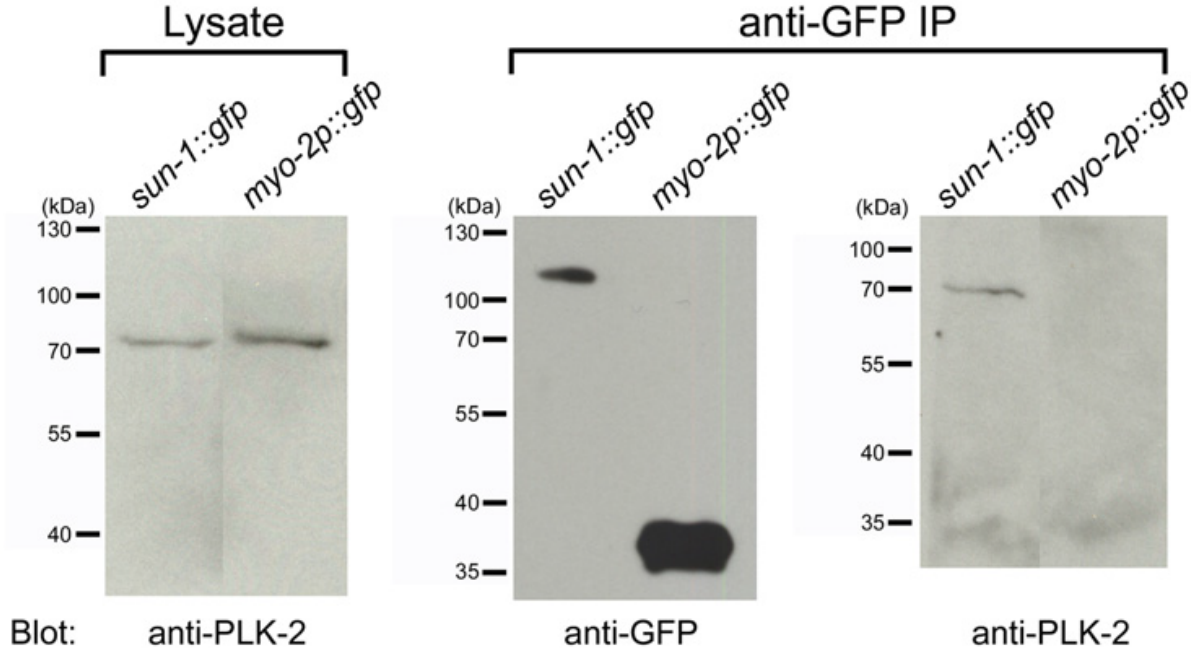

Figure 11. PLK-2 co-purifies with SUN-1. Western blot analysis of whole-worm extracts and pull-downs (IP) from *sun-1::gfp; sun-1(ok1282); spe-26(hc138); (sun-1::gfp)* and *sun-1(ok1282)/nT1(qIs51); (myo-2p::gfp)* strains. 15% of lysate input for the pull-down probed with anti-PLK-2 detects a band of the predicted molecular weight for PLK-2 (72.1 kDa). SUN-1::GFP and PLK-2 can be detected in anti-GFP immunoprecipitates probed with anti-GFP and anti-PLK-2, respectively. PLK-2 cannot be detected in anti-GFP immunoprecipitates from whole-worm lysates derived from the *qIs51*-bearing control strain expressing soluble GFP.

Nevertheless all SUN-1 phosphorylations and aggregate formation still occur in *plk-2(ok1936)* deletion mutants (Figure 12, only SUN-1 S12 phosphorylation is shown). Only when the homolog of PLK-2, PLK-1 is co-depleted in *plk-2(ok1936)* by *plk-1(RNAi),* SUN-1 aggregate formation and meiotic phosphorylation of S12 was strongly decreased or completely absence. Phosphorylation of other serines was not affected (data not shown). Therefore PLK-1 and PLK-2 can act redundantly to phosphorylate SUN-1S12 and to induce movement competent SUN-1 aggregates.

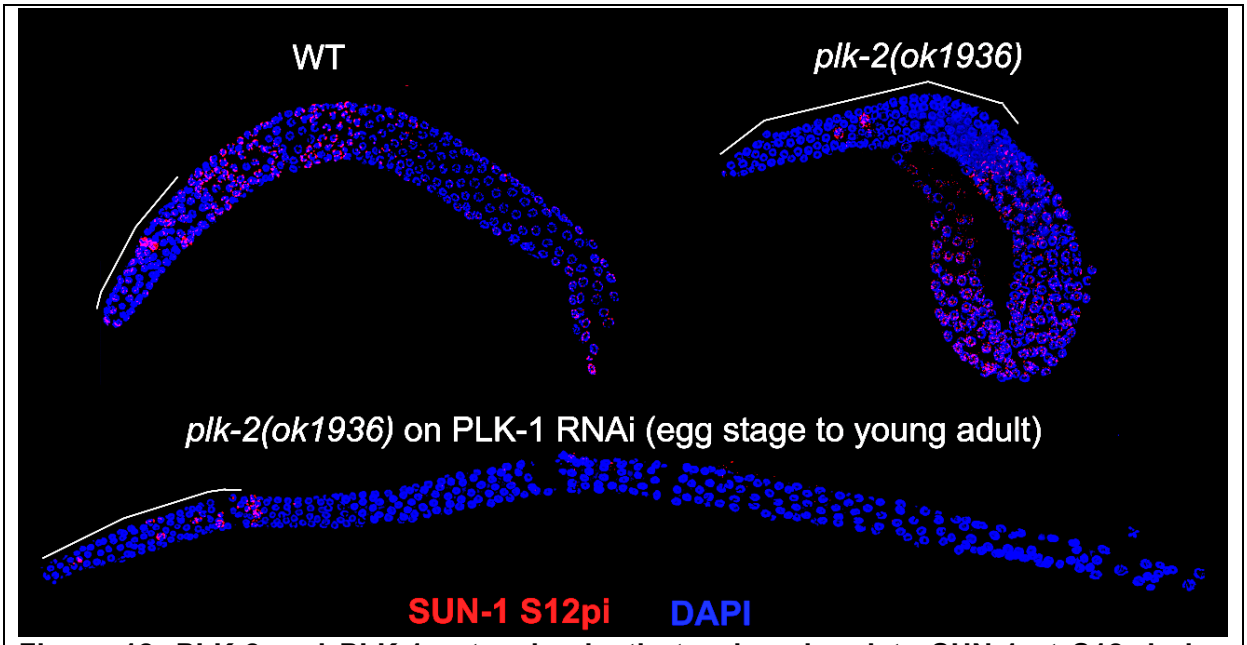

Figure 12. PLK-2 and PLK-1 act redundantly to phosphorylate SUN-1 at S12 during meiosis. WT (top left), *plk-2(ok1936)* (top right) and *plk-2(ok1936); plk-1(RNAi)* (bottom) hermaphrodite gonad stained with DAPI (blue) and anti-SUN-1 S12Pi (red). Meiotic phosphorylation of SUN-1 S12 is almost completely absent in *plk-2(ok1936); plk-1(RNAi).* The white line from the distal tip marks the mitotic zone of the gonad.

Nevertheless in the wild-type PLK-2 is probably doing this job alone. Sara Labella found that PLK-1 does not localize to chromosome ends in the presence of wild-type PLK-2. However in a *plk-2(ok1936)* deletion mutant she could detect PLK-1 on chromosome ends, where normally PLK-2 would be localized (Labella, Woglar et al. 2011). Further evidence that PLK-2 was required in the wild type for SUN-1 aggregate formation and phosphorylation on S12 was provided by a *plk-2* allele isolated by the Zetka lab.

plk-2(vv44) is a missense mutation resulting in a P197L amino acid exchange. P197 is a residue in the highly conserved activation loop of the kinase domain of PLK-2. *plk-2(vv44)* phenolcopies the co-depletion of PLK-1 and PLK-2 concerning absence

of SUN-1 aggregates and SUN-1 phosphorylation on S12. These features of *plk-2(vv4)* are not caused by a lack of recruitment of PLK-2(P197L) to chromosome ends, since PLK-2(P1977L) foci were detected normally upon entry into meiosis at the nuclear envelope. Also localization to pairing center proteins to the same sites is not affected in *plk-2(vv44)* (Labella, Woglar et al. 2011). Therefore we speculated, that *plk-2(vv44)* encoded for a kinase dead version of PLK-2 that would exclude the normally compensating PLK-1 protein from the respective targets.

To test for this idea I wanted to compare the kinase activity of PLK-2 and PLK-2(P197L). Therefore I expressed HA tagged PLK-2 and PLK-2(P197L) in *S. cerevisiae* and purified them with anti-HA beads (Figure 13A). The canonical substrate for Polo-kinases is α-casein (Golsteyn, Mundt et al. 1995), which is commercially available. The kinase activity of both PLK-2 version was tested on HA pull down extracts containing the kinases supplied with dephosphorylated α-casein in a kinase reaction buffer. In the control IP (the solely expressed HA tag) no phosphorylated casein was detectable (Figure 13B, middle lane), demonstrating that the HA purified fraction from yeast cells was not contaminated with endogenous kinases activity from yeast, active on α-casein. PLK-2 shows strong phosphorylation activity on α-casein (Figure 13B left lane). In comparison casein incubated with PLK-2(P197L) shows only faint signals on the autoradiograph plot (Figure 13B, right lane). Therefore PLK-2(P197L) represents a strongly kinase decreased, but not a completely kinase dead version of PLK-2 *in vitro*. This finding strongly supports the hypothesis, that *plk-2(vv44)* encodes for a version of PLK-2 that is not able to confer phosphorylation *in vivo* due to decreased kinase activity.

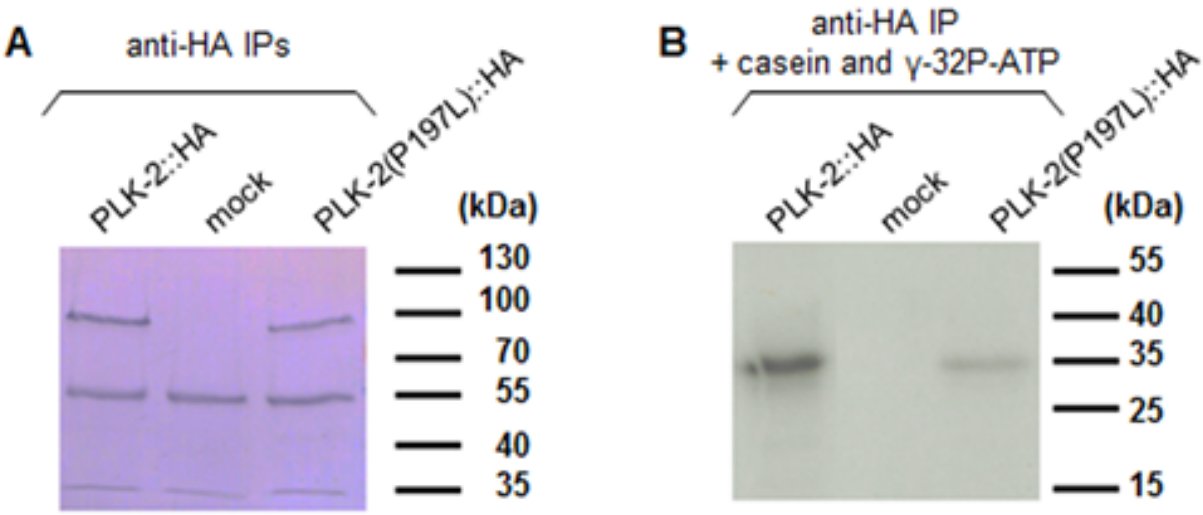

Figure 13. PLK-2(P197L) displays strongly reduced phosphorylation activity. (A) Western blot analysis of anti-HA pull-downs of budding yeast lysates expressing PLK-2::HA (left lane), empty vector (middle lane) and PLK-2(P197L) (right lane). At roughly 55 and 25 kDa the heavy and the light chain of the anti-HA antibody (used for the IP) shows a signal. (B) Autoradiography blot followed incubation of pull downs with 5 µg of dephosphorylated α-casein in a kinase reaction buffer supplied with γ-32p-ATP.

Chapter 2.10 SUN-1 phosphorylation is required for stable PLK-2 localization under challenged conditions

plk-2(ok1936) not only rescues the meiotic progression delay induced by *syp-1(me17)*, but also leads to suppression of asynapsis triggered apoptosis (Harper, Rillo et al. 2011). Since PLK-2 is required for SUN-1 S12 phosphorylation we wanted to know whether phosphorylation of SUN-1 is a mediator for synapsis-dependent apoptosis. Unlike the *plk-2* deletion, expression of *sun-1(allA)* was not able to reduce the synapsis checkpoint triggered elevated numbers of apoptotic corpses (visualized by SYTO 12 live staining) in *syp-2* mutants; therefore, SUN-1 is not the responsible target for *plk-2* with respect to apoptosis induction. Consistent with this observation, the number of apoptotic corpses did not increase in *sun-1(6E)* germlines mimicking constitutive phosphorylation (Table 5, counting of apoptotic corps was performed by Adele Adamo and Adriana LaVolpe, CNR, Naples, Italy).

	Apoptotic corpses/gonad arm	*n*
WT	3.5 ± 0.17	56
sun-1(wt)	3.37 ± 0.28	40
sun-1(6E)	3.35 ± 0.016	136
sun-1(allA)	3.56 ± 0.16	123
syp-2; sun-1(wt)	14.72 ± 0.72	67
syp-2; sun-1(allA)	13.24 ± 0.58	84
syp-2; sun-1(6E)	10.25 ± 0.48	61

Table 5. Number of apoptotic corpses per gonad arm. Age-matched hermaphrodites were stained with SYTO 12. Positive nuclei were scored as apoptotic corpses. Variations indicate the standard error of the mean (SEM). Each genotype was analyzed in at least three independent experiments. *n*, number of scored gonad arms.

To gain more mechanistic insight into how SUN-1 phosphorylation mediates *plk-2*-dependent leptotene/zygotene arrest, and why *sun-1(allA)* partially, but not completely, phenocopies the *plk-2* deletion, we analyzed PLK-2 localization in the *syp-2; sun-1(allA) and syp-2; sun-1(wt)*–expressing lines. In *syp-2; sun-1(wt),* multiple PLK-2 foci per nucleus localized to all movement-competent SUN-1 aggregates over almost the entire length of the gonad. Only in the last cell rows of the meiotic gonad, where there was reduced movement, did PLK-2 localization diminish; most of the time, only one PLK-2 focus per nucleus was visible (Figure 10). In contrast, PLK-2 localized to SUN-1 aggregates only in the first cell rows after meiotic entry in *syp-2; sun-1(allA)*–expressing germlines. Analogous to the smaller nonphosphorylatable

aggregates formed in *syp-2; sun-1(allA)*–expressing germlines, PLK-2 signals were much weaker in *sun-1(allA)* germlines from the beginning of the TZ onwards (Figure 10). In the remainder of the gonad, PLK-2 signals were strongly decreased or absent at the autosomal pairing centers and only persisted at the X-chromosomal pairing center in *syp-2; sun-1(allA)* (Figure 10 and data not shown).

Localization of the ZIMs to the autosomal pairing centers at the nuclear envelope is required for SUN-1 aggregate formation, chromosome movement, and PLK-2 localization as it was shown by complete depletion of all ZIMs. In this case PLK-2 was no longer localized to the nuclear envelope (Harper, Rillo et al. 2011; Labella, Woglar et al. 2011). Therefore, I tested whether ZIM localization was affected in *syp-2; sun-1(allA)*–expressing germlines by following ZIM-3, the pairing-center binding protein for chromosomes I and IV (Phillips and Dernburg 2006). ZIM-3 was present at the nuclear envelope, and colocalized with SUN-1 aggregates throughout the gonad in *syp-2; sun-1(wt)* (Figure 14); a similar pattern was observed in *syp-2; sun-1(allA)*–expressing lines. Therefore, instability of ZIM localization at the nuclear envelope cannot account for the premature reduction in PLK-2 localization, accompanied by premature chromosome end movement cessation and SUN-1 aggregate dissolution observed in syp-2*; sun-1(allA).*

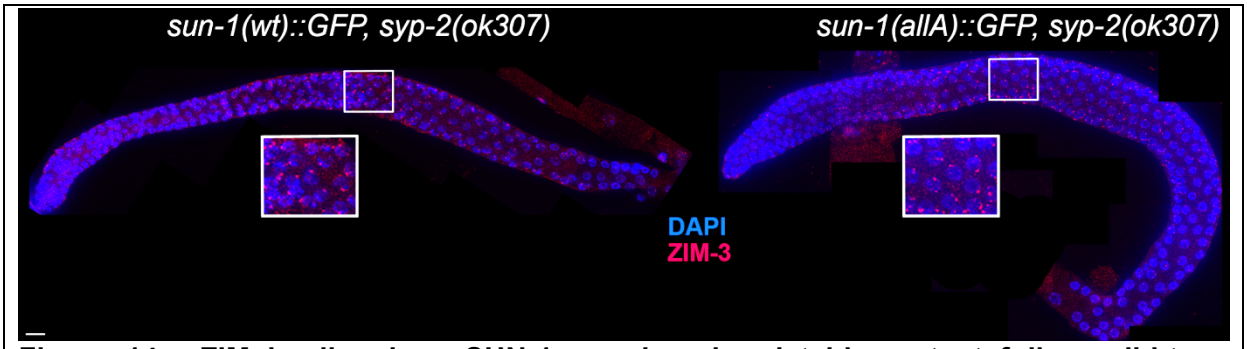

Figure 14. ZIM loading in a SUN-1 nonphosphorylatable mutant follow wild-type kinetics. *sun-1(wt); sun-1(ok1282)* and *sun-1(allA); sun-1(ok1282)* (bottom) hermaphrodite gonads stained with DAPI (top, blue in merged), anti-GFP (middle, green in merged), and anti-ZIM-3 (bottom, red in merged). Scale bar, 10 µm.

These results demonstrate that SUN-1 phosphorylation is required, not only for SUN-1 aggregate stability, but also for robust localization of PLK-2 to the autosomal pairing centers. The consequences of this become most apparent under challenging conditions. Because PLK-2 interacts with SUN-1 and phosphorylates it and, in return, depends on SUN-1 phosphomodification to localize to chromosome end

attachments, we propose the existence of a self-reinforcing feedback loop between PLK-2 localization and SUN-1 phosphorylation at chromosomal attachment sites at the nuclear envelope. Under challenging conditions, this feedback loop maintains PLK-2 at the nuclear envelope and thereby allows chromosome mobility. Therefore, the delay in meiotic progression observed in synapsis mutants is dependent on SUN-1 phosphorylation.

Discussion

In summary we could show that at the onset of meiosis in *C. elegans* the inner nuclear envelope protein SUN-1 transiently changes its localization. From being uniformly distributed throughout the entire nuclear envelope in the mitotic region of the germline, SUN-1 is found enriched at chromosome attachment sites at the nuclear envelope in early meiotic prophase.

By transmitting dynein dependent forces (Sato, Isaac et al. 2009) through the nuclear envelope spanning SUN/KASH bridge (mediated by SUN-1 and ZYG-12) SUN-1 aggregates move chromosome ends within a restricted, crescent shaped, volume of the nucleus. This movement shuffles chromosome ends and thereby enables homologous pairing and inhibits formation of the SC between non-homologous chromosomes (Penkner, Tang et al. 2007).

SUN-1 is phosphorylated on the entire population at the onset of meiosis on several N-terminal residues and additionally at least S12 is phosphorylated exclusively in the SUN-1 population enriched at aggregates. Formation of these aggregates, pairing and homologous synapsis is dependent on the localization of the ZIMs to the pairing center at the nuclear envelope. Loading of ZIMs is dependent on CHK-2 (Phillips and Dernburg 2006). By that also formation and phosphorylation of SUN-1 aggregates depends on CHK-2 kinase.

PLK-2 activity induces meiotic SUN-1 aggregates, presumably phosphorylates them on S12 and initializes the homology search. In absence of PLK-2, PLK-1 can substitute for the induction of SUN-1 aggregates. PLK-2 localizes to chromosome ends in leptotene/zygotene and co-purifies together with SUN-1. Also PLK-2 relocates from pairing centers to synapsed chromosomes and promotes homologous synapsis by counteracting non-homologous synaptic engagements. Furthermore PLK-2 is required to sustain a meiotic progression arrest due to synaptic failure (Harper, Rillo et al. 2011).

Phosphorylation of SUN-1 is dispensable for chromosome pairing, loading, and maintenance of pairing center proteins at the nuclear envelope and for induction of SUN-1 aggregates. However, the nonphosphorylatable SUN-1 aggregates are smaller. Similar to *plk-2* mutants, non-phosphorylatable SUN-1 fails to arrest nuclei with leptotene/zygotene characteristic mobile chromosomes when synapsis is

challenged. This is accompanied by a failure to maintain the colocalization of PLK-2 on pairing centers of autosomes beyond zygotene.

We also could demonstrate that, besides synaptic failure, also unrepaired DSBs and the absence of a crossover or a certain crossover intermediate induces a cytological manifested meiotic progression arrest including SUN-1 phosphorylation, aggregate persistence and chromatin clustering.

Since PLK-2 phosphorylates and interacts with SUN-1 we speculate that SUN-1 phosphorylation might mediate a self-reinforcing feedback loop involving SUN-1 aggregate stability and PLK-2 localization. This checkpoint mechanism sustains leptotene/zygotene-characteristic chromosome mobility under challenging conditions, such as asynapsis. In agreement with this hypothesis we observed that only nuclei in leptotene/zygotene are susceptible to SUN-1 modifications, and we therefore propose that this particular surveillance mechanism cannot be reinstalled later than zygotene (TZ).

Furthermore, we demonstrated that SUN-1 phosphorylation in agreement with the proposed role in a meiotic surveillance mechanism is required for full wild-type offspring viability and meiotic chromosome segregation under challenging conditions and is also required to synapse homologous chromosomes with wild-type kinetics.

SUN-1 phosphomodification as part of a checkpoint that monitors incomplete meiotic tasks

Meiocytes enter meiosis in leptotene with unpaired and unsynapsed chromosome axes. In the TZ, DSBs are generated to give rise to the vital crossover between homologous chromosomes. The data presented in this thesis showed that SUN-1 phosphorylation was sustained until chromosome axes were synapsed and DSB repair progresses beyond a certain stage.

Interestingly, in the absence of DSBs in *spo-11* germlines, SUN-1 phosphorylation also persisted, suggesting that crossover recombination needs to progress to a certain stage to permit SUN-1 dephosphorylation. SUN-1 phosphorylation correlated with ATM/ATL-dependent phosphorylation of CHK-1. The prolonged phosphorylation observed in *spo-11* mutants can be mitigated by treatment with low doses of ionizing radiation that were sufficient to rescue bivalent formation, but too low to induce

checkpoint activation in all nuclei. This suggests that damage signals must be emanating from fully synapsed pairs of homologous chromosomes that have not yet formed a certain crossover intermediate. Independently, SUN-1 phosphorylation was sustained in synapsis-defective mutants in leptotene/zygotene.
These results suggest that multiple checkpoint/DNA-damage signaling events lead to prolonged SUN-1 phosphorylation, consistent with the observation that individual loss of any of the known checkpoint players (*atm-1, atl-1, hus-1, cep-1,* and *pch-2*) does not reduce SUN-1 phosphomodification or the time spent in leptotene/zygotene (unpublished data). Furthermore we propose that it were not only meiotically induced DSBs that elicit damage signaling in leptotene/zygotene since CHK-1 appears activated even in the absence of *spo-11*. Therefore, the modifications are part of a surveillance machinery that monitors ongoing meiotic tasks. In contrast to synapsis-defective mutants, however, constitutive SUN-1 phosphorylation was not sufficient to fully arrest meiocytes in leptotene/zygotene, suggesting that other components participate in executing the meiotic arrest.

The role of SUN-1 phosphorylation in PLK-2 orchestrated meiotic prophase progression

PLK-2 fulfills several roles during early prophase in *C. elegans*: In redundancy with PLK-1, PLK-2 is required to induce SUN-1 aggregates and phosphorylation of them on S12 accompanied by initiation of homology search. In the absence of PLK-2 synapsis is delayed but finally established prematurely between non-homologous chromosomes. Furthermore PLK-2 is required to sustain a leptotene/zygotene arrest in the absence of synapsis and asynapsis triggered apoptosis depends on PLK-2 (Harper, Rillo et al. 2011).
Initial aggregate formation, chromosome end mobility and homologous pairing did not depend on SUN-1 phosphorylations. This observation let us conclude that SUN-1 was not the key substrate of Polo-kinases to initiated SUN-1 aggregate formation and homology search by chromosome end–led movement.
Nevertheless nonphosphorylatable SUN-1 aggregates were significantly smaller. Further, in a synapsis deficient background, these aggregates became unstable over time and fail to maintained chromosome mobility beyond transition zone. In addition I

observed that less PLK-2 was recruited to pairing centers at nuclear envelope attachment sites in nonphosphoylatable *sun-1* mutants. Furthermore, PLK-2 was not stably maintained at autosomal pairing centers in a synapsis-defective mutant, despite the fact that the pairing center proteins were appropriately localized to these pairing centers. The depletion of PLK-2 at pairing centers correlated with restricted movement of chromosomal ends under challenging conditions. Under these conditions, in nonphosphorylatable *sun-1* mutants, wild-type-like movement occurred only in the first rows of TZ, thereby resembling the *plk-2* deletion mutant (Harper, Rillo et al. 2011; Labella, Woglar et al. 2011).

Consequently, we propose that phosphorylation of SUN-1 may be part of a self-reinforcing feedback loop between PLK-2-dependent SUN-1 phosphomodification and SUN-1 phosphorylation–dependent PLK-2 localization; this loop remains activated upon detection of unfinished meiotic tasks. After meiotic entry, meiotic chromosomal axes are defined by specific components, such as HTP-1-3 and HIM-3 (MacQueen and Villeneuve 2001; Goodyer, Kaitna et al. 2008; Martinez-Perez, Schvarzstein et al. 2008). Formation of meiotic axes is independent of CHK-2 (MacQueen and Villeneuve 2001). One can speculate that unsynapsed axes emit a *chk-2*-dependent signal that results in the phosphorylation of SUN-1 on several residues (in particular, serines 8, 24, and 43) and loading of the pairing center–binding proteins onto their respective pairing centers, which then recruit PLK-2. This ultimately results in the induction of SUN-1 aggregates, SUN-1 phosphorylation on serine 12 by PLK-2, and transmission of cytoplasmic kinetic forces to pairing centers (Harper, Rillo et al. 2011; Labella, Woglar et al. 2011). PLK-2-dependent modification of the pairing center–binding proteins and other unknown targets may then lead to directed movement of chromosome ends (Harper, Rillo et al. 2011). We speculate that phosphorylation of SUN-1 increases its ability to bind PLK-2 to stabilize it at the pairing centers, where PLK-2 reinforces the stability of SUN-1 aggregates and supports directed movement of chromosome ends until certain meiotic tasks are accomplished. Consistent with this model, PLK-2 was found in a protein complex with SUN-1.

Role of SUN-1 phosphorylation during synapsis

SUN-1 phosphorylation is required for wild-type kinetics of SC polymerization, but it is dispensable for pairing. Several interpretations of this result are possible. PLK-2 is required for a fully developed SC with wild-type kinetics that is likely to assemble in a processive manner from the pairing centers (MacQueen, Colaiacovo et al. 2002; Harper, Rillo et al. 2011; Labella, Woglar et al. 2011). In leptotene/zygotene, PLK-2 localizes to SUN-1 aggregates, and from there it seems to be transferred onto synapsed parts of the chromosomes (Figure 1). In nonphosphorylatable SUN-1 aggregates, PLK-2 localization is unstable. Therefore, it is possible that the amount of PLK-2 that can effuse from the pairing center downwards along the axes is insufficient to fulfill its function there. However, we cannot exclude a direct involvement of SUN-1 phosphorylation in SC progression. Alternatively, we could speculate that smaller/weaker SUN-1 aggregates in the nonphosphorylatable background transmit less of the kinetic forces that are required to drive SC formation with wild-type kinetics between homologous chromosomes. Chromosome end–led movements have frequently been suggested not only to contribute to the search for the homologous partner, but also to play a role in resolving topological entanglements, interlocks, and unwanted interactions that might impede successful recombinational repair and SC formation (Koszul and Kleckner 2009). Furthermore, chromosome motions might even provide the energy for recombinational repair (Kosaka, Shinohara et al. 2008). Therefore, we propose that the coupling of SUN-1-mediated progression delay with chromosome movement is an elegant means to ensure chromosome motion until a crossover has been established on each chromosome.

Reduction of *sun-1* gene dosage alters meiotic behavior

Initially, we observed stronger phenotypes in *sun-1* substitution lines generated by particle bombardment (biolistic transformation) compared to the phenotypes observed with Mos single-copy insertion lines. In phosphomimetic mutants, the TZ was prolonged and SUN-1 aggregates persisted more dramatically. Also this phosphomimetic lines generated by biolistic transformation display a much stronger

accumulation and delayed disappearance of RAD-51 foci and greater meiotic chromosome mis-segregation (Penkner, Fridkin et al. 2009). It is likely that these lines were not single-copy lines and were subjected to germline silencing, because over generations, the GFP signals of the transgenes and the fertility of these lines decreased (the novel Mos lines did not show silencing over >20 generations). RNAi depletion of *sun-1* in a new Mos-generated line phenocopied the defects seen in the biolistically generated lines, suggesting that the previously reported phenotypes were due to incomplete rescue. SUN-1 aggregates and tightly clustered chromatin persisted and RAD-51 foci accumulated. These phenotypes, which resembled those of the lines generated by biolistic transformation, were more frequently induced by feeding SUN-1 RNAi to *sun-1(S12E)* and *sun-1(6E)* lines, but could also be observed when feeding SUN-1 RNAi to wild-type (*sun-1(wt)*) control animals. These phenotypes correlated with a reduction in SUN-1 and therefore offer an explanation for the differences observed when using transgenic lines that were generated by different methods (Figure 15B). Moreover, a homologous pairing defect, as reported for one of the biolistically generated substitution lines (Penkner, Fridkin et al. 2009), could be induced when even more SUN-1 protein was depleted (Figure 15A).

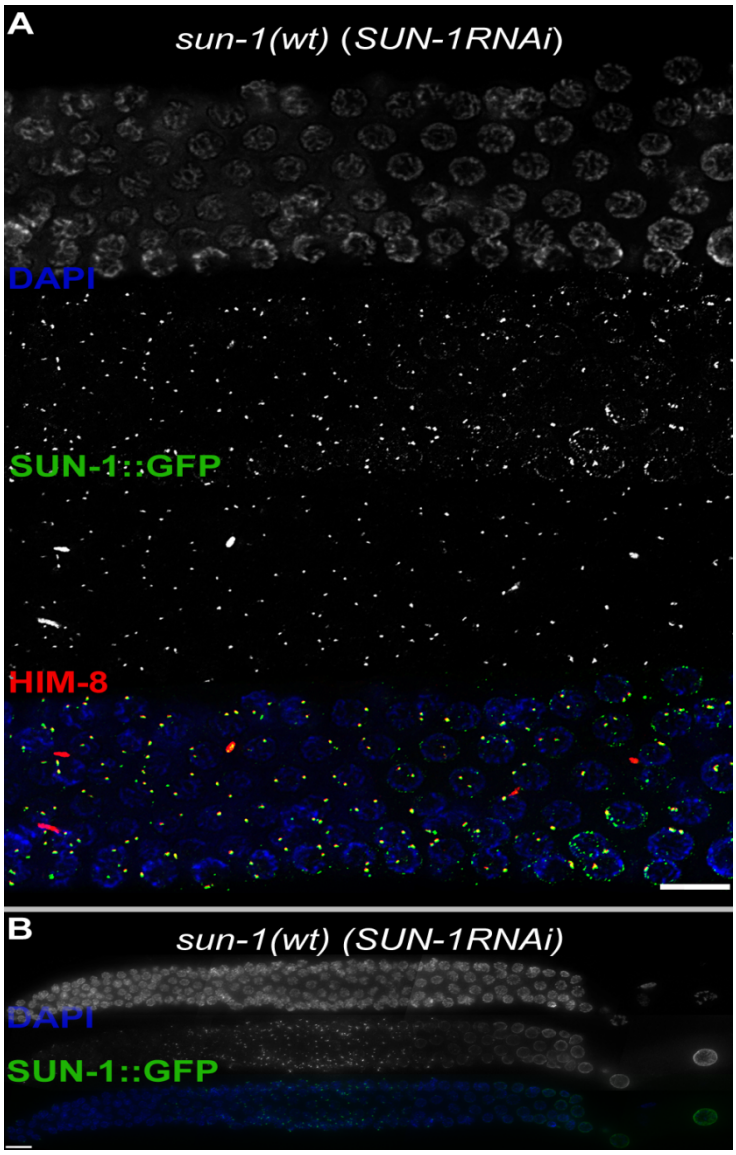

Figure 15. Decreased SUN-1 protein leads to SUN-1 aggregate persistence and failure of chromosome pairing. (A) Pachytene hermaphrodite *sun-1(wt); sun-1(ok1282)* gonads subjected to *sun-1* RNAi stained with DAPI (top, blue in merge), anti-GFP (middle, green in merge), and anti-HIM-8 (bottom, red in merge). Two HIM-8 signals in one nucleus represent unpaired pairing centers of the X chromosome. (B) Reduction in SUN-1 protein dosage leads to prolonged SUN-1 aggregation and chromatin clustering. *sun-1(wt); sun-1(ok1282)* hermaphrodite gonads subjected to *sun-1* RNAi stained with DAPI (top, blue in merge) and anti-GFP (bottom, green in merge). Scale bar, 10 μm.

Male *C. elegans*: an example of the biological relevance of the SUN-1 mediated checkpoint

C. elegans hermaphrodites have the karyotype X/X, whereas males arise by spontaneous nondisjunction of the X chromosome and display the X/O karyotype. The lone X chromosome is therefore unable to undergo pairing and synapsis with a homologous partner. While in hermaphrodites, any unsynapsed chromosome would trigger a cell cycle delay MacQueen 2002, the failure of the single X chromosome to undergo synapsis in *C. elegans* males does not activate the meiotic checkpoint (whereas asynapsis of autosomes does). Therefore, the single X chromosome in males must have adapted a mechanism that shields it from the synapsis checkpoint (Jaramillo-Lambert and Engebrecht 2010).

Anahita Daryabeigi in the lab of Verena Jantsch could show recently that at the nuclear envelope–associated end of the lone male X chromosome, SUN-1 is not phosphorylated at S12; nevertheless a mobile SUN-1 aggregate is induced by the lone X chromosomal pairing center (Anahita Daryabeigi, personal communication). This is consistent with a model in which SUN-1 phosphorylation installs a checkpoint mechanism that is competent to delay meiotic progression. We propose that an absence of this phosphorylation may be part of the mechanism to hide the single X from the checkpoint machinery that responds to unsynapsed chromosomes, which, in turn, precludes the checkpoint machinery from responding to signals emanating from the unsynapsed X. It will be interesting to learn whether the repressive chromatin environment of the single X chromosome (Kelly, Schaner et al. 2002) in males acts on PLK-2 activity, or if an as-yet unknown phosphatase “overrides” PLK-2 kinase activity at the X chromosome.

Not in line with our hypothesis glutamic acid substitution of SUN-1 phosphosites delayed the cell cycle progression in males only slightly, similar to hermaphrodites, and failed to generate a complete synapsis checkpoint response for the lone X chromosome (Anahita Darybeigi, personal communication). This suggests that the checkpoint response might be supported by additional factors, or that glutamic acid substitutions do not sufficiently mimic phosphorylation.

A G2 meiotic checkpoint

This thesis presents evidence for the existence of a meiotic prophase checkpoint system at the nuclear envelope that responds to unfinished meiotic tasks, such as incomplete synapsis or recombination, by delaying meiotic progression. Most importantly, the SUN-1-mediated “checkpoint” system can only integrate a signal when the cell is still in a responsive state (zygotene and early pachytene), and long before the G2/M transition. I observed that nuclei that had progressed beyond early pachytene were unable to reestablish SUN-1 and CHK-1 phosphorylation. Recently, it was shown that a DNA-damage checkpoint at the G2/M transition was only responsive to very high doses of the DNA-damaging agent etoposide in mouse oocytes (Marangos and Carroll 2012). Moderate doses led to activation of DNA-damage responses, such as production of gamma H2AX chromatin, but ATM

signaling and subsequent CHK1 signaling were not enough to elicit an efficient response. The potential surveillance mechanism for unfinished meiotic tasks proposed here (provided it also exists in vertebrates) may have been undetected by Marangos and Caroll because, in their study, oocytes were exposed to DNA-damaging agents past the stage of meiotic prophase in which SUN-1 phosphorylation is observed in *C. elegans*. Recently, vertebrate Sun1$^{-/-}$ Sun2$^{-/-}$ embryonic fibroblasts were shown to accumulate DNA damage more rapidly and failed to arrest cell cycle progression in response to certain genotoxic agents (Lei, Zhu et al. 2012). This suggests a potentially conserved role for SUN-domain proteins in the DNA-damage response. Because leptotene/zygotene bouquet formation (SUN/KASH-dependent chromosome end attachment with prominent Sun protein relocation and concentration into chromosome ends) is conserved in mammals (Ding, Xu et al. 2007; Schmitt, Benavente et al. 2007), it will be worthwhile in future investigations to determine whether mammalian oocytes have adapted a similar checkpoint mechanism to slow down progression, leading to prolonged letotene/zygotene chromosome movement when unfinished meiotic tasks are detected.

Material and Methods

Genetics

Maintenance and cultivation of worms were based on standard protocols (Brenner 1974). Following strains were used in this study:

- N2 (Nicholas, Dougherty et al. 1959)
- *ced-3(n717)* (Ellis and Horvitz 1986)
- *syp-2(ok307)*/nT1[qIs51](IV:V) (Colaiacovo, MacQueen et al. 2003)
- *rad-51(ok2218)*/nT1[qIs51](IV:V)
- *spo-11(ok79)*/nT1[qIs51] (IV:V) (Dernburg, McDonald et al. 1998)
- *ttTi5605*, *unc-119(ed3)* (Frokjaer-Jensen, Davis et al. 2008)
- *atm-1(gk186)*; *atl-1(tm853)*/nT1[qIs51] (IV;V) (Penkner, Fridkin et al. 2009)
- *syp-2(ok307); spo-11(me44)*/nT1[qIs51](IV:V) (Penkner, Fridkin et al. 2009)
- *plk-2(ok1936)* (Harper, Rillo et al. 2011; Labella, Woglar et al. 2011)
- *plk-2(vv44)* (Labella, Woglar et al. 2011)
- *sun-1::gfp; sun-1(ok1282); spe-26(hc138)* (Penkner, Fridkin et al. 2009)
- *sun-1(ok1282)/* nT1[qIs51] (IV;V)

Following genotypes were generated during this study:

- *sun-1(ok1282)/*nT1[qIs51](IV;V); *ttTi5605 jfSi1[Psun-1::GFP cb-unc-119(+)]*
- *sun-1(ok1282)/*nT1[qIs51](IV;V); *ttTi5605 jfSi3[Psun-1S12E::GFP cb-unc-119(+)*]
- *sun-1(ok1282)/*nT1[qIs51](IV;V); *ttTi5605 jfSi23[Psun-1(S8, 12, 24, 43, 58, 62E)::GFP cb-unc-119(+)]*
- *sun-1(ok1282)/*nT1[qIs51](IV;V); *ttTi5605 jfSi4[Psun-1(12A)::GFP cb-unc-119(+)]*
- *sun-1(ok1282)/*nT1 [qIs51](IV;V); *ttTi5605 jfSi9[Psun-1(8, 12, 24, 36, 43, 58, 62A)::GFP cb-unc-119(+)]*
- *syp-2(ok307), sun-1(ok1282)/*nT1[qIs51](IV;V)*; ttTi5605 jfSi1[Psun-1::GFP cb-unc-119(+)]*
- *syp-2(ok307)*, *sun-1(ok1282)/*nT1[qIs51](IV;V)*; ttTi5605 jfSi3[Psun-1S12E::GFP cb-unc-119(+)*]

- *syp-2(ok307), sun-1(ok1282)/*nT1[qIs51](IV;V)*; ttTi5605 jfSi23[Psun-1(S8, 12, 24, 43, 58, 62E)::GFP cb-unc-119(+)]*
- *syp-2(ok307), sun-1(ok1282)/*nT1[qIs51](IV;V); *ttTi5605 jfSi4[Psun-1(12A)::GFP cb-unc-119(+)]*
- *syp-2(ok307)*, *sun-1(ok1282)/*nT1[qIs51](IV;V)*; ttTi5605 jfSi9[Psun-1(8, 12, 24, 36, 43, 58, 62A)::GFP cb-unc-119(+)]*

Generation of transgenic lines using MosSCI method

We generated different SUN-1 phosphosite mutants by using the MosSCI system, which allows integration of a transgene at a defined locus in the genome as a single copy (Frokjaer-Jensen, Davis et al. 2008). Following plasmid mix was injected into EG4322 (*ttTi5605; unc-119(ed3)* (injections were carried out by Verena Jantsch):

- 20-50 ng/µl pCFJ151 (our SUN-1 transgenes were cloned between the XhoI and the AflII sites driven by the endogenous promoter and 3'UTR)
- 50 ng/µl pJL44 (*Phsp-16-48::transposase*)
- 5 ng/µl pGH8 (*Prab-3::mCherry*)
- 2.5 ng/µl pCFJ90 (*Pmyo-2::mCherry*)

Injected animals (24h post L4 at 16°C) were recovered for 1 h post injection in M9 buffer before transferred individually onto NGM plates and incubated at 16°C overnight, before shifted to 25°C. Plates were scored for restoration of the *unc-199(ed3)* conferred immobility after roughly one week (when no food was left on the plate anymore). Plates with mobile worms were chunked and after further incubation at 25°C scored for loss of the selection markers for the extra chromosomal array.

We generated five different mutant transgenic *sun-1* lines, all C-terminally tagged with GFP and crossed them to the *sun-1(ok1282)* deletion background. The wild type control (referred to as *sun-1(wt)*) was compared to two different glutamic acid substitution lines, referred to as *sun-1(S12E)* and *sun-1(6E)*, in which all six serines doubtlessly identified as target sites were exchanged to glutamic acid (mass spec analysis could not differentiate between S35 and T36). In addition the wild type control was compared to two non-phosphorylatable lines (referred to as *sun-1(S12A)* and *sun-1(allA)*, in which all residues found to be phosphorylated, including T36,

were replaced by alanine). Subjecting this latter line to mass spectrometry analysis did not detect residual SUN-1 phospho-signals (data not shown).

Cytological preparations and immunofluorescence analysis

For Figures 1, 2ABD, 3, 4, 5, 6, 7AB, 9, 12, 14 and 15 gonads were dissected in 1xPBS supplied with 5 mM Levamisol. After fixation for 5 minutes in 1% formaldehyde under a coverslip slides were froze in liquid nitrogen for 10 min and a freeze-crack was performed before dehydrating specimens for 1 min in Methanol (-20°). Slides were washed 3x in 1x PBS-T and blocked in 3% BSA for 15 min before application of the primary antibody (4°C over night). After washing 3x with PBS-T, secondary detection was performed for 2 h on 30°C before washing slides 3x in 1 PBS-T for 5 min. Specimens were mounted in Vectashield (Vector) supplied with 2 μl/ml and sealed with nail polish.

For Figure 2C, 7F and 10 gonads were dissected in 10 μl EBT buffer (for 1ml: 110 μl 10X egg buffer, 10 μl, 10% Tween, 50 μl of 100 mM Levamisol, 1 μl 0.15M spermidine and 850 μl of water). Specimens were fixed for 5 min on room temperature by adding 10 μl of fixative (2% formaldehyde in 1x egg buffer). Freeze-crack and staining was performed as described above.

Following antibodies were used:

- rat anti-SUN-1 phospho-serine 43 (1:1000) (antisera were produced against the following phospho-peptide: CVT RRD S(PO_3H_2)QP G)
- guinea pig anti-SUN-1 phospho-serine 12 (1:1500) (Penkner, Fridkin et al. 2009), rabbit anti-RAD-51 (1:100) (Colaiacovo, MacQueen et al. 2003)
- rabbit anti-SYP-1 (1:200) (MacQueen, Colaiacovo et al. 2002)
- mouse anti-GFP (1:500) (Roche Diagnostics)
- rabbit anti HIM-8 (1:5000) (Novus)
- guinea pig anti HIM-8 (1:500) (Phillips, Wong et al. 2005)
- guinea pig anti-ZIM-3 (1:100) (Penkner, Fridkin et al. 2009)
- guinea pig anti-SUN-1 phospho-serine 8 (1:700) (Penkner, Fridkin et al. 2009)
- rabbit anti-PLK-2 (1:15) (Labella, Woglar et al. 2011)

- guinea pig anti HTP-3 (1:500) (Goodyer, Kaitna et al. 2008)
- alexa fluor 568 goat anti-guinea pig (1:500) (Invitrogen)
- rabbit anti-Chk1 (S345Pi) (1:100) (Cell Signaling)
- alexa fluor 488 goat anti-guinea pig (1:500) (Invitrogen)
- alexa fluor 568 goat anti-rabbit (1:500) (Invitrogen)
- alexa fluor 488 goat anti-rabbit (1:500) (Invitrogen)
- alexa fluor 488 goat anti-mouse (1:500) (Invitrogen).

Microscopic evaluation of fixed samples

A Zeiss Axioskop epifluorescence microscope was used in combination with a cooled CCD camera (Photometrics). Z-stacks of one horizontal layer of nuclei within a gonad were taken with MetaVue software (Universal Imaging), deconvolved with AutoDeblur software (AutoQuant Imaging) and projected with Helicon Focus software (Helicon Soft Ltd.). Alternatively, a Deltavision deconvolution microscope and SoftWoRx image analysis deconvolution software system (both Applied Precision, Inc.) was used. Data analysis was performed using ImageJ (NIH). The Z-stacks (on both systems) comprised a series of 18–45 optical sections in increments of 200 nm.

Assessment of meiotic prophase duration

To define the duration of meiotic prophase I stages with respect to chromosome movement and SUN-1 aggregate behavior I quantified how many nuclei per cell row in the gonadal tube from TZ to cellularization displayed more than one SUN-1 aggregate (paralleled by tightly clustered chromatin), one SUN-1 aggregate (paralleled by loosely clustered chromatin) or no SUN-1 aggregate (accompanied by chromatin distributed throughout the nuclear volume). If the majority of nuclei per cell row met one of the three criteria the cell row was scored as “TZ” (more than one aggregate), “early pachytene” (one aggregate) or “full pachytene” (no aggregate) (Figure 3C). The length of these zones was normalized to the shape and length of the meiotic gonad.

Fluorescence in situ hybridization

FISH was performed as described in (Penkner, Tang et al. 2007) using a PCR generated probe against the 5 S ribosomal locus. FISH was performed by Cornelia Habacher.

Irradiation assay

Hermaphrodites were exposed to ionizing irradiation from a $_{137}$Cs source (90, 70, 50 or 7.5Gy). Dissection and cytological analysis were done 20 min, 90min, 120min, 8 h, or 27 h post-irradiation.

Time-lapse microscopy of SUN-1::GFP aggregates

For time lapse microscopy, adult hermaphrodites 24 h post L4 stadium were mounted in 10 mM Levamisol on a 2% Agarose pad and covered with a coverslip (sealed with melted Vaseline). On a delta vision deconvolution microscopy system (Applied Precision, Inc) every 5 sec (for 5 min total recording time) a Z-stack of 800 nm thick sections was taken through a 8000-12000 nm depth within the gonad (of total 10-15 pictures per stack to allow imaging one horizontal layer of nuclei). Standard exposure condition for recording: GFP channel, 100%ND, exposure time 50 msec, objective 60x. Live imaging was performed between 21-24°C. Z-stacks were deconvolved and 2D-projected (maximum intensity) by using Softworx software (Applied Precision). Analysis of aggregate movement in these 2D-ploted 16 frames per second movies was performed in ImageJ (NIH). Movement of the whole worm or gonad was reduced by using the plugin Stackreg. For aggregates tracking single nuclei were centered and aggregates were tracked for 3 minutes by using the plug in Manual Tracking. When two aggregates split, tracking of the larger aggregate was continued. Then movement of the second aggregate was recorded from the splitting point on.

RNA interference

RNAi feeding targeting *sun-1* was performed as described in (Kamath, Martinez-Campos et al. 2001). L1 to L4 larvae were pre-selected and incubated at 20°C until the animals reached 24 h post L4 stadium when gonads were dissected and stained. For *plk-1* depletion the second generation of animals on RNAi feeding plates was analyzed as adults 24 h post L4.
In vitro transcription of dsRNA for *cdk-2* was performed with T7 Megascript (Ambion). Microinjection of 400 ng/ul dsRNA in water into both arms of the gonad was performed under standard conditions by Verena Jantsch. For all RNAi application (for bacterial expression or as template for in vitro transcription, clones from the Ahringer library (Kamath, Martinez-Campos et al. 2001; Kamath, Fraser et al. 2003)) were obtained.

Apoptosis quantification

L4 larvae were pre-selected and incubated for 24-36 hours at 20^{o}C. Worms were collected into M9 solution containing 33 µM SYTO-12 (Molecular Probes) for 90 min in the dark. Worms were transferred to seeded plates for 30 min and then mounted on 2% agarose pads in 2 mM levamisole. The quantitative analysis was performed using a Leica DM6000 fluorescence microscope, Leica DC 350 FX camera under the control of Leica LAS AF 6000 software. Apoptosis auantification was performed by Adrian LaVolpe and Adele Adamo.

Immunoprecipitation

Worms were sonicated (5 3 30 s; 28% output) in 13 homogenization buffer (15 mM HEPES (pH 7.6), 10 mM KCl, 1.5 mM $MgCl_2$, 70 mM NaCl, 0.1 nM EDTA, 0.5 mM EGTA, 1 mM DTT, 44 mM Sucrose, 0,1% Triton X-100, 1 mM PMSF, protease inhibiter cocktail (Roche); 50 mM NaF, 0.1 mM Na_3VO_4, 60 mM b-glycerophosphate). The GFP trap (ChromoTek) was used to immunoprecipitate SUN-1::GFP. Beads were washed once with homogenization buffer and two times with washing buffer (10

mM Tris (pH 7.5), 175 mM NaCl, 0.5 mM EDTA, 1 mM PMSF, protease inhibitor cocktail (Roche)).

Antibodies used for western blot detection in these experiments;

- rabbit anti-PLK-2 (1:15) (Labella, Woglar et al. 2011)
- mouse anti-GFP (1:2500) (Roch)
- HRP goat anti-mouse (1:5000) (Rockland)
- HRP goat anti-rabbit (1:10000) (Pierce)

Mass spectrometry

For mass spectrometry SUN-1 GFP was precipitated as described above from 25 g of adult, synchronous worms with 0.2 ml of GFP trap agarose beads (Chromtek). Samples were eluted by boiling in Laemmli buffer (BioRad) and proteins were resolved for 1 cm on a 7.5% pre-casted SDS-PAGE gel (BioRad). The gel was fixed and silver-stained as described in (Blum, Beier et al. 1987). The lanes of interest were cut and subjected to the mass spectrometry facility. When SUN-1(allA)::GFP purified from *sun-1(allA)* was subjected to mass spectrometry no phosphorylation of S35 could be detected. Mass spectrometry was performed as described previously in (Penkner, Fridkin et al. 2009) by the MFPL mass spectrometry unit.

Expression and Purification of HA-HIM-8, HA-SUN-1 and HA-PLK-2 in budding yeast

cDNA clones of Him-8, Sun-1 and PLK-2 were cloned into the pPR3-N vector (Mobitec). Yeast strains (NMY51, Mobitec) were co-transformed with empty pBT3-N vector (Mobitec) and constructs of interest followed by selection on SC-Leu-Trp solid medium. Expression was verified by probing against HA on a western plot. For purification 100 ml SC-Leu-Trp liquid media was inoculated with 0.5 ml of an overnight culture and grown to an OD_{660} of 0.8. Pellets were harvested by centrifugation (3000 rpm, 5min) and washed twice in ddH2O before resupension in 0.4 ml Homogenization buffer (15 mM Hepes pH=7.6, 250 mM NaCl, 0.1 mM EDTA, 0.5 mM EGTA, 0,1% Triton 100, 0.1 mM DTT, 50 mM Sucrose, 0.1 mM AEBSF,

1:200 Aprotinine, 5 mM Benzamidine, 50 mM NaF, 0.1 mM Na_3VO_4, 60 mM beta-glycero phosphate and complete protease inhibitor tablets (1/10 ml, Roche)).
Cells were transferred in a 1.5 ml test tube which was filled with glass beads (0.4-0.6mm, Satorius). Cells were broken by incubation for 30-60 min on a vibrating platform (4°C). The lysate was collected and the beads were washed two times with homogenization buffer. The cell lysate was sonicated 1x (amplitude 28%) for 30 seconds, before spinning at 14000 rpm for 30 min. The supernatant was used for IP. Per 100 ml yeast culture 50 ul Dynabeads pan-mouse IgG (Invitrogen) overnight coupled to mouse-anti-HA antibody (Covance) were added. IP was performed for 3-5 h on 4°C. Beads were washed 1x with homogenization buffer 3x with 1xPBS + 0.1% BSA and 2x with kinase reaction buffer before kinase reaction was performed.

in vitro kinase reaction

The kinase activity of PLK-2(vv44) was assessed as previously described for the budding yeast polo kinase Cdc5p (St-Pierre, Douziech et al. 2009), with some minor modifications. Similar amounts of wild-type PLK-2 or PLK-2(vv44) (estimated by western plot analysis judging the amount of PLK-2 after immunoprecipitation) was incubated at 25˚C for 30 min in a kinase reaction buffer containing 5 µg of dephosphoorylated-casein (Sigma), 25 mM Tris-HCl pH 7.5, 2 mM DTT, 10 mM $MgCl_2$, 100 µM ATP and 1 µCi ATPγ^{32}P, 0.5 mM EDTA, 5 nM microcystin, 25 µM bromolevamisole oxalate, 5 mM β-glycerophosphate 1 mM AEBSF, 10 µM pepstatin A, 10 µM E-64, 0.2 mM tungstate and 0.1 mM Na_3VO_4. The reactions were terminated by the addition of 2X sample buffer containing β-mercaptoethanol followed by 5 min incubation at 95˚C. Samples were loaded onto a standard 11% SDS-PAGE gel (Laemmli buffer system; BioRad). Protein phosphorylation was detected by monitoring 32P-labelled bands in dried gels using Fuji Medical X-Ray Films (Fujifilm Life Science).

Abbreviations

SC… synaptonemal complex

DSBs… DNA double strand breaks

GFP… green fluorescent protein

RNAi… RNA interference

DAPI… 4',6-diamidino-2-phenylindole

ZIMs… ZIM-1, ZIM-2, ZIM-3 and HIM-8

HIM… high incidence of males

SEM... standard error of the mean

TZ… transition zone

References

Adamo, A., P. Montemauri, et al. (2008). "BRC-1 acts in the inter-sister pathway of meiotic double-strand break repair." EMBO reports **9**(3): 287-292.

Agarwal, S. and G. S. Roeder (2000). "Zip3 provides a link between recombination enzymes and synaptonemal complex proteins." Cell **102**(2): 245-255.

Allers, T. and M. Lichten (2001). "Differential timing and control of noncrossover and crossover recombination during meiosis." Cell **106**(1): 47-57.

Alpi, A., P. Pasierbek, et al. (2003). "Genetic and cytological characterization of the recombination protein RAD-51 in Caenorhabditis elegans." Chromosoma **112**(1): 6-16.

Aravind, L. and E. V. Koonin (1998). "The HORMA domain: a common structural denominator in mitotic checkpoints, chromosome synapsis and DNA repair." Trends in biochemical sciences **23**(8): 284-286.

Bahler, J., T. Wyler, et al. (1993). "Unusual nuclear structures in meiotic prophase of fission yeast: a cytological analysis." The Journal of cell biology **121**(2): 241-256.

Bai, X., B. N. Peirson, et al. (1999). "Isolation and characterization of SYN1, a RAD21-like gene essential for meiosis in Arabidopsis." The Plant cell **11**(3): 417-430.

Bailly, A. P., A. Freeman, et al. (2010). "The Caenorhabditis elegans homolog of Gen1/Yen1 resolvases links DNA damage signaling to DNA double-strand break repair." PLoS genetics **6**(7): e1001025.

Barber, L. J., J. L. Youds, et al. (2008). "RTEL1 maintains genomic stability by suppressing homologous recombination." Cell **135**(2): 261-271.

Barchi, M., S. Mahadevaiah, et al. (2005). "Surveillance of different recombination defects in mouse spermatocytes yields distinct responses despite elimination at an identical developmental stage." Molecular and cellular biology **25**(16): 7203-7215.

Barchi, M., I. Roig, et al. (2008). "ATM promotes the obligate XY crossover and both crossover control and chromosome axis integrity on autosomes." PLoS genetics **4**(5): e1000076.

Bardhan, A. (2010). "Many functions of the meiotic cohesin." Chromosome research : an international journal on the molecular, supramolecular and evolutionary aspects of chromosome biology **18**(8): 909-924.

Bardhan, A., H. Chuong, et al. (2010). "Meiotic cohesin promotes pairing of nonhomologous centromeres in early meiotic prophase." Molecular biology of the cell **21**(11): 1799-1809.

Barlow, C., S. Hirotsune, et al. (1996). "Atm-deficient mice: a paradigm of ataxia telangiectasia." Cell **86**(1): 159-171.

Baudat, F., K. Manova, et al. (2000). "Chromosome synapsis defects and sexually dimorphic meiotic progression in mice lacking Spo11." Molecular cell **6**(5): 989-998.

Baudrimont, A., A. Penkner, et al. (2010). "Leptotene/zygotene chromosome movement via the SUN/KASH protein bridge in Caenorhabditis elegans." PLoS Genet **6**(11): e1001219.

Baudrimont, A., A. Penkner, et al. (2011). "A new thermosensitive smc-3 allele reveals involvement of cohesin in homologous recombination in C. elegans." PloS one **6**(9): e24799.

Bell, L. and B. Byers (1983). "Separation of branched from linear DNA by two-dimensional gel electrophoresis." Analytical biochemistry **130**(2): 527-535.
Bell, L. R. and B. Byers (1983). "Homologous association of chromosomal DNA during yeast meiosis." Cold Spring Harbor symposia on quantitative biology **47 Pt 2**: 829-840.
Benson, F. E. and S. C. West (1994). "Substrate specificity of the Escherichia coli RuvC protein. Resolution of three- and four-stranded recombination intermediates." The Journal of biological chemistry **269**(7): 5195-5201.
Bhalla, N. and A. F. Dernburg (2005). "A conserved checkpoint monitors meiotic chromosome synapsis in Caenorhabditis elegans." Science **310**(5754): 1683-1686.
Bhalla, N., D. J. Wynne, et al. (2008). "ZHP-3 acts at crossovers to couple meiotic recombination with synaptonemal complex disassembly and bivalent formation in C. elegans." PLoS genetics **4**(10): e1000235.
Bickel, J. S., L. Chen, et al. (2010). "Structural maintenance of chromosomes (SMC) proteins promote homolog-independent recombination repair in meiosis crucial for germ cell genomic stability." PLoS genetics **6**(7): e1001028.
Bishop, D. K. (1994). "RecA homologs Dmc1 and Rad51 interact to form multiple nuclear complexes prior to meiotic chromosome synapsis." Cell **79**(6): 1081-1092.
Blat, Y., R. U. Protacio, et al. (2002). "Physical and functional interactions among basic chromosome organizational features govern early steps of meiotic chiasma formation." Cell **111**(6): 791-802.
Bolcun-Filas, E., Y. Costa, et al. (2007). "SYCE2 is required for synaptonemal complex assembly, double strand break repair, and homologous recombination." The Journal of cell biology **176**(6): 741-747.
Borner, G. V., A. Barot, et al. (2008). "Yeast Pch2 promotes domainal axis organization, timely recombination progression, and arrest of defective recombinosomes during meiosis." Proceedings of the National Academy of Sciences of the United States of America **105**(9): 3327-3332.
Borner, G. V., N. Kleckner, et al. (2004). "Crossover/noncrossover differentiation, synaptonemal complex formation, and regulatory surveillance at the leptotene/zygotene transition of meiosis." Cell **117**(1): 29-45.
Boulton, S. J., A. Gartner, et al. (2002). "Combined functional genomic maps of the C. elegans DNA damage response." Science **295**(5552): 127-131.
Brenner, S. (1974). "The genetics of Caenorhabditis elegans." Genetics **77**(1): 71-94.
Carpenter, A. T. (1975). "Electron microscopy of meiosis in Drosophila melanogaster females: II. The recombination nodule--a recombination-associated structure at pachytene?" Proceedings of the National Academy of Sciences of the United States of America **72**(8): 3186-3189.
Cartagena-Lirola, H., I. Guerini, et al. (2008). "Role of the Saccharomyces cerevisiae Rad53 checkpoint kinase in signaling double-strand breaks during the meiotic cell cycle." Molecular and cellular biology **28**(14): 4480-4493.
Chen, S. Y., T. Tsubouchi, et al. (2008). "Global analysis of the meiotic crossover landscape." Developmental cell **15**(3): 401-415.
Chikashige, Y., C. Tsutsumi, et al. (2006). "Meiotic proteins bqt1 and bqt2 tether telomeres to form the bouquet arrangement of chromosomes." Cell **125**(1): 59-69.
Chin, G. M. and A. M. Villeneuve (2001). "C. elegans mre-11 is required for meiotic recombination and DNA repair but is dispensable for the meiotic G(2) DNA damage checkpoint." Genes & development **15**(5): 522-534.

Chua, P. R. and G. S. Roeder (1997). "Tam1, a telomere-associated meiotic protein, functions in chromosome synapsis and crossover interference." Genes & development **11**(14): 1786-1800.
Ciosk, R., M. Shirayama, et al. (2000). "Cohesin's binding to chromosomes depends on a separate complex consisting of Scc2 and Scc4 proteins." Molecular cell **5**(2): 243-254.
Clejan, I., J. Boerckel, et al. (2006). "Developmental modulation of nonhomologous end joining in Caenorhabditis elegans." Genetics **173**(3): 1301-1317.
Colaiacovo, M. P., A. J. MacQueen, et al. (2003). "Synaptonemal complex assembly in C. elegans is dispensable for loading strand-exchange proteins but critical for proper completion of recombination." Dev Cell **5**(3): 463-474.
Conrad, M. N., A. M. Dominguez, et al. (1997). "Ndj1p, a meiotic telomere protein required for normal chromosome synapsis and segregation in yeast." Science **276**(5316): 1252-1255.
Conrad, M. N., C. Y. Lee, et al. (2007). "MPS3 mediates meiotic bouquet formation in Saccharomyces cerevisiae." Proceedings of the National Academy of Sciences of the United States of America **104**(21): 8863-8868.
Cooper, J. P., Y. Watanabe, et al. (1998). "Fission yeast Taz1 protein is required for meiotic telomere clustering and recombination." Nature **392**(6678): 828-831.
Costa, Y., R. Speed, et al. (2005). "Two novel proteins recruited by synaptonemal complex protein 1 (SYCP1) are at the centre of meiosis." Journal of cell science **118**(Pt 12): 2755-2762.
Couteau, F., K. Nabeshima, et al. (2004). "A component of C. elegans meiotic chromosome axes at the interface of homolog alignment, synapsis, nuclear reorganization, and recombination." Current biology : CB **14**(7): 585-592.
Couteau, F. and M. Zetka (2005). "HTP-1 coordinates synaptonemal complex assembly with homolog alignment during meiosis in C. elegans." Genes & development **19**(22): 2744-2756.
Cremer, T., M. Cremer, et al. (2006). "Chromosome territories--a functional nuclear landscape." Current opinion in cell biology **18**(3): 307-316.
Crittenden, S. L., K. A. Leonhard, et al. (2006). "Cellular analyses of the mitotic region in the Caenorhabditis elegans adult germ line." Molecular biology of the cell **17**(7): 3051-3061.
Crittenden, S. L., E. R. Troemel, et al. (1994). "GLP-1 is localized to the mitotic region of the C. elegans germ line." Development **120**(10): 2901-2911.
Cromie, G. A., R. W. Hyppa, et al. (2006). "Single Holliday junctions are intermediates of meiotic recombination." Cell **127**(6): 1167-1178.
de Carvalho, C. E., S. Zaaijer, et al. (2008). "LAB-1 antagonizes the Aurora B kinase in C. elegans." Genes & development **22**(20): 2869-2885.
de los Santos, T., N. Hunter, et al. (2003). "The Mus81/Mms4 endonuclease acts independently of double-Holliday junction resolution to promote a distinct subset of crossovers during meiosis in budding yeast." Genetics **164**(1): 81-94.
De Muyt, A., L. Jessop, et al. (2012). "BLM helicase ortholog Sgs1 is a central regulator of meiotic recombination intermediate metabolism." Molecular cell **46**(1): 43-53.
de Vries, F. A., E. de Boer, et al. (2005). "Mouse Sycp1 functions in synaptonemal complex assembly, meiotic recombination, and XY body formation." Genes & development **19**(11): 1376-1389.

Dernburg, A. F., K. McDonald, et al. (1998). "Meiotic recombination in C. elegans initiates by a conserved mechanism and is dispensable for homologous chromosome synapsis." Cell **94**(3): 387-398.
Dernburg, A. F., J. Zalevsky, et al. (2000). "Transgene-mediated cosuppression in the C. elegans germ line." Genes & development **14**(13): 1578-1583.
Derry, W. B., R. Bierings, et al. (2007). "Regulation of developmental rate and germ cell proliferation in Caenorhabditis elegans by the p53 gene network." Cell death and differentiation **14**(4): 662-670.
Di Giacomo, M., M. Barchi, et al. (2005). "Distinct DNA-damage-dependent and -independent responses drive the loss of oocytes in recombination-defective mouse mutants." Proceedings of the National Academy of Sciences of the United States of America **102**(3): 737-742.
Ding, D. Q., Y. Chikashige, et al. (1998). "Oscillatory nuclear movement in fission yeast meiotic prophase is driven by astral microtubules, as revealed by continuous observation of chromosomes and microtubules in living cells." Journal of cell science **111 (Pt 6)**: 701-712.
Ding, D. Q., K. Okamasa, et al. (2012). "Meiosis-specific noncoding RNA mediates robust pairing of homologous chromosomes in meiosis." Science **336**(6082): 732-736.
Ding, X., R. Xu, et al. (2007). "SUN1 is required for telomere attachment to nuclear envelope and gametogenesis in mice." Developmental cell **12**(6): 863-872.
Eijpe, M., H. Offenberg, et al. (2003). "Meiotic cohesin REC8 marks the axial elements of rat synaptonemal complexes before cohesins SMC1beta and SMC3." The Journal of cell biology **160**(5): 657-670.
Ellis, H. M. and H. R. Horvitz (1986). "Genetic control of programmed cell death in the nematode C. elegans." Cell **44**(6): 817-829.
Fekairi, S., S. Scaglione, et al. (2009). "Human SLX4 is a Holliday junction resolvase subunit that binds multiple DNA repair/recombination endonucleases." Cell **138**(1): 78-89.
Fire, A., S. Xu, et al. (1998). "Potent and specific genetic interference by double-stranded RNA in Caenorhabditis elegans." Nature **391**(6669): 806-811.
Fridkin, A., E. Mills, et al. (2004). "Matefin, a Caenorhabditis elegans germ line-specific SUN-domain nuclear membrane protein, is essential for early embryonic and germ cell development." Proceedings of the National Academy of Sciences of the United States of America **101**(18): 6987-6992.
Frokjaer-Jensen, C., M. W. Davis, et al. (2010). "Targeted gene deletions in C. elegans using transposon excision." Nature methods **7**(6): 451-453.
Frokjaer-Jensen, C., M. W. Davis, et al. (2008). "Single-copy insertion of transgenes in Caenorhabditis elegans." Nature genetics **40**(11): 1375-1383.
Fung, J. C., B. Rockmill, et al. (2004). "Imposition of crossover interference through the nonrandom distribution of synapsis initiation complexes." Cell **116**(6): 795-802.
Garcia, V., H. Bruchet, et al. (2003). "AtATM is essential for meiosis and the somatic response to DNA damage in plants." The Plant cell **15**(1): 119-132.
Garcia-Muse, T. and S. J. Boulton (2005). "Distinct modes of ATR activation after replication stress and DNA double-strand breaks in Caenorhabditis elegans." The EMBO journal **24**(24): 4345-4355.
Gartner, A., S. Milstein, et al. (2000). "A conserved checkpoint pathway mediates DNA damage--induced apoptosis and cell cycle arrest in C. elegans." Mol Cell **5**(3): 435-443.

Gerton, J. L. and R. S. Hawley (2005). "Homologous chromosome interactions in meiosis: diversity amidst conservation." Nature reviews. Genetics **6**(6): 477-487.
Gillespie, P. J. and T. Hirano (2004). "Scc2 couples replication licensing to sister chromatid cohesion in Xenopus egg extracts." Current biology : CB **14**(17): 1598-1603.
Giroux, C. N., M. E. Dresser, et al. (1989). "Genetic control of chromosome synapsis in yeast meiosis." Genome / National Research Council Canada = Genome / Conseil national de recherches Canada **31**(1): 88-94.
Golsteyn, R. M., K. E. Mundt, et al. (1995). "Cell cycle regulation of the activity and subcellular localization of Plk1, a human protein kinase implicated in mitotic spindle function." The Journal of cell biology **129**(6): 1617-1628.
Goodyer, W., S. Kaitna, et al. (2008). "HTP-3 links DSB formation with homolog pairing and crossing over during C. elegans meiosis." Developmental cell **14**(2): 263-274.
Grelon, M., D. Vezon, et al. (2001). "AtSPO11-1 is necessary for efficient meiotic recombination in plants." The EMBO journal **20**(3): 589-600.
Gumienny, T. L., E. Lambie, et al. (1999). "Genetic control of programmed cell death in the Caenorhabditis elegans hermaphrodite germline." Development **126**(5): 1011-1022.
Haering, C. H., J. Lowe, et al. (2002). "Molecular architecture of SMC proteins and the yeast cohesin complex." Molecular cell **9**(4): 773-788.
Haering, C. H., D. Schoffnegger, et al. (2004). "Structure and stability of cohesin's Smc1-kleisin interaction." Molecular cell **15**(6): 951-964.
Hagstrom, K. A. and B. J. Meyer (2003). "Condensin and cohesin: more than chromosome compactor and glue." Nature reviews. Genetics **4**(7): 520-534.
Hamer, G., K. Gell, et al. (2006). "Characterization of a novel meiosis-specific protein within the central element of the synaptonemal complex." Journal of cell science **119**(Pt 19): 4025-4032.
Harper, N. C., R. Rillo, et al. (2011). "Pairing centers recruit a Polo-like kinase to orchestrate meiotic chromosome dynamics in C. elegans." Dev Cell **21**(5): 934-947.
Harrison, J. C. and J. E. Haber (2006). "Surviving the breakup: the DNA damage checkpoint." Annual review of genetics **40**: 209-235.
Hayashi, M., G. M. Chin, et al. (2007). "C. elegans germ cells switch between distinct modes of double-strand break repair during meiotic prophase progression." PLoS genetics **3**(11): e191.
Hayashi, M., S. Mlynarczyk-Evans, et al. (2010). "The synaptonemal complex shapes the crossover landscape through cooperative assembly, crossover promotion and crossover inhibition during Caenorhabditis elegans meiosis." Genetics **186**(1): 45-58.
Heidinger-Pauli, J. M., E. Unal, et al. (2008). "The kleisin subunit of cohesin dictates damage-induced cohesion." Molecular cell **31**(1): 47-56.
Herman, R. K. and C. K. Kari (1989). "Recombination between small X chromosome duplications and the X chromosome in Caenorhabditis elegans." Genetics **121**(4): 723-737.
Herman, R. K., C. K. Kari, et al. (1982). "Dominant X-chromosome nondisjunction mutants of Caenorhabditis elegans." Genetics **102**(3): 379-400.
Heyer, W. D., K. T. Ehmsen, et al. (2010). "Regulation of homologous recombination in eukaryotes." Annual review of genetics **44**: 113-139.

Hillers, K. J. and A. M. Villeneuve (2003). "Chromosome-wide control of meiotic crossing over in C. elegans." Current biology : CB **13**(18): 1641-1647.
Hirsh, D., D. Oppenheim, et al. (1976). "Development of the reproductive system of Caenorhabditis elegans." Developmental biology **49**(1): 200-219.
Hodgkin, J., H. R. Horvitz, et al. (1979). "Nondisjunction Mutants of the Nematode CAENORHABDITIS ELEGANS." Genetics **91**(1): 67-94.
Hofmann, E. R., S. Milstein, et al. (2002). "Caenorhabditis elegans HUS-1 is a DNA damage checkpoint protein required for genome stability and EGL-1-mediated apoptosis." Current biology : CB **12**(22): 1908-1918.
Holliday, R. (1964). "The Induction of Mitotic Recombination by Mitomycin C in Ustilago and Saccharomyces." Genetics **50**: 323-335.
Hsu, J. Y., Z. W. Sun, et al. (2000). "Mitotic phosphorylation of histone H3 is governed by Ipl1/aurora kinase and Glc7/PP1 phosphatase in budding yeast and nematodes." Cell **102**(3): 279-291.
Hunter, N. and N. Kleckner (2001). "The single-end invasion: an asymmetric intermediate at the double-strand break to double-holliday junction transition of meiotic recombination." Cell **106**(1): 59-70.
Ivanov, D. and K. Nasmyth (2007). "A physical assay for sister chromatid cohesion in vitro." Molecular cell **27**(2): 300-310.
Jantsch, V., P. Pasierbek, et al. (2004). "Targeted gene knockout reveals a role in meiotic recombination for ZHP-3, a Zip3-related protein in Caenorhabditis elegans." Molecular and cellular biology **24**(18): 7998-8006.
Jaramillo-Lambert, A. and J. Engebrecht (2010). "A single unpaired and transcriptionally silenced X chromosome locally precludes checkpoint signaling in the Caenorhabditis elegans germ line." Genetics **184**(3): 613-628.
Jaramillo-Lambert, A., Y. Harigaya, et al. (2010). "Meiotic errors activate checkpoints that improve gamete quality without triggering apoptosis in male germ cells." Curr Biol **20**(23): 2078-2089.
Jensen, R. B., A. Carreira, et al. (2010). "Purified human BRCA2 stimulates RAD51-mediated recombination." Nature **467**(7316): 678-683.
Jessop, L. and M. Lichten (2008). "Mus81/Mms4 endonuclease and Sgs1 helicase collaborate to ensure proper recombination intermediate metabolism during meiosis." Molecular cell **31**(3): 313-323.
Jiang, L., M. Xia, et al. (2007). "The Arabidopsis cohesin protein SYN3 localizes to the nucleolus and is essential for gametogenesis." The Plant journal : for cell and molecular biology **50**(6): 1020-1034.
Joyce, E. F. and K. S. McKim (2009). "Drosophila PCH2 is required for a pachytene checkpoint that monitors double-strand-break-independent events leading to meiotic crossover formation." Genetics **181**(1): 39-51.
Kamath, R. S., A. G. Fraser, et al. (2003). "Systematic functional analysis of the Caenorhabditis elegans genome using RNAi." Nature **421**(6920): 231-237.
Kamath, R. S., M. Martinez-Campos, et al. (2001). "Effectiveness of specific RNA-mediated interference through ingested double-stranded RNA in Caenorhabditis elegans." Genome biology **2**(1): RESEARCH0002.
Katis, V. L., J. J. Lipp, et al. (2010). "Rec8 phosphorylation by casein kinase 1 and Cdc7-Dbf4 kinase regulates cohesin cleavage by separase during meiosis." Developmental cell **18**(3): 397-409.
Keeney, S., C. N. Giroux, et al. (1997). "Meiosis-specific DNA double-strand breaks are catalyzed by Spo11, a member of a widely conserved protein family." Cell **88**(3): 375-384.

Kelly, K. O., A. F. Dernburg, et al. (2000). "Caenorhabditis elegans msh-5 is required for both normal and radiation-induced meiotic crossing over but not for completion of meiosis." Genetics **156**(2): 617-630.
Kelly, W. G., C. E. Schaner, et al. (2002). "X-chromosome silencing in the germline of C. elegans." Development **129**(2): 479-492.
Kerrebrock, A. W., D. P. Moore, et al. (1995). "Mei-S332, a Drosophila protein required for sister-chromatid cohesion, can localize to meiotic centromere regions." Cell **83**(2): 247-256.
Ketting, R. F. and R. H. Plasterk (2000). "A genetic link between co-suppression and RNA interference in C. elegans." Nature **404**(6775): 296-298.
Kim, K. P., B. M. Weiner, et al. (2010). "Sister cohesion and structural axis components mediate homolog bias of meiotic recombination." Cell **143**(6): 924-937.
Kimble, J. E. and J. G. White (1981). "On the control of germ cell development in Caenorhabditis elegans." Developmental biology **81**(2): 208-219.
Kitajima, T. S., S. A. Kawashima, et al. (2004). "The conserved kinetochore protein shugoshin protects centromeric cohesion during meiosis." Nature **427**(6974): 510-517.
Kitajima, T. S., T. Sakuno, et al. (2006). "Shugoshin collaborates with protein phosphatase 2A to protect cohesin." Nature **441**(7089): 46-52.
Klein, F., P. Mahr, et al. (1999). "A central role for cohesins in sister chromatid cohesion, formation of axial elements, and recombination during yeast meiosis." Cell **98**(1): 91-103.
Kosaka, H., M. Shinohara, et al. (2008). "Csm4-dependent telomere movement on nuclear envelope promotes meiotic recombination." PLoS genetics **4**(9): e1000196.
Koszul, R., K. P. Kim, et al. (2008). "Meiotic chromosomes move by linkage to dynamic actin cables with transduction of force through the nuclear envelope." Cell **133**(7): 1188-1201.
Koszul, R. and N. Kleckner (2009). "Dynamic chromosome movements during meiosis: a way to eliminate unwanted connections?" Trends Cell Biol **19**(12): 716-724.
Kouznetsova, A., H. Wang, et al. (2009). "BRCA1-mediated chromatin silencing is limited to oocytes with a small number of asynapsed chromosomes." Journal of cell science **122**(Pt 14): 2446-2452.
Krejci, L., V. Altmannova, et al. (2012). "Homologous recombination and its regulation." Nucleic acids research **40**(13): 5795-5818.
Krejci, L., B. Song, et al. (2002). "Interaction with Rad51 is indispensable for recombination mediator function of Rad52." The Journal of biological chemistry **277**(42): 40132-40141.
Labella, S., A. Woglar, et al. (2011). "Polo kinases establish links between meiotic chromosomes and cytoskeletal forces essential for homolog pairing." Dev Cell **21**(5): 948-958.
Lamelza, P. and N. Bhalla (2012). "Histone methyltransferases MES-4 and MET-1 promote meiotic checkpoint activation in Caenorhabditis elegans." PLoS genetics **8**(11): e1003089.
Lao, J. P., S. D. Oh, et al. (2008). "Rad52 promotes postinvasion steps of meiotic double-strand-break repair." Molecular cell **29**(4): 517-524.
Lee, J. and T. Hirano (2011). "RAD21L, a novel cohesin subunit implicated in linking homologous chromosomes in mammalian meiosis." The Journal of cell biology **192**(2): 263-276.

Lee, J., T. Iwai, et al. (2003). "Temporally and spatially selective loss of Rec8 protein from meiotic chromosomes during mammalian meiosis." Journal of cell science **116**(Pt 13): 2781-2790.
Lei, K., X. Zhu, et al. (2012). "Inner Nuclear Envelope Proteins SUN1 and SUN2 Play a Prominent Role in the DNA Damage Response." Current biology : CB **22**(17): 1609-1615.
Lengronne, A., Y. Katou, et al. (2004). "Cohesin relocation from sites of chromosomal loading to places of convergent transcription." Nature **430**(6999): 573-578.
Lightfoot, J., S. Testori, et al. (2011). "Loading of meiotic cohesin by SCC-2 is required for early processing of DSBs and for the DNA damage checkpoint." Current biology : CB **21**(17): 1421-1430.
Llano, E., R. Gomez, et al. (2008). "Shugoshin-2 is essential for the completion of meiosis but not for mitotic cell division in mice." Genes & development **22**(17): 2400-2413.
Loidl, J. (1990). "The initiation of meiotic chromosome pairing: the cytological view." Genome / National Research Council Canada = Genome / Conseil national de recherches Canada **33**(6): 759-778.
Loidl, J. and H. Scherthan (2004). "Organization and pairing of meiotic chromosomes in the ciliate Tetrahymena thermophila." Journal of cell science **117**(Pt 24): 5791-5801.
Longhese, M. P., D. Bonetti, et al. (2009). "DNA double-strand breaks in meiosis: checking their formation, processing and repair." DNA repair **8**(9): 1127-1138.
Lorenz, A., J. L. Wells, et al. (2004). "S. pombe meiotic linear elements contain proteins related to synaptonemal complex components." Journal of cell science **117**(Pt 15): 3343-3351.
Losada, A., M. Hirano, et al. (1998). "Identification of Xenopus SMC protein complexes required for sister chromatid cohesion." Genes & development **12**(13): 1986-1997.
MacQueen, A. J., M. P. Colaiacovo, et al. (2002). "Synapsis-dependent and -independent mechanisms stabilize homolog pairing during meiotic prophase in C. elegans." Genes Dev **16**(18): 2428-2442.
MacQueen, A. J., C. M. Phillips, et al. (2005). "Chromosome sites play dual roles to establish homologous synapsis during meiosis in C. elegans." Cell **123**(6): 1037-1050.
MacQueen, A. J. and A. M. Villeneuve (2001). "Nuclear reorganization and homologous chromosome pairing during meiotic prophase require C. elegans chk-2." Genes & development **15**(13): 1674-1687.
Maguire, M. P. (1966). "The relationship of crossing over to chromosome synapsis in a short paracentric inversion." Genetics **53**(6): 1071-1077.
Mailhes, J. B., C. Hilliard, et al. (2003). "Okadaic acid, an inhibitor of protein phosphatase 1 and 2A, induces premature separation of sister chromatids during meiosis I and aneuploidy in mouse oocytes in vitro." Chromosome research : an international journal on the molecular, supramolecular and evolutionary aspects of chromosome biology **11**(6): 619-631.
Malone, C. J., L. Misner, et al. (2003). "The C. elegans hook protein, ZYG-12, mediates the essential attachment between the centrosome and nucleus." Cell **115**(7): 825-836.
Marangos, P. and J. Carroll (2012). "Oocytes Progress beyond Prophase in the Presence of DNA Damage." Current biology : CB **22**(11): 989-994.

Martin, J. S., N. Winkelmann, et al. (2005). "RAD-51-dependent and -independent roles of a Caenorhabditis elegans BRCA2-related protein during DNA double-strand break repair." Molecular and cellular biology **25**(8): 3127-3139.
Martinez-Perez, E., M. Schvarzstein, et al. (2008). "Crossovers trigger a remodeling of meiotic chromosome axis composition that is linked to two-step loss of sister chromatid cohesion." Genes & development **22**(20): 2886-2901.
Martinez-Perez, E. and A. M. Villeneuve (2005). "HTP-1-dependent constraints coordinate homolog pairing and synapsis and promote chiasma formation during C. elegans meiosis." Genes & development **19**(22): 2727-2743.
Martini, E., R. L. Diaz, et al. (2006). "Crossover homeostasis in yeast meiosis." Cell **126**(2): 285-295.
McKee, B. D. (1996). "The license to pair: identification of meiotic pairing sites in Drosophila." Chromosoma **105**(3): 135-141.
McKim, K. S., B. L. Green-Marroquin, et al. (1998). "Meiotic synapsis in the absence of recombination." Science **279**(5352): 876-878.
McKim, K. S., A. M. Howell, et al. (1988). "The effects of translocations on recombination frequency in Caenorhabditis elegans." Genetics **120**(4): 987-1001.
Melby, T. E., C. N. Ciampaglio, et al. (1998). "The symmetrical structure of structural maintenance of chromosomes (SMC) and MukB proteins: long, antiparallel coiled coils, folded at a flexible hinge." The Journal of cell biology **142**(6): 1595-1604.
Mets, D. G. and B. J. Meyer (2009). "Condensins regulate meiotic DNA break distribution, thus crossover frequency, by controlling chromosome structure." Cell **139**(1): 73-86.
Minn, I. L., M. M. Rolls, et al. (2009). "SUN-1 and ZYG-12, mediators of centrosome-nucleus attachment, are a functional SUN/KASH pair in Caenorhabditis elegans." Molecular biology of the cell **20**(21): 4586-4595.
Moses, M. J. (1958). "The relation between the axial complex of meiotic prophase chromosomes and chromosome pairing in a salamander (Plethodon cinereus)." The Journal of biophysical and biochemical cytology **4**(5): 633-638.
Nabeshima, K., A. M. Villeneuve, et al. (2005). "Crossing over is coupled to late meiotic prophase bivalent differentiation through asymmetric disassembly of the SC." The Journal of cell biology **168**(5): 683-689.
Nabeshima, K., A. M. Villeneuve, et al. (2004). "Chromosome-wide regulation of meiotic crossover formation in Caenorhabditis elegans requires properly assembled chromosome axes." Genetics **168**(3): 1275-1292.
Nasmyth, K. and C. H. Haering (2009). "Cohesin: its roles and mechanisms." Annual review of genetics **43**: 525-558.
Nimmo, E. R., A. L. Pidoux, et al. (1998). "Defective meiosis in telomere-silencing mutants of Schizosaccharomyces pombe." Nature **392**(6678): 825-828.
Niu, H., L. Wan, et al. (2009). "Regulation of meiotic recombination via Mek1-mediated Rad54 phosphorylation." Molecular cell **36**(3): 393-404.
Obeso, D. and D. S. Dawson (2010). "Temporal characterization of homology-independent centromere coupling in meiotic prophase." PloS one **5**(4): e10336.
Oh, S. D., J. P. Lao, et al. (2008). "RecQ helicase, Sgs1, and XPF family endonuclease, Mus81-Mms4, resolve aberrant joint molecules during meiotic recombination." Molecular cell **31**(3): 324-336.
Page, S. L. and R. S. Hawley (2001). "c(3)G encodes a Drosophila synaptonemal complex protein." Genes & development **15**(23): 3130-3143.

Panizza, S., M. A. Mendoza, et al. (2011). "Spo11-accessory proteins link double-strand break sites to the chromosome axis in early meiotic recombination." Cell **146**(3): 372-383.
Parisi, S., M. J. McKay, et al. (1999). "Rec8p, a meiotic recombination and sister chromatid cohesion phosphoprotein of the Rad21p family conserved from fission yeast to humans." Molecular and cellular biology **19**(5): 3515-3528.
Pasierbek, P., M. Fodermayr, et al. (2003). "The Caenorhabditis elegans SCC-3 homologue is required for meiotic synapsis and for proper chromosome disjunction in mitosis and meiosis." Experimental cell research **289**(2): 245-255.
Pasierbek, P., M. Jantsch, et al. (2001). "A Caenorhabditis elegans cohesion protein with functions in meiotic chromosome pairing and disjunction." Genes & development **15**(11): 1349-1360.
Penkner, A., Z. Portik-Dobos, et al. (2007). "A conserved function for a Caenorhabditis elegans Com1/Sae2/CtIP protein homolog in meiotic recombination." The EMBO journal **26**(24): 5071-5082.
Penkner, A., L. Tang, et al. (2007). "The nuclear envelope protein Matefin/SUN-1 is required for homologous pairing in C. elegans meiosis." Dev Cell **12**(6): 873-885.
Penkner, A. M., A. Fridkin, et al. (2009). "Meiotic chromosome homology search involves modifications of the nuclear envelope protein Matefin/SUN-1." Cell **139**(5): 920-933.
Peoples, T. L., E. Dean, et al. (2002). "Close, stable homolog juxtaposition during meiosis in budding yeast is dependent on meiotic recombination, occurs independently of synapsis, and is distinct from DSB-independent pairing contacts." Genes & development **16**(13): 1682-1695.
Petalcorin, M. I., V. E. Galkin, et al. (2007). "Stabilization of RAD-51-DNA filaments via an interaction domain in Caenorhabditis elegans BRCA2." Proceedings of the National Academy of Sciences of the United States of America **104**(20): 8299-8304.
Petalcorin, M. I., J. Sandall, et al. (2006). "CeBRC-2 stimulates D-loop formation by RAD-51 and promotes DNA single-strand annealing." Journal of molecular biology **361**(2): 231-242.
Petronczki, M., M. F. Siomos, et al. (2003). "Un menage a quatre: the molecular biology of chromosome segregation in meiosis." Cell **112**(4): 423-440.
Phillips, C. M. and A. F. Dernburg (2006). "A family of zinc-finger proteins is required for chromosome-specific pairing and synapsis during meiosis in C. elegans." Dev Cell **11**(6): 817-829.
Phillips, C. M., X. Meng, et al. (2009). "Identification of chromosome sequence motifs that mediate meiotic pairing and synapsis in C. elegans." Nat Cell Biol **11**(8): 934-942.
Phillips, C. M., C. Wong, et al. (2005). "HIM-8 binds to the X chromosome pairing center and mediates chromosome-specific meiotic synapsis." Cell **123**(6): 1051-1063.
Rasmussen, S. W. and P. B. Holm (1984). "The synaptonemal complex, recombination nodules and chiasmata in human spermatocytes." Symposia of the Society for Experimental Biology **38**: 271-292.
Reddy, K. C. and A. M. Villeneuve (2004). "C. elegans HIM-17 links chromatin modification and competence for initiation of meiotic recombination." Cell **118**(4): 439-452.

Riedel, C. G., V. L. Katis, et al. (2006). "Protein phosphatase 2A protects centromeric sister chromatid cohesion during meiosis I." Nature **441**(7089): 53-61.
Rinaldo, C., P. Bazzicalupo, et al. (2002). "Roles for Caenorhabditis elegans rad-51 in meiosis and in resistance to ionizing radiation during development." Genetics **160**(2): 471-479.
Rogers, E., J. D. Bishop, et al. (2002). "The aurora kinase AIR-2 functions in the release of chromosome cohesion in Caenorhabditis elegans meiosis." The Journal of cell biology **157**(2): 219-229.
Rollins, R. A., M. Korom, et al. (2004). "Drosophila nipped-B protein supports sister chromatid cohesion and opposes the stromalin/Scc3 cohesion factor to facilitate long-range activation of the cut gene." Molecular and cellular biology **24**(8): 3100-3111.
Rose, A. M., D. L. Baillie, et al. (1984). "Meiotic pairing behavior of two free duplications of linkage group I in Caenorhabditis elegans." Molecular & general genetics : MGG **195**(1-2): 52-56.
Rosenbluth, R. E. and D. L. Baillie (1981). "The genetic analysis of a reciprocal translocation, eT1(III; V), in Caenorhabditis elegans." Genetics **99**(3-4): 415-428.
Rosu, S., D. E. Libuda, et al. (2011). "Robust crossover assurance and regulated interhomolog access maintain meiotic crossover number." Science **334**(6060): 1286-1289.
Saito, T. T., F. Mohideen, et al. (2012). "SLX-1 is required for maintaining genomic integrity and promoting meiotic noncrossovers in the Caenorhabditis elegans germline." PLoS genetics **8**(8): e1002888.
Saito, T. T., J. L. Youds, et al. (2009). "Caenorhabditis elegans HIM-18/SLX-4 interacts with SLX-1 and XPF-1 and maintains genomic integrity in the germline by processing recombination intermediates." PLoS genetics **5**(11): e1000735.
San-Segundo, P. A. and G. S. Roeder (1999). "Pch2 links chromatin silencing to meiotic checkpoint control." Cell **97**(3): 313-324.
Sanford, C. and M. D. Perry (2001). "Asymmetrically distributed oligonucleotide repeats in the Caenorhabditis elegans genome sequence that map to regions important for meiotic chromosome segregation." Nucleic acids research **29**(14): 2920-2926.
Sato, A., B. Isaac, et al. (2009). "Cytoskeletal forces span the nuclear envelope to coordinate meiotic chromosome pairing and synapsis." Cell **139**(5): 907-919.
Scherthan, H. (2001). "A bouquet makes ends meet." Nat Rev Mol Cell Biol **2**(8): 621-627.
Schild-Prufert, K., T. T. Saito, et al. (2011). "Organization of the synaptonemal complex during meiosis in Caenorhabditis elegans." Genetics **189**(2): 411-421.
Schmitt, J., R. Benavente, et al. (2007). "Transmembrane protein Sun2 is involved in tethering mammalian meiotic telomeres to the nuclear envelope." Proceedings of the National Academy of Sciences of the United States of America **104**(18): 7426-7431.
Schramm, S., J. Fraune, et al. (2011). "A novel mouse synaptonemal complex protein is essential for loading of central element proteins, recombination, and fertility." PLoS genetics **7**(5): e1002088.
Schumacher, B., K. Hofmann, et al. (2001). "The C. elegans homolog of the p53 tumor suppressor is required for DNA damage-induced apoptosis." Current biology : CB **11**(21): 1722-1727.

Schumacher, B., C. Schertel, et al. (2005). "C. elegans ced-13 can promote apoptosis and is induced in response to DNA damage." Cell death and differentiation **12**(2): 153-161.
Schwacha, A. and N. Kleckner (1995). "Identification of double Holliday junctions as intermediates in meiotic recombination." Cell **83**(5): 783-791.
Seitan, V. C., P. Banks, et al. (2006). "Metazoan Scc4 homologs link sister chromatid cohesion to cell and axon migration guidance." PLoS biology **4**(8): e242.
Severson, A. F., L. Ling, et al. (2009). "The axial element protein HTP-3 promotes cohesin loading and meiotic axis assembly in C. elegans to implement the meiotic program of chromosome segregation." Genes & development **23**(15): 1763-1778.
Sheridan, S. and D. K. Bishop (2006). "Red-Hed regulation: recombinase Rad51, though capable of playing the leading role, may be relegated to supporting Dmc1 in budding yeast meiosis." Genes & development **20**(13): 1685-1691.
Shin, Y. H., Y. Choi, et al. (2010). "Hormad1 mutation disrupts synaptonemal complex formation, recombination, and chromosome segregation in mammalian meiosis." PLoS genetics **6**(11): e1001190.
Smolikov, S., A. Eizinger, et al. (2007). "Synapsis-defective mutants reveal a correlation between chromosome conformation and the mode of double-strand break repair during Caenorhabditis elegans meiosis." Genetics **176**(4): 2027-2033.
Smolikov, S., A. Eizinger, et al. (2007). "SYP-3 restricts synaptonemal complex assembly to bridge paired chromosome axes during meiosis in Caenorhabditis elegans." Genetics **176**(4): 2015-2025.
Smolikov, S., K. Schild-Prufert, et al. (2008). "CRA-1 uncovers a double-strand break-dependent pathway promoting the assembly of central region proteins on chromosome axes during C. elegans meiosis." PLoS genetics **4**(6): e1000088.
Smolikov, S., K. Schild-Prufert, et al. (2009). "A yeast two-hybrid screen for SYP-3 interactors identifies SYP-4, a component required for synaptonemal complex assembly and chiasma formation in Caenorhabditis elegans meiosis." PLoS genetics **5**(10): e1000669.
Sosa, B. A., A. Rothballer, et al. (2012). "LINC complexes form by binding of three KASH peptides to domain interfaces of trimeric SUN proteins." Cell **149**(5): 1035-1047.
St-Pierre, J., M. Douziech, et al. (2009). "Polo kinase regulates mitotic chromosome condensation by hyperactivation of condensin DNA supercoiling activity." Molecular cell **34**(4): 416-426.
Stergiou, L., K. Doukoumetzidis, et al. (2007). "The nucleotide excision repair pathway is required for UV-C-induced apoptosis in Caenorhabditis elegans." Cell death and differentiation **14**(6): 1129-1138.
Sturtevant, A. H. (1913). "A Third Group of Linked Genes in Drosophila Ampelophila." Science **37**(965): 990-992.
Sugiyama, T., J. H. New, et al. (1998). "DNA annealing by RAD52 protein is stimulated by specific interaction with the complex of replication protein A and single-stranded DNA." Proceedings of the National Academy of Sciences of the United States of America **95**(11): 6049-6054.
Sun, H., D. Treco, et al. (1991). "Extensive 3'-overhanging, single-stranded DNA associated with the meiosis-specific double-strand breaks at the ARG4 recombination initiation site." Cell **64**(6): 1155-1161.

Sym, M., J. A. Engebrecht, et al. (1993). "ZIP1 is a synaptonemal complex protein required for meiotic chromosome synapsis." Cell **72**(3): 365-378.
Szostak, J. W., T. L. Orr-Weaver, et al. (1983). "The double-strand-break repair model for recombination." Cell **33**(1): 25-35.
Tabara, H., A. Grishok, et al. (1998). "RNAi in C. elegans: soaking in the genome sequence." Science **282**(5388): 430-431.
Tang, L., T. Machacek, et al. (2010). "Mutations in Caenorhabditis elegans him-19 show meiotic defects that worsen with age." Molecular biology of the cell **21**(6): 885-896.
Timmons, L. and A. Fire (1998). "Specific interference by ingested dsRNA." Nature **395**(6705): 854.
Tonkin, E. T., T. J. Wang, et al. (2004). "NIPBL, encoding a homolog of fungal Scc2-type sister chromatid cohesion proteins and fly Nipped-B, is mutated in Cornelia de Lange syndrome." Nature genetics **36**(6): 636-641.
Trelles-Sticken, E., C. Adelfalk, et al. (2005). "Meiotic telomere clustering requires actin for its formation and cohesin for its resolution." The Journal of cell biology **170**(2): 213-223.
Trelles-Sticken, E., M. E. Dresser, et al. (2000). "Meiotic telomere protein Ndj1p is required for meiosis-specific telomere distribution, bouquet formation and efficient homologue pairing." The Journal of cell biology **151**(1): 95-106.
Trowbridge, K., K. McKim, et al. (2007). "Synthetic lethality of Drosophila in the absence of the MUS81 endonuclease and the DmBlm helicase is associated with elevated apoptosis." Genetics **176**(4): 1993-2001.
Tsubouchi, H. and G. S. Roeder (2006). "Budding yeast Hed1 down-regulates the mitotic recombination machinery when meiotic recombination is impaired." Genes & development **20**(13): 1766-1775.
Tsubouchi, T. and G. S. Roeder (2005). "A synaptonemal complex protein promotes homology-independent centromere coupling." Science **308**(5723): 870-873.
Tzur, Y. B., A. Margalit, et al. (2006). "Matefin/SUN-1 is a nuclear envelope receptor for CED-4 during Caenorhabditis elegans apoptosis." Proceedings of the National Academy of Sciences of the United States of America **103**(36): 13397-13402.
Uhlmann, F., F. Lottspeich, et al. (1999). "Sister-chromatid separation at anaphase onset is promoted by cleavage of the cohesin subunit Scc1." Nature **400**(6739): 37-42.
Villeneuve, A. M. (1994). "A cis-acting locus that promotes crossing over between X chromosomes in Caenorhabditis elegans." Genetics **136**(3): 887-902.
Wang, F., J. Yoder, et al. (2003). "Caenorhabditis elegans EVL-14/PDS-5 and SCC-3 are essential for sister chromatid cohesion in meiosis and mitosis." Molecular and cellular biology **23**(21): 7698-7707.
Watrin, E., A. Schleiffer, et al. (2006). "Human Scc4 is required for cohesin binding to chromatin, sister-chromatid cohesion, and mitotic progression." Current biology : CB **16**(9): 863-874.
Watt, F. M. and B. L. Hogan (2000). "Out of Eden: stem cells and their niches." Science **287**(5457): 1427-1430.
Webber, H. A., L. Howard, et al. (2004). "The cohesion protein ORD is required for homologue bias during meiotic recombination." The Journal of cell biology **164**(6): 819-829.
Weiner, B. M. and N. Kleckner (1994). "Chromosome pairing via multiple interstitial interactions before and during meiosis in yeast." Cell **77**(7): 977-991.

Whitby, M. C., F. Osman, et al. (2003). "Cleavage of model replication forks by fission yeast Mus81-Eme1 and budding yeast Mus81-Mms4." The Journal of biological chemistry **278**(9): 6928-6935.
Woglar, A., A. Daryabeigi, et al. (2013). "Matefin/SUN-1 Phosphorylation Is Part of a Surveillance Mechanism to Coordinate Chromosome Synapsis and Recombination with Meiotic Progression and Chromosome Movement." PLoS genetics **9**(3): e1003335.
Wojtasz, L., K. Daniel, et al. (2009). "Mouse HORMAD1 and HORMAD2, two conserved meiotic chromosomal proteins, are depleted from synapsed chromosome axes with the help of TRIP13 AAA-ATPase." PLoS genetics **5**(10): e1000702.
Wood, A. J., T. W. Lo, et al. (2011). "Targeted genome editing across species using ZFNs and TALENs." Science **333**(6040): 307.
Wu, H. Y. and S. M. Burgess (2006). "Two distinct surveillance mechanisms monitor meiotic chromosome metabolism in budding yeast." Current biology : CB **16**(24): 2473-2479.
Xu, L., B. M. Weiner, et al. (1997). "Meiotic cells monitor the status of the interhomolog recombination complex." Genes & development **11**(1): 106-118.
Yildiz, O., S. Majumder, et al. (2002). "Drosophila MUS312 interacts with the nucleotide excision repair endonuclease MEI-9 to generate meiotic crossovers." Molecular cell **10**(6): 1503-1509.
Yokoo, R., K. A. Zawadzki, et al. (2012). "COSA-1 reveals robust homeostasis and separable licensing and reinforcement steps governing meiotic crossovers." Cell **149**(1): 75-87.
Youds, J. L., D. G. Mets, et al. (2010). "RTEL-1 enforces meiotic crossover interference and homeostasis." Science **327**(5970): 1254-1258.
Zakharyevich, K., S. Tang, et al. (2012). "Delineation of joint molecule resolution pathways in meiosis identifies a crossover-specific resolvase." Cell **149**(2): 334-347.
Zalevsky, J., A. J. MacQueen, et al. (1999). "Crossing over during Caenorhabditis elegans meiosis requires a conserved MutS-based pathway that is partially dispensable in budding yeast." Genetics **153**(3): 1271-1283.
Zanders, S. and E. Alani (2009). "The pch2Delta mutation in baker's yeast alters meiotic crossover levels and confers a defect in crossover interference." PLoS genetics **5**(7): e1000571.
Zetka, M. C., I. Kawasaki, et al. (1999). "Synapsis and chiasma formation in Caenorhabditis elegans require HIM-3, a meiotic chromosome core component that functions in chromosome segregation." Genes & development **13**(17): 2258-2270.
Zhang, W., N. Miley, et al. (2012). "HAL-2 promotes homologous pairing during Caenorhabditis elegans meiosis by antagonizing inhibitory effects of synaptonemal complex precursors." PLoS genetics **8**(8): e1002880.
Zhao, H. and H. Piwnica-Worms (2001). "ATR-mediated checkpoint pathways regulate phosphorylation and activation of human Chk1." Molecular and cellular biology **21**(13): 4129-4139.
Zickler, D. (1977). "Development of the synaptonemal complex and the "recombination nodules" during meiotic prophase in the seven bivalents of the fungus Sordaria macrospora Auersw." Chromosoma **61**(4): 289-316.

Curriculum vitae

Name:	Alexander Woglar
Date of birth:	16.12.1983
Place of birth:	Salzburg
Nationality:	Austria

Education and working experience

1990 - 1994	Elementary school Elixhausen
1994 - 2002	Christian Doppler Gymnasium Salzburg
June 2002	Matriculation examination („Matura“ CD-Gymnasium Salzburg)
October 2002 - October 2003	Civil servant (Red Cross organization Salzburg)
October 2003 - May 2008	Biology at the University of Wien
Oktober 2006 - May 2008	Diploma thesis in molecular genetics (Franz Klein lab at the Dep. of Chromosome Biology at the MFPL, University of Wien (Mag.rer. nat)
May 2008 - March 2009	CTA at the MFPL, University of Vienna (Dep. of Chromosome Biology)
May 2009 - March 2013	PhD studies (Verena Jantsch lab) at the Dep. of Chromosome Biology (MFPL) supported by a DOC-scholarship (3 years) from the Austrian Academy of science (OeAdW)

Appendix

Cell

Meiotic Chromosome Homology Search Involves Modifications of the Nuclear Envelope Protein Matefin/SUN-1

Alexandra M. Penkner,[1,*] Alexandra Fridkin,[2,*] Jiradet Gloggnitzer,[1] Antoine Baudrimont,[1] Thomas Machacek,[1] Alexander Woglar,[1] Edina Csaszar,[3] Pawel Pasierbek,[4] Gustav Ammerer,[3] Yosef Gruenbaum,[2] and Verena Jantsch[1,*]
[1]Department of Chromosome Biology, Max F. Perutz Laboratories, University of Vienna, 1030-Vienna, Austria
[2]Department of Genetics, Hebrew University of Jerusalem, 91904 Jerusalem, Israel
[3]Mass Spectrometry Unit, Max F. Perutz Laboratories, University of Vienna, 1030-Vienna, Austria
[4]Research Institute of Molecular Pathology, 1030-Vienna, Austria
*Correspondence: alexandra.penkner@univie.ac.at (A.M.P.), moloko@cc.huji.ac.il (A.F.), verena.jantsch@univie.ac.at (V.J.)
DOI 10.1016/j.cell.2009.10.045

SUMMARY

Genome haploidization during meiosis depends on recognition and association of parental homologous chromosomes. The *C. elegans* SUN/KASH domain proteins Matefin/SUN-1 and ZYG-12 have a conserved role in this process. They bridge the nuclear envelope, connecting the cytoplasm and the nucleoplasm to transmit forces that allow chromosome movement and homolog pairing and prevent nonhomologous synapsis. Here, we show that Matefin/SUN-1 forms rapidly moving aggregates at putative chromosomal attachment sites in the meiotic transition zone (TZ). We analyzed requirements for aggregate formation and identified multiple phosphotarget residues in the nucleoplasmic domain of Matefin/SUN-1. These CHK-2 dependent phosphorylations occur in leptotene/zygotene, diminish during pachytene and are involved in pairing. Mimicking phosphorylation causes an extended TZ and univalents at diakinesis. Our data suggest that the properties of the nuclear envelope are altered during the time window when homologs are sorted and Matefin/SUN-1 aggregates form, thereby controling the movement, homologous pairing and interhomolog recombination of chromosomes.

INTRODUCTION

Homologous chromosomes are segregated to opposite cell poles at the first meiotic division to accomplish genome haploidization. To assure their proper alignment on the metaphase spindle, homologs have to identify each other to allow the generation of a physical connection between them. How homolog recognition and correct pairing is established is a question under intense investigation (for review, see Petronczki et al., 2003; Pawlowski and Cande, 2005; Bhalla and Dernburg, 2008).

Integral nuclear envelope (NE) proteins play a conserved role in homolog pairing in eukaryotes (for review, see Fridkin et al., 2009; Alsheimer, 2009; Starr, 2009). Inner and outer nuclear membrane proteins (SUN/KASH proteins) bridge the NE by the interaction of their conserved C-terminal domains within the perinuclear space. While the N terminus of the SUN domain protein faces the nucleoplasm, the N terminus of the KASH domain protein protrudes into the cytoplasm, thus allowing the connection of nuclear components to cytoplasmic structures, such as the cytoskeleton (Tzur et al., 2006).

Chromosome ends attachment to the NE is dependent on SUN domain-bearing inner NE proteins as shown for yeast and mammals. SUN domain proteins aggregate at the site of telomere attachment to the NE, and their absence causes a randomized localization of telomeres within the nucleus (Conrad et al., 2007, 2008; Chikashige et al., 2006; Ding et al., 2007). In rodents, SUN domain proteins are engaged in the formation of attachment plaques, electron-dense plates observed at the site where conically thickened chromosome ends attach to the nucleoplasmic side of the NE (Schmitt et al., 2007). At these sites, the nuclear membrane is spanned by fibrils that are connected to cytoplasmic structures (Alsheimer, 2009; Scherthan, 2007).

During meiotic prophase I, chromosomes display pronounced movements. In *S. cerevisiae*, the motility of chromosome ends during prophase I is driven by actin-based motors, whereas in *S. pombe*, tubulin motors likely drive chromosome ends into the bouquet and the chromosomes in a horsetail configuration (Trelles-Sticken et al., 2005; Scherthan et al., 2007; Koszul et al., 2008; Ding et al., 1998; Yamamoto et al., 1999; Chikashige et al., 2006). In yeast and mammals, chromosomes also transiently adopt a polarized configuration termed the "chromosomal bouquet." The timing of telomere clustering coincides with chromosome pairing, synapsis, and recombination (for review, see Scherthan, 2007; Harper et al., 2004). Interference with SUN domain proteins or their interactors abrogates bouquet formation (Conrad et al., 2007; Ding et al., 2007; Chikashige et al., 2006; Tang et al., 2006).

Once homologs have paired, a proteinaceous structure, the synaptonemal complex (SC), assembles between them. Stable,

close juxtaposition of homologs is a prerequisite for the repair of deliberately induced DNA double-strand breaks (DSBs) to generate crossovers by homologous recombination. In budding yeast, the timely repair of meiotic DSBs depends on chromosome movement during very early steps in meiotic recombination. This movement supports the removal of nonspecific chromosomal interactions and entanglements, thus ensuring homolog juxtaposition along the entire length of the chromosome. Additionally, these chromosome movements promote later steps during recombination, possibly by affecting chromatin structure (Koszul et al., 2008; Conrad et al., 2008; Kosaka et al., 2008; Wanat et al., 2008).

The *C. elegans* inner NE protein Matefin/SUN-1 is expressed in the germline in adult hermaphrodites and in embryos (Fridkin et al., 2004). A missense mutation within the conserved SUN domain strongly reduces the retention of the KASH protein ZYG-12 at the outer membrane of the NE and completely abrogates homolog alignment. Instead, nonhomologous synapsis is prematurely established (Penkner et al., 2007).

In *C. elegans*, only the pairing center (PC)-carrying chromosome end attaches to the NE upon entry into meiosis (Goldstein and Slaton, 1982; Phillips et al., 2005; Phillips and Dernburg, 2006). The PC or homolog recognition region (HRR) comprises a *cis*-acting chromosomal region responsible for the pairing and synapsis of homologs (MacQueen et al., 2005). PC regions have to interact with one of four zinc-finger proteins termed ZIM-1, ZIM-2, ZIM-3, and HIM-8 (Phillips et al., 2005; Phillips and Dernburg, 2006) and are sufficient to mediate pairing and synapsis when ectopically inserted into a different chromosome (Phillips et al., 2009). Independent of recombination, the PCs establish the first contacts between homologous chromosomes in the transition zone (TZ) corresponding to the leptotene/zygotene stage in *C. elegans* (MacQueen et al., 2005; Phillips et al., 2005; Phillips and Dernburg, 2006; Dernburg et al., 1998). Clustering of chromosomes within a subvolume of the nucleus strongly correlates with an ongoing homology search (Couteau et al., 2004; MacQueen and Villeneuve, 2001). In pachytene, when chromosomes are synapsed, chromosomes disperse and adopt a homogeneous arrangement at the nuclear periphery. At this stage DSBs are repaired by homologous recombination.

Here, we describe a dramatic change in properties of the NE protein Matefin/SUN-1, especially during the time window of ongoing homologous pairing and chromosome movement. Matefin/SUN-1 forms dynamic local aggregates at the site of the chromosome end attachment to the NE. Chromosome end movement in the TZ requires a functional SUN domain. An intact SUN domain correlates with size changes of Matefin/SUN-1 aggregates and chromatin clustering and is essential for homologous pairing. At the same time, the nuclear N terminus of Matefin/SUN-1 is phosphorylated at multiple serines and the presence of the modification correlates with the presence of polarized chromatin. Phosphorylations of Matefin/SUN-1 impact faithful bivalent formation and suggest a connection to the regulation of Matefin/SUN-1 aggregate formation/resolution. Furthermore, we have examined triggers and factors responsible for Matefin/SUN-1 phosphorylation during leptotene/zygotene.

RESULTS

Matefin/SUN-1 Redistributes during the Time Window of Homologous Pairing

A C-terminally GFP-tagged Matefin/SUN-1 transgene was generated to allow high-resolution cytological analysis and biochemical purification. The transgene is fully functional as it rescues the highly reduced brood size and the embryonic lethality of *mtf-1/sun-1(ok1282)* knockout worms (Table S1 available online). The expression and localization patterns of SUN-1::GFP fully overlap with those of the endogenous protein (Figure 1B and data not shown; hereafter, we refer to Matefin/SUN-1 as SUN-1). SUN-1::GFP localizes to the NE of germline nuclei in hermaphrodites (Figure 1A) (Fridkin et al., 2004; Penkner et al., 2007) and males (data not shown). SUN-1 colocalizes with ZYG-12ABC::GFP in mitosis (Malone et al., 2003) (data not shown) and during meiotic prophase I (Figure 1B). This and the fact that we could coprecipitate both proteins (Figure 1E) support the assumption that SUN-1 and ZYG-12 interact in vivo. Furthermore, the western blot demonstrates that SUN-1 forms dimers/multimers in vivo.

The progressive developmental stages of meiotic prophase I can be found in a spatial gradient from distal to proximal in the *C. elegans* gonad. Mitotic precursor cells display a uniform rim-like GFP signal enclosing the chromatin and highlighting the centrosome as evidenced by the colocalization with the centrosomal marker SPD-5 (Hamill et al., 2002) (Figures 1A and 1D). Once germline nuclei enter the TZ, SUN-1 redistributes and forms aggregates of variable size and number (see also Sato et al., 2009). In contrast to mitosis, SUN-1 aggregates in the TZ do not mark the centrosome (Figure 1D) (Penkner et al., 2007).

In addition to the local enrichment of SUN-1::GFP, a weak protein signal is detectable along the remaining NE. The majority of aggregates are observed in the TZ. SUN-1 aggregates disassemble concomitantly with the redispersal of chromosomes in mid-prophase (Figure 1A). In nuclei in later prophase I, SUN-1::GFP distributes uniformly. We conclude that SUN-1/ZYG-12 protein complexes undergo extensive reorganization within the nuclear periphery during prophase I.

The localization pattern of SUN-1 and ZYG-12::GFP in the TZ is reminiscent of the distribution of all four PC-binding proteins (Phillips and Dernburg, 2006). In the TZ, the signal of the PC-proteins HIM-8 (X chromosome) and ZIM-3 (chromosomes I and IV) overlaps with SUN-1 aggregates (Figure 1C, ii and iv), demonstrating that PC-containing chromosome ends localize to the nuclear periphery at the sites of SUN-1 aggregation. SUN-1 aggregates likely represent an equivalent to chromosomal attachment plaques to the NE.

The Formation of SUN-1 Aggregates Requires Establishment of Chromosome Axes, CHK-2 Kinase Activity, and Chromosome Movement

We next analyzed genes that are likely to play a role in the establishment and/or kinetics of SUN-1 aggregates. SUN-1::GFP and HIM-8 were coimmunostained in various mutant gonads subdivided into six zones of equal length. We counted the number and size of aggregates per nucleus for each zone and analyzed their colocalization with HIM-8 (Figures 2A and S1). Spherical

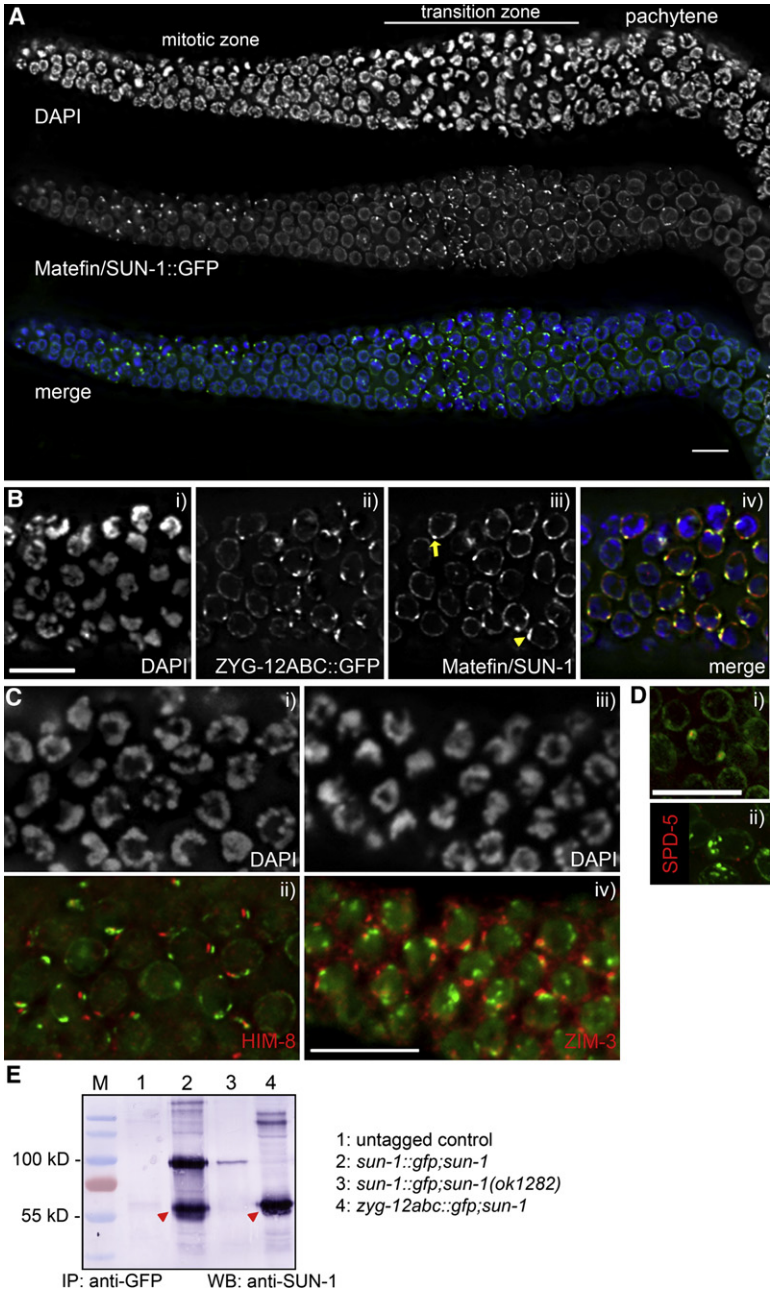

Figure 1. SUN-1 Forms Aggregates at the Nuclear Envelope during the Time of Ongoing Homolog Pairing

(A) A *mtf-1/sun-1::gfp;mtf-1/sun-1(ok1282)* hermaphrodite gonad expressing SUN-1::GFP (middle, green in merge) was stained for DNA with DAPI (top, blue in merge).

(B) SUN-1 staining (iii, red in merge) of hermaphrodite gonads expressing ZYG-12ABC::GFP (ii, green in merge). i, DAPI; iv, merge. The yellow arrowhead marks the position of a patch, while the yellow arrow highlights a focus.

(C) DAPI staining (i, iii) and antibody staining (ii, iv). PC-binding proteins HIM-8 or ZIM-3 (red) are shown in combination with SUN-1::GFP (green). The green channel is shifted to the right to allow better visualization of green and red signals.

(D) Centrosome marked by SPD-5 staining (red) in mitotic (i) and meiotic (ii, transition zone) nuclei expressing SUN-1::GFP (green). Scale bars represent 10 μm.

(E) Western blot to show the in vivo interaction of ZYG-12ABC::GFP and endogenous SUN-1 (54 kD, red arrowheads). Coimmunoprecipitations were performed with anti-GFP antibodies. SUN-1 was detected with anti-SUN-1 antibodies. Genotypes are on the right.

SUN-1::GFP aggregates with a diameter <1.1 μm were classified as foci (yellow arrow in Figure 2B). Aggregates elongated in one dimension (≥1.1 μm) were termed patches (yellow arrowhead in Figure 2B).

In hermaphrodite gonads expressing the transgenic SUN-1::GFP and lacking endogenous SUN-1 (referred to as wild-type), zones 2 to 4, including the TZ and early pachytene, showed both foci and patches (Figure 2A). Maximum aggregate formation was observed in zone 3, with 75% of nuclei displaying mostly two to three and up to four patches. In zone 3, in addition to patches, 30% of the nuclei formed foci, usually one to two. In contrast to the zone 2, where almost all nuclei displayed both foci and patches, more than half of the nuclei with aggregates did not form foci (Figure 2A). Combined, zones 2 and 3 (the TZ) nuclei had an average of 1.9 patches (n = 137, SD = 1.3) and 1.0 focus (SD = 1.4) (Table S2).

While most patches disassembled within zone 4 (early pachytene), the patch colocalizing with HIM-8 remained into zone 5 (mid-pachytene) (Figure S1), suggesting that X chromosome aggregates persist longer than autosomal ones.

SYP-2 comprises a central element component of the SC. Besides a defect in the assembly of the SC, *syp-2(ok307)* is defective in the timely redistribution of chromatin, as seen by a prolongation of the TZ (Colaiácovo et al., 2003). In *syp-2(ok307)*, SUN-1 aggregates extend into zone 5. Foci are even present until late pachytene (zone 6). Maximum patch formation is observed from zones 2–4. While patch formation is slightly reduced as compared to that of the wild-type (an average of 1.4 patches is seen in zones 2 and 3 [SD = 0.9, n = 122]), SUN-1 foci are significantly more abundant in *syp-2(ok307)* (x = 3.4, SD = 2.2 in zones 2 and 3; Student's t test, p = 6.33E-22) (Table S2). Foci are already seen upon entry into meiosis (zone 1) and reach a maximum in zone 4, concomitant with the start of disassembly of patches. Interestingly, while wild-type nuclei always display foci in addition to patches, *syp-2* nuclei in zones 2–4 can display foci without having patches.

him-3(gk149) lacks the chromosome axis component HIM-3, which is essential for homologous pairing, synapsis, and spatial chromatin rearrangement (Couteau et al., 2004). In *him-3,* SUN-1 foci form, but no more than one patch was observed in zone 2. The reduced patch formation is reflected by an average of 0.5 patches in zones 2 and 3 (n = 129, SD = 0.5; Student's t test, p = 3.14E-24), while an average of 1.8 foci (SD = 1.4) documents

an increase in focus formation (Student's t test; p = 2.89E-06) (Table S2). SUN-1 foci are present from zone 2 until zone 5, with the maximum number of nuclei displaying foci in zone 3 (90%). These data demonstrate that HIM-3 is required for efficient aggregate formation.

The serine/threonine kinase mutant *chk-2(me64)* lacks a TZ. It is deficient in homologous alignment and DSB formation (MacQueen and Villeneuve, 2001). SUN-1 aggregates were not observed in *chk-2(me64)*.

A point mutation within the SUN domain of SUN-1 (*mtf-1/sun-1(jf18)*) causes reduced ZYG-12 retention at the NE and a failure in homolog alignment and chromatin polarization (Penkner et al., 2007). A GFP transgene engineered with this mutation, SUN-1 (G311V)::GFP, does not form patches. Instead, numerous foci ($x = 9.6 \pm 1.6$ aggregates; ranging from 7 to 12 foci; n = 17 nuclei) are present in early meiotic nuclei (Figure 2B) that colocalize with PC-binding proteins such as HIM-8 and ZIM-3 (Figure 2B and data not shown). They mark sites of chromosome end attachment to the NE. Time-lapse microscopy of SUN-1::GFP aggregates showed displacement tracks distributed over a subarea of the NE covering the underlying polarized chromatin. In striking contrast, SUN-1(G311V)::GFP aggregates were only mildly shifted, suggesting that chromosome ends barely moved (Figure 2C and Movies S1–S3; detailed analysis of chromosome movement will be published elsewhere).

Taken together, our data demonstrate a correlation between chromatin polarization and SUN-1 aggregate formation. Patches were only observed at the NE of nuclei with clustered chromatin, consistent with the observations that they require CHK-2 activity and that they disassemble concomitantly with chromatin rearrangement in pachytene. The data also suggest that chromosome ends are moved in the TZ by a mechanism that requires a functional SUN domain of SUN-1. Chromosome clustering is a consequence of the movement of chromosome ends and not a consequence of relocating the nucleolus.

In both wild-type and mutant situations, unpaired HIM-8 foci overlapped with SUN-1 foci. We therefore hypothesize that these foci mark the NE attachment sites of single chromosome ends. Consistently, patches correspond to areas where multiple chromosome ends meet. Patches are not formed in the absence of chromosome end movement.

The N Terminus of SUN-1 Is Modified in Leptotene/Zygotene

Antibodies recognizing an N-terminal peptide of SUN-1 (Fridkin et al., 2004) disclosed an unexpected staining pattern in wild-type hermaphrodite gonads (compare SUN-1 levels in Figures 3A and 3B). While germline nuclei in the mitotic zone and later prophase I showed a clear reactivity with these antibodies, the signal intensity was strikingly weaker in nuclei in leptotene/zygotene (TZ). Asynchronous, interspersed nuclei, which display a uniform distribution of chromatin, also exhibit enhanced SUN-1 signals compared to nuclei that surround the TZ (Figure 3B, red stars).

The reduced staining of the nuclear periphery could be correlated with polarization of the chromatin characteristic for TZ nuclei, over a prolonged zone like in *syp-2(ok307)*, conversely reduced to a few nuclei [*him-3(gk149)*] or was completely absent [*chk-2(me64)*], (Figure 3C). We hypothesized that the N-terminal epitope/s recognized by the antibodies is/are transiently and reversibly masked during the time of homolog pairing.

The N Terminus of SUN-1 Is Phosphorylated at Multiple Serines

To determine potential posttranslational modifications of SUN-1, we performed mass spectrometry analysis on immunoprecipitated SUN-1::GFP from strains producing embryos or devoid of embryos. Multiple phosphorylated residues in SUN-1's N terminus were identified (protein coverage of ~90%; Figures 4B and S2) No differential phosphorylation sites could be uncovered from extracts devoid of embryos (Figure S3). In total, six phosphorylated serines (Ser8, Ser12, Ser24, Ser43, Ser58, and Ser62) and one phosphorylated serine or threonine (Ser35 or Thr36) showed reproducible mass spectrometry results (Figure 4B). Difficulties arose from the discrimination between putative phosphorylations of Ser12 or Ser16. Ser12, however, is considered to be the most probable candidate for a phosphorylation site (see below and Figures S2 and S3). Moreover, Ser35 and Thr36 are equally likely to be phosphorylated.

Antibodies directed against the phosphoepitope of Ser8 (S8-Pi) were raised and their specificity verified [dot blot experiments and lack of immunofluoresence of the SUN-1(S8A)::GFP line, data not shown]. In the mitotic zone, S8-Pi antibodies stained the NE and centrosomes. The rim-like staining at the nuclear periphery was observed from prometaphase onward, concomitant with the beginning of chromatin condensation (Figure 4C). Interestingly, the phosphorylation signal became stronger as the nuclei proceeded through mitosis. A strong signal was also detected in diakinesis nuclei.

In meiosis, staining of S8-Pi was first detected in the TZ, highlighting SUN-1 protein localized in foci and patches, as well as over the rest of the NE (Figure 4C). S8-Pi was most prevalent until early pachytene, when the aggregates disappeared. The signal became continuously weaker and eventually disappeared in later pachytene. Prolonged S8-Pi staining was observed in *syp-2(ok307)*, which develops an extended TZ. The peak of staining was seen in nuclei with clustered chromatin (Figure S4A). SUN-1 Ser12 and Ser24 exhibit a comparable phosphorylation pattern in wild-type and *syp-2(ok307)* hermaphrodite gonads. Centrosomal SUN-1 is detectable in mitosis, and the antibodies highlight the SUN-1 population located in aggregates during early meiosis (Figures S4B and S4C).

The phosphorylations of SUN-1 during the time window of ongoing homology search, when chromatin is polarized and SUN-1::GFP aggregates are formed, and the dephosphorylations concomitant with the redistribution of paired chromosomes support a potential role for SUN-1 phosphorylation in homologous pairing.

The CHK-2 Kinase Is Required for SUN-1 Phosphorylation in Meiosis

We analyzed the regulation of Matefin Ser8, Ser12, and Ser24 phosphorylation. Early meiotic *chk-2(me64)* nuclei showed no S8-Pi, S12-Pi, and S24-Pi staining above background level, whereas mitotic NE or centrosome staining remained as in wild-type nuclei (Figures 4D, S4B, and S4C). These results

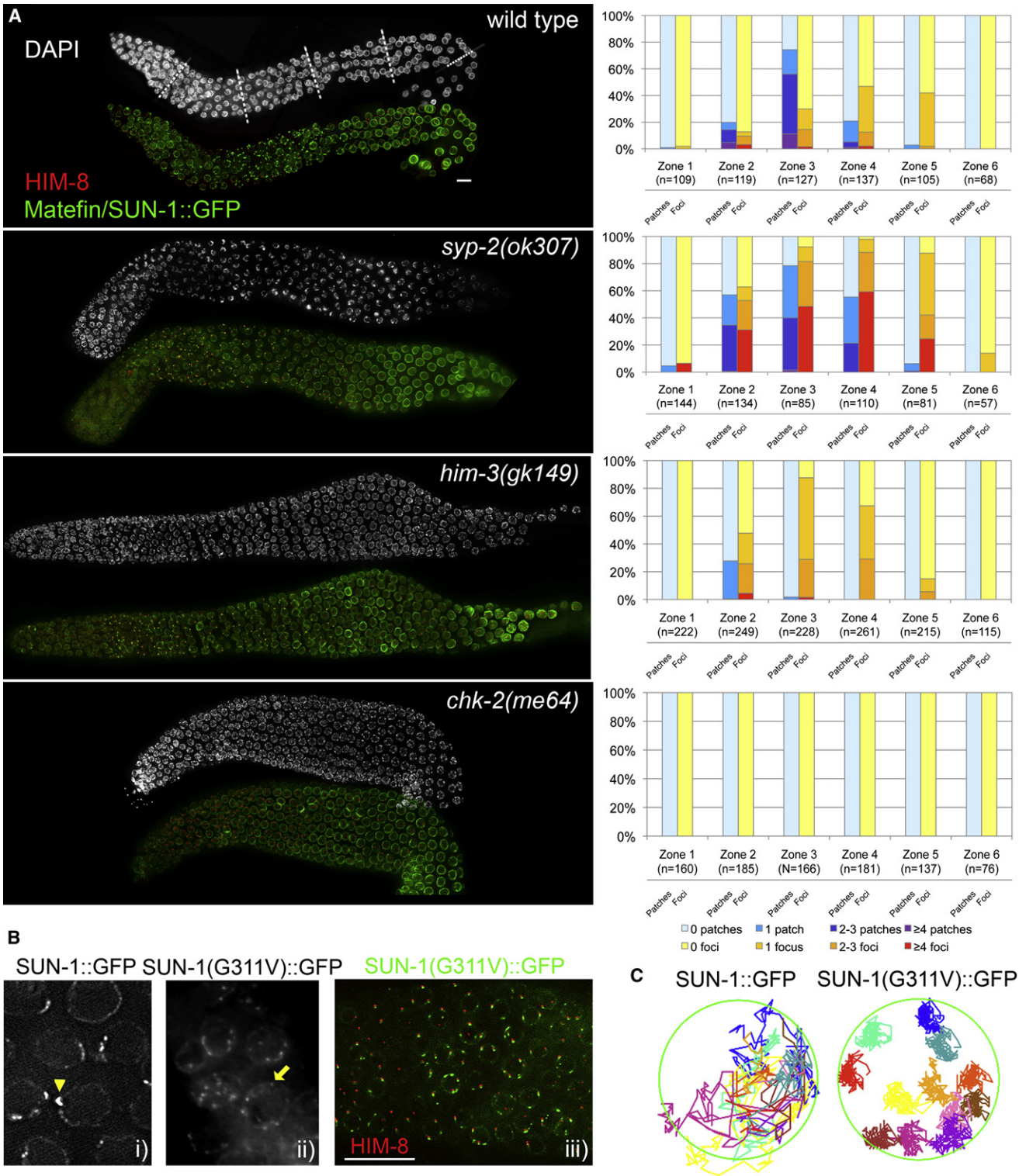

Figure 2. The Formation of SUN-1 Aggregates Requires Chromosome Axes, the Kinase CHK-2, and Chromosome Movement

(A) Analysis of SUN-1::GFP aggregates in various mutant backgrounds. White, DAPI staining; green, SUN-1::GFP; red, HIM-8. Wild-type: *mtf-1/sun-1::gfp;mtf-1/sun-1(ok1282)*. *syp-2(ok307)*: *syp-2(ok307);mtf-1/sun-1::gfp;mtf-1/sun-1(ok1282)*. *him-3(gk149)*: *him-3(gk149);mtf-1/sun-1::gfp;mtf-1/sun-1(ok1282)*. *chk-2(me64)*: *chk-2(me64);mtf-1/sun-1::gfp;mtf-1/sun-1(ok1282)*. Dotted lines in the wild-type DAPI-stained gonad indicate subdivision into six zones. Quantification of aggregate forms (foci and patches) and numbers are shown in the right panel.

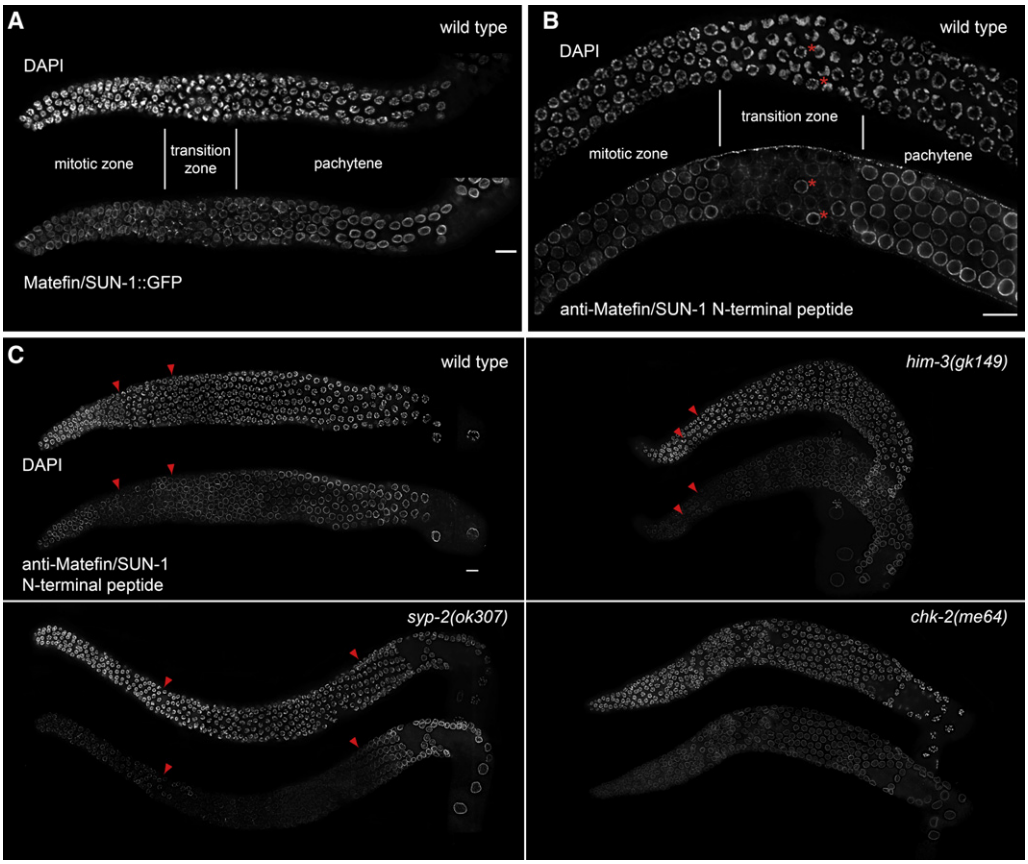

Figure 3. The N Terminus of SUN-1 Is Not Recognized by N Terminus-Specific Matefin Antibodies in the Transition Zone

(A) A wild-type hermaphrodite gonad expressing SUN-1::GFP.

(B) Labeling of SUN-1 in wild-type (N2) hermaphrodite gonads with antibodies recognizing an N-terminal peptide (number 3663). Red stars mark the asynchronous nuclei interspersed in the transition zone.

(C) Analysis of wild-type (N2), *syp-2(ok307)*, *him-3(gk149)*, and *chk-2(me64)* mutants representing varying development of transition zone. The SUN-1 staining is weak at the nuclear periphery of nuclei displaying the typical polarized chromatin configuration of transition zone nuclei. Red arrowheads mark the beginning and the end of the TZ [in wild-type and *syp-2(ok307)*] and TZ-nuclei in *him-3(gk149)*.

Scale bars represent 10 μm.

suggest that CHK-2 is required for the early meiotic phosphorylation of Ser8, Ser12, and Ser24, but not for phosphorylation in mitosis or diakinesis.

Activation of CHK-2, however, is not or not solely dependent on the ATM/ATR orthologs of *C. elegans* (Chen and Poon, 2008; Perona et al., 2008; Stergiou et al., 2007; Garcia-Muse and Boulton, 2005), since *atm-1(gk186)*, *atl-1(tm853)*, or double *atm-1(gk186);atl-1(tm853)* mutants did not display a reduction in S8-Pi staining (Figure 4F and data not shown).

Since *chk-2(me64)* is defective in both homologous chromosome alignment and DSBs formation, we investigated *htp-1 (gk174)* (Figure 4G) and *him-3(gk149)* (data not shown), both defective in homologous alignment (Couteau and Zetka, 2005; Martinez-Perez and Villeneuve, 2005; Couteau et al., 2004), to determine which process affects Ser8 phosphorylation. We also analyzed S8-Pi staining in *spo-11(me44)* (Figure 4E) and *mre-11(ok179)* (data not shown), which are deficient in DSB initiation but competent for homologous pairing (Dernburg et al., 1998; Chin and Villeneuve, 2001). In all mutant backgrounds, SUN-1 was phosphorylated at Ser8 (Figure 4 and data not shown), demonstrating that the absence of DSBs or defective homologous alignment alone do not interfere with the

(B) Comparison of SUN-1::GFP (i) and SUN-1(G311V)::GFP (ii) aggregates at the NE of nuclei proximal to the mitotic zone. The yellow arrowhead marks the position of a patch, while the yellow arrow highlights a focus. iii, costaining of SUN-1(G311V)::GFP foci (green) and the PC-binding protein HIM-8 (red; channel shifted upward).

(C) Displacement tracks of SUN-1::GFP and SUN-1(G311V)::GFP aggregates in a representative nucleus in the transition zone. Various colors correspond to individual aggregates analyzed. The yellow SUN-1::GFP displacement track documents a protuberance of the NE. SUN-1 aggregates were analyzed in live specimen.

Scale bars represent 10 μm.

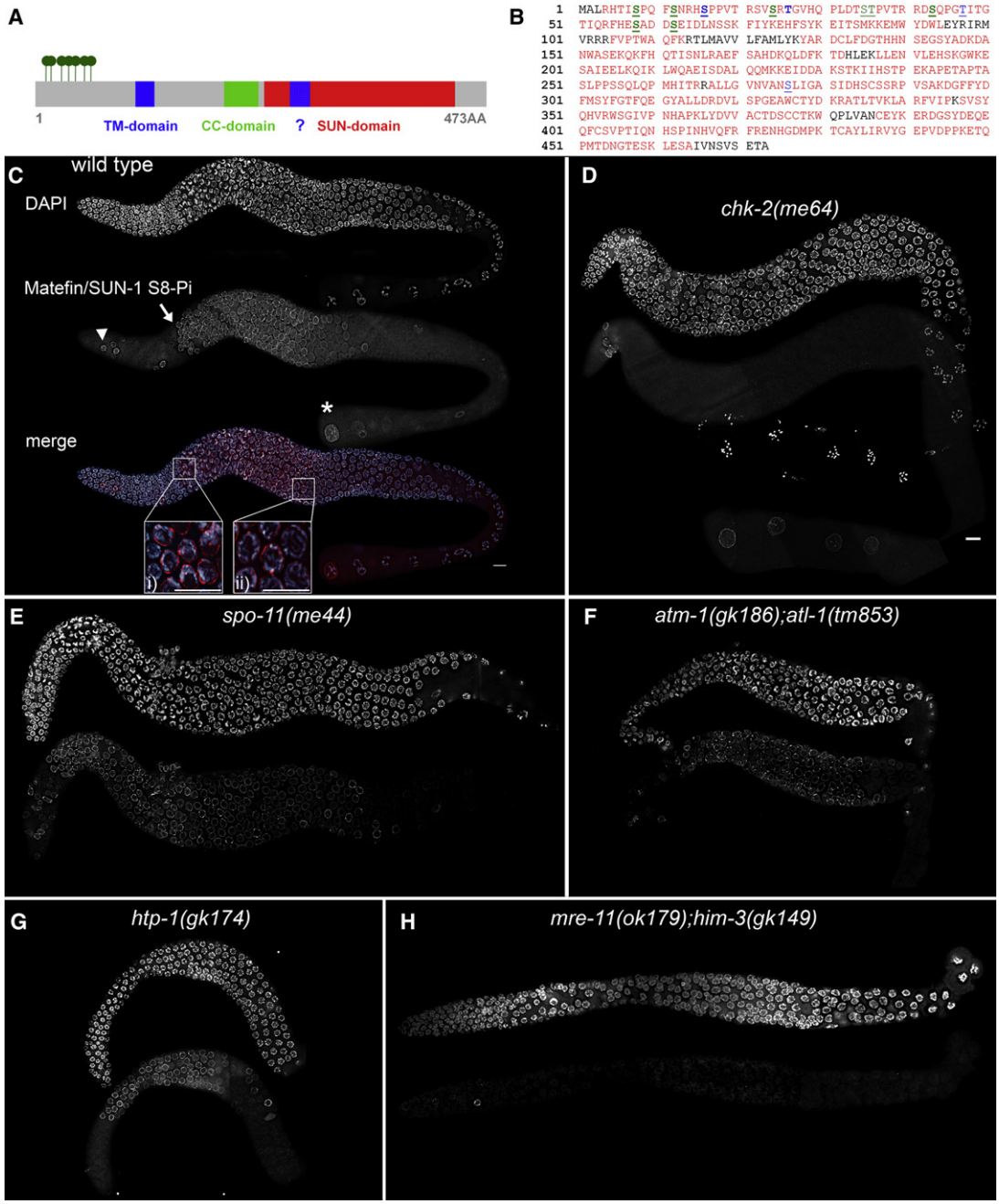

Figure 4. SUN-1 Is Phosphorylated at Its N Terminus

(A) Schematic representation of the SUN-1 protein. The position of the six phosphorylated serines and one serine or threonine at the N-terminal domain are marked (dark green). Also indicated are the positions of the putative transmembrane domains (TM and ?), the putative coiled-coil domain (CC) and the SUN domain.

(B) A single letter sequence of SUN-1. Residues covered by mass spectrometry are in red. Phosphorylated serine/threonine residues are in green. Phosphorylated residues in a mixture of embryonically and germline-expressed SUN-1 are shown with bold letters, and phosphorylations in the germline are underlined. Blue letters designate not-certified phosphorylations.

(C) Wild-type hermaphrodite gonad costained with DAPI (top and blue in merge) and with antibodies that recognize the phosphoepitope of serine8, SUN-1 S8-Pi (middle and red in merge). Insets display magnified nuclei of transition zone (i) and mid-pachytene (ii). The arrowhead marks a mitotic nucleus. The arrow indicates the beginning of TZ, and the star highlights a diakinesis nucleus.

(D–H) Mutant hermaphrodite gonads: *chk-2(me64)* (D), *spo-11(me44)* (E), *atm(gk186);atl(tm853)* (F), *htp-1(gk174)* (G), and *mre-11(ok179);him-3(gk149)* (H). Note that there is only background S8-Pi staining of transition zone and early pachytene nuclei in *chk-2(me64)* and *mre-11(ok179);him-3(gk149)* mutant backgrounds. Scale bars represent 10 μm.

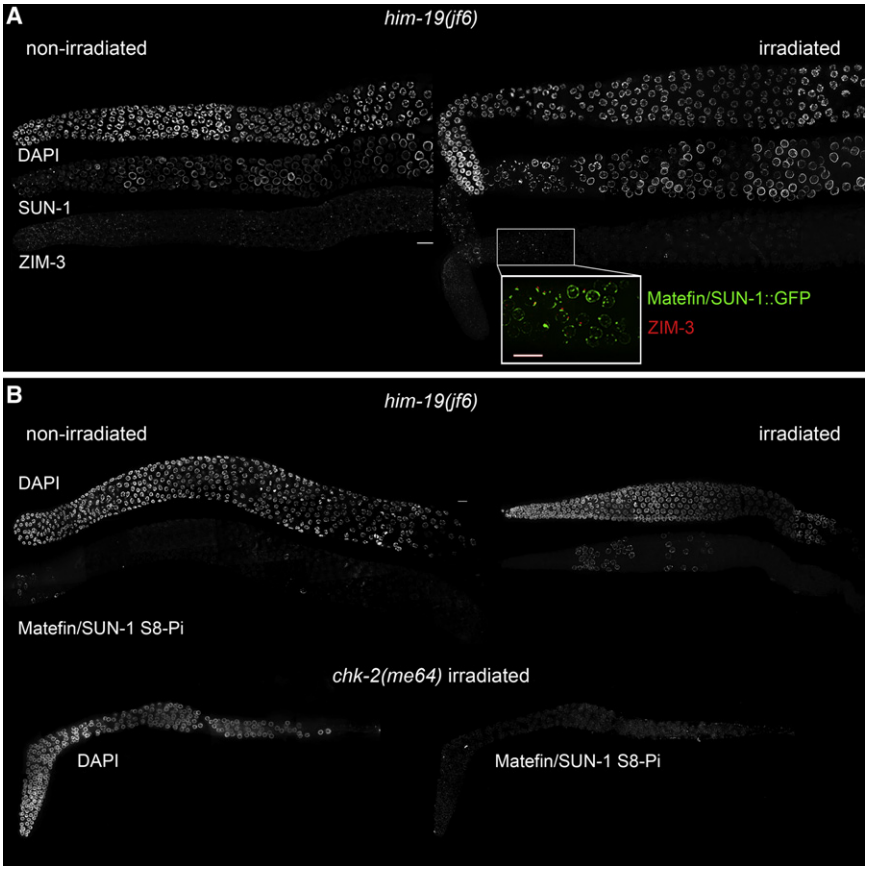

Figure 5. DNA Damage Can Induce SUN-1 Aggregation and Phosphorylation on Serine8

(A) SUN-1::GFP aggregates and ZIM-3 loading in germline nuclei proximal to the mitotic zone are induced by ionizing radiation of 2-day-old *him-19(jf6)* hermaphrodites. SUN-1::GFP (green in merge) and ZIM-3 (red in merge) colocalize (red channel is shifted upwards).

(B) SUN-1 S8-Pi staining in unirradiated (left) and irradiated (right) 2-day-old *him-19(jf6)* hermaphrodites. SUN-1 Ser8 does not become phosphorylated after ionizing radiation in *chk-2(me64)* mutants.

Scale bars represent 10 μm.

phosphorylation of Ser8. However, in 46.2% (n = 13 gonads) of *mre-11(ok179);him-3(gk149)* double-mutant gonads the meiotic phosphorylation of Ser8 was undetectable (Figure 4H). These data suggest that elimination of both DSB initiation and an intact chromosomal axis prevents CHK-2 from influencing SUN-1 phosphorylation.

DNA Damage Induces the Phosphorylation of SUN-1 at Ser8

him-19 is an early meiotic regulator necessary for homologous pairing, chromatin clustering, synapsis, and recombination. The phenotype only becomes cytologically apparent in 2-day-old hermaphrodites (L. Tang and V.J., unpublished data). Two-day-old adult *him-19(jf6)* animals are most probably defective in the initiation of DSBs, as judged by the absence of repair intermediates marked by RAD-51. Importantly, gamma radiation-induced DSBs restored the clustering of chromosomes in *him-19(jf6)* nuclei proximal to the mitotic zone.

In accordance with a pairing defect and an absent TZ, SUN-1 aggregates could barely be detected in aged *him-19(jf6)* hermaphrodites (Figure 5A, left panel, and Figure S5). Because chromosome clustering could be induced by gamma radiation, we assayed whether polarization coincides with the restoration of SUN-1 aggregates. After irradiation, meiotic nuclei in the TZ region adopted the polarized chromatin configuration with SUN-1 patches and foci (Figure 5A, right panel). These displayed dynamic movement along the nuclear surface (A.B. and V.J., unpublished data) and appeared to be colocalized with reloaded ZIM proteins, as revealed by ZIM-3 immunolocalization (Figure 5A, inset).

Consistent with the severe defect in chromatin polarization, phosphorylation of SUN-1 at Ser8 was rarely detected in unirradiated aged *him-19(jf6)* hermaphrodite gonads (Figure 5B, left panel). The phospho-specific immunostaining of SUN-1 was restored in irradiated *him-19(jf6)* nuclei progressing through early meiotic prophase I, but not in gamma-irradiated *chk-2(me64)* hermaphrodites (Figure 5B, right panel and lower panel). We conclude that induction of artificial DSBs in the *him-19(jf6)* background restores the characteristics of TZ nuclei, including chromatin reorganization and phosphorylation of the SUN-1 N terminus, probably by activation of the CHK-2 kinase.

Mutation of SUN-1 Phospho-Sites Elicits Meiotic Defects

We substituted each of the phosphoserines either for alanine (nonphosphorylatable) or for glutamic acid (to mimic constitutively phosphorylated SUN-1). Only a subset of the substitutions could be recovered as viable transgenic lines, possibly because of disruption of other essential functions of SUN-1 (Fridkin et al., 2004).

Animals expressing SUN-1(S12E)::GFP with no endogenous SUN-1 (referred to as S12E) displayed a reduced brood size, embryonic lethality, and a Him phenotype (Table S1). SUN-1(S12E)::GFP hermaphrodites display a lack of chiasmata, with an average of 8.6 DAPI-positive structures at diakinesis, ranging from six to 12 (n = 54; Figure 6A, ii and iii) compared to six in the wild-type (n = 57). SUN-1(S12E)::GFP-expressing hermaphrodites display an extended TZ with tightly clustered chromatin (Figure 6A). Accordingly, SUN-1(S12E) aggregates are detected at the NE and colocalize with PC-binding proteins such as HIM-8 and ZIM-3 in the elongated TZ (Figures 6A and 6B). Those "artificial" aggregates are movement competent, as shown in Movies S4 and S5.

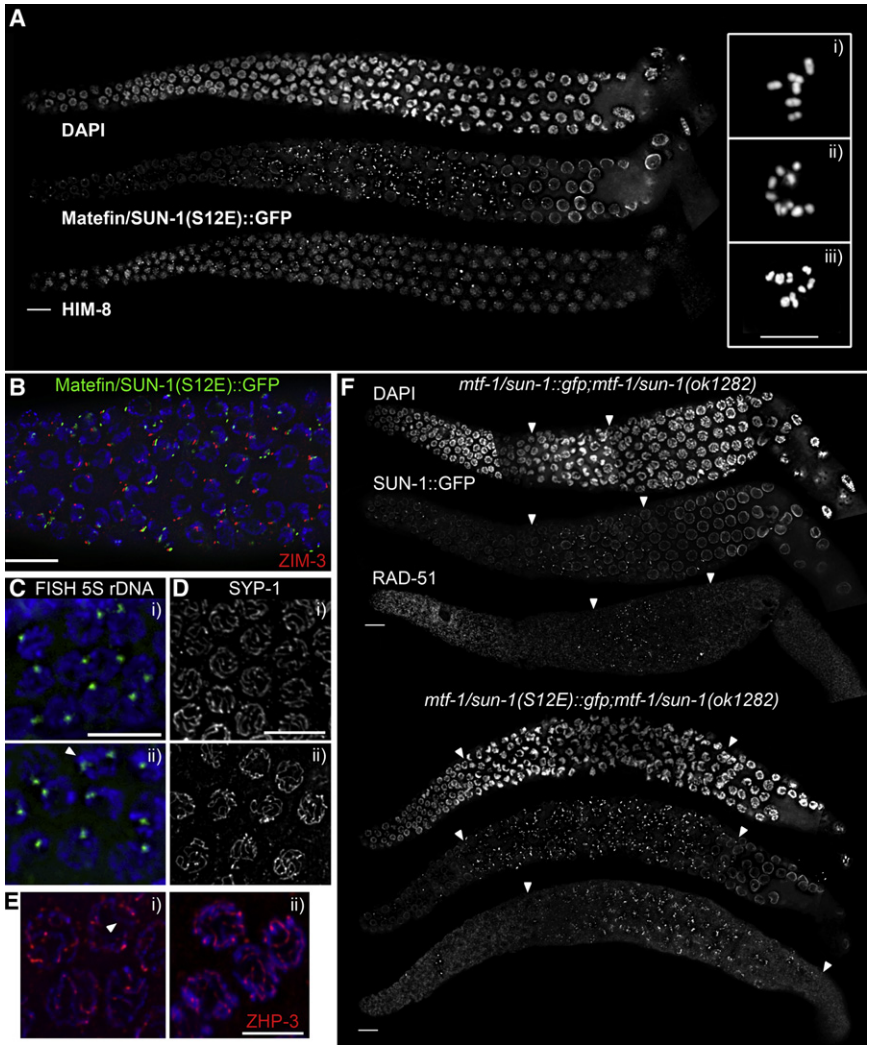

Figure 6. Dephosphorylation of SUN-1 Serine12 Promotes Timely Exit from the Transition Zone and Proper DNA Repair

(A) Chromatin clustering, SUN-1(S12E)::GFP aggregation, and HIM-8 localization in hermaphrodite gonads expressing solely SUN-1(S12E)::GFP. i, diakinesis in *mtf-1/sun-1::gfp;mtf-1/sun-1 (ok1282)* (wild-type); ii and iii, diakinesis in *mtf-1/sun-1(S12E)::gfp;mtf-1/sun-1(ok1282)*.

(B) Costaining of SUN-1(S12E)::GFP (green) aggregates and ZIM-3 (red, channel shifted to the left). Blue, DAPI staining.

(C) Paired FISH signals (green) marking LG V right arm in a region corresponding to mid-pachytene of wild-type (i) and mutant (ii) gonads. White arrowhead marks a nucleus with unpaired FISH signals in the mutant.

(D) SYP-1 assembly in the wild-type situation (i) and in *mtf-1/sun-1(S12E)::gfp;mtf-1/sun-1 (ok1282)* (ii) gonads (pachytene region shown).

(E) ZHP-3 (red) disassembly in diplotene of wild-type and mutant hermaphrodites. Blue, DAPI staining. Arrowhead highlights ZHP-3-free chromosome region.

(F) RAD-51 staining in SUN-1(S12E)::GFP-expressing transgenic worms and in hermaphrodites expressing the wild-type protein. Arrowheads border the zones of tight chromatin clustering (DAPI staining), SUN-1::GFP and SUN-1(S12E)::GFP aggregation, and RAD-51 staining. Scale bars represent 10 μm.

Defects in the timely exit from the TZ are characteristic of mutants affecting the assembly of the SC (MacQueen et al., 2002, Colaiácovo et al., 2003; Smolikov et al., 2007a). In SUN-1(S12E), SYP-1 was loaded normally and elongated into linear structures (Figure 6D). Almost full-pairing levels were reached for chromosomes X and V, (Figures 6A, 6C, and S6A). Interestingly, in late S12E pachytene nuclei (zone 6), the percentage of paired homologs decreased, indicating that the pairing is not completely stabilized (Figure S6A). Therefore, a pairing defect is not the primary reason for the decrease in bivalent formation.

Extending the zone of polarized chromatin can be the consequence of a defect in the timely repair of DSBs and can be suppressed by the absence of SPO-11 (Carlton et al., 2006). In order to monitor recombination, we visualized the repair protein RAD-51 (Alpi et al., 2003; Colaiácovo et al., 2003). In SUN-1::GFP-expressing worms, RAD-51 is detected from the late TZ to mid-pachytene. In contrast, in SUN-1(S12E), RAD-51 foci are present from the mid-TZ until diplotene and in greater numbers (Figures 6F and S6B). Persistence of RAD-51 into late pachytene and its subsequent disappearance in diplotene, combined with the failure to observe chiasmata on all chromosomes, is indicative of DSB repair from the sister chromatid. This conclusion is supported by the fact that ZHP-3, whose asymmetric disassembly at the end of pachytene is dependent on crossover establishment (Bhalla et al., 2008) (Figure 6E, i), did not disappear as in the wild-type but rather remained in SUN-1(S12E)::GFP-expressing animals as elongated structures decorating the whole chromosome in late pachytene and in diplotene (Figure 6E, ii).

As the tight chromatin clustering of SUN-1(S12E)::GFP transgenic worms is still observed in the *spo-11(me44)* background (Figure S6C), we conclude that the dephosphorylation of SUN-1 S12 directly regulates the timely redispersal of chromosomes upon exit from the TZ. Moreover, we suggest that the timely exit from the TZ regulates proper DNA repair to generate crossovers.

Worms expressing SUN-1(S62E)::GFP with no endogenous SUN-1 displayed a prolonged early pachytene zone characterized by the relaxed clustering of chromatin (Carlton et al., 2006) (Figure S6D). The brood size and embryonic viability was reduced accompanied by an increase in DAPI-positive structures at diakinesis (x = 6.9, n = 38 diakinesis) and a Him phenotype (Table S1). The S62E line reproduces the extended clustering phenotype seen with S12E, therefore strongly supporting the specificity of this phenotype.

We also analyzed the single-alanine substitution of Ser8. These lines showed reduced embryonic viability and a Him phenotype accompanied by an increase of DAPI-positive bodies at diakinesis (Table S1). Seventeen and a half percent of diakinesis nuclei display more than six DAPI signals, ranging from seven to 12 (n = 120 diakinesis).

Hermaphrodites expressing transgenic SUN-1(S12A,S16A)::GFP display defects in meiotic prophase I entailing univalent formation, described in detail below (Figure 7 and Table S1). The single S16A substitution line, however, did not display a cytologically detectable meiotic phenotype (Figure S7A and data not shown). Consistently, six signals at diakinesis (n = 101 diakinesis of 30 hermaphrodites; inset in Figure S6A) were seen. Therefore, we concluded that the meiotic prophase I phenotype seen in SUN-1(S12A,S16A) represents the loss of Ser12Pi.

In SUN-1(S12A,S16A)::GFP, an average of 11.7 DAPI signals (SD = 0.6; n = 22 diakinesis, ten gonads) were counted at diakinesis, documenting failed bivalent formation. Consistently, RAD-51 is present longer (from the mid-TZ until diplotene) and in greater numbers as compared to wild-type transgenes (Figure 7A), indicating a defect in DSB repair. SUN-1(S12A,S16A)::GFP aggregates are formed upon entry into meiosis, and they colocalize with the PC-binding protein HIM-8 (Figure 7A and data not shown). However, fewer large aggregates (patches) can be detected (Figures 7A and S7C), correlating with the lack of pronounced chromatin clustering. Despite HIM-8 localization at aggregates, X chromosome pairing is defective (Figure 7B). However, the SC central component SYP-1 is timely and extensively loaded in the mutant worms (Figure 7C), suggesting the presence of nonhomologous synapsis.

Nonhomologous synapsis is also observed in the movement-defective SUN-domain mutated *jf18* allele caused by the loss of ZYG-12 from the outer NE. Immunostaining for ZYG-12 in SUN-1(S12A,S16A)::GFP-expressing lines showed that ZYG-12 is retained at the outer NE (Figure S7B). This is consistent with time-lapse analysis of movement competent SUN-1(S12A,S16A)::GFP aggregates (see Movies S6 and S7).

To address how this substitution elicits nonhomologous synapsis, we analyzed the size distribution of the SUN-1 aggregates. A reduced number of patches can be seen in the mutant line in comparison to the wild-type SUN-1 and SUN-1(S16A) (Figure S7C). Importantly, the size of single chromosome SUN-1(S12A,S16A)::GFP attachment foci is comparable to the wild-type. Despite the lack of transgenic lines with Ser to Ala exchanges for all the phospho-target sites, the SUN-1(S12A,S16A)::GFP-expressing transgenic line suggests that the modification is required for proper homolog pairing. The reduction of large SUN-1 patches proposes a defect in the homology check.

DISCUSSION

The Induction of SUN-1 Aggregates in Early Meiosis

Our data reveal a strong correlation between SUN-1 aggregate formation and PC protein binding to one chromosome end. The foci and patches of SUN-1 form upon entry into the TZ, concomitantly with the attachment of PC-containing chromosome ends at the NE. PC-binding proteins colocalize with SUN-1 aggregates and ZIM-1 and ZIM-3 could be coprecipitated with SUN-1 (see the model in Figure 7; data not shown). While the autosome-associated ZIM-proteins are detectable in the TZ up to early pachytene, HIM-8, the PC-binding protein of the X chromosome, is present until later stages of meiotic prophase, where it colocalizes with the only persisting SUN-1 aggregate.

In chromosome axis mutants, such as HIM-3 and HTP-1, SUN-1 aggregates are strongly reduced. Moreover, in aged *him-19(jf6)* hermaphrodite gonads, the restoration of SUN-1 aggregates by artificially induced DSBs correlates with the reassociation of ZIM-3 with the chromosomes. Full chromosomal association of PC-binding proteins, except for HIM-8, depends on CHK-2 activity (Phillips and Dernburg, 2006), whereas in *chk-2(me64)* SUN-1 aggregates are completely absent. These observations could be explained by a model in which PC-binding proteins, perhaps in a phosphorylated form, are involved in the induction of SUN-1 aggregates at the beginning of the TZ. The aggregates are induced as soon as *chk-2*-dependent modified PC-binding proteins associate with chromosome ends and attach to the inner NE (Figure 7). Consistently, Sato et al. (2009) show that in the *him-8* missense allele *me4* (S85F), HIM-8 still localizes to chromosome ends and the NE, but colocalizing SUN-1 aggregates cannot be detected. S85 might be a potential CHK-2 target site.

Alternatively, the *chk-2*-dependent phosphorylation of SUN-1 indirectly influences the recruitment of the ZIM proteins to chromosomal ends. Deciphering the regulatory mechanisms leading to CHK-2 activation is a challenge for future studies.

The Function of SUN-1 Aggregates

The local enrichment of the SUN-1/ZYG-12 NE bridge provides a powerful connective interface for mechanically stable attachment of chromosome ends to the nuclear periphery. Small SUN-1 foci appear earlier and mature into larger SUN-1 patches as nuclei progress through the TZ and into pachytene.

Several lines of evidence suggest that SUN-1 foci with a diameter <1.1 μm are the primary aggregates formed upon attachment of chromosome ends to the NE, while larger aggregates or patches constitute sites where different chromosome ends coalesce to assess homology and initiate synapsis. First, the SUN-1(G311V)::GFP line only forms movement impaired foci. Second, SUN-1 patches could only be observed in nuclei with clustered chromatin (an indicator of chromosome movement). Third, in *him-19(jf6)* large aggregates could only be observed in nuclei where the clustering of chromatin is restored concomitantly with movement. Finally, in mutants deficient for homologous alignment or synapsis, only a few patches but an increased number of SUN-1 foci could be seen. If the homologous partner is not available, as in *htp-1*, chromosome ends remain mobile and patches would be broken into smaller foci (Figure 7). The presence of an increased number of SUN-1 foci would, therefore, be consistent with an ongoing homology search, where chromosomes move randomly over one hemisphere of the nucleus, meet, and coalesce. Chromosome movement not only assists in the homology search process as a "mixing force," but additionally acts as a "repelling force," preventing nonhomologous synapsis.

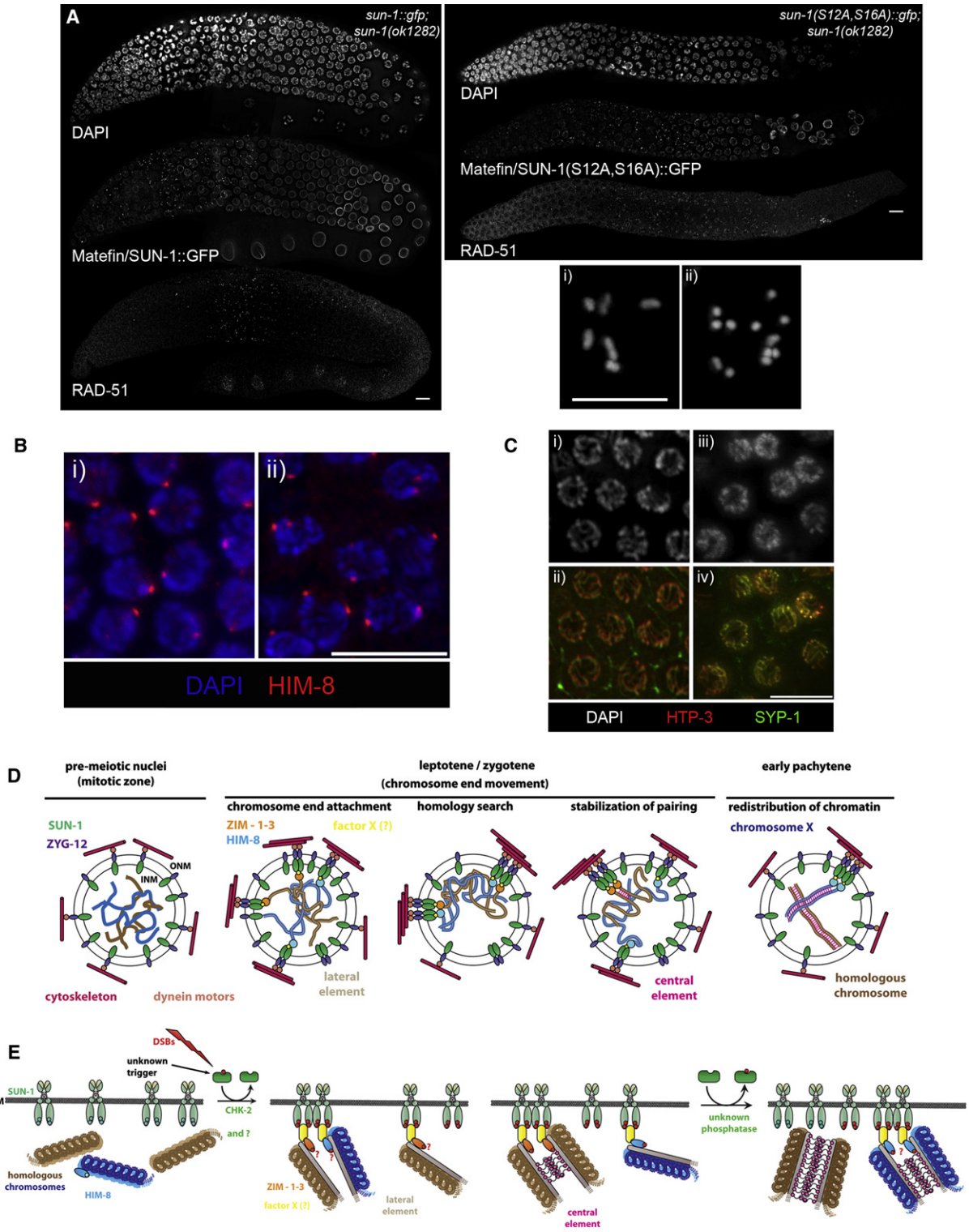

Figure 7. Unphosphorylatable Serine12 Elicits a Meiotic Pairing Defect

(A) Chromatin clustering, SUN-1::GFP aggregation, and RAD-51 staining in hermaphrodite gonads expressing solely SUN-1(S12A,S16A)::GFP or wild-type SUN-1::GFP. i, diakinesis in *mtf-1/sun-1::gfp;mtf-1/sun-1(ok1282)* (wild-type); ii, diakinesis in *mtf-1/sun-1(S12A,S16A)::gfp;mtf-1/sun-1(ok1282)*.

(B) HIM-8 localization in hermaphrodite gonads solely expressing SUN-1(S12A,S16A)::GFP. Blue, DAPI staining; red, HIM-8 staining. Paired HIM-8 signals in wild-type pachytene (i) and unpaired HIM-8 signals in *mtf-1/sun-1(S12A,S16A)::gfp;mtf-1/sun-1(ok1282)* pachytene region (ii) are shown.

Interestingly, the special allele *me42* of the SC component SYP-3 results in a C-terminal truncation and leads to a premature exit from the TZ. *syp-3(me42)* is synapsis defective and appears to employ an alternative meiotic repair pathway (Smolikov et al., 2007a, 2007b). This suggests that a specific synapsis and/or recombination intermediate activates the phosphatase to act on SUN-1. We hypothesize that chromosomes continue to move as a united parental chromosomal pairs once synapsed followed by the concerted resolution of aggregates mediated by the so far unknown phosphatase. This is supported by the fact that the average number of four patches remains constant throughout the TZ.

Phosphorylation of the SUN-1 N Terminus and Functional Implications

Six N-terminally located serines and one serine or threonine are phosphorylated in germline-expressed SUN-1. Our cytological analysis of phosphorylations has revealed a cell cycle-specific phosphorylation in mitosis, peaking toward anaphase, and a meiotic phosphorylation pattern overlapping with the time window of homologous pairing and reappearing later on in diakinesis nuclei.

In meiotic prophase I, phosphorylated serines of SUN-1 overlap with clustered chromatin and the presence of SUN-1 aggregates in the TZ. As nuclei enter early pachytene, S8-Pi staining becomes progressively weaker, eventually disappearing concomitantly with homogenous redispersion of the chromatin throughout the nucleus. This suggests that S8-Pi is first dephosphorylated in SUN-1 aggregates and that the dephosphorylated protein redistributes throughout the NE, resulting in gradually weaker signals as nuclei progress through meiotic prophase I.

In meiosis, the phosphorylation might influence the binding affinity of chromatin-binding proteins or the nuclear lamina to the NE. We found that in an unphosphorylatable SUN-1 mutant chromosomes nonhomologously synapse despite retaining aggregate mobility. The phosphorylation of SUN-1 could promote the interaction to the PC proteins directly or indirectly (PC proteins can be found in a SUN-1 protein complex by mass spectrometry analysis, data not shown). The PC proteins were proposed to have a prominent role in licensing synapsis (Sato et al., 2009). The weakening of this connection could account for the reduced amount of large SUN-1 patches representing the ongoing homology check. We therefore conclude that the phosphorylation is required for the induction of functional chromosomal attachment plaques. Stable association of chromosome ends at the nuclear periphery is a prerequisite for pronounced chromosome movement. Furthermore, we hypothesize that the phosphorylations of the SUN-1 N terminus impact the mobility of chromosomal attachment plaques by influencing its capability to self-oligomerize or support the mobility of the protein within the inner nuclear membrane, while dephosphorylation of SUN-1 regulates the dissolution of aggregates.

Dramatic phenotypes were observed in the phosphomimic S12E mutation, suggesting that timely dephosphorylation of SUN-1 is required for aggregate dissociation and chromatin redistribution. Consistently, the TZ prolongation phenotype was also observed in S8E and S62E mutants. The data also suggest that the dephosphorylation is necessary for ongoing DSB repair. Possibly, the movement out from the TZ clustering allows for the polymerization of the SC central element along the length of the entire chromosome, a prerequisite for crossover formation. Also in yeast, chromosome movement influences recombinational repair by resolving chromosome entanglements, ectopic contacts, and/or restructuring chromosomes (Koszul et al., 2008; Wanat et al., 2008; Kosaka et al., 2008).

The trigger for the induction of SUN-1 Ser8, 12, and 24 phosphorylation is less clear. We favor the idea that CHK-2 is directly involved in the phosphorylation of the SUN-1 N terminus. It is possible that CHK-2 recruited by PC-binding proteins phosphorylates the inner nuclear membrane protein, as soon as chromosome ends attach to the NE. The induction of DSBs is apparently involved in S8-Pi induction, as demonstrated by the restoration of the phosphorylation pattern upon irradiation of *him-19(jf6)* aged hermaphrodites. In *C. elegans*, full homolog pairing and synapsis are independent of SPO-11 (Dernburg et al., 1998). Consistently, we found that the elimination of DSBs is not sufficient to prevent phosphorylation of SUN-1, arguing for redundant pathways that lead to CHK-2 activation to induce SUN-1 phosphorylation.

Concomitantly with chromosome recruitment of PC proteins, chromosomes are moved over the surface of the nucleus searching proper and repelling improper interactions (see also Sato et al., 2009). Our study strongly supports a model in which the modification of SUN-1, a core component of the movement apparatus, adds the temporal frame to the searching process.

(C) SYP-1 (green) and HTP-3 (red) assembly in wild-type (ii) and in *mtf-1/sun-1(S12A,S16A)::gfp;mtf-1/sun-1(ok1282)* (iv) pachytene regions. Gray, DAPI staining in wild-type (i) and in *mtf-1/sun-1(S12A,S16A)::gfp;mtf-1/sun-1(ok1282)* (iii).

Scale bars represent 10 μm.

(D and E) A model of SUN-1-mediated homologous chromosome pairing.

(D) Overview of chromosome pairing. Homologous chromosomes depicted as blue (chromosome X) and brown (an autosome) lines.

(E) Chromosome attachment and SUN-1 modifications.

Green ellipses, SUN-1. For simplicity, only the inner nuclear membrane (INM) with associated proteins is drawn. Upon entry into meiosis, PC-binding proteins (blue and orange ellipses), most likely CHK-2-dependent phosphorylated (small red circles), associate with the respective chromosome ends. PC-containing chromosome ends attach to SUN-1 at the NE. The N terminus of Matefin/SUN-1 is phosphorylated (Ser8 and Ser12 are marked) in a CHK-2-dependent manner activated by DSBs or a so far unknown trigger. SUN-1/ZYG-12 (violet ellipses in D) form aggregates at chromosomal attachment sites to establish a proteinaceous bridge across the NE. Chromosome ends are, thereby, connected through motors (brick in D) to the cytoskeleton (dark pink bars in D) to provide a link between the motile forces in the cytoplasm and chromosome ends in the nuclear interior. When chromosome ends meet, small SUN-1 aggregates coalesce to form larger patches that likely represent sites of ongoing homology check. If the homologous partner is not available, chromosome ends are moved further. As homology is successfully assessed, the SC (magenta lines and circles) polymerizes. Autosomal PC-binding proteins are lost from chromosome ends and the respective SUN-1 aggregates dissolve in early pachytene after dephosphorylation. HIM-8 remains bound to the X chromosome until mid-pachytene.

EXPERIMENTAL PROCEDURES

Cytological Preparation of Gonads and Immunostaining

Hermaphrodite gonads were dissected and fixed as described in Martinez-Perez and Villeneuve (2005). For immunostaining, gonads were blocked in 3% BSA/1× PBS for 20 min. Antibodies were diluted in 1× PBS/0.01% sodium azide as follows: anti-SUN-1 (antibody against an N-terminal peptide, this study) 1:700, anti-SUN-1 (antibody against an N-terminal peptide, Fridkin et al. [2004]) 1:700, anti-SUN-1 Ser8-Pi (this study) 1:700, anti-GFP (Roche Diagnostics, #11814460001) 1:300, anti-HIM-8 (Phillips et al., 2005) 1:500, anti-ZIM-3 (this study) 1:100, anti-RAD-51 (Alpi et al., 2003) 1:300, anti-SYP-1 (MacQueen et al., 2002) 1:200, anti-SPD-5 (Pelletier et al., 2004) 1:2000, and anti-ZYG-12 (Malone et al., 2003) 1:400.

Fluorescence In Situ Hybridization

5S ribosomal DNA (rDNA) was used as a probe for the right arm of chromosome V. 5S rDNA was labeled by PCR with digoxigenin-11-dUTP (Pasierbek et al., 2001). Digoxigenin-labeled probes were detected with FITC-conjugated anti-digoxigenin antibodies (1:100).

Microscopy and Evaluation

Evaluation of cytological phenotypes was performed in animals kept at 20°C, 18–24 hr after L4. A Zeiss Axioskop epifluorescence microscope was used in combination with a cooled CCD camera (Photometrics, Tucson, AZ). 3D stacks of images were taken (MetaVue software, Universal Imaging, Downingtown, PA), deconvolved (AutoDeblur software, AutoQuant Imaging, Troy, NY) and projected (Helicon Focus software, http://helicon.com.ua/heliconfocus/). Artificial coloring and merging were done with Adobe Photoshop 7.0 (Adobe Systems).

Live Imaging of SUN-1::GFP Constructs

Worms were mounted in 10 mM levamisol in M9 buffer on 2% agarose, covered with a coverslip, and sealed with melted Vaseline. Images were acquired at room temperature every 5 s for 15 min as stacks of optical sections with 1 μm intervals with a Deltavision deconvolution microscopy system (Applied Precision, Issaquah, WA). The following conditions were used: FITC fluorescence filter, 10% ND, bin 1 × 1, exposure time 200 ms, objective 60× (CoolSNAP HQ digital camera from photometrics).

Maximum-intensity projections with Softworx software (Applied Precision) were created and the collection of files saved as stack files with Metamorph Offline (Molecular Devices, Downingtown, PA). Nonspecific signals of the stack pictures were removed with Autoquant X2 (AutoQuant Imaging), and the slices realigned with the first slice used as a reference. With Metamorph Offline, the position of the dots was followed manually. The position of the dots was plotted with Gnuplot software (http://www.gnuplot.info/).

Aggregate movements were recorded with a Deltavision microscope scanning through the gonad every 5 s. After projection, the image sequences were saved as movies (Quicktime) with a rate of six frames per second. Therefore, aggregates move 30 times faster than in real time.

Irradiation Assay

Hermaphrodites were exposed to 5000 rads of γ-radiation from a ^{137}Cs source. Cytological analysis was performed 120 min after irradiation.

Immunoprecipitation and Silver Staining of SUN-1::GFP

Worms were harvested in 1× homogenization buffer, frozen in liquid nitrogen, thawed on ice, and sonicated twice on ice (5–7× 30 s bursts at an amplitude of 28%). Protein lysates were added to anti-GFP (Roche Diagnostics, #11814460001) coupled Dynabeads Pan Mouse IgG (Dynal Biotech, #110.41) and incubated overnight at 4°C.

Precipitated proteins were washed four times in 1× PBS and eluted at 60°C for 10 min in SDS-sample buffer. Samples were loaded onto SDS-PAGE gels (Bio-Rad Laboratories) and silver stained (Shevchenko et al., 1996).

Mass Spectrometry Analysis

See the Supplemental Data.

SUPPLEMENTAL DATA

Supplemental Data include Supplemental Experimental Procedures, seven figures, two tables, and seven movies and can be found with this article online at http://www.cell.com/supplemental/S0092-8674(09)01371-3.

ACKNOWLEDGMENTS

We thank Christian Pflügl, Ella Kaplan, Sonja Kolar, and Sophie Wöhrer for technical assistance. We are grateful to Chris Malone, Tony Hyman, Abby Dernburg, Anton Gartner, Anne Villeneuve, Monique Zetka, and the Caenorhabditis Genetics Center for strains, plasmids, and antibodies. We are indebted to Abby Dernburg for sharing unpublished results. We are grateful to Peter Carlton, Cécile Brocard, and Simon Boulton for helpful suggestions. We thank Iain Wilson, Maria Siomos, Yudith Yanowitz, and Josef Loidl for discussion. This work was supported by grants from the FWF (P-21107 and SFB-F3402), the WWTF (LS05009), the University of Vienna (I031-B), as well as an Elise-Richter grant to V.J., a DOC scholarship to A.W., an Israel Science Foundation grant to Y.G., and a Clore scholarship to A.F.

Received: June 5, 2009
Revised: October 16, 2009
Accepted: October 30, 2009
Published online: November 12, 2009

REFERENCES

Alpi, A., Pasierbek, P., Gartner, A., and Loidl, J. (2003). Genetic and cytological characterization of the recombination protein RAD-51 in Caenorhabditis elegans. Chromosoma *112*, 6–16.

Alsheimer, M. (2009). The dance floor of meiosis: evolutionary conservation of nuclear envelope attachment and dynamics of meiotic telomeres. Genome Dyn. *5*, 81–93.

Bhalla, N., and Dernburg, A.F. (2008). Prelude to a division. Annu. Rev. Cell Dev. Biol. *24*, 397–424.

Bhalla, N., Wynne, D.J., Jantsch, V., and Dernburg, A.F. (2008). ZHP-3 acts at crossovers to couple meiotic recombination with synaptonemal complex disassembly and bivalent formation in C. elegans. PLoS Genet. *4*, e1000235.

Carlton, P.M., Farruggio, A.P., and Dernburg, A.F. (2006). A link between meiotic prophase progression and crossover control. PLoS Genet. *2*, e12.

Chen, Y., and Poon, R.Y.C. (2008). The multiple checkpoint functions of CHK1 and CHK2 in maintenance of genome stability. Front Biosci. *13*, 5016–5029.

Chikashige, Y., Tsutsumi, C., Yamane, M., Okamasa, K., Haraguchi, T., and Hiraoka, Y. (2006). Meiotic proteins bqt1 and bqt2 tether telomeres to form the bouquet arrangement of chromosomes. Cell *125*, 59–69.

Chin, G.M., and Villeneuve, A.M. (2001). C. elegans mre-11 is required for meiotic recombination and DNA repair but is dispensable for the meiotic G(2) DNA damage checkpoint. Genes Dev. *15*, 522–534.

Colaiácovo, M.P., MacQueen, A.J., Martinez-Perez, E., McDonald, K., Adamo, A., Volpe, A.L., and Villeneuve, A.M. (2003). Synaptonemal complex assembly in C. elegans is dispensable for loading strand-exchange proteins but critical for proper completion of recombination. Dev. Cell *5*, 463–474.

Conrad, M.N., Lee, C.-Y., Wilkerson, J.L., and Dresser, M.E. (2007). MPS3 mediates meiotic bouquet formation in Saccharomyces cerevisiae. Proc. Natl. Acad. Sci. USA *104*, 8863–8868.

Conrad, M.N., Lee, C.-Y., Chao, G., Shinohara, M., Kosaka, H., Shinohara, A., Conchello, J.-A., and Dresser, M.E. (2008). Rapid telomere movement in meiotic prophase is promoted by NDJ1, MPS3, and CSM4 and is modulated by recombination. Cell *133*, 1175–1187.

Couteau, F., and Zetka, M. (2005). HTP-1 coordinates synaptonemal complex assembly with homolog alignment during meiosis in C. elegans. Genes Dev. *19*, 2744–2756.

Couteau, F., Nabeshima, K., Villeneuve, A., and Zetka, M. (2004). A component of C. elegans meiotic chromosome axes at the interface of homolog alignment, synapsis, nuclear reorganization, and recombination. Curr. Biol. *14*, 585–592.

Dernburg, A.F., McDonald, K., Moulder, G., Barstead, R., Dresser, M., and Villeneuve, A.M. (1998). Meiotic recombination in C. elegans initiates by a conserved mechanism and is dispensable for homologous chromosome synapsis. Cell *94*, 387–398.

Ding, D.Q., Chikashige, Y., Haraguchi, T., and Hiraoka, Y. (1998). Oscillatory nuclear movement in fission yeast meiotic prophase is driven by astral microtubules, as revealed by continuous observation of chromosomes and microtubules in living cells. J. Cell Sci. *111*, 701–712.

Ding, X., Xu, R., Yu, J., Xu, T., Zhuang, Y., and Han, M. (2007). SUN1 is required for telomere attachment to nuclear envelope and gametogenesis in mice. Dev. Cell *12*, 863–872.

Fridkin, A., Mills, E., Margalit, A., Neufeld, E., Lee, K.K., Feinstein, N., Cohen, M., Wilson, K.L., and Gruenbaum, Y. (2004). Matefin, a Caenorhabditis elegans germ line-specific SUN-domain nuclear membrane protein, is essential for early embryonic and germ cell development. Proc. Natl. Acad. Sci. USA *101*, 6987–6992.

Fridkin, A., Penkner, A., Jantsch, V., and Gruenbaum, Y. (2009). SUN-domain and KASH-domain proteins during development, meiosis and disease. Cell. Mol. Life Sci. *66*, 1518–1533.

Garcia-Muse, T., and Boulton, S.J. (2005). Distinct modes of ATR activation after replication stress and DNA double-strand breaks in Caenorhabditis elegans. EMBO J. *24*, 4345–4355.

Goldstein, P., and Slaton, D.E. (1982). The synaptonemal complexes of caenorhabditis elegans: comparison of wild-type and mutant strains and pachytene karyotype analysis of wild-type. Chromosoma *84*, 585–597.

Hamill, D.R., Severson, A.F., Carter, J.C., and Bowerman, B. (2002). Centrosome maturation and mitotic spindle assembly in C. elegans require SPD-5, a protein with multiple coiled-coil domains. Dev. Cell *3*, 673–684.

Harper, L., Golubovskaya, I., and Cande, W.Z. (2004). A bouquet of chromosomes. J. Cell Sci. *117*, 4025–4032.

Kosaka, H., Shinohara, M., and Shinohara, A. (2008). Csm4-dependent telomere movement on nuclear envelope promotes meiotic recombination. PLoS Genet. *4*, e1000196.

Koszul, R., Kim, K.P., Prentiss, M., Kleckner, N., and Kameoka, S. (2008). Meiotic chromosomes move by linkage to dynamic actin cables with transduction of force through the nuclear envelope. Cell *133*, 1188–1201.

MacQueen, A.J., and Villeneuve, A.M. (2001). Nuclear reorganization and homologous chromosome pairing during meiotic prophase require C. elegans chk-2. Genes Dev. *15*, 1674–1687.

MacQueen, A.J., Colaiácovo, M.P., McDonald, K., and Villeneuve, A.M. (2002). Synapsis-dependent and -independent mechanisms stabilize homolog pairing during meiotic prophase in C. elegans. Genes Dev. *16*, 2428–2442.

MacQueen, A.J., Phillips, C.M., Bhalla, N., Weiser, P., Villeneuve, A.M., and Dernburg, A.F. (2005). Chromosome sites play dual roles to establish homologous synapsis during meiosis in C. elegans. Cell *123*, 1037–1050.

Malone, C.J., Misner, L., Bot, N.L., Tsai, M.-C., Campbell, J.M., Ahringer, J., and White, J.G. (2003). The C. elegans hook protein, ZYG-12, mediates the essential attachment between the centrosome and nucleus. Cell *115*, 825–836.

Martinez-Perez, E., and Villeneuve, A.M. (2005). HTP-1-dependent constraints coordinate homolog pairing and synapsis and promote chiasma formation during C. elegans meiosis. Genes Dev. *19*, 2727–2743.

Pasierbek, P., Jantsch, M., Melcher, M., Schleiffer, A., Schweizer, D., and Loidl, J. (2001). A Caenorhabditis elegans cohesion protein with functions in meiotic chromosome pairing and disjunction. Genes Dev. *15*, 1349–1360.

Pawlowski, W.P., and Cande, W.Z. (2005). Coordinating the events of the meiotic prophase. Trends Cell Biol. *15*, 674–681.

Pelletier, L., Ozlü, N., Hannak, E., Cowan, C., Habermann, B., Ruer, M., Müller-Reichert, T., and Hyman, A.A. (2004). The Caenorhabditis elegans centrosomal protein SPD-2 is required for both pericentriolar material recruitment and centriole duplication. Curr. Biol. *14*, 863–873.

Penkner, A., Tang, L., Novatchkova, M., Ladurner, M., Fridkin, A., Gruenbaum, Y., Schweizer, D., Loidl, J., and Jantsch, V. (2007). The nuclear envelope protein Matefin/SUN-1 is required for homologous pairing in C. elegans meiosis. Dev. Cell *12*, 873–885.

Perona, R., Moncho-Amor, V., Machado-Pinilla, R., Belda-Iniesta, C., and Pérez, I.S. (2008). Role of CHK2 in cancer development. Clin. Transl. Oncol. *10*, 538–542.

Petronczki, M., Siomos, M.F., and Nasmyth, K. (2003). Un ménage à quatre: the molecular biology of chromosome segregation in meiosis. Cell *112*, 423–440.

Phillips, C.M., and Dernburg, A.F. (2006). A family of zinc-finger proteins is required for chromosome-specific pairing and synapsis during meiosis in C. elegans. Dev. Cell *11*, 817–829.

Phillips, C.M., Wong, C., Bhalla, N., Carlton, P.M., Weiser, P., Meneely, P.M., and Dernburg, A.F. (2005). HIM-8 binds to the X chromosome pairing center and mediates chromosome-specific meiotic synapsis. Cell *123*, 1051–1063.

Phillips, C.M., Meng, X., Zhang, L., Chretien, J.H., Urnov, F.D., and Dernburg, A.F. (2009). Identification of chromosome sequence motifs that mediate meiotic pairing and synapsis in C. elegans. Nat. Cell Biol. *11*, 934–942.

Sato, A., Isaac, B., Phillips, C.M., Rillo, R., Carlton, P.M., Wynne, D.J., Roshni, A., Kasad, R.A., and Dernburg, A.F. (2009). Cytoskeletal forces span the nuclear envelope to coordinate meiotic chromosome pairing and synapsis. Cell *139*, this issue, 907–919.

Scherthan, H. (2007). Telomere attachment and clustering during meiosis. Cell. Mol. Life Sci. *64*, 117–124.

Scherthan, H., Wang, H., Adelfalk, C., White, E.J., Cowan, C., Cande, W.Z., and Kaback, D.B. (2007). Chromosome mobility during meiotic prophase in Saccharomyces cerevisiae. Proc. Natl. Acad. Sci. USA *104*, 16934–16939.

Schmitt, J., Benavente, R., Hodzic, D., Höög, C., Stewart, C.L., and Alsheimer, M. (2007). Transmembrane protein Sun2 is involved in tethering mammalian meiotic telomeres to the nuclear envelope. Proc. Natl. Acad. Sci. USA *104*, 7426–7431.

Shevchenko, A., Wilm, M., Vorm, O., and Mann, M. (1996). Mass spectrometric sequencing of proteins silver-stained polyacrylamide gels. Anal. Chem. *68*, 850–858.

Smolikov, S., Eizinger, A., Schild-Prufert, K., Hurlburt, A., McDonald, K., Engebrecht, J., Villeneuve, A.M., and Colaiácovo, M.P. (2007a). SYP-3 restricts synaptonemal complex assembly to bridge paired chromosome axes during meiosis in Caenorhabditis elegans. Genetics *176*, 2015–2025.

Smolikov, S., Eizinger, A., Hurlburt, A., Rogers, E., Villeneuve, A.M., and Colaiácovo, M.P. (2007b). Synapsis-defective mutants reveal a correlation between chromosome conformation and the mode of double-strand break repair during Caenorhabditis elegans meiosis. Genetics *176*, 2027–2033.

Starr, D.A. (2009). A nuclear-envelope bridge positions nuclei and moves chromosomes. J. Cell Sci. *122*, 577–586.

Stergiou, L., Doukoumetzidis, K., Sendoel, A., and Hengartner, M.O. (2007). The nucleotide excision repair pathway is required for UV-C-induced apoptosis in Caenorhabditis elegans. Cell Death Differ. *14*, 1129–1138.

Tang, X., Jin, Y., and Cande, W.Z. (2006). Bqt2p is essential for initiating telomere clustering upon pheromone sensing in fission yeast. J. Cell Biol. *173*, 845–851.

Trelles-Sticken, E., Adelfalk, C., Loidl, J., and Scherthan, H. (2005). Meiotic telomere clustering requires actin for its formation and cohesin for its resolution. J. Cell Biol. *170*, 213–223.

Tzur, Y.B., Wilson, K.L., and Gruenbaum, Y. (2006). SUN-domain proteins: 'Velcro' that links the nucleoskeleton to the cytoskeleton. Nat. Rev. Mol. Cell Biol. *7*, 782–788.

Wanat, J.J., Kim, K.P., Koszul, R., Zanders, S., Weiner, B., Kleckner, N., and Alani, E. (2008). Csm4, in collaboration with Ndj1, mediates telomere-led chromosome dynamics and recombination during yeast meiosis. PLoS Genet. *4*, e1000188.

Yamamoto, A., West, R.R., McIntosh, J.R., and Hiraoka, Y. (1999). A cytoplasmic dynein heavy chain is required for oscillatory nuclear movement of meiotic prophase and efficient meiotic recombination in fission yeast. J. Cell Biol. *145*, 1233–1249.

Cell, Volume *139*

Supplemental Data

Meiotic Chromosome Homology Search

Involves Modifications of the Nuclear

Envelope Protein Matefin/SUN-1

Alexandra M. Penkner, Alexandra Fridkin, Jiradet Gloggnitzer, Antoine Baudrimont, Thomas Machacek, Alexander Woglar, Edina Csaszar, Pawel Pasierbek, Gustav Ammerer, Yosef Gruenbaum, Verena Jantsch

Supplemental Experimental Procedures

Nematode strains, strain construction and culture conditions

All *C. elegans* strains were cultured using standard techniques (Brenner, 1974).
C. elegans strains used: N2 Bristol, RB1276 *mtf-1/sun-1(ok1282)*, WH223 ojIs9 *[zyg-12ABC::GFP unc-119(ed3)]; unc-119(ed3)* (Malone et al., 2003), AV276 *syp-2(ok307)* (Colaiacovo et al., 2003), VC418 *him-3(gk149)* (Couteau et al., 2004), *chk-2(me64)* (MacQueen and Villeneuve, 2001), BA821 *spe-26(hc138)* (Van Voorhies, 1992), AV393 *htp-1(gk174)* (Martinez-Perez and Villeneuve, 2005), AV157 *spo-11(me44)* (Hayashi et al., 2007), VC381 *atm-1(gk186)* (Stergiou et al., 2007), DW101 *atl-1(tm853)* (Garcia-Muse and Boulton, 2005), UV21 *him-19(jf6)* (Tang and Jantsch, unpublished).
Nematode strains were provided by the *Caenorhabditis Genetics Center*, which is funded by the NIH National Center for Research Resources (NCRR).

Matefin/SUN-1::GFP-expressing transgenic worm strains were generated by microparticle bombardment (Praitis et al., 2001). The *mtf-1/sun-1*-coding locus including 2.8 kb of its 5' sequence and 780 bp of its 3' regulatory sequence was inserted into the pEGFP-1 vector of BD Biosciences Clontech (#6086-1) and co-bombarded with plasmid pDP#mm051 carrying the *unc-119* locus into the *C. elegans* mutant *unc-119(ed3)*. Mutated forms of Matefin/SUN-1::GFP were generated by site-directed mutagenesis. Mutated Matefin/SUN-1::GFP proteins were analyzed in the homozygous *mtf-1/sun-1(ok1282)* deletion background.

Immunoprecipitation and silver staining of Matefin/SUN-1::GFP

1x homogenization buffer: 15 mM Hepes pH7.6, 10 mM KCl, 250 mM NaCl, 1.5 mM $MgCl_2$, 0.1 mM EDTA, 0.5 mM EGTA, 0,2% Triton*100, 1 mM DTT, 44 mM sucrose, 0.1 mM AEBSF, 5 mM benzamidine, 1:200 aprotinin, 50 mM NaF, 0.1 mM Na_3VO_4, 60 mM β-glycerophosphate, Roche® Complete Mini protease inhibitor cocktail tablets (#11836170001).
SDS-sample buffer: 55 mM Tris/HCl pH6.8, 6 M Urea, 2% (w/v) SDS, 0.1 mM EDTA, 5% (v/v) β-mercaptoethanol, 6% glycerol, 0.025% bromophenol blue.

Mass spectrometry analysis

Enzymatic digest, LC-MS/MS analysis and data analysis

Silver stained gel bands were used for nano-electrospray LC-MS/MS analysis. The gel bands were cut, chopped and washed several times with high quality water. Proteins were reduced by dithiothreitol (DTT) and alkylated by iodoacetamide, trypsin digested overnight at 37°C and stopped by acidifying to 1% with formic acid. We used an HPLC UltiMate™ system equipped with a PepMap C18 purification column (300 µm x 5 mm) and a 75 µm x 150 mm analytical column of the same material. 0.1% TFA was used on the Switchos module for the binding of the peptides and a linear gradient of acetonitrile and 0.1% formic acid in water was used for the elution. LC-MS/MS analyses were carried out with the UltiMate™ system interfaced to an LTQ (Thermo; San Jose, CA, USA) linear ion trap mass spectrometer. The nanospray source of Proxeon (Odense, Denmark) was used with the distal coated silica capillaries of New Objective (Woburn, MA, USA). The electrospray voltage was set to 1500 V. Peptide spectra were recorded over the mass range of m/z 450-1600, MS/MS spectra were recorded in information dependent data acquisition and the default charge state was set to 3; the mass range for MS/MS measurements was calculated according to the masses of the parent ions. One full spectrum was recorded followed by 4 MS/MS spectra for the most intense ions, automatic gain control was applied and the collision energy was set to the arbitrary value of 35. Neutral loss dependent MS/MS/MS experiments were carried out to enhance the fragmentation of phosphopeptides. It was used as collision gas. The instrument was operated in data-dependent modus; fragmented ions were set onto an exclusion list for 20 sec.
Raw spectra were interpreted by Mascot 2.2.04 (Matrix Science Ltd, London, UK) using Mascot Daemon 2.2.2. and Bioworks 3.3 (Thermo; San Jose, CA, USA). Peptide tolerance was set to +/-2 Da, MS/MS tolerance was set to +/-0.8 Da. Carbamidomethylcysteine was set as static modification, oxidation of M, phosphorylation of STY residues and water loss of ST residues were set as variable modifications for both search programs.
The database used for Mascot search was the nr protein database of NIH (NCBI Resources, NIH, Bethesda, MD, USA); taxonomy was *C. elegans*. In order to reduce the search time, the Bioworks search was carried out with a homemade database prepared by the extraction (Bioworks) of all *C. elegans* entries out of the NIH nr database. Ion score cut off was set to 30 for Mascot.
Xcorr versus charge state was set as the filter for Bioworks with the following values: 1.5, 2.00, 2.50, 3.00 for singly, doubly, triply and quadruply charged ions, respectively. Peptide spectra indicated to contain phosphorylated residues were validated manually in both cases.

Live imaging of Matefin/SUN-1::GFP constructs
M9 buffer: 0.6% (w/v) Na_2HPO_4 x$(H_2O)_7$, 0.3% (w/v) KH_2PO_4, 0.5% (w/v) NaCl, 0.02% (w/v) $MgSO_4$ x$(H_2O)_7$

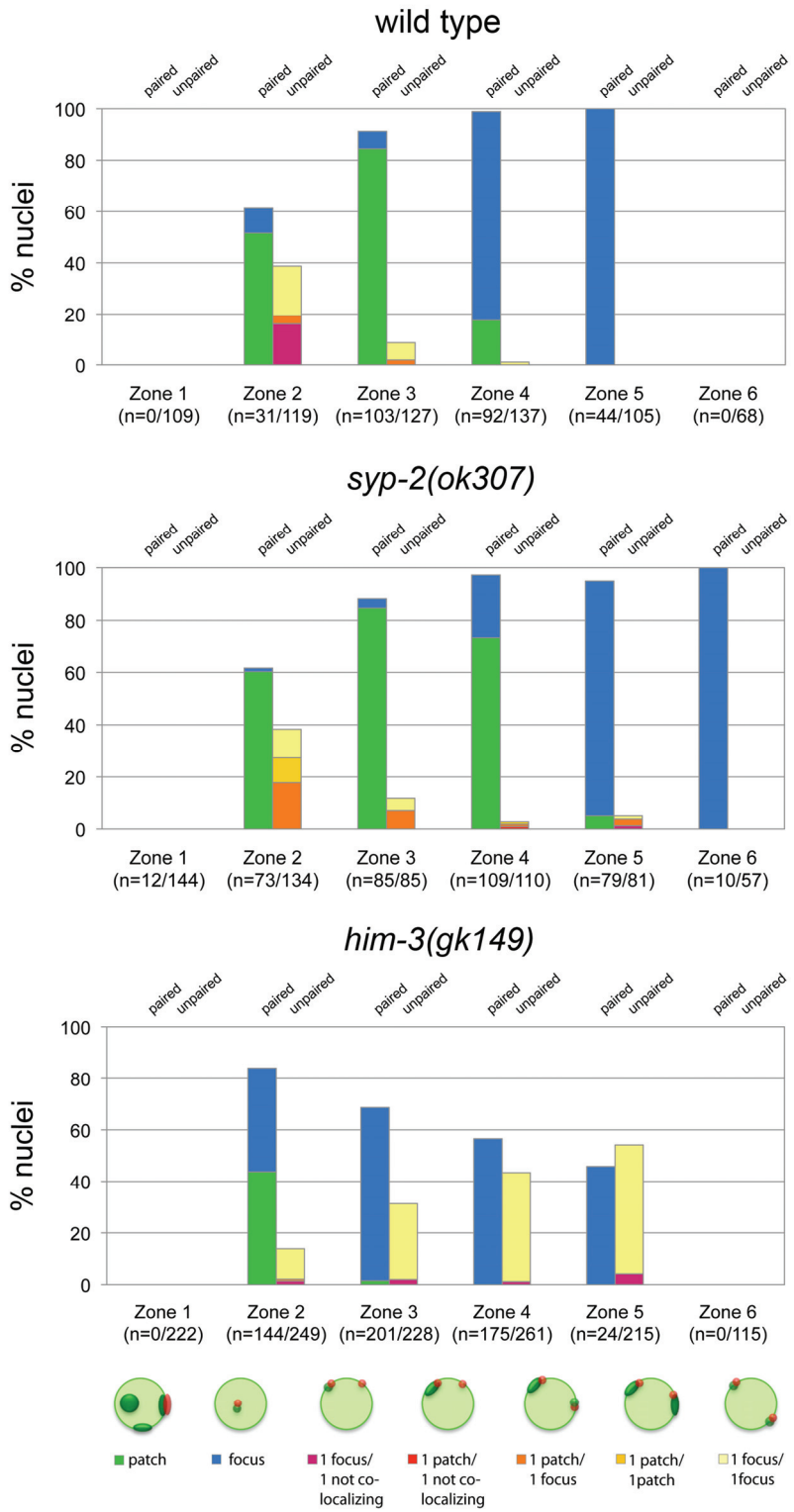

Figure S1. Analysis of the co-localization of Matefin/SUN-1 aggregates and the X chromosome-specific pairing center-binding protein HIM-8 in nuclei displaying aggregates as well as HIM-8 foci. Diagrams of wild type (*mtf-1/sun-1::gfp;mtf-1/sun-1(ok1282)*), *syp-2(ok307)* (*syp-2(ok307);mtf-1/sun-1::gfp;mtf-1/sun-1(ok1282)*) and *him-*

3(gk149) (*him-3(gk149);mtf-1/sun-1::gfp;mtf-1/sun-1(ok1282)*) are shown. The number of nuclei analyzed per total number of nuclei is given for each zone.

Figure S2. Mass spectrometry analysis of Matefin/SUN-1::GFP purified from *mtf-1/sun-1::gfp;mtf-1/sun-1(ok1282)* hermaphrodites.

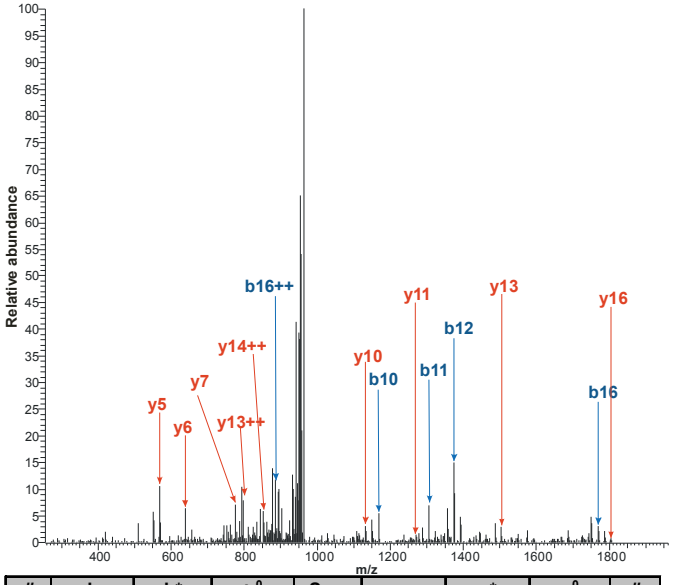

#	b	b*	b^0	Seq.	y	y*	y^0	#
1	138.07			H				17
2	239.11		221.1	T	1805.94	1788.91	1787.93	16
3	352.2		334.19	I	1704.89	1687.87	1686.88	15
4	439.23		421.22	S	1591.81	1574.78	1573.8	14
5	536.28		518.27	P	1504.78	1487.75	1486.77	13
6	664.34	647.31	646.33	Q	1407.72	1390.7	1389.71	12
7	811.41	794.38	793.4	F	1279.67	1262.64	1261.65	11
8	898.44	881.42	880.43	S	1132.6	1115.57	1114.59	10
9	1012.48	995.46	994.47	N	1045.57	1028.54	1027.55	9
10	1168.59	1151.56	1150.58	R	931.52	914.5	913.51	8
11	1305.64	1288.62	1287.63	H	775.42	758.39	757.41	7
12	1374.67	1357.64	1356.66	S@	638.36	621.34	620.35	6
13	1471.72	1454.69	1453.71	P	569.34	552.31	551.33	5
14	1568.77	1551.75	1550.76	P	472.29	455.26	454.28	4
15	1667.84	1650.81	1649.83	V	375.24	358.21	357.22	3
16	1768.89	1751.86	1750.88	T	276.17	259.14	258.16	2
17				R	175.12	158.09		1

Figure S2.1 Positive ionization low energy CID fragmentation spectrum of the singly phosphorylated peptide HTISPQFSNRHSPPVTR originating from the Matefin/SUN-1::GFP; *mtf-1/sun-1(ok1282)* sample

MS^3 spectrum of the doubly charged peptide. The position of the dehydro-alanine generated by the loss of phosphoric acid from the phosphorylated serine residue was labeled with "@". Identified b and y fragment ions detected in the measurement are colored in the fragmentation table and labeled blue and red, respectively in the spectrum. Identified satellite ions originating from the loss of water (b0 or y0 ions) or ammonia (b* or y* ions) are also labeled in the table. Although the peptide was doubly charged, it contains several basic residues which account for the doubly charged fragment ions.

#	b	b^{++}	Seq.	y	y^{++}	#
1	138.07	69.54	H			17
2	239.11	120.06	T	1805.94	903.47	16
3	352.2	176.6	I	1704.89	852.95	15
4	439.23	220.12	S	1591.81	796.41	14
5	536.28	268.64	P	1504.78	752.89	13
6	664.34	332.67	Q	1407.72	704.37	12
7	811.41	406.21	F	1279.67	640.34	11
8	898.44	449.72	S	1132.6	566.8	10
9	1012.48	506.75	N	1045.57	523.29	9
10	1168.59	584.8	R	931.52	466.26	8
11	1305.64	653.33	H	775.42	388.21	7
12	1374.67	687.84	S@	638.36	319.68	6
13	1471.72	736.36	P	569.34	285.17	5
14	1568.77	784.89	P	472.29	236.65	4
15	1667.84	834.42	V	375.24	188.12	3
16	1768.89	884.95	T	276.17	138.59	2
17			R	175.12	88.06	1

#	b	b^{++}	Seq.	y	y^{++}	#
1	138.07	69.54	H			17
2	239.11	120.06	T	1805.94	903.47	16
3	352.2	176.6	I	1704.89	852.95	15
4	421.22	211.11	S@	1591.81	796.41	14
5	518.27	259.64	P	1522.79	761.9	13
6	646.33	323.67	Q	1425.73	713.37	12
7	793.4	397.2	F	1297.68	649.34	11
8	880.43	440.72	S	1150.61	575.81	10
9	994.47	497.74	N	1063.58	532.29	9
10	1150.58	575.79	R	949.53	475.27	8
11	1287.63	644.32	H	793.43	397.22	7
12	1374.67	687.84	S	656.37	328.69	6
13	1471.72	736.36	P	569.34	285.17	5
14	1568.77	784.89	P	472.29	236.65	4
15	1667.84	834.42	V	375.24	188.12	3
16	1768.89	884.95	T	276.17	138.59	2
17			R	175.12	88.06	1

#	b	b^{++}	Seq.	y	y^{++}	#
1	138.07	69.54	H			17
2	239.11	120.06	T	1805.94	903.47	16
3	352.2	176.6	I	1704.89	852.95	15
4	439.23	220.12	S	1591.81	796.41	14
5	536.28	268.64	P	1504.78	752.89	13
6	664.34	332.67	Q	1407.72	704.37	12
7	811.41	406.21	F	1279.67	640.34	11
8	880.43	440.72	S@	1132.6	566.8	10
9	994.47	497.74	N	1063.58	532.29	9
10	1150.58	575.79	R	949.53	475.27	8
11	1287.63	644.32	H	793.43	397.22	7
12	1374.67	687.84	S	656.37	328.69	6
13	1471.72	736.36	P	569.34	285.17	5
14	1568.77	784.89	P	472.29	236.65	4
15	1667.84	834.42	V	375.24	188.12	3
16	1768.89	884.95	T	276.17	138.59	2
17			R	175.12	88.06	1

Figure S2.2 Assignment of the phosphorylation site in the peptide HTISPQFSNRHSPPVTR

Fragment ion coverages for three possible phosphorylation sites. Identified b and y fragment ions detected in the MS^3 measurement are colored red in the fragmentation table. The position of the dehydro-alanine was labeled with "@". Although this peptide was fragmented several times, the unambiguous identification of the modification site was not possible. The phosphorylation was identified by both applied search engines (Mascot and Sequest), but three possible positions were proposed with nearly identical score values. Manual assignment of the fragment ions did not make the differentiation possible either. We concluded, that this spectrum was a mixture of different singly phosphorylated species, which eluted and were fragmented simultaneously. This peptide version with one missed cleavage site was only present in the phosphorylated version. The unphosphorylated peptide was always cleaved C-terminal to R14 by trypsin. This fact supports the phosphorylation on S12. The doubly phosphorylated version of the peptide was also detected (Figure S2.3).

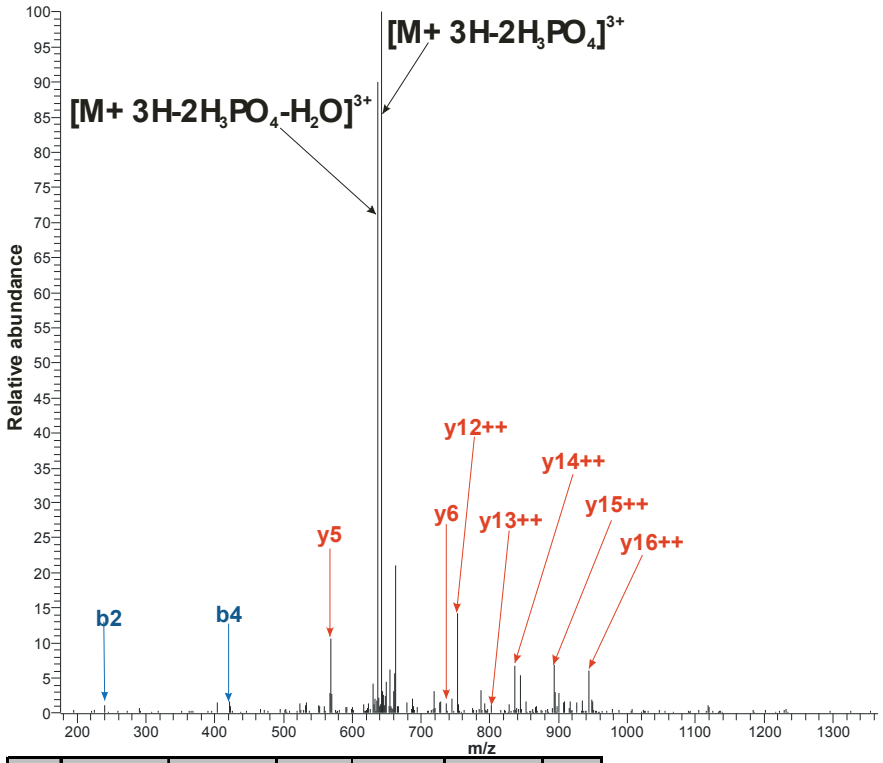

#	b	b++	Seq.	y	y++	#
1	138.07	69.54	H	-	-	17
2	239.11	120.06	T	1885.92	943.46	16
3	352.2	176.6	I	1784.87	892.94	15
4	421.23	211.12	S@	1671.79	836.4	14
5	518.28	259.64	P	1602.75	801.88	13
6	646.34	323.67	Q	1505.7	753.35	12
7	793.41	397.21	F	1377.64	689.32	11
8	880.44	440.72	S	1230.57	615.79	10
9	994.48	497.75	N	1143.54	572.27	9
10	1150.59	575.8	R	1029.5	515.25	8
11	1287.64	644.33	H	873.4	437.2	7
12	1454.64	727.83	S#	736.34	368.67	6
13	1551.7	776.35	P	569.34	285.17	5
14	1648.75	824.88	P	472.29	236.65	4
15	1747.82	874.41	V	375.24	188.12	3
16	1848.86	924.94	T	276.17	138.59	2
17	-	-	R	175.12	88.06	1

#	b	b^{++}	Seq.	y	y^{++}	#
1	138.07	69.54	H	-	-	17
2	239.11	120.06	T	1983.88	992.45	16
3	352.2	176.6	I	1882.84	941.92	15
4	519.2	260.1	S#	1769.75	885.38	14
5	616.25	308.63	P	1602.75	801.88	13
6	744.31	372.66	Q	1505.7	753.35	12
7	891.38	446.19	F	1377.64	689.32	11
8	978.41	489.71	S	1230.57	615.79	10
9	1092.45	546.73	N	1143.54	572.27	9
10	1248.55	624.78	R	1029.5	515.25	8
11	1385.61	693.31	H	873.4	437.2	7
12	1552.61	776.81	S#	736.34	368.67	6
13	1649.66	825.33	P	569.34	285.17	5
14	1746.71	873.86	P	472.29	236.65	4
15	1845.78	923.4	V	375.24	188.12	3
16	1946.83	973.92	T	276.17	138.59	2
17	-	-	R	175.12	88.06	1

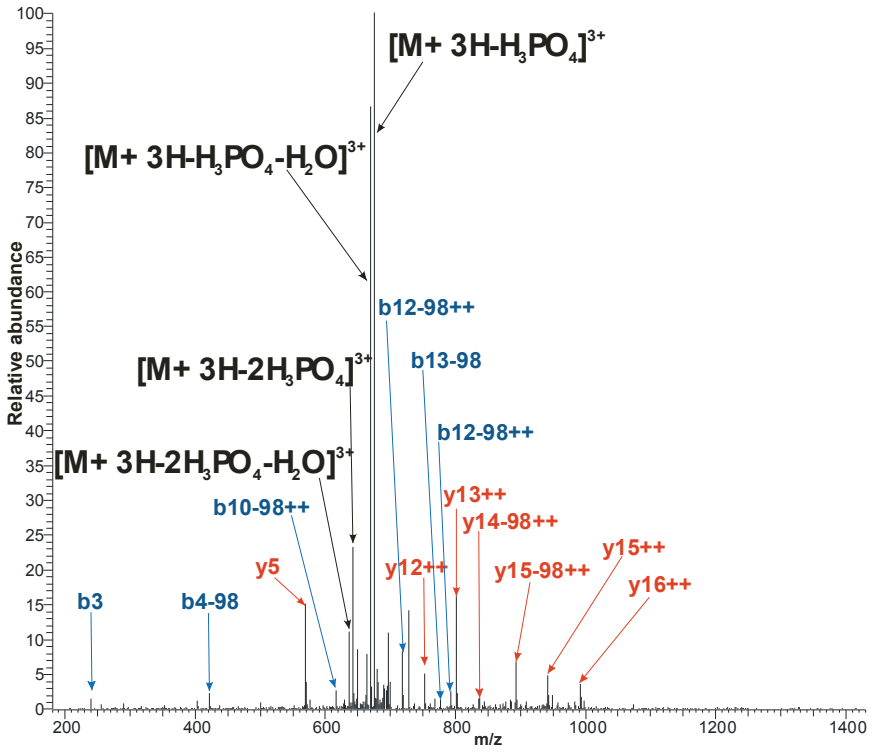

Figure S2.3 Positive ionization low energy CID fragmentation spectrum of the doubly phosphorylated peptide HTISPQFSNRHSPPVTR originating from the Matefin/SUN-1::GFP; *mtf-1/sun-1(ok1282)* sample

MS^2 (a) and MS^3 (b) spectrum of the triply charged peptide. The position of the phosphorylated residue was labeled with "#", the position of dehydro-alanine in the MS^3 spectrum was labeled with "@". Identified b and y fragment ions detected in the measurement are colored in the fragmentation table and labeled blue and red, respectively, in the spectrum. Identified satellite ions originating from the loss of water (b0 or y0 ions) or ammonia (b* or y* ions) are also labeled in the table. Although the fragmentation was poor, important characteristic ions (neutral losses, water loss, intensive fragmentation at prolines) could be easily recognized.

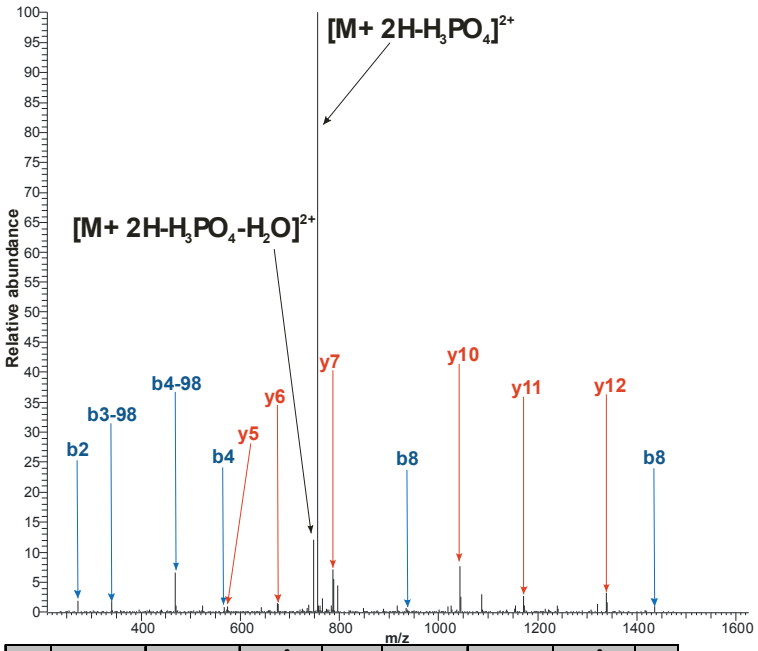

#	b	b*	b^0	Seq.	y	y*	y^0	#
1	157.11	140.08		R				14
2	272.14	255.11	254.12	D	1453.67	1436.64	1435.66	13
3	439.13	422.11	421.12	S#	1338.64	1321.61	1320.63	12
4	567.19	550.17	549.18	Q	1171.64	1154.62	1153.63	11
5	664.25	647.22	646.23	P	1043.58	1026.56	1025.57	10
6	721.27	704.24	703.26	G	946.53	929.51	928.52	9
7	822.31	805.29	804.3	T	889.51	872.48	871.5	8
8	935.4	918.37	917.39	I	788.46	771.44	770.45	7
9	1036.45	1019.42	1018.44	T	675.38	658.35	657.37	6
10	1093.47	1076.44	1075.46	G	574.33	557.3	556.32	5
11	1194.52	1177.49	1176.5	T	517.31	500.28	499.3	4
12	1307.6	1290.57	1289.59	I	416.26	399.24		3
13	1435.66	1418.63	1417.65	Q	303.18	286.15		2
14				R	175.12	158.09		1

#	b	b*	b^0	Seq.	y	y*	y^0	#
1	157.11	140.08		R				14
2	272.14	255.11	254.12	D	1355.69	1338.66	1337.68	13
3	341.16	324.13	323.15	S@	1240.66	1223.64	1222.65	12
4	469.22	452.19	451.2	Q	1171.64	1154.62	1153.63	11
5	566.27	549.24	548.26	P	1043.58	1026.56	1025.57	10
6	623.29	606.26	605.28	G	946.53	929.51	928.52	9
7	724.34	707.31	706.33	T	889.51	872.48	871.5	8
8	837.42	820.39	819.41	I	788.46	771.44	770.45	7
9	938.47	921.44	920.46	T	675.38	658.35	657.37	6
10	995.49	978.46	977.48	G	574.33	557.3	556.32	5
11	1096.54	1079.5	1078.53	T	517.31	500.28	499.3	4
12	1209.62	1192.6	1191.61	I	416.26	399.24		3
13	1337.68	1320.7	1319.67	Q	303.18	286.15		2
14				R	175.12	158.09		1

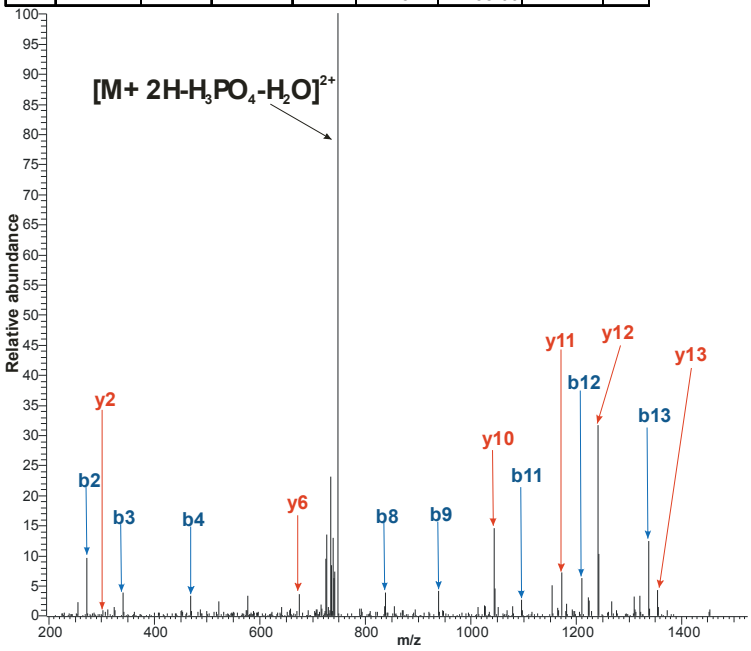

Figure S2.4 Positive ionization low energy CID fragmentation spectrum of the singly phosphorylated peptide RDSQPGTITGTIQR originating from the Matefin/SUN-1::GFP; *mtf-1/sun-1(ok1282)* sample

MS^2 (a) and MS^3 (b) spectrum of the doubly charged peptide. The position of the phosphorylated residue was labeled with "#", the position of the dehydro-alanine in the MS^3 spectrum was labeled with "@". Identified b and y fragment ions detected in the measurement are colored in the fragmentation table and labeled blue and red, respectively, in the spectrum. Identified satellite ions originating from the loss of water (b0 or y0 ions) or ammonia (b* or y* ions) are also labeled in the table.

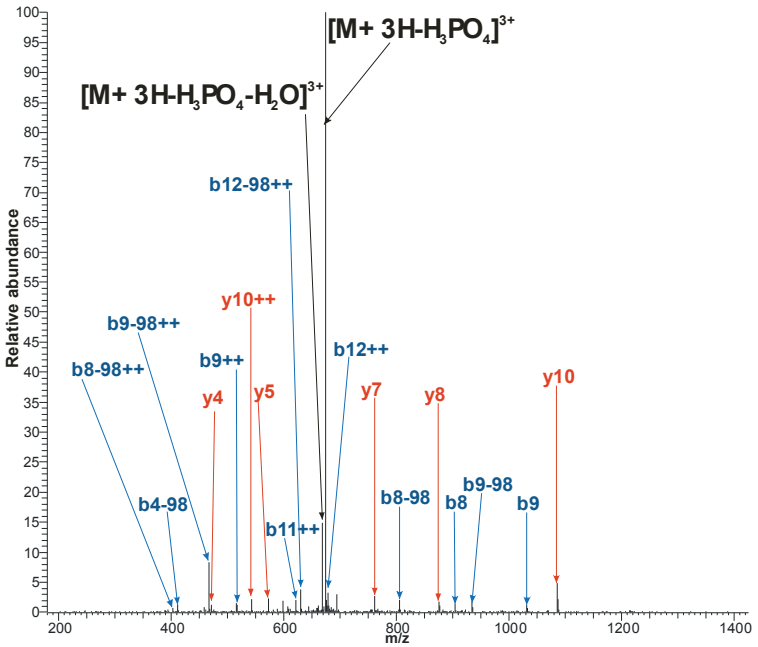

#	b	b^{++}	b*	b*$^{++}$	b^{0}	b^{0++}	Seq.	y	y^{++}	y*	y*$^{++}$	y^{0}	y^{0++}	#
1	88.0393	44.52329			70.02874	35.51801	S							19
2	187.1077	94.0575			169.0972	85.05221	V	1933.025	967.0161	1915.998	958.5029	1915.014	958.0109	18
3	256.1292	128.5682			238.1186	119.5629	S#	1833.957	917.4819	1816.93	908.9687	1815.946	908.4767	17
4	412.2303	206.6188	395.2037	198.1055	394.2197	197.6135	R	1764.935	882.9712	1747.909	874.4579	1746.925	873.9659	16
5	513.278	257.1426	496.2514	248.6294	495.2674	248.1373	T	1608.834	804.9206	1591.807	796.4074	1590.823	795.9154	15
6	570.2994	285.6534	553.2729	277.1401	552.2889	276.6481	G	1507.786	754.3968	1490.76	745.8835	1489.776	745.3915	14
7	669.3678	335.1876	652.3413	326.6743	651.3573	326.1823	V	1450.765	725.8861	1433.738	717.3728	1432.754	716.8808	13
8	806.4268	403.717	789.4002	395.2037	788.4162	394.7117	H	1351.696	676.3519	1334.67	667.8386	1333.686	667.3466	12
9	934.4853	467.7463	917.4588	459.233	916.4748	458.741	Q	1214.638	607.8224	1197.611	599.3091	1196.627	598.8171	11
10	1031.538	516.2727	1014.512	507.7594	1013.528	507.2674	P	1086.579	543.7931	1069.552	535.2799	1068.568	534.7878	10
11	1144.622	572.8147	1127.596	564.3014	1126.612	563.8094	L	989.5262	495.2667	972.4997	486.7535	971.5156	486.2615	9
12	1259.649	630.3282	1242.623	621.8149	1241.639	621.3229	D	876.4421	438.7247	859.4156	430.2114	858.4316	429.7194	8
13	1360.697	680.852	1343.67	672.3388	1342.686	671.8468	T	761.4152	381.2112	744.3887	372.698	743.4046	372.206	7
14	1447.729	724.368	1430.702	715.8548	1429.718	715.3628	S	660.3675	330.6874	643.341	322.1741	642.357	321.6821	6
15	1548.776	774.8919	1531.75	766.3786	1530.766	765.8866	T	573.3355	287.1714	556.3089	278.6581	555.3249	278.1661	5
16	1645.829	823.4183	1628.803	814.905	1627.819	814.413	P	472.2878	236.6475	455.2613	228.1343	454.2772	227.6423	4
17	1744.898	872.9525	1727.871	864.4392	1726.887	863.9472	V	375.2351	188.1212	358.2085	179.6079	357.2245	179.1159	3
18	1845.945	923.4763	1828.919	914.963	1827.935	914.471	T	276.1666	138.587	259.1401	130.0737	258.1561	129.5817	2
19							R	175.119	88.06311	158.0924	79.54984			

Figure S2.5 Positive ionization low energy CID spectrum of the singly phosphorylated peptide SVSRTGVHQPLDTSTPVTR originating from the Matefin/SUN-1::GFP; *mtf-1/sun-1(ok1282)* sample

MS^2 spectrum of the triply charged peptide. The position of the phosphorylated residue was labeled with "#". Identified b and y fragment ions are labeled in the fragmentation table and colored (b* or y* ions) are also labeled in the table. According to the information provided by the fragmentation it was not possible to unambiguously localize the phosphorylation site to S22 or S24. Because of the presence of a missed cleavage site at R25 we assumed, that the phosphorylation was probably on S24. This missed cleavage site was only detected in the phosphorylated peptide.

#	b	b*	b^0	Seq.	y	y*	y^0	#
1	148.08			F				16
2	285.13			H	1806.65	1789.62	1788.64	15
3	414.18		396.17	E	1669.59	1652.56	1651.58	14
4	581.18		563.16	S#	1540.55	1523.52	1522.53	13
5	652.21		634.2	A	1373.55	1356.52	1355.54	12
6	767.24		749.23	D	1302.51	1285.48	1284.5	11
7	882.27		864.26	D	1187.48	1170.46	1169.47	10
8	1049.26		1031.25	S#	1072.46	1055.43	1054.45	9
9	1178.31		1160.3	E	905.46	888.43	887.45	8
10	1291.39		1273.38	I	776.41	759.39	758.4	7
11	1406.42		1388.41	D	663.33	646.3	645.32	6
12	1519.5		1501.49	L	548.3	531.28	530.29	5
13	1633.55	1616.52	1615.53	N	435.22	418.19	417.21	4
14	1720.58	1703.55	1702.57	S	321.18	304.15	303.17	3
15	1807.61	1790.58	1789.6	S	234.14	217.12	216.13	2
16				K	147.11	130.09		1

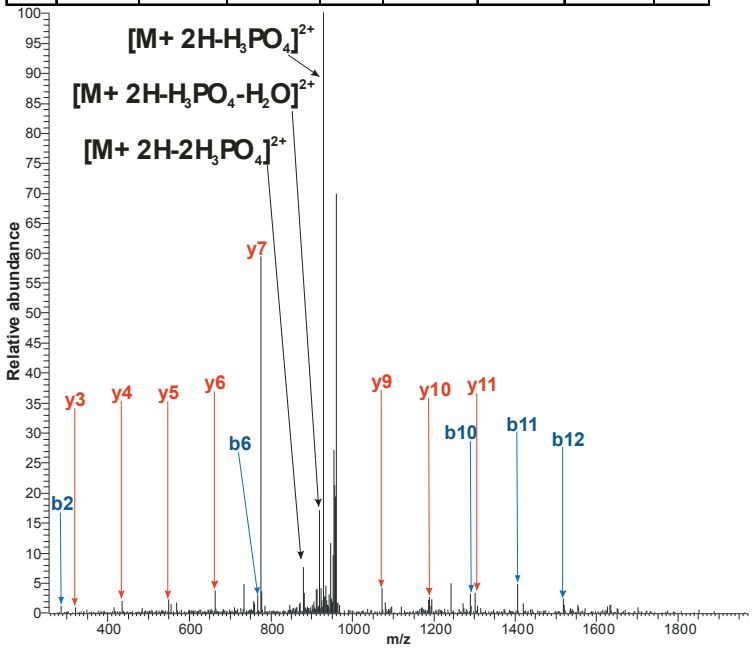

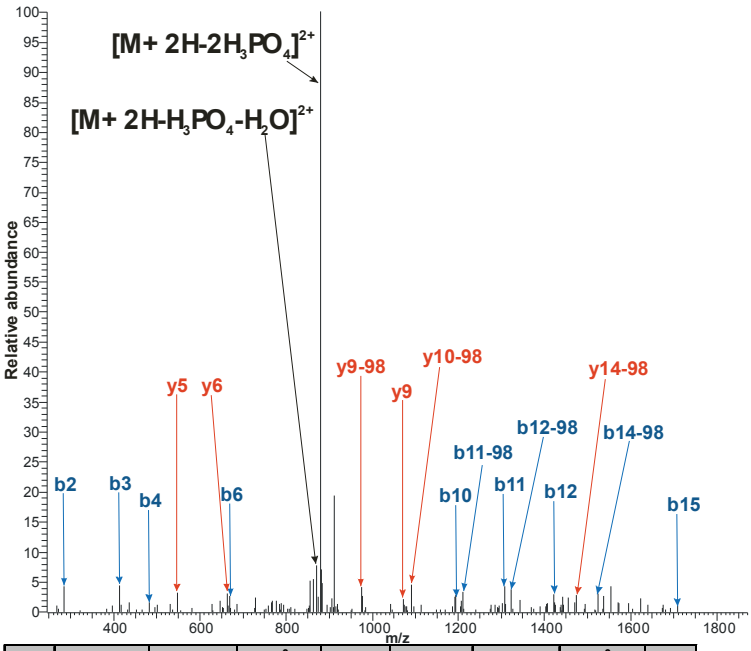

#	b	b*	b^0	Seq.	y	y*	y^0	#
1	148.08			F				16
2	285.13			H	1708.67	1691.64	1690.66	15
3	414.18		396.17	E	1571.61	1554.58	1553.6	14
4	483.2		465.19	S@	1442.57	1425.54	1424.56	13
5	554.24		536.23	A	1373.55	1356.52	1355.54	12
6	669.26		651.25	D	1302.51	1285.48	1284.5	11
7	784.29		766.28	D	1187.48	1170.46	1169.47	10
8	951.29		933.28	S#	1072.46	1055.43	1054.45	9
9	1080.33		1062.32	E	905.46	888.43	887.45	8
10	1193.41		1175.4	I	776.41	759.39	758.4	7
11	1308.44		1290.43	D	663.33	646.3	645.32	6
12	1421.53		1403.52	L	548.3	531.28	530.29	5
13	1535.57	1518.54	1517.56	N	435.22	418.19	417.21	4
14	1622.6	1605.57	1604.59	S	321.18	304.15	303.17	3
15	1709.63	1692.61	1691.62	S	234.14	217.12	216.13	2
16				K	147.11	130.09		1

Figure S2.6 Positive ionization low energy CID spectrum of the doubly phosphorylated peptide FHESADDSEIDLNSSK originating from the Matefin/SUN-1::GFP; *mtf-1/sun-1(ok1282)* sample

MS^2 (a) and MS^3 (b) spectrum of the doubly charged peptide. The positions of the phosphorylated residue and dehydro-alanine were labeled by "#" and "@". Identified b and y fragment ions are colored blue and red, respectively, in the spectrum and labeled in the fragmentation tables (a,b) Identified satellite ions originating from the loss of water (b0 or y0 ions) or ammonia (b* or y* ions) are also labeled in the fragmentation tables. Only the doubly phosphorylated peptide was detected.

Figure S3. Mass spectrometry analysis of Matefin/SUN-1::GFP purified from *mtf-1/sun-1::gfp;spe-26(hc138)* hermaphrodites.

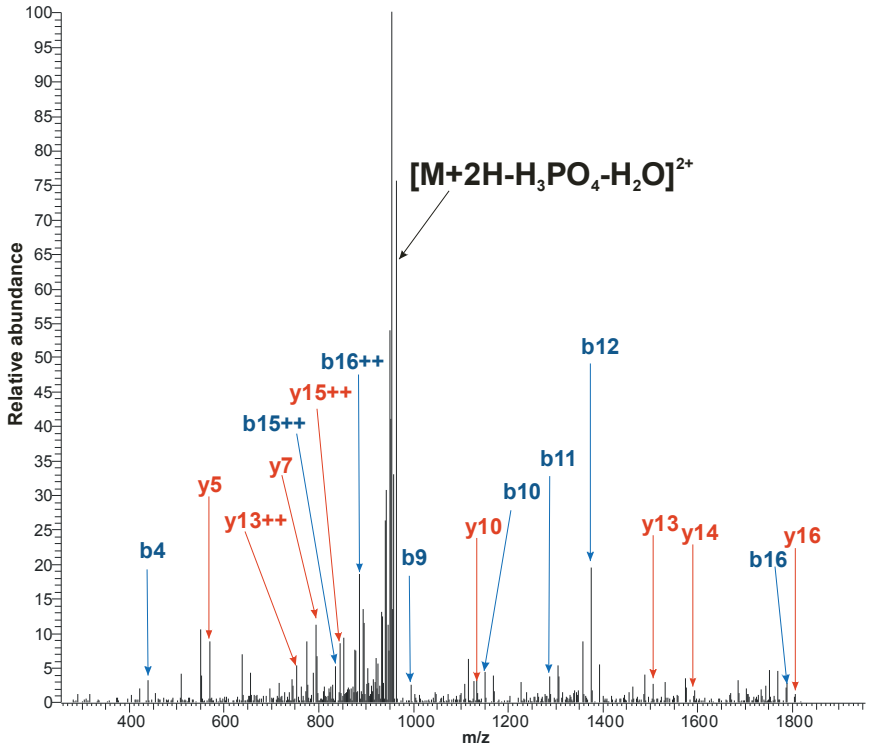

#	b	b++	b*	b*++	b0	b0++	Seq.	y	y++	y*	y*++	y0	y0++	#
1	138.07	69.54					H							17
2	239.11	120.06			221.1	111.06	T	1805.94	903.47	1788.91	894.96	1787.93	894.47	16
3	352.2	176.6			334.19	167.6	I	1704.89	852.95	1687.87	844.44	1686.88	843.94	15
4	439.23	220.12			421.22	211.11	S	1591.81	796.41	1574.78	787.89	1573.8	787.4	14
5	536.28	268.64			518.27	259.64	P	1504.78	752.89	1487.75	744.38	1486.77	743.89	13
6	664.34	332.67	647.31	324.16	646.33	323.67	Q	1407.72	704.37	1390.7	695.85	1389.71	695.36	12
7	811.41	406.21	794.38	397.7	793.4	397.2	F	1279.67	640.34	1262.64	631.82	1261.65	631.33	11
8	880.43	440.72	863.4	432.21	862.42	431.71	S@	1132.6	566.8	1115.57	558.29	1114.59	557.8	10
9	994.47	497.74	977.45	489.23	976.46	488.74	N	1063.58	532.29	1046.55	523.78	1045.56	523.29	9
10	1150.58	575.79	1133.55	567.28	1132.56	566.79	R	949.53	475.27	932.51	466.76	931.52	466.26	8
11	1287.63	644.32	1270.61	635.81	1269.62	635.32	H	793.43	397.22	776.4	388.71	775.42	388.21	7
12	1374.67	687.84	1357.64	679.32	1356.66	678.83	S	656.37	328.69	639.35	320.18	638.36	319.68	6
13	1471.72	736.36	1454.69	727.85	1453.71	727.36	P	569.34	285.17	552.31	276.66	551.33	276.17	5
14	1568.77	784.89	1551.75	776.38	1550.76	775.88	P	472.29	236.65	455.26	228.13	454.28	227.64	4
15	1667.84	834.42	1650.81	825.91	1649.83	825.42	V	375.24	188.12	358.21	179.61	357.22	179.12	3
16	1768.89	884.95	1751.86	876.43	1750.88	875.94	T	276.17	138.59	259.14	130.07	258.16	129.58	2
17							R	175.12	88.06	158.09	79.55			1

Figure S3.1 Positive ionization low energy CID fragmentation spectrum of the singly phosphorylated peptide HTISPQFSNRHSPPVTR originating from the Matefin/SUN-1::GFP; *mtf-1/sun-1(ok1282);spe-26(hc138)* sample

MS3 spectrum of the triply charged peptide. The position of the dehydro-alanine generated by the loss of phosphoric acid from the phosphorylated serine residue was labeled with "@". Identified b and y fragment ions detected in the MS3 measurement are labeled in the fragmentation table and colored blue and red, respectively, in the spectrum. Identified satellite ions originating from the loss of water (b0 or y0 ions) or ammonia (b* or y* ions) are also labeled in the table. Even the intensive fragmentation of the ion in the MS^3 measurement did not make the unambiguous localization of the phosphorylation site possible. Fragment ions indicating the phosphorylation of residues S8, S12 and S16 were detected, which indicated that in this spectrum, a mixture of isobaric, singly phosphorylated peptide species were fragmented. The interpretation of

MS^3 spectra by Mascot and Sequest resulted in very similar fragment ion coverages (Figure S2.2) and score values for all three phosphorylation sites. The phosphorylated peptide contains a missed cleavage site at R14. This indicates the phosphorylation of the S16 residue. The shorter version of the peptide (HTISPQFSNR) was only detected unphosphorylated.

The doubly phosphorylated version of the peptide was also detected and the phosphorylation sites were localized either on S8 and S12 or on S8 and S16. This verified the assumption that the spectrum of the singly phosphorylated peptide was derived from a mixture.

#	b	b++	Seq.	y	y++	#	#	b	b^{++}	Seq.	y	y^{++}	#	#	b	b^{++}	Seq.	y	y^{++}	#
1	138.07	69.54	H			17	1	138.07	69.54	H			17	1	138.07	69.54	H			17
2	239.11	120.06	T	1805.94	903.47	16	2	239.11	120.06	T	1805.94	903.47	16	2	239.11	120.06	T	1805.94	903.47	16
3	352.2	176.6	I	1704.89	852.95	15	3	352.2	176.6	I	1704.89	852.95	15	3	352.2	176.6	I	1704.89	852.95	15
4	439.23	220.12	S	1591.81	796.41	14	4	439.23	220.12	S	1591.81	796.41	14	4	421.22	211.11	S@	1591.81	796.41	14
5	536.28	268.64	P	1504.78	752.89	13	5	536.28	268.64	P	1504.78	752.89	13	5	518.27	259.64	P	1522.79	761.9	13
6	664.34	332.67	Q	1407.72	704.37	12	6	664.34	332.67	Q	1407.72	704.37	12	6	646.33	323.67	Q	1425.73	713.37	12
7	811.41	406.21	F	1279.67	640.34	11	7	811.41	406.21	F	1279.67	640.34	11	7	793.4	397.2	F	1297.68	649.34	11
8	880.43	440.72	S@	1132.6	566.8	10	8	898.44	449.72	S	1132.6	566.8	10	8	880.43	440.72	S	1150.61	575.81	10
9	994.47	497.74	N	1063.58	532.29	9	9	1012.48	506.75	N	1045.57	523.29	9	9	994.47	497.74	N	1063.58	532.29	9
10	1150.58	575.79	R	949.53	475.27	8	10	1168.59	584.8	R	931.52	466.26	8	10	1150.58	575.79	R	949.53	475.27	8
11	1287.63	644.32	H	793.43	397.22	7	11	1305.64	653.33	H	775.42	388.21	7	11	1287.63	644.32	H	793.43	397.22	7
12	1374.67	687.84	S	656.37	328.69	6	12	1374.67	687.84	S@	638.36	319.68	6	12	1374.67	687.84	S	656.37	328.69	6
13	1471.72	736.36	P	569.34	285.17	5	13	1471.72	736.36	P	569.34	285.17	5	13	1471.72	736.36	P	569.34	285.17	5
14	1568.77	784.89	P	472.29	236.65	4	14	1568.77	784.89	P	472.29	236.65	4	14	1568.77	784.89	P	472.29	236.65	4
15	1667.84	834.42	V	375.24	188.12	3	15	1667.84	834.42	V	375.24	188.12	3	15	1667.84	834.42	V	375.24	188.12	3
16	1768.89	884.95	T	276.17	138.59	2	16	1768.89	884.95	T	276.17	138.59	2	16	1768.89	884.95	T	276.17	138.59	2
17			R	175.12	88.06	1	17			R	175.12	88.06	1	17			R	175.12	88.06	1

Figure S3.2 Fragment ion coverages in the MS^3 spectrum of the singly phosphorylated peptide HTISPQFSNRHSPPVTR

The possible positions of the dehydro-alanine generated by the loss of phosphoric acid from the phosphorylated serine residue was labeled with "@". Identified b and y fragment ions are colored red in the fragmentation table.

#	b	b*	b0	Seq.	y	y*	y0	#
1	157.11	140.08		R				14
2	272.14	255.11	254.12	D	1355.69	1338.66	1337.68	13
3	341.16	324.13	323.15	S@	1240.66	1223.64	1222.65	12
4	469.22	452.19	451.2	Q	1171.64	1154.62	1153.63	11
5	566.27	549.24	548.26	P	1043.58	1026.56	1025.57	10
6	623.29	606.26	605.28	G	946.53	929.51	928.52	9
7	724.34	707.31	706.33	T	889.51	872.48	871.5	8
8	837.42	820.39	819.41	I	788.46	771.44	770.45	7
9	938.47	921.44	920.46	T	675.38	658.35	657.37	6
10	995.49	978.46	977.48	G	574.33	557.3	556.32	5
11	1096.54	1079.51	1078.53	T	517.31	500.28	499.3	4
12	1209.62	1192.6	1191.61	I	416.26	399.24		3
13	1337.68	1320.65	1319.67	Q	303.18	286.15		2
14				R	175.12	158.09		1

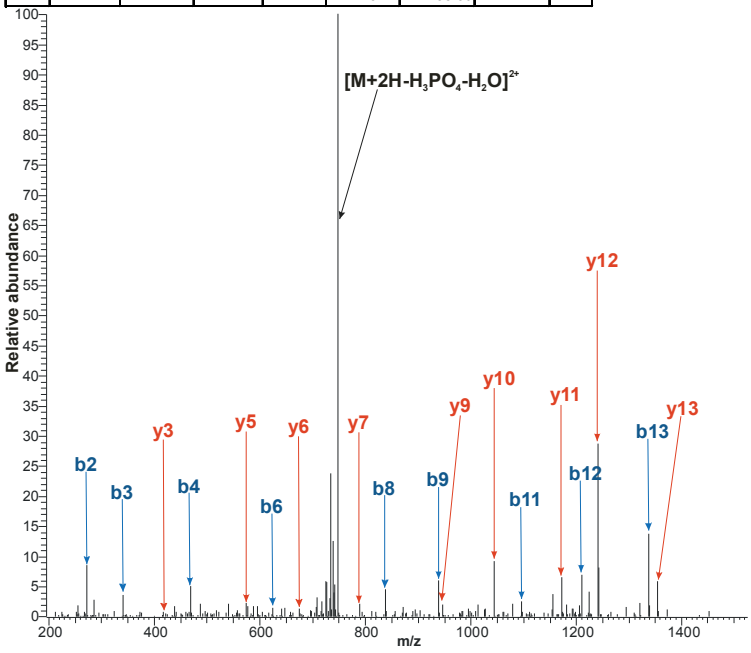

Figure S3.3 Positive ionization low energy CID spectrum of the singly phosphorylated peptide RDSQPGTITGTIQR originating from the Matefin/SUN-1::GFP; *mtf-1/sun-1(ok1282);spe-26(hc138)* sample

MS^3 spectrum of the doubly charged peptide. The position of the dehydro-alanine generated by the loss of phosphoric acid from the phosphorylated serine residue was labeled with "@". Identified b and y fragment ions are labeled in the fragmentation table and colored blue and red, respectively, in the spectrum. Identified satellite ions originating from the loss of water (b0 or y0 ions) or ammonia (b* or y* ions) are also labeled in the table. The localization of the phosphorylated residue was unambiguous and the presence of the missed cleavage at residue R41 verifies the modification of S43.

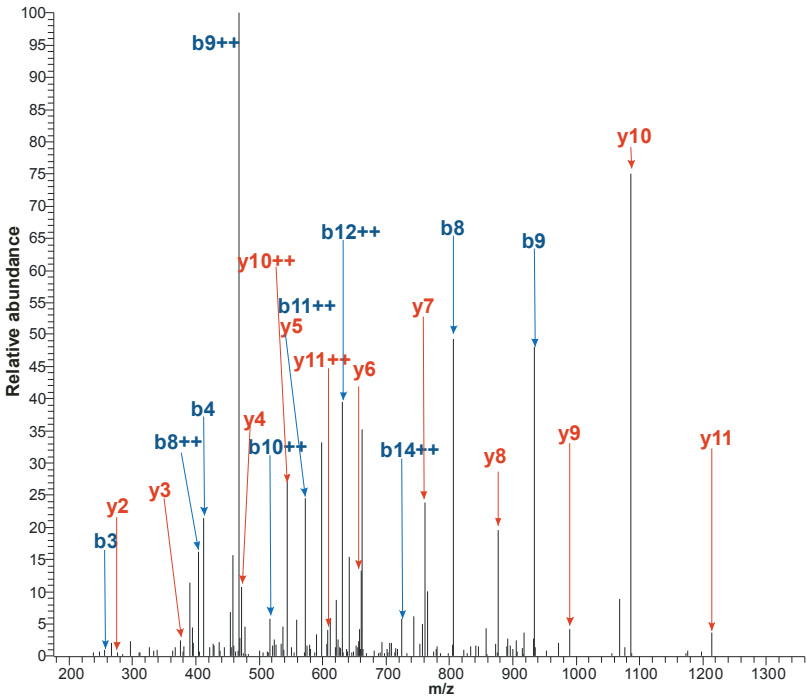

#	b	b++	b*	b*++	b0	b0++	Seq.	y	y++	y*	y*++	y0	y0++	#
1	88.04	44.52			70.03	35.52	S							19
2	187.11	94.06			169.1	85.05	V	1933.03	967.02	1916	958.5	1915.01	958.01	18
3	256.13	128.57			238.12	119.56	S@	1833.96	917.48	1816.93	908.97	1815.95	908.48	17
4	412.23	206.62	395.2	198.11	394.22	197.61	R	1764.94	882.97	1747.91	874.46	1746.92	873.97	16
5	513.28	257.14	496.25	248.63	495.27	248.14	T	1608.83	804.92	1591.81	796.41	1590.82	795.92	15
6	570.3	285.65	553.27	277.14	552.29	276.65	G	1507.79	754.4	1490.76	745.88	1489.78	745.39	14
7	669.37	335.19	652.34	326.67	651.36	326.18	V	1450.76	725.89	1433.74	717.37	1432.75	716.88	13
8	806.43	403.72	789.4	395.2	788.42	394.71	H	1351.7	676.35	1334.67	667.84	1333.69	667.35	12
9	934.49	467.75	917.46	459.23	916.47	458.74	Q	1214.64	607.82	1197.61	599.31	1196.63	598.82	11
10	1031.54	516.27	1014.51	507.76	1013.53	507.27	P	1086.58	543.79	1069.55	535.28	1068.57	534.79	10
11	1144.62	572.81	1127.6	564.3	1126.61	563.81	L	989.53	495.27	972.5	486.75	971.52	486.26	9
12	1259.65	630.33	1242.62	621.81	1241.64	621.32	D	876.44	438.72	859.42	430.21	858.43	429.72	8
13	1360.7	680.85	1343.67	672.34	1342.69	671.85	T	761.42	381.21	744.39	372.7	743.4	372.21	7
14	1447.73	724.37	1430.7	715.85	1429.72	715.36	S	660.37	330.69	643.34	322.17	642.36	321.68	6
15	1548.78	774.89	1531.75	766.38	1530.77	765.89	T	573.34	287.17	556.31	278.66	555.32	278.17	5
16	1645.83	823.42	1628.8	814.91	1627.82	814.41	P	472.29	236.65	455.26	228.13	454.28	227.64	4
17	1744.9	872.95	1727.87	864.44	1726.89	863.95	V	375.24	188.12	358.21	179.61	357.22	179.12	3
18	1845.95	923.48	1828.92	914.96	1827.93	914.47	T	276.17	138.59	259.14	130.07	258.16	129.58	2
19							R	175.12	88.06	158.09	79.55			

Figure S3.4 Positive ionization low energy CID spectrum of the singly phosphorylated peptide SVSRTGVHQPLDTSTPVTR originating from the Matefin/SUN-1::GFP; *mtf-1/sun-1(ok1282);spe-26(hc138)* sample

MS^3 spectrum of the triply charged peptide. The position of the dehydro-alanine generated by the loss of phosphoric acid from the phosphorylated serine residue was labeled with "@". Identified b and y fragment ions are labeled in the fragmentation table and colored blue and red, respectively, in the spectrum. Identified satellite ions originating from the loss of water (b0 or y0 ions) or ammonia (b* or y* ions) are also labeled in the table. According to the information provided by the fragmentation, it was not possible to ambiguously localize the phosphorylation site to S22 or S24. Because of the presence of a missed cleavage site at R25 we assumed, that the phosphorylation is probably on S24. This missed cleavage site was only detected in the phosphorylated peptide.

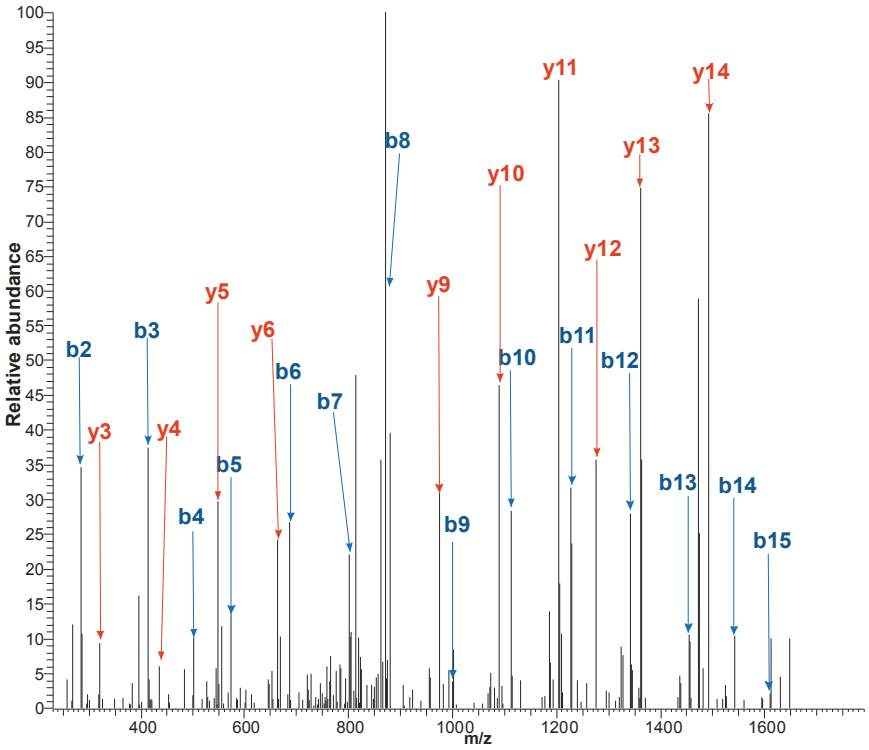

#	b	b*	b0	Seq.	y	y*	y0	#	#	b	b*	b0	Seq.	y	y*	y0	#
1	148.08			F				16	1	148.08			F				16
2	285.13			H	1628.7	1611.68	1610.69	15	2	285.13			H	1628.7	1611.68	1610.69	15
3	414.18		396.17	E	1491.64	1474.62	1473.63	14	3	414.18		396.17	E	1491.64	1474.62	1473.63	14
4	501.21		483.2	S	1362.6	1345.58	1344.59	13	4	483.2		465.19	S@	1362.6	1345.58	1344.59	13
5	572.25		554.24	A	1275.57	1258.54	1257.56	12	5	554.24		536.23	A	1293.58	1276.55	1275.57	12
6	687.27		669.26	D	1204.53	1187.51	1186.52	11	6	669.26		651.25	D	1222.54	1205.52	1204.53	11
7	802.3		784.29	D	1089.51	1072.48	1071.5	10	7	784.29		766.28	D	1107.52	1090.49	1089.51	10
8	871.32		853.31	S@	974.48	957.45	956.47	9	8	871.32		853.31	S	992.49	975.46	974.48	9
9	1000.36		982.35	E	905.46	888.43	887.45	8	9	1000.36		982.35	E	905.46	888.43	887.45	8
10	1113.45		1095.44	I	776.41	759.39	758.4	7	10	1113.45		1095.44	I	776.41	759.39	758.4	7
11	1228.48		1210.46	D	663.33	646.3	645.32	6	11	1228.48		1210.46	D	663.33	646.3	645.32	6
12	1341.56		1323.55	L	548.3	531.28	530.29	5	12	1341.56		1323.55	L	548.3	531.28	530.29	5
13	1455.6	1438.58	1437.59	N	435.22	418.19	417.21	4	13	1455.6	1438.58	1437.59	N	435.22	418.19	417.21	4
14	1542.63	1525.61	1524.62	S	321.18	304.15	303.17	3	14	1542.63	1525.61	1524.62	S	321.18	304.15	303.17	3
15	1629.67	1612.64	1611.66	S	234.14	217.12	216.13	2	15	1629.67	1612.64	1611.66	S	234.14	217.12	216.13	2
16				K	147.11	130.09		1	16				K	147.11	130.09		1

Figure S3.5 Positive ionization low energy CID spectrum of the singly phosphorylated peptide FHESADDSEIDLNSSK originating from the Matefin/SUN-1::GFP; *mtf-1/sun-1(ok1282);spe-26(hc138)* sample

MS^3 spectrum of the doubly charged peptide. The position of the dehydro-alanine generated by the loss of phosphoric acid from the phosphorylated serine residue was labeled with "@". Identified b and y fragment ions are colored blue and red in the spectrum, respectively, and labeled in the fragmentation tables (a,b) Identified fragment ions are labeled in the spectrum according to table "a". Identified satellite ions originating from the loss of water (b0 or y0 ions) or ammonia (b* or y* ions) are also labeled in the fragmentation tables. This peptide contains a second serine residue (S58). The presence of the fragment ions b4-b7 in the MS3 spectrum verifies the phosphorylation of S62. There are also some fragment ions, which support the phosphorylation of S58. (b), but they are less significant in the spectrum. Indeed, according to the mass spectrometry

data, it cannot be ruled out, that the spectrum was generated from a mixture of both peptide species and this residue was phosphorylated as well. The doubly phosphorylated peptide was not detected.

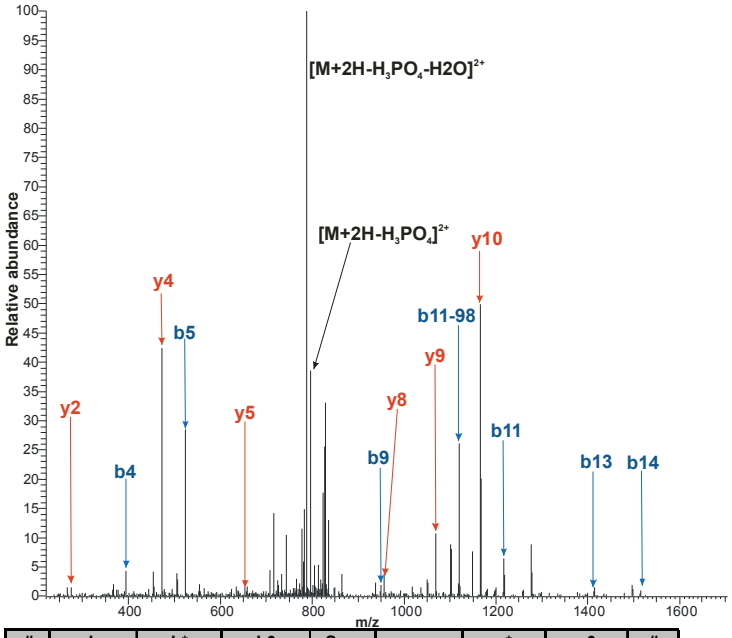

#	b	b*	b0	Seq.	y	y*	y0	#
1	102.05		84.04	T				15
2	159.08		141.07	G	1587.75	1570.73	1569.74	14
3	258.14		240.13	V	1530.73	1513.7	1512.72	13
4	395.2		377.19	H	1431.66	1414.64	1413.65	12
5	523.26	506.24	505.25	Q	1294.6	1277.58	1276.59	11
6	620.32	603.29	602.3	P	1166.55	1149.52	1148.53	10
7	733.4	716.37	715.39	L	1069.49	1052.47	1051.48	9
8	848.43	831.4	830.42	D	956.41	939.38	938.4	8
9	949.47	932.45	931.46	T	841.38	824.35	823.37	7
10	1036.51	1019.48	1018.5	S	740.33	723.31	722.32	6
11	1217.52	1200.49	1199.51	T#	653.3	636.28	635.29	5
12	1314.57	1297.55	1296.56	P	472.29	455.26	454.28	4
13	1413.64	1396.61	1395.63	V	375.24	358.21	357.22	3
14	1514.69	1497.66	1496.68	T	276.17	259.14	258.16	2
15				R	175.12	158.09		1

Figure S3.6 Positive ionization low energy CID spectrum of the singly phosphorylated peptide TGVHQPLDTSTPVTR originating from the Matefin/SUN-1::GFP; *mtf-1/sun-1(ok1282);spe-26(hc138)* sample

MS^2 spectrum of the doubly charged peptide. The characteristic neutral loss was labeled in the spectrum. The position of the phosphothreonine is indicated with "#" in the fragment ion table. Identified b and y fragment ions are labeled in the fragmentation table and colored blue and red, respectively, in the spectrum. Identified satellite ions originating from the loss of water (b0 or y0 ions) or ammonia (b* or y* ions) are also labeled in the table. The peak generated by the loss of phosphoric acid was not under the three most intensive ions, thus no MS^3 measurement was triggered, but the fragmentation of the peptide made it possible to localize the modification site to T36.

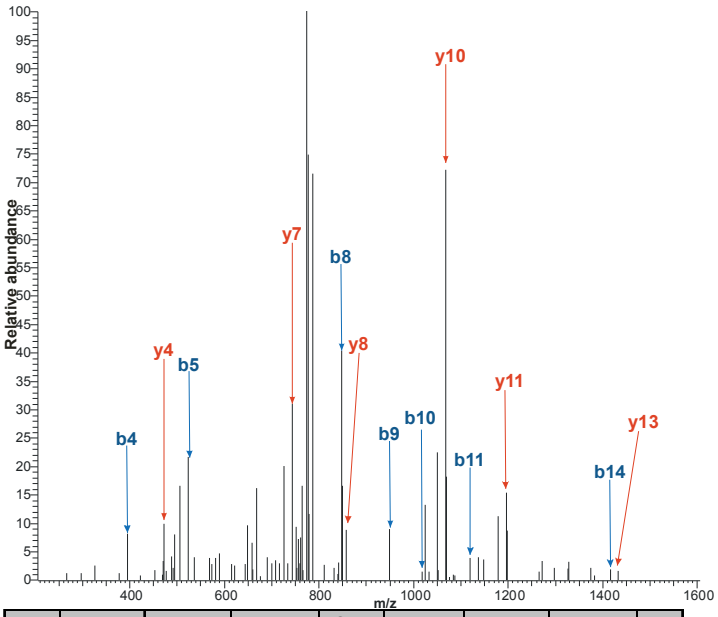

#	b	b*	b0	Seq.	y	y*	y0	#
1	102.05		84.04	T				15
2	159.08		141.07	G	1489.78	1472.75	1471.77	14
3	258.14		240.13	V	**1432.75**	1415.73	1414.74	13
4	**395.2**		**377.19**	H	1333.69	1316.66	1315.68	12
5	**523.26**	506.24	**505.25**	Q	**1196.63**	**1179.6**	**1178.62**	11
6	620.32	603.29	602.3	P	**1068.57**	**1051.54**	**1050.56**	10
7	733.4	716.37	715.39	L	971.52	954.49	953.51	9
8	**848.43**	831.4	830.42	D	858.43	841.41	840.42	8
9	**949.47**	932.45	931.46	T	**743.4**	726.38	**725.39**	7
10	**1018.5**	1001.47	1000.48	S@	642.36	625.33	624.35	6
11	**1119.54**	1102.52	1101.53	T	573.34	556.31	555.32	5
12	1216.6	1199.57	1198.59	P	**472.29**	455.26	**454.28**	4
13	1315.66	1298.64	**1297.65**	V	375.24	358.21	357.22	3
14	**1416.71**	1399.69	1398.7	T	276.17	259.14	258.16	2
15				R	175.12	158.09		1

Figure S3.7 Positive ionization low energy CID spectrum of the singly phosphorylated peptide TGVHQPLDTSTPVTR originating from the Matefin/SUN-1::GFP; *mtf-1/sun-1(ok1282);spe-26(hc138)* sample

MS^3 spectrum of the doubly charged peptide. The position of the dehydro-alanine was labeled with "@". Identified b and y fragment ions are labeled red in the fragmentation table and colored blue and red, respectively, in the spectrum. Identified satellite ions originating from the loss of water (b0 or y0 ions) or ammonia (b* or y* ions) are also labeled in the table. The peptides in Figure 1.6 and 1.7 have the same mass, but slightly different elution times. The peptide, which was identified as being phosphorylated at the S35 residue had a retention time of 26.93 min; the peptide phosphorylated at T35 eluted at 25.14 min. This fact and the different fragmentation characteristics of the two peptides may confirm the existence of the two different phosphorylated residues.

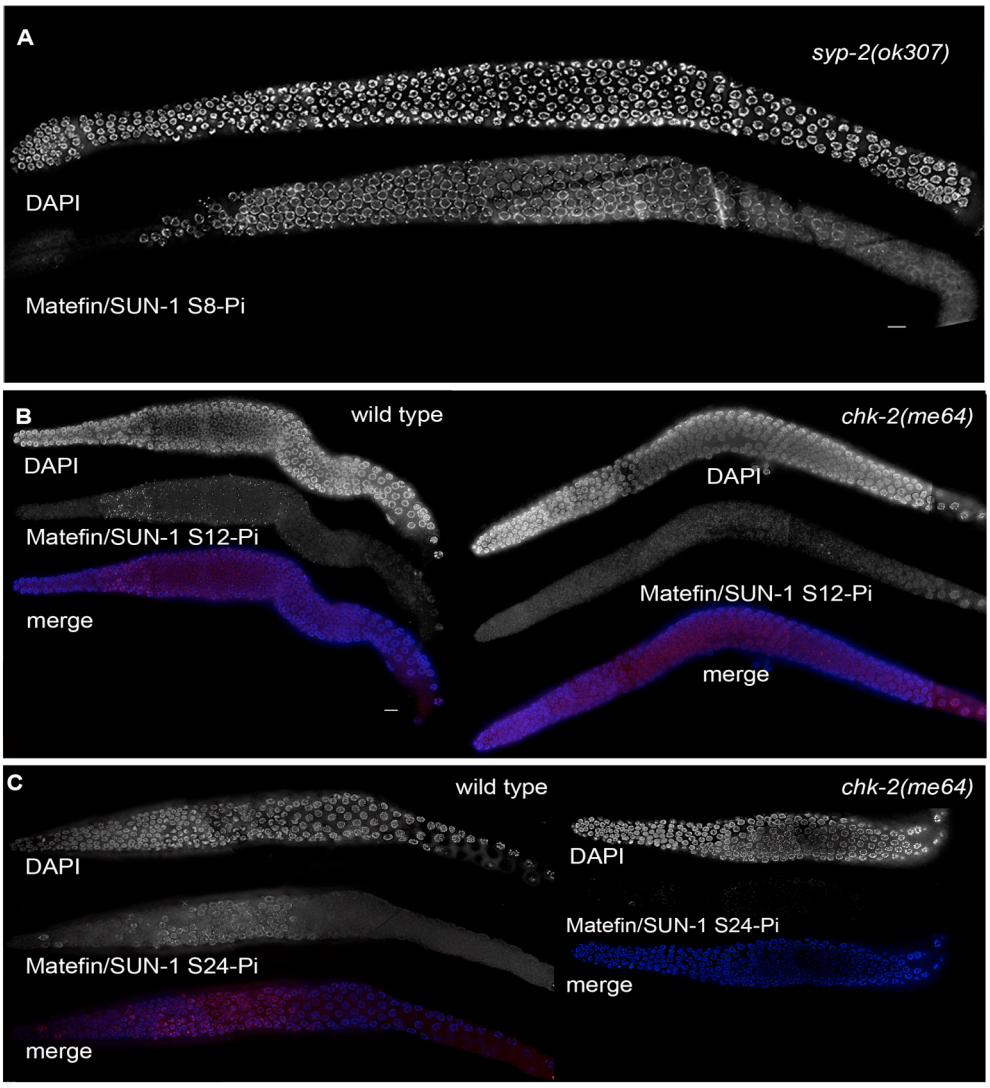

Figure S4. (A) Matefin/SUN-1 S8-Pi staining in *syp-2(ok307)* mutant gonads. The persistence of the immunostaining correlates with the prolongation of the transition zone. (B) Wild-type and *chk-2(me64)* hermaphrodite gonads co-stained with DAPI (top and blue in merge) and with antibodies against Matefin/SUN-1 S12-Pi (middle and red in merge). (C) Wild-type and *chk-2(me64)* hermaphrodite gonads co-stained with DAPI (top and blue in merge) and with antibodies against Matefin/SUN-1 S24-Pi (middle and red in merge).
Scale bars: 10 µm.

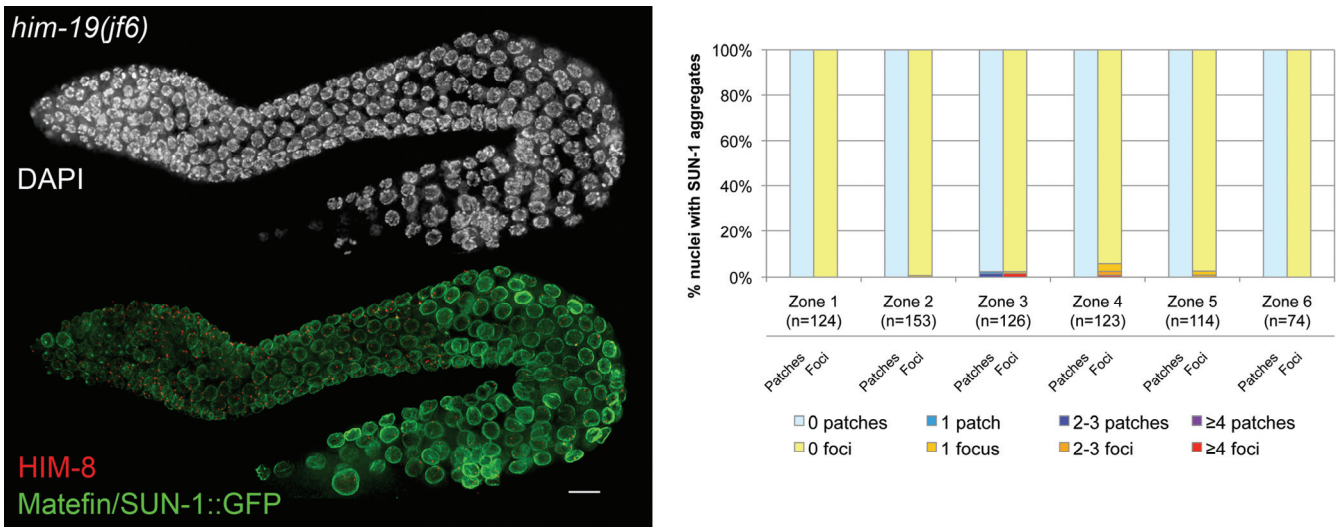

Figure S5. Analysis of Matefin/SUN-1::GFP aggregate formation in *him-19(jf6)* mutants. White: DAPI staining, green: Matefin/SUN-1::GFP, red: HIM-8.
Scale bars: 10 µm.

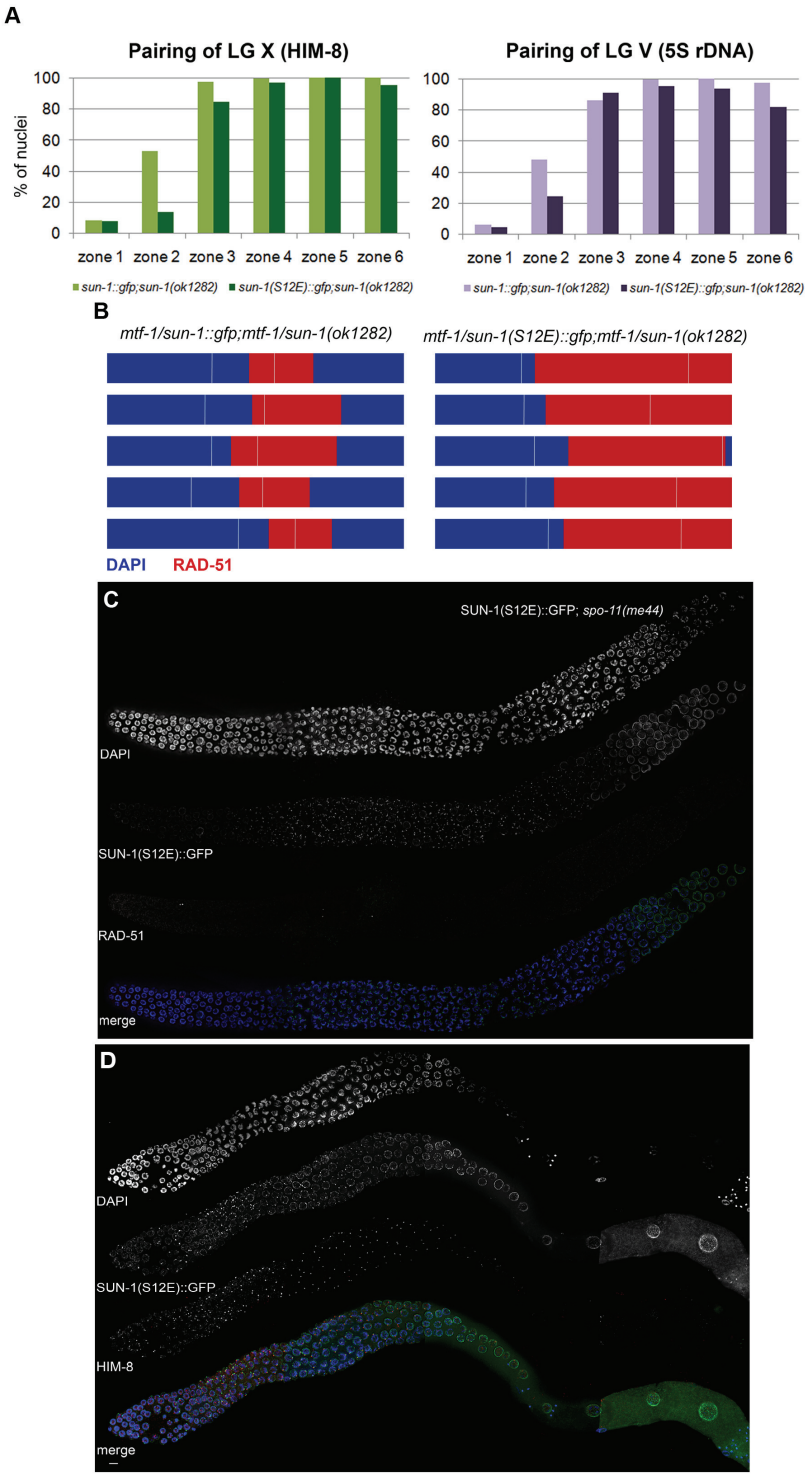

Figure S6. (A) Pairing of the X chromosome within the germline of *mtf-1/sun-1::gfp*;*mtf-1/sun-1(ok1282)* and *mtf-1/sun-1(S12E)::gfp*;*mtf-1/sun-1(ok1282)* worms as assessed by immunostaining of the pairing center-binding protein HIM-8. zone 1: n=80/77 nuclei, zone 2: n=149/108, zone 3: n=178/167, zone 4: n=157/174, zone 5: n=120/117, zone 6: n=54/43 (5 gonads counted for each genotype). Pairing of chromosome V within the germline of *mtf-1/sun-1::gfp*;*mtf-1/sun-1(ok1282)* and *mtf-1/sun-1(S12E)::gfp*;*mtf-1/sun-1(ok1282)* worms as assessed by FISH of the 5S rDNA locus. zone 1: n=129/108

nuclei, zone 2: n=193/128, zone 3: n=173/162, zone 4: n=155/166, zone 5: n=113/126, zone 6: n=72/105 (5 gonads counted for each genotype). (B) RAD-51-positive zones (in red) of 5 individual gonads of *mtf-1/sun-1::gfp*; *mtf-1/sun-1(ok1282)* and *mtf-1/sun-1(S12E)::gfp*;*mtf-1/sun-1(ok1282)* hermaphrodites. White vertical lines mark the beginning and the end of the zone displaying clustered chromatin. (C) Matefin/SUN-1(S12E)::GFP aggregates and RAD-51 staining in *mtf-1/sun-1(S12E)::gfp*;*mtf-1/sun-1(ok1282);spo-11(me44)* hermaphrodite gonads; compare to figure 6 for stainings of wild type and the S12E substitution. (D) Highlighting of chromatin clustering, Matefin/SUN-1(S62E)::GFP aggregation and HIM-8 localization in hermaphrodite gonads expressing solely Matefin/SUN-1(S62E)::GFP. blue: DAPI staining, green: Matefin/SUN-1(S62E)::GFP, red: HIM-8.
Scale bars: 10 µm.

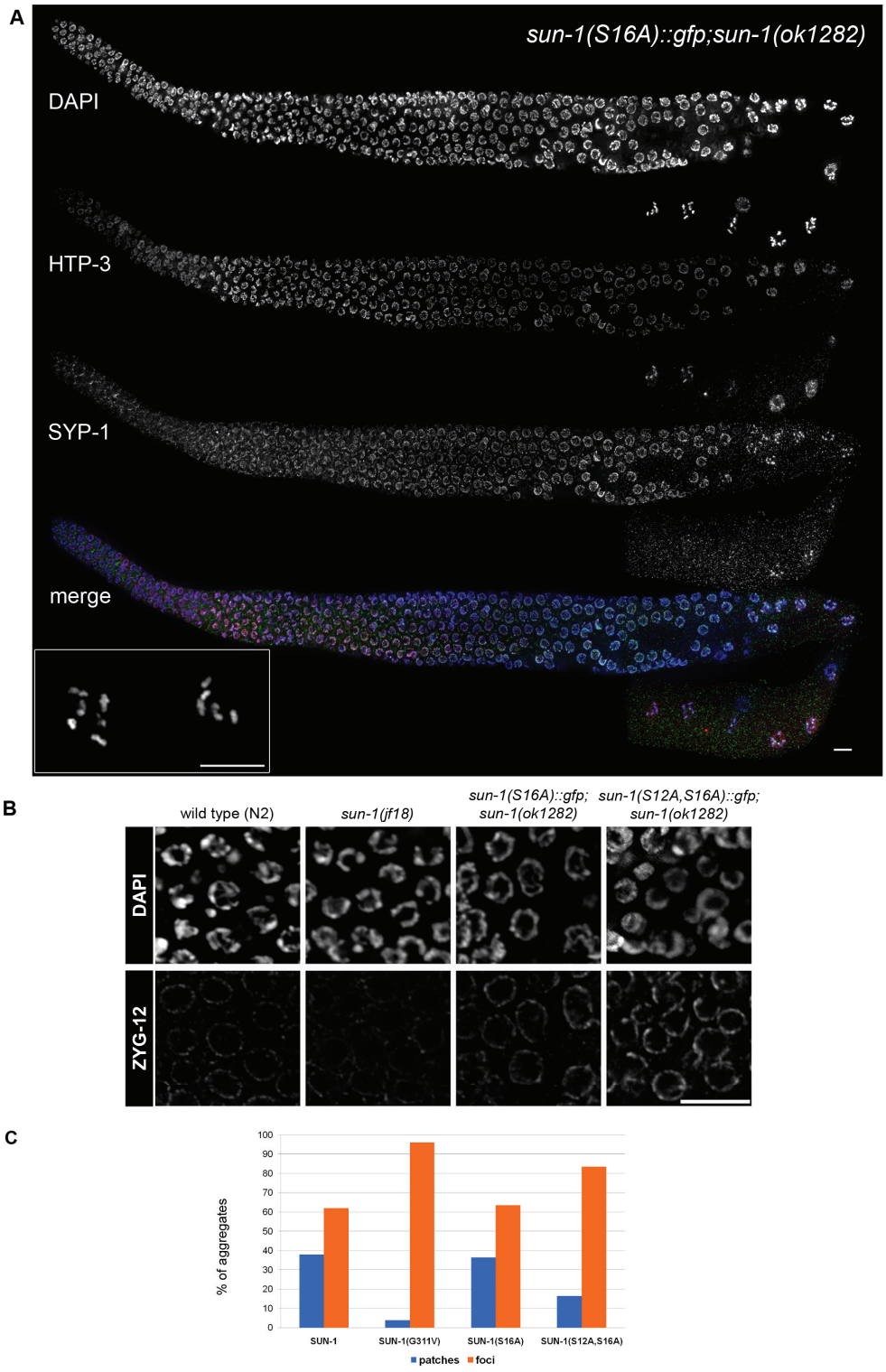

Figure S7. (A) Highlighting of the SC components HTP-3 (red in merge), SYP-1 (green in merge) and DAPI staining (blue in merge) in *sun-1(S16A)::gfp;sun-1(ok1282)* hermaphrodite gonads. inset: DAPI staining of diakinesis nuclei. (B) ZYG-12 staining (lower panel) of nuclei in the pachytene region of hermaphrodite gonads of wild type,

sun-1(jf18), *sun-1(S16A)::gfp;sun-1(ok1282)* and *sun-1(S12A,S16A)::gfp;sun-1(ok1282)*. DAPI staining: upper panel. (C) Distribution of patches and foci formed by Matefin/SUN-1::GFP (n=250 aggregates), Matefin/SUN-1(G311V)::GFP (n=130 aggregates), Matefin/SUN-1(S16A)::GFP (n=315 aggregates) and Matefin/SUN-1(S12A,S16A)::GFP (n=206 aggregates).

Table S1.

Genotype	Viability	n (eggs/ hermaphrodites)	Brood size	Males in surviving offspring
sun-1(ok1282)	0±0%	6/7	0.86±0.9	n.d.
sun-1::gfp;sun-1(ok1282)	98.2±1.4%	653/5	130.6±17.5	0%
sun-1(S12E)::gfp;sun-1(ok1282)	25.1±11.1%	1542/9	171.3±35.9	4.7%
sun-1(S62E)::gfp;sun-1(ok1282)	73.6±22.3%	482/14	34.4±15.9	4.7%
sun-1(S8A)::gfp;sun-1(ok1282)	24.6±7.2%	736/n.d.	n.d.	4.5%
*sun-1(*S16A*)::gfp;sun-1(ok1282)*	89±25%	2593/15	172.9±49.7	n.d.
*sun-1(*S12A,S16A*)::gfp;sun-1(ok1282)*	3.9±3.4%	597/13	45.9±20.4	n.d.

Summary of viability, broodsize and Him counts for various SUN-1 wild-type and serine mutated transgenic lines.

Table S2.

Genotype	Scored zone	n (nuclei)	Mean number	
			patches (p-value)	foci (p-value)
wild type	2+3	137	1.9±1.3	1.0±1.4
syp-2(ok307)	2+3	122	1.4±0.9 (p=1.2E-3)	3.4±2.2 (p=6.3E-22)
him-3(gk149)	2	129	0.5±0.5 (p=3.1E-24)	1.8±1.4 (p=2.9E-6)
chk-2(me64)	-	-	-	-
him-19(jf6)	-	-	-	-

Analysis of Matefin/SUN-1::GFP aggregates in various mutant backgrounds (wild type: *mtf-1/sun-1::gfp;mtf-1/sun-1(ok1282)*. *syp-2(ok307)*: *syp-2(ok307);mtf-1/sun-1::gfp;mtf-1/sun-1(ok1282)*. *him-3(gk149)*: *him-3(gk149);mtf-1/sun-1::gfp;mtf-1/sun-1(ok1282)*. *chk-2(me64)*: *chk-2(me64);mtf-1/sun-1::gfp;mtf-1/sun-1(ok1282)*). *him-19(jf6): him-19(jf6);mtf-1/sun-1::gfp;mtf-1/sun-1(ok1282)*. The mean of Matefin/SUN-1::GFP patches and foci is listed. Four independent gonads were scored per genotype. Values were compared using a two-tailed Student's t-test with a significance level below p=0.05.

Supplemental References

Brenner, S. (1974). The genetics of Caenorhabditis elegans. *Genetics 77*, 71-94.

Colaiácovo, M. P.; MacQueen, A. J.; Martinez-Perez, E.; McDonald, K.; Adamo, A.; Volpe, A. L. & Villeneuve, A. M. (2003). Synaptonemal complex assembly in C. elegans is dispensable for loading strand-exchange proteins but critical for proper completion of recombination. *Dev Cell 5*, 463-474.

Couteau, F.; Nabeshima, K.; Villeneuve, A. & Zetka, M. (2004). A component of C. elegans meiotic chromosome axes at the interface of homolog alignment, synapsis, nuclear reorganization, and recombination. *Curr Biol 14*, 585-592.

Garcia-Muse, T. & Boulton, S. J. (2005). Distinct modes of ATR activation after replication stress and DNA double-strand breaks in Caenorhabditis elegans. *EMBO J 24*, 4345-4355.

Hayashi, M.; Chin, G. M. & Villeneuve, A. M. (2007). C. elegans germ cells switch between distinct modes of double-strand break repair during meiotic prophase progression. *PLoS Genet 3*, e191.

MacQueen, A. J. & Villeneuve, A. M. (2001). Nuclear reorganization and homologous chromosome pairing during meiotic prophase require C. elegans chk-2. *Genes Dev 15*, 1674-1687.

Malone, C. J.; Misner, L.; Bot, N. L.; Tsai, M.-C.; Campbell, J. M.; Ahringer, J. & White, J. G. (2003). The C. elegans hook protein, ZYG-12, mediates the essential attachment between the centrosome and nucleus. *Cell 115*, 825-836.

Martinez-Perez, E. & Villeneuve, A. M. (2005). HTP-1-dependent constraints coordinate homolog pairing and synapsis and promote chiasma formation during C. elegans meiosis. *Genes Dev 19*, 2727-2743.

Praitis, V.; Casey, E.; Collar, D. & Austin, J. (2001). Creation of low-copy integrated transgenic lines in Caenorhabditis elegans. *Genetics 157*, 1217-1226.

Stergiou, L.; Doukoumetzidis, K.; Sendoel, A. & Hengartner, M. O. (2007). The nucleotide excision repair pathway is required for UV-C-induced apoptosis in Caenorhabditis elegans. *Cell Death Differ 14*, 1129-1138.

Tang L., Machacek T., Mamnun Y.M., Gloggnitzer J., Penkner A., Konrat R., Jantsch M., Loidl J., and Jantsch V. (2009) Mutations in *C. elegans* HIM-19 show meiotic defects that worsen with age (*submitted*)

Voorhies, W. A. V. (1992). Production of sperm reduces nematode lifespan. *Nature 360*, 456-458.

OPEN ACCESS Freely available online

PLoS GENETICS

Leptotene/Zygotene Chromosome Movement Via the SUN/KASH Protein Bridge in *Caenorhabditis elegans*

Antoine Baudrimont[1], Alexandra Penkner[1], Alexander Woglar[1], Thomas Machacek[1], Christina Wegrostek[1], Jiradet Gloggnitzer[1¤], Alexandra Fridkin[2], Franz Klein[1], Yosef Gruenbaum[2], Pawel Pasierbek[3,4], Verena Jantsch[1]*

1 Department of Chromosome Biology, Max F. Perutz Laboratories, University of Vienna, Vienna, Austria, **2** Department of Genetics, Hebrew University, Jerusalem, Israel, **3** Institute of Molecular Biotechnology of the Austrian Academy of Sciences, Vienna, Austria, **4** Institute of Molecular Pathology, Vienna, Austria

Abstract

The *Caenorhabditis elegans* inner nuclear envelope protein matefin/SUN-1 plays a conserved, pivotal role in the process of genome haploidization. CHK-2–dependent phosphorylation of SUN-1 regulates homologous chromosome pairing and interhomolog recombination in *Caenorhabditis elegans*. Using time-lapse microscopy, we characterized the movement of matefin/SUN-1::GFP aggregates (the equivalent of chromosomal attachment plaques) and showed that the dynamics of matefin/SUN-1 aggregates remained unchanged throughout leptonene/zygotene, despite the progression of pairing. Movement of SUN-1 aggregates correlated with chromatin polarization. We also analyzed the requirements for the formation of movement-competent matefin/SUN-1 aggregates in the context of chromosome structure and found that chromosome axes were required to produce wild-type numbers of attachment plaques. Abrogation of synapsis led to a deceleration of SUN-1 aggregate movement. Analysis of matefin/SUN-1 in a double-strand break deficient mutant revealed that repair intermediates influenced matefin/SUN-1 aggregate dynamics. Investigation of movement in meiotic regulator mutants substantiated that proper orchestration of the meiotic program and effective repair of DNA double-strand breaks were necessary for the wild-type behavior of matefin/SUN-1 aggregates.

Citation: Baudrimont A, Penkner A, Woglar A, Machacek T, Wegrostek C, et al. (2010) Leptotene/Zygotene Chromosome Movement Via the SUN/KASH Protein Bridge in *Caenorhabditis elegans*. PLoS Genet 6(11): e1001219. doi:10.1371/journal.pgen.1001219

Editor: Monica Colaiácovo, Harvard University, United States of America

Received April 23, 2010; **Accepted** October 25, 2010; **Published** November 24, 2010

Funding: This work was supported by grants from the FWF (V11B12, P-21107, SFB-F34, "Chromosome Dynamics"), the WWTF (LS05009), the University of Vienna (IO31-B), an Israel Science Foundation (ISF) grant to YG, and a Clore scholarship to AF. The Caenorhabditis Genetics Center is funded by the NIH National Canter for Research Resources (NCRR). The funders had no role in study design, data collection and analysis, decision to publish, or preparation of the manuscript.

Competing Interests: The authors have declared that no competing interests exist.

* E-mail: verena.jantsch@univie.ac.at

¤ Current address: Gregor Mendel Institute of Molecular Plant Biology, Austrian Academy of Sciences, Vienna, Austria

Introduction

During the first meiotic division, homologous parental chromosomes must accomplish numerous tasks that eventually result in their connection via homologous recombination. They must recognize one another, align, synapse via the tripartite proteinaceous synaptonemal complex (SC), and repair programmed double-strand breaks (DSBs); a subset of DSBs is repaired using the homologous partner as a template [1]. During this period, the chromosomes are connected to the nuclear envelope at one or both ends [2]. The highly conserved protein interaction module of SUN/KASH domain proteins has emerged as a core element for the attachment of chromosomal ends to the nuclear envelope, and for telomere-led chromosomal movement. The mechanism for moving chromosomes during early prophase I inside the nucleus via the SUN/KASH bridge, which provides a connection to various cytoskeletal forces in the cytoplasm, appears to be a general, evolutionarily conserved phenomenon (for reviews see [3–5]). Studies in *Saccharomyces cerevisiae* [6,7], *Schizosaccharomyces pombe* [8], and maize [9] discovered differences among organisms with regard to which factors are employed to build the connection of the chromosome ends to the SUN-domain proteins in the inner nuclear envelope, and which cytoskeletal forces drive the movement. For example, in *S. cerevisiae*, telomere-led chromosome movement has been observed during meiotic prophase I, from leptotene to pachytene [6,7,10]. Interference with prophase chromosome movement in *S. cerevisiae* results in delayed pairing and DSB processing, aberrant crossover formation, and loss of crossover interference [6,7,11–16].

In many organisms, formation of the synaptonemal complex requires the formation of programmed meiotic DSBs; however, in *C. elegans*, synapsis is independent of DSBs [17]. In *C. elegans*, the SC is comprised of the lateral element components HTP-1 to 3 and HIM-3, and the central region components SYP-1 to SYP-4 [18,19]. HTP-1, in addition to being part of the lateral element, also plays a role in licensing synapsis [20,21].

Another characteristic of *C. elegans* is that the pairing of homologs involves homolog recognition regions (HRRs), also called pairing center (PC) regions, which are enriched in heterochromatic repeats localized at one end of each chromosome. HRRs were shown to be required to initiate the subsequent key features of meiosis I, recombination and disjunction [22–24]. The PC proteins ZIM-1 to ZIM-3 and HIM-8 bind to HRRs, and specifically localize to either one or two chromosomes [25–27]. When extrachromosomal arrays of the heterochromatic repeats found in HRRs are introduced into *C. elegans* germline cells, they

Author Summary

During meiosis, homologous chromosomes from each parent must pair, synapse, and recombine before being assorted to the gametes. In *Caenorhabditis elegans*, to find the correct pairing partner, telomere-led chromosome movement occurs in a restricted subvolume of the nucleus. This feature is comparable to the widely conserved meiotic bouquet, a configuration where telomeres cluster in a limited area at the nuclear periphery. Chromosomes are moved by cytoskeletal forces transmitted via the SUN/KASH bridge across the nuclear envelope, and abrogation of movement leads to precocious nonhomologous synapsis. Using live cell imaging, we followed the movement of matefin/SUN-1 aggregates, which highlight chromosome ends. Instead of single chromosome ends looking for their homologous partners, we observed that duplets/multiplets and single chromosome ends were brought together into "patches" by the ongoing movement during the leptotene/zygotene stages of meiosis. Chromosome ends then shuffled through these patches in search of the correct partner. This study was a comprehensive analysis of matefin/SUN-1 aggregate dynamics in wild type, known *Caenorhabditis elegans* pairing mutants, and the recombination mutant *spo-11*; and it examined the contributions of these genotypes to leptotene/zygotene chromosome movement.

recruit PC proteins and the arrays localize to the nuclear periphery [27].

In *C. elegans*, the protein matefin/SUN-1 (referred to as SUN-1 from this point forward) and its interacting partner ZYG-12 bridge the nuclear membranes and play a central role in the pairing of homologous chromosomes and the licensing of synapsis [28,29]. The PC proteins colocalize with SUN-1, and are thought to connect chromosome ends to SUN-1 [28,29]. A point mutation in the SUN domain of *C. elegans* SUN-1 revealed that prophase movement is required for chromosomes to find each other and to prevent nonhomologous synapsis [29,30]. Recently, it was found that in worms, microtubules and dynein motors act through the nuclear envelope bridge formed by matefin/SUN-1 and ZYG-12, and that these components are at the core of licensing synapsis only for properly aligned bivalents [29].

Progression of meiosis is tightly regulated in *C. elegans*, and involves the checkpoint protein kinase CHK-2 at the meiotic entry. CHK-2 is responsible for the polarization of the chromatin, which is characteristic of the transition zone (TZ) [31], and is involved in induction of DSBs and proper SC polymerization, as well as the phosphorylation of SUN-1 [28]. PROM-1, an F-box–containing protein, controls progression of early meiosis; its depletion leads to an extended meiotic entry zone followed by nonhomologous synapsis [32]. The newly identified meiotic regulator HIM-19 is involved in chromatin polarization, formation of DSBs, and elongation of the SC. It encodes a protein with an RNA helicase domain, as determined by metastructure analysis [33]. In *cra-1* mutants, central-region components of the SC first fail to localize extensively to chromosomes; later, they instead polymerize along chromosomal axes, leading to unconnected bivalents. The tetratricopeptide repeat domain–bearing protein CRA-1 uncouples the polymerization of the central region components of the SC from the repair of DSBs [34].

In this study, we used live imaging microscopy to show that chromosome ends, highlighted as SUN-1 aggregates, were highly dynamic and contributed to chromosome movement in the leptotene/zygotene stages of *C. elegans* prophase I; they came together, coalesced and dispersed. Disruption of the SUN/KASH interaction in *mtf-1/sun-1(jf18)* mutants resulted in an absence of motion of the SUN-1 aggregates. We also analyzed the SUN-1-GFP aggregates in different mutant backgrounds affecting phosphorylation of SUN-1 and structural components of the lateral and central region of the SC, the DSB inducing enzyme SPO-11 and a group of genes that play a regulatory role during prophase I in *C. elegans*. Abrogation of synapsis led to a deceleration of SUN-1 aggregate movement. Aggregate behavior was influenced by recombination. Quantification of SUN-1 aggregates in meiotic regulators suggested that mere chromosome collisions driven by movement of nuclear envelope–attached chromosomes were insufficient for successful homologous pairing.

Results

Erratic movement of SUN-1 aggregates at one pole of the nucleus

C. elegans gonads recapitulate the progression of nuclei through meiotic prophase I in a spatial manner [35]. The mitotic zone is followed by the TZ, with its characteristically polarized chromatin (corresponding to leptotene/zygotene). In the next stage (pachytene), chromatin is redistributed and forms parallel tracks of DNA. Later, chromosomes condense (diplotene) and connected bivalents become apparent at diakinesis. SUN-1 forms foci and patches (the equivalent of the chromosomal attachment plaque seen in vertebrates) in the TZ [28–30].

We followed the movement of a functional SUN-1::GFP transgene integrated into the corresponding deletion background *sun-1(ok1282)* using in vivo imaging microscopy [28]. By additionally applying Hoechst 33342, we recorded both the motion of chromatin and the movement of SUN-1::GFP (Figure 1A, Video S1). SUN-1::GFP formed both large and small aggregates that moved in an erratic manner on one half of the nuclear periphery. Small and large aggregates met, fused and dispersed during the leptotene/zygotene stage of prophase I. Small aggregates, termed foci, likely define single chromosome end attachments, whereas large aggregates, termed patches, likely define multiple chromosome ends that are locally enriched. Indeed, only a single patch was visible at $t = 425$ s (Figure 1A), whereas at an earlier timepoint ($t = 140$ s), one patch and five foci were observed. Later ($t = 555$ s), we observed three foci and one patch. The coalescence of foci and patches were often very transient: in less than 130 s, we observed three foci driven out from the patch. Once two foci or one focus and a patch fused, they dispersed within a short time.

SUN-1::GFP aggregates, via cytoplasmic forces, also triggered protrusion of the chromatin, deforming the nuclear membranes. At $t = 140$ s, the chromatin was pulled outward by the SUN-1::GFP patch, which moved at the periphery of the nucleus (Figure 1A, white arrow; $t = 140$ s).

SUN-1 aggregates are highly dynamic

General features of SUN-1 aggregates. Because of unreliable Hoechst staining, as reported by [7], only SUN-1::GFP dynamics were recorded during this study. To study the dynamics of SUN-1 aggregates, we manually followed their movement and characterized features such as the number of aggregates, distribution of the projected speed, the distance traveled, number of fusion/splitting events, and coalescence time. No distinction was made between patches and foci when tracking their movement; therefore, both SUN-1 patches and foci are referred to as aggregates.

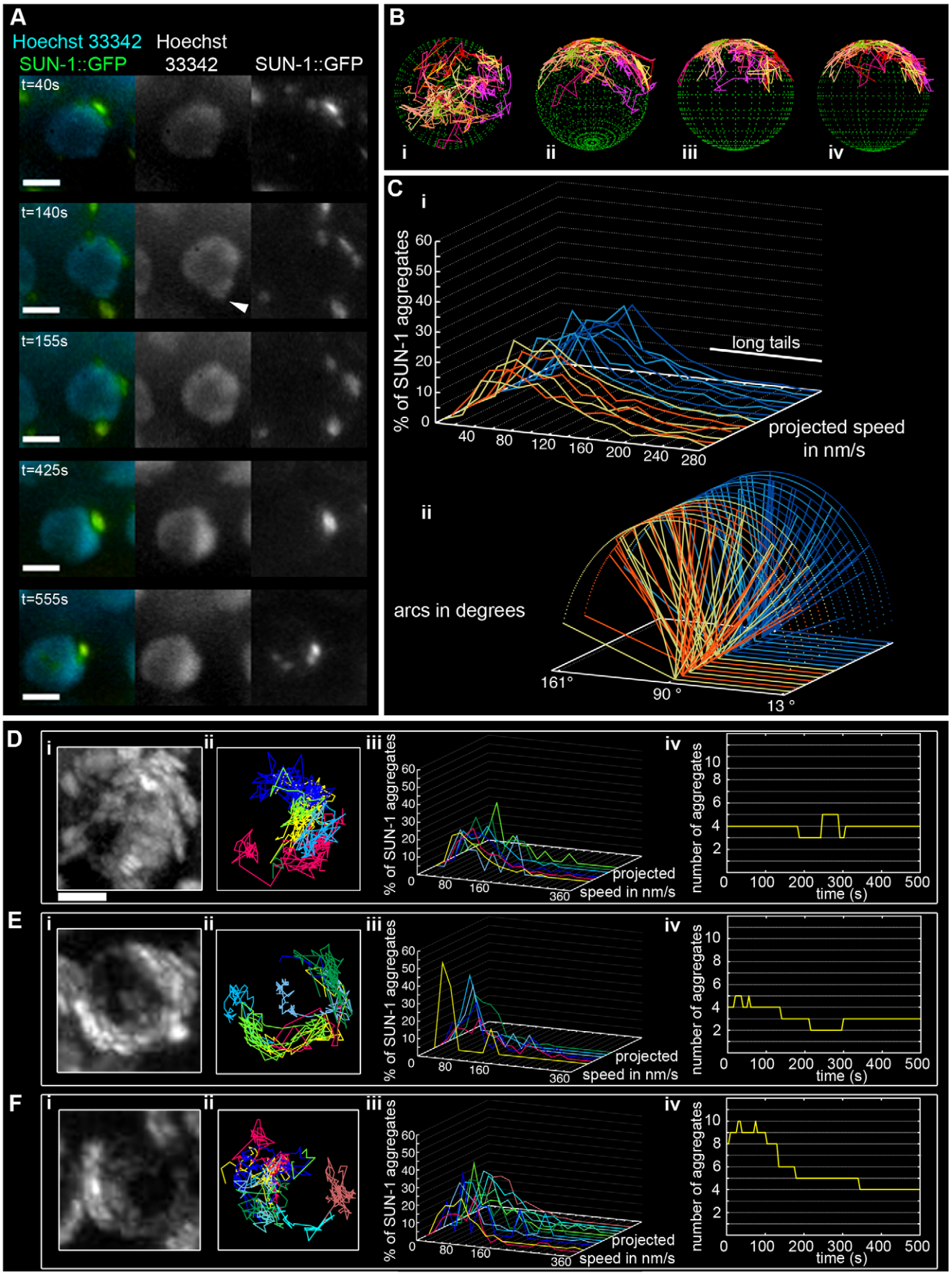
A
Hoechst 33342
SUN-1::GFP
Hoechst 33342
SUN-1::GFP
t=40s
t=140s
t=155s
t=425s
t=555s
B
i
ii
iii
iv
C
i
% of SUN-1 aggregates
long tails
projected speed in nm/s
ii
arcs in degrees
161°
90 °
13 °
D
E
F
projected speed in nm/s
number of aggregates
time (s)

Figure 1. Dynamics of SUN-1 aggregates. (A) Frames from a movie showing the movement of SUN-1::GFP (green); chromatin stained with Hoechst 33342 (blue). White arrowhead highlights protrusion of chromatin. (B) Three-dimensional reconstruction of SUN-1::GFP displacement track dynamics. View from top (i), 30° z-axis rotation and 60° x-axis rotation (ii), and view from right side (iii) and left side (iv). (C) (i) Each line represents the distribution of the projected speed of all SUN-1 aggregates inside a nucleus from individual movies (yellow and orange: tracks from first movie, seven nuclei shown; light and dark blue: tracks from second movie, seven nuclei shown). (ii) Arcs show distance traveled for each SUN-1 track inside a nucleus. Yellow and orange: tracks from first movie, seven nuclei shown; light and dark blue: tracks from second movie, seven nuclei shown). Nuclei in the distal (D), central (E), and proximal (F) TZ, with projection of the cumulative movement of SUN-1::GFP (i), displacement tracks with different colors for each track (ii), distribution of speed for each track, using the same color code as for displacement tracks (iii), and number of SUN-1 aggregates as a function of time (iv). See Table 1 for number of nuclei analyzed. Scale bar: 2 μm.
doi:10.1371/journal.pgen.1001219.g001

Throughout the entire TZ, there were a minimum of 2.4±1.1 (standard deviation [SD], $n = 27$ nuclei) aggregates and a maximum of 6.1±2.8 (SD, $n = 27$ nuclei) aggregates. During the recorded time, on average, 3.9±1.4 (SD, $n = 27$ nuclei) aggregates (Table 1) per frame moved in an erratic manner over the surface of the nuclear membrane of single wild-type nuclei throughout the TZ (Video S2). The movement of SUN-1 aggregates was restricted to one hemisphere of the nucleus (Figure 1Di, 1Ei, and 1Fi; Video S1). The resulting displacement tracks of SUN-1 aggregates overlapped. In most cases, the projected movement of SUN-1 aggregates on the surface of the nucleus resembled the polarized conformation of the chromatin characteristic of leptotene/zygotene (Figure 1Dii, 1Eii, and 1Fii). In rare cases, the movement of the attachment plaques was observed from the top of the nuclei (Figure 1Bi). We reconstructed the 3D movement by considering that aggregates traveled only on one hemisphere of a spherical nucleus. (Figure 1Bi–iv). This reconstructed movement displayed undirected movement of chromosome ends. In addition, SUN-1::GFP aggregates moved outward toward the boundary of the nuclei (Figure 1Bii), (Figure 1A, $t = 140$ s), leading to bulging of the nuclear membrane. Aggregates usually moved randomly over short distances, but occasionally they traveled longer distances (Figure 1B).

We also defined background motion in the filmed germ cells. To assess background motion, we measured the movement of SUN-1::GFP aggregates in animals killed with sodium azide. The values for the projected speed defined the background projected speed between 0 and 40 nm/s (Figure S1A).

The projected speed of SUN-1::GFP aggregates did not display a normal distribution, but rather a "Maxwellian-shaped" distribution (Figure 1Ci; see Figure S1B for an explanation of the term). Overall, more than half of the SUN-1 aggregates inside a nucleus (66%) moved within a range of 40–160 nm/s; approximately 10% of the aggregates showed a higher projected speed of up to 260 nm/s (long tails), and 24% were in the range of the background projected speed ($n = 27$ nuclei, taken from two movies, illustrated by the orange and blue colors in the figures).

Table 1. Numbers of aggregates in the region proximal to the mitotic zone for the different genotypes.

		number of aggregates			
		average	**minimum**	**maximum**	**n**
SUN-1::GFP	entire TZ	3.9±1.4	2.4±1.1	6.1±2.8	27
	distal part of TZ	3.5±1.1	2.1±0.7	5.7±2.0	10
	central part of TZ	4.6±1.1	2.3±1.6	7.5±2.5	4
	proximal part of TZ	3.9±1.6	2.1±0.9	5.4±3.0	9
SUN-1(G311V)::GFP		7.8±2.3	7.8±2.3	7.8±2.3	8
him-3(gk149); SUN-1::GFP		1.1±0.3	1.1±0.3	1.1±0.3	82
htp-1(gk174); SUN-1::GFP		3.1±08	2.6±1.0	3.9±1.0	14
syp-2(ok307); SUN-1::GFP	distal part	2.8±1.0	1.7±1	3.5±1.1	30
	proximal part	3.3±0.9	2.0±1.0	4.2±1.2	45
syp-3(me42); SUN-1::GFP	entire TZ	3.0±0.9	1.7±0.6	4.3±1.4	14
htp-1(gk149); *syp-1(RNAi)*; SUN-1::GFP	distal part of TZ	3.5±0.6	2.4±0.8	4.5±0.9	23
	proximal part of TZ	2.8±0.6	2.2±0.6	3.3±0.8	24
spo-11(me44); SUN-1::GFP	entire TZ	3.0±0.6	1.9±0.6	4.1±0.9	18
spo-11(me44); SUN-1::GFP irradiated	entire TZ	3.6±0.6	2.3±0.6	4.7±0.9	23
prom-1(ok1140); SUN-1::GFP	dispersed nuclei	3.4±0.9	2.7±0.9	3.8±1.1	37
him-19(jf6); SUN-1::GFP	dispersed nuclei	2.8±0.8	1.9±0.6	4.0±1.3	8
him-19(jf6); SUN-1::GFP irradiated	entire TZ	3.9±1.5	3.2±1.7	4.7±1.5	34
SUN-1::GFP irradiated	entire TZ	3.7±0.9	2.8±1.0	4.6±1.1	24
cra-1(tm2144); SUN-1::GFP	entire TZ	3.7±0.7	2.3±0.8	5.4±1.0	22

The variations indicated correspond to the standard deviation. It should be noted that the number of nuclei analyzed for SUN-1::GFP in the distal, central, and proximal parts of the TZ do not add up to the number of nuclei for the entire TZ, because nuclei that where localized in the middle of these zones (distal and central or central and proximal) were not assigned to any specific part.
n, number of nuclei.
doi:10.1371/journal.pgen.1001219.t001

To analyze the distance traveled, we extrapolated that the aggregates were moving on the periphery of a circle (projected nucleus), and measured the angle formed by the most extreme points of the tracks (Figure S2). Arcs do not express the absolute distance traveled; instead, they measure the area covered on the circle (a measurement of how vigorously aggregates move). We followed the arc for each track inside a nucleus, and also recorded the overall minimum and maximum values for the observed arcs (Figure 1Cii). Note that 180° is placed on the left of the x-axis, because angles were computed in a trigonometric circle. When the aggregate moved more than 180°/half plane, the radius of the circle increased, and the line representing this "arc" is dashed. Arc values for SUN-1 aggregates were not centered, but were evenly distributed between 13° and 163° (Figure 1Cii).

Because SUN-1 aggregates appeared to transiently coalesce (Figure 1A), we counted the number of fusion or splitting events of the aggregates during the first 15 min of the recordings (Figure 2A). The two most representative classes for the number of fusion/splitting events were 1–5 and 6–10 fusion/splitting events during the 15 min measuring period. A representative number of nuclei displayed between 11–15 fusion/splitting events, with an observed maximum of 25 exchanges. To assess how often exchanges take place, we looked at the time period between two fusion/splitting events. The "coalescence time" between aggregates was <1 min before splitting/fusing in 71% of cases, 1–3 min in 22% of cases, and >3 min in 7% of cases (Figure 2B).

Wild-type SUN-1 aggregates were particularly dynamic: they were movement-competent (traveled a distance of up to 160°) and able to reach high projected speeds (>160 nm/s). They fused and dispersed with high frequency (up to 15 fusion/splitting events during a 15 min interval of filming) during the leptotene/zygotene stage.

SUN-1 aggregate dynamics are independent of the position of the nucleus inside the TZ. To analyze whether SUN-1 aggregate behavior changes as the homology search progresses, we compared the aggregates in different parts of the TZ: distal (first row of cells of the TZ), proximal (last row of cells of the TZ), and central (row of cells clearly in the middle of the TZ). The appearance of tracks of SUN-1 aggregates was similar in each case. First, they exhibited the crescent form characteristic of the leptotene/zygotene stage (Figure 1Dii, 1Eii, and 1Fii). Second, no distinctions among the nuclei (from different positions in the TZ) could be made when looking at the distribution of the projected speeds. Aggregates in the three nuclei shown displayed the two classes of projected speed distribution: with or without long tails (Figure 1Diii, 1Eiii, 1Fiii). Aggregate numbers increased and decreased during the recorded time, independent of their position inside the TZ (Figure 1Div, 1Eiv, and 1Fiv). The distance traveled did not show a distinct pattern corresponding to the position in the TZ (Figure S3). No differences were found in the number of aggregates exchanged or the periodicity of these exchanges (data not shown). Therefore, we concluded that SUN-1 aggregates showed identical behavior, irrespective of their position in the TZ and the progress of homologous chromosome pairing.

Leptotene/zygotene characteristic chromatin polarization requires connection of the chromosome ends to the cytoskeleton via a functional SUN/KASH bridge

A point mutation in the SUN domain of SUN-1 results in the absence of a defined TZ, and disturbs the interaction of SUN-1 with ZYG-12 [30]. In the cytoplasm, ZYG-12 interacts with the cytoskeleton via a dynein motor [29,36]. We performed a time-lapse analysis of the mutated SUN-1(G311V)::GFP transgenic line in the *sun-1(ok1282)* deletion background and found that, on average, 7.8 ± 2.3 (SD) aggregates inside a nucleus exhibited restrained movement (Table 1, Figure 3A and 3B, and Video S3). The distribution of the projected speed of these aggregates was a sharp bell, with 95% of the aggregates moving within a range of 10–100 nm/s (Figure 3C); the projected speed was significantly reduced compared to wild-type aggregates (Mann-Whitney test, $p<0.001$). The displacement tracks indicated weak local oscillatory movement (Figure 3B), and the distances traveled were significantly reduced. The arcs varied between 27° and 59° (Figure 3D). No exchange of SUN-1 aggregates was seen (Figure 2A). A functional SUN/KASH bridge mediating the connection to the cytoskeleton was, thus, necessary for the movement of SUN-1 aggregates and correlated with the absence of polarized chromatin.

Loading of SC components is required for the formation of functional SUN-1 aggregates

The SC is a "zipper-like" structure that stabilizes the close pairing of parental chromosomes. This complex is composed of lateral elements on chromosome axes bridged by central region components [18]. We explored the behavior of SUN-1 aggregates in the SC mutants *him-3(gk149)*, *htp-1(gk174)*, *syp-2(ok307)*, and *syp-3(me42)*. HIM-3 is a major constituent of the lateral element, and HTP-1, in addition to being part of the lateral element, licenses synapsis [20,21]. The central region components of the SC, SYP-1, SYP-2, SYP-3 and SYP-4 zip up paired homologs [37,38,19]. An allele of the central region component SYP-3 revealed that SYP-3 plays a role in meiotic repair pathway decisions, in addition to its role in SC formation [39].

The *him-3(gk149)* null allele displays loss of the polarized conformation of chromatin in the TZ of the gonad and lacks presynaptic alignment [40]. Depleting HIM-3 resulted in 1.1 ± 0.3 (SD, $n=53$) SUN-1 aggregates moving inside a nucleus (Table 1), and, on rare occasions, up to two aggregates (Figure 4Ai and 4Aii) unable to fuse (Figure 2A, Video S4). The projected speed distribution of the aggregates was "Gaussian-shaped," with 95% of the aggregates moving within a range of 10–100 nm/s (Figure 4Aiii); this was significantly reduced compared to wild type (Mann-Whitney test, $p<0.001$). Depletion of HIM-3 also reduced the distance traveled by the SUN-1 aggregates: arc values only varied between 23° and 91° (Figure 4Aiv). HIM-8 is one of the four PC proteins, and binds specifically to the X chromosome [25]. In *him-3(gk149)*, HIM-8 always colocalizes with SUN-1::GFP, as shown by immunostaining [28]. Thus, the single SUN-1 aggregate moving with a reduced projected speed corresponds to the X chromosome and HIM-3 is, therefore, required for the formation of autosomal chromosome attachment plaques ([28] and this study). To test whether the formation of SUN-1 aggregates was impaired in *him-3(gk149)* due to mis-localization of the PC proteins, we stained *him-3(gk149)* with the PC protein ZIM-3 (marker for chromosomes I and IV). In *him-3(gk149)* mutant worms, the PC protein ZIM-3 did not colocalize with SUN-1 aggregates, although chromatin-associated signals were observed (Figure S4, Text S2). Therefore, we hypothesize that defective lateral elements of the SC impeded functional attachment plaque formation.

htp-1 mutants precociously synapse with the wrong partner despite proper loading of HIM-3 [20,21]. In *htp-1(gk174)*, the average number of aggregates was reduced (Mann-Whitney test, $p<0.05$). The maximum number of aggregates was comparable to the average number of SUN-1 aggregates in wild-type worms (Table 1). The displacement tracks of SUN-1::GFP in this

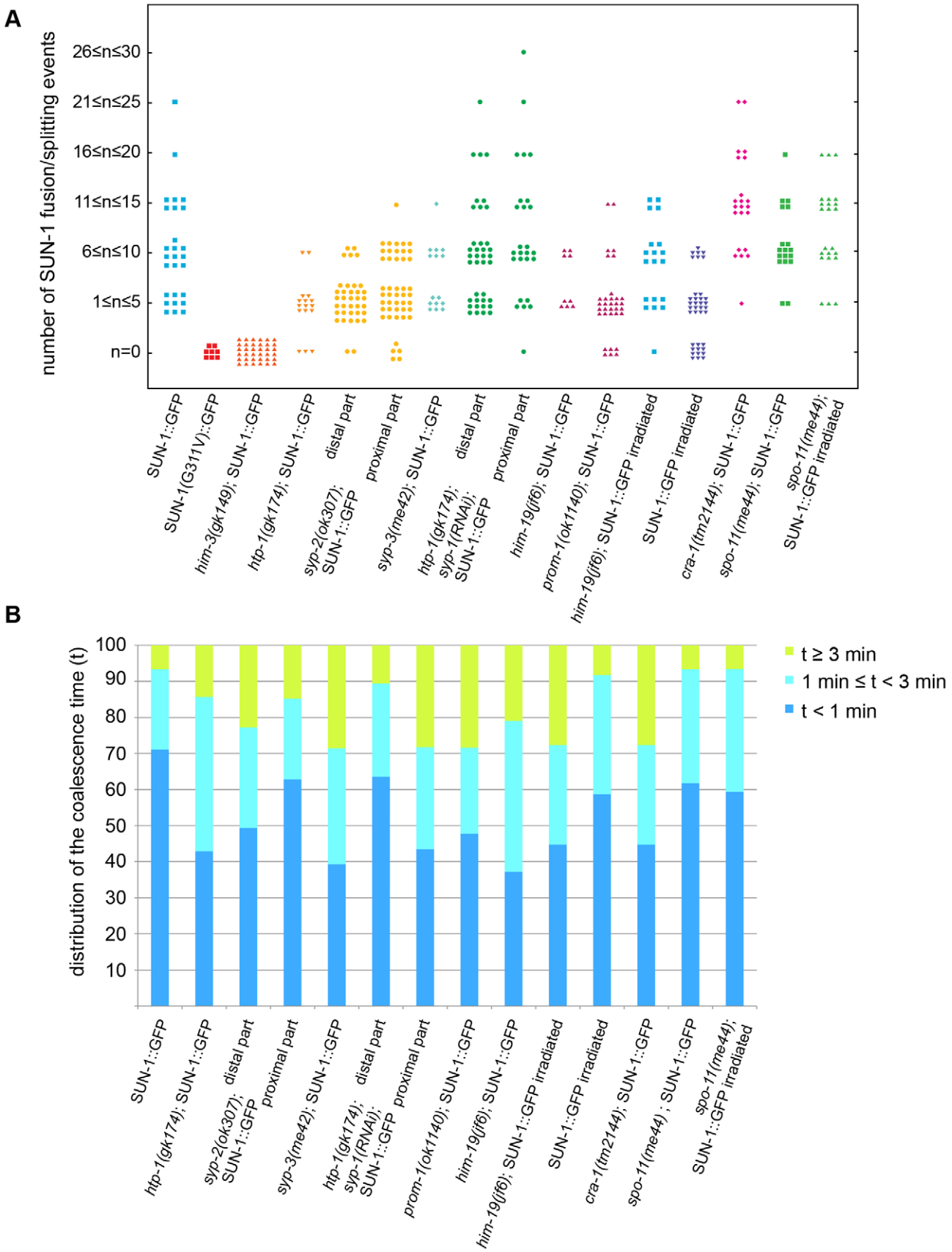
A
number of SUN-1 fusion/splitting events
26≤n≤30
21≤n≤25
16≤n≤20
11≤n≤15
6≤n≤10
1≤n≤5
n=0
SUN-1::GFP
SUN-1(G311V)::GFP
him-3(gk149); SUN-1::GFP
htp-1(gk174); SUN-1::GFP
syp-2(ok307); SUN-1::GFP distal part
syp-2(ok307); SUN-1::GFP proximal part
syp-3(me42); SUN-1::GFP
htp-1(gk174); syp-1(RNAi); SUN-1::GFP distal part
htp-1(gk174); syp-1(RNAi); SUN-1::GFP proximal part
him-19(jf6); SUN-1::GFP
prom-1(ok1140); SUN-1::GFP
him-19(jf6); SUN-1::GFP irradiated
SUN-1::GFP irradiated
cra-1(tm2144); SUN-1::GFP
spo-11(me44); SUN-1::GFP
spo-11(me44); SUN-1::GFP irradiated
B
distribution of the coalescence time (t)
100
90
80
70
60
50
40
30
20
10
t ≥ 3 min
1 min ≤ t < 3 min
t < 1 min
SUN-1::GFP
htp-1(gk174); SUN-1::GFP
syp-2(ok307); SUN-1::GFP distal part
syp-2(ok307); SUN-1::GFP proximal part
syp-3(me42); SUN-1::GFP
htp-1(gk174); syp-1(RNAi); SUN-1::GFP distal part
htp-1(gk174); syp-1(RNAi); SUN-1::GFP proximal part
prom-1(ok1140); SUN-1::GFP
him-19(jf6); SUN-1::GFP
him-19(jf6); SUN-1::GFP irradiated
SUN-1::GFP irradiated
cra-1(tm2144); SUN-1::GFP
spo-11(me44) ; SUN-1::GFP
spo-11(me44); SUN-1::GFP irradiated

Figure 2. Dynamics of fusion/splitting events of SUN-1 aggregates for all genotypes studied (15 min recording). (A) Number of SUN-1 fusion/splitting events grouped into classes. (B) Quantification of the coalescence time (t) grouped into classes ($t<1$ min, 1 min$\leq t<3$ min, and $t\geq 3$ min).
doi:10.1371/journal.pgen.1001219.g002

background recapitulated the polarization of the chromatin characteristic of the TZ (Figure 4Bi and 4Bii; Video S5). The projected speed distribution within a nucleus was comparable to that in *him-3(gk149)*. For most SUN-1 aggregates (>95%), the projected speed varied between 10 and 100 nm/s (Figure 4Biii). The distance traveled was significantly reduced compared to *him-3(gk149)* (Mann-Whitney test, $p<0.001$): arc values ranged from 20° to 62° (Figure 4Biv). The precocious synapsis in *htp-1(gk174)* mutant worms likely inhibits the mobility of SUN-1 aggregates (see below). This interpretation was reinforced by a significant decrease in the number of fusion/splitting events (Figure 2A and Table S1) and a significant increase in the time without exchange (Figure 2B and Table S2). Indeed, SUN-1 aggregates coalesced for longer than 1 min in 60% of cases. Although ZIM-3 loading was defective in *him-3(gk149)*, it was unaffected in *htp-1(gk174)*, with 2–4 ZIM-3 signals overlapping with SUN-1 aggregates (Figure S4). We conclude that *htp-1(gk174)* mutant worms readily formed single chromosomal attachment plaques.

The SC central region component mutant *syp-2(ok307)* has an extended TZ, characteristic of SC mutants [38]. We compared the dynamics of SUN-1 aggregates in distal (first half of the TZ, Video S6) and proximal (second half of the TZ, Video S7) positions in the prolonged TZ. In the distal part, on average, 2.8±1 (SD, $n=30$) SUN-1 aggregates showed reduced movement (Figure 4Ci and 4Cii); in addition, the maximum number of SUN-1 aggregates was reduced (3.5±1.1; SD, $n=30$) compared to wild type (Table 1; Mann-Whitney test, $p<0.05$). Although the projected speed distribution of 95% of SUN-1 aggregates was 10–100 nm/s (Figure 4Ciii), comparable to *him-3(gk149)*, the distribution was more Maxwellian-shaped. The distance traveled by SUN-1::GFP aggregates was reduced (from 16° up to 90°, with the exception of one track that went up to 163°; Figure 4Civ) compared to wild type. Depletion of SYP-2 also reduced the number of SUN-1::GFP fusion/splitting events in the distal part of the TZ (Figure 2A and Table S1), with mostly 1–5 fusion/splitting events occurring within 15 min. The time of coalescence between SUN-1 aggregates was increased. Indeed, only 50% of SUN-1 aggregates coalesced for less than 1 min, while 22% of them coalesced for more than 3 min (Figure 2B and Table S2).

syp-2(ok307) SUN-1::GFP aggregates in the proximal part of the TZ traveled longer distances. The arcs were between 20° and 150° (Figure 4Civ'), which is in accordance with a broader projected speed distribution. The projected speed distribution for 95% of the aggregates ranged between 15 and 140 nm/s (Figure 4Ciii'), and adopted a more Maxwellian-shaped distribution than in the early TZ, with the distribution shifted towards the higher speed. In the proximal part of the TZ, the displacement tracks were more reminiscent of the crescent shape of the chromatin than in the distal part of the TZ (compare Figure 4Ci and 4Ci'). In the proximal part of the TZ, the maximum number of SUN-1 aggregates went up to 4.2±1.2 (SD, $n=45$) (Table 1); nevertheless, their average number remained decreased compared to wild type (Mann-Whitney test, $p<0.05$). The number of SUN-1::GFP fusion/splitting events also differed from those seen in wild-type worms; there were less than ten exchanges within 15 min (Figure 2A and Table S1). The periodicity of the exchanges was similar to wild type (Figure 2B and Table S2). Disruption of synapsis resulted in a lack of long tails in the speed distribution and a decrease in the number of SUN-1 aggregates exchanged in both the distal and proximal parts of the TZ.

The *syp-3* allele *me42* is special because it has a shortened TZ and appears to use a different repair pathway for the repair of meiotic DSBs [39]. In contrast to SC-deficient mutants, in *me42*, the central region component SYP-1 was found to be polymerized on univalents. The displacement tracks of SUN-1::GFP in *syp-3(me42)* followed a half-moon shape (Figure 4Di and 4Dii; Video S8). The number of SUN-1 aggregates was significantly decreased compared to wild-type values (Table 1; Mann-Whitney test, $p<0.001$). The distribution of the projected speed was more Maxwellian-shaped and comparable to the distribution of SUN-1::GFP aggregates in the distal part of the *syp-2(ok307)* mutants (Figure 4Diii). The distance traveled was greater than in *syp-2(ok307)* mutant worms, and covered angles from 37° to 100° (Figure 4Div). The number of SUN-1::GFP fusion/splitting events was comparable to those in wild-type worms (Figure 2A and Table S1), but the frequency of the exchanges was significantly decreased (Figure 2B and Table S2).

To test the idea that restricted aggregate behavior in *htp-1(gk174)* was due to nonhomologous synapsis, we depleted SYP-1 in *htp-1(gk174)* mutants. Surprisingly, in *htp-1(gk174)*; *syp-1(RNAi)* SUN-1 aggregates were extended and not restricted to the first cell row where chromatin is strongly polarized (Figure S5). SUN-1 aggregates were still detectable in nuclei with more loosely clustered chromatin. We divided the zone with aggregates into distal (Video S9) and proximal (Video S10) for analysis. In the distal part of *htp-1(gk174)*; *syp-1(RNAi)* the average number of SUN-1 aggregates (3.5±0.6, SD, n = 23, Table 1) was close to wild type, but their maximum number was significantly reduced (Mann-Whitney test, $p<0.05$). Displacement tracks adopted a circular form, in contrast to the crescent shape seen in wild type (Figure 5A and 5B, 11 out of 23 nuclei), where movement pushes the nucleolus to one side of the nucleus. Here the tracks are found at the periphery, with chromatin likely rotating around the nucleolus. SYP-1 depletion in *htp-1(gk174)* significantly increased the projected speed of SUN-1 aggregates when compared to *htp-1(gk174)*, nevertheless the percentage of long tails (4%) was significantly below wild-type values (Figure 5C, Mann-Whitney test, $p<0.05$). The distance traveled was also significantly increased in *htp-1(gk174)*; *syp-1(RNAi)*, with arc values reaching 156° (compare Figure 4Biv and Figure 5D, Mann-Whitney test, $p<0.05$). Depletion of SYP-1 in *htp-1(gk174)* resulted in an increase of exchanged aggregates (Figure 2A, Table S1) and restored the periodicity of these exchanges to the wild type value (Figure 2B, Table S2).

In the proximal region of *htp-1(gk174)*; *syp-1(RNAi)* gonads the number of SUN-1 aggregates was significantly reduced compared to the distal part (Mann-Whitney test, $p<0.05$) with an average of 2.8±0.6 (SD, n = 24, Table 1). Of the 23 nuclei analyzed, 16 nuclei displayed circular displacement tracks (Figure 5A' and 5B'). The distribution of the projected speed was significantly increased compared to the distal part (6% long tails, Figure 5C', Mann-Whitney test, $p<0.05$), but still below wild-type values (Mann-Whitney test, $p<0.05$). SUN-1 aggregates traveled longer distances in the proximal part than in the distal (Figure 5D', Mann-Whitney test, $p<0.05$), but the distances traveled, the exchanges, and the frequencies were still below wild-type values (Mann-Whitney test, $p<0.05$). (Figure 2A and 2B, Tables S1 and S2).

Our analysis of the behavior of SUN-1 aggregates in mutants defective in SC formation confirmed that intact lateral elements of

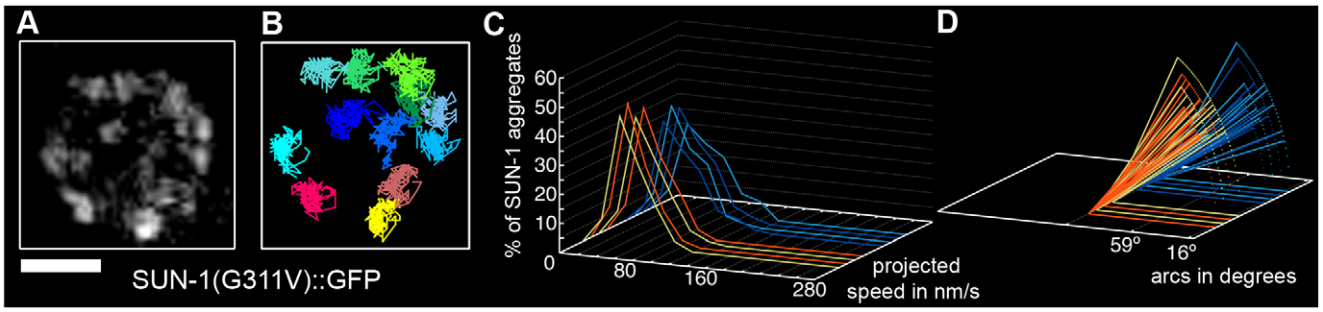

Figure 3. Disruption of the SUN/KASH bridge abrogates SUN-1 aggregate movement. Restrained movement in SUN-1(G311V)::GFP (A), displacement tracks (B), distribution of the projected speed of all SUN-1 aggregates inside a nucleus (C), and arcs representing the traveled distance for each track inside a nucleus (D). Blue lines represent values from the first movie, orange lines from the second. Eight out of the eight nuclei analyzed are shown. See Table 1 for number of nuclei analyzed. Scale bar: 2 μm.
doi:10.1371/journal.pgen.1001219.g003

the SC were necessary for the formation of functional SUN-1 aggregates. We showed that SC components played a role in the exchange of SUN-1 aggregates. HTP-1 has an inhibitory influence on the exchange of aggregates as we observed reduced exchanges in *htp-1(gk174)* and *syp-2(ok307)* single mutants, whereas exchanges were increased to wild type values in *htp-1(gk174)*; *syp-1(RNAi)*). Strikingly, defects in SC polymerization reduced the projected speed of aggregates, whereas decreasing synapsis in the *htp-1* mutant increased the projected speed of SUN-1 aggregates. The persistent aggregates in the *syp-1 htp-1* double mutant formed circular displacement tracks concomitant with only loosely clustered chromatin.

Modulation of SUN-1 aggregate properties by meiotic regulators CHK-2, HIM-19, PROM-1, and CRA-1

To date, known early meiotic regulators with a role in chromosome pairing in *C. elegans* include CHK-2, HIM-19, PROM-1, and CRA-1. Depletion of CHK-2 results in a lack of SUN-1 aggregates in *chk-2* [28]; therefore, no live imaging can be shown. HIM-19 is a newly identified meiotic regulator. In *him-19(jf6)* mutants, meiotic defects are aggravated with age. In 2-day-old (2-d-old) *him-19(jf6)* mutant worms, the TZ is not defined, DSB formation is likely defective, and elongation of the SC is restricted and nonhomologous [33]. PROM-1 is involved in the progression of meiosis I, and its depletion elicits nonhomologous synapsis. *prom-1(ok1140)* mutant worms lack a defined TZ and instead display dispersed nuclei with a polarized conformation after a prolonged meiotic entry zone [32]. CRA-1 regulates SC formation. Unlike *chk-2*, *prom-1*, and *him-19*, *cra-1* mutant worms display an extended TZ. In addition, *cra-1(tm2144)* mutant worms are defective in the formation of the SC central region [34].

In dispersed nuclei with a TZ-like appearance in *prom-1(ok1140)* mutant worms, SUN-1::GFP aggregates were movement competent (Video S11), and their tracking reconstructed the crescent shape of the chromatin (Figure 6Ai and 6Aii). The number of SUN-1 aggregates in *prom-1(ok1140)* was reduced compared to wild type (Mann-Whitney test, $p<0.05$), despite a similar average number of aggregates (Table 1). In this background, SUN-1 aggregates displayed a Maxwellian-shaped projected speed distribution and lacked long tails (Figure 6Aiii; Mann-Whitney test, $p<0.05$ compared to wild type), although the distance traveled by SUN-1::GFP aggregates was unaffected (from 19° up to 143°; Figure 6Aiv; Mann-Whitney test, $p>0.05$). Depletion of PROM-1 also reduced the number of exchanged aggregates (Figure 2A). Indeed, in a significant number of nuclei, SUN-1 aggregates were unable to fuse or split, and the number of nuclei showing 6–10 fusion/splitting events was considerably reduced (Table S1). The time period without exchange was significantly increased in *prom-1(ok1140)* compared to wild type: 47% of SUN-1::GFP aggregates were found to coalesce for less than 1 min and 23% for more than 3 min (Figure 2B and Table S2).

In *prom-1(ok1140)*, it is likely that the delayed orchestration of the meiotic program led to a reduction in the speed of SUN-1 aggregates without affecting the distance traveled. In addition, the number and frequency of exchanges were reduced in *prom-1(ok1140)* mutants.

The formation of SUN-1 aggregates in 2-d-old *him-19(jf6)* mutants was restricted to the few dispersed nuclei with a polarized chromatin conformation, but could be augmented by γ-irradiation (Figure 6B and [28]). In aged *him-19(jf6)* worms, a few SUN-1::GFP aggregates were movement competent (Video S12), and their displacement tracks resembled a crescent shape (Figure 6Bi and 6Bii). Both the average number of SUN-1 aggregates (2.8 ± 0.8; SD, $n=8$)) and the maximum number of aggregates was decreased (4.0 ± 1.3; SD, $n=8$) (Table 1; Mann-Whitney test, $p<0.05$). In addition, the projected speed distribution of SUN-1::GFP aggregates was reduced compared to wild type (Mann-Whitney test, $p<0.05$): it was similar to the speed of SUN-1::GFP aggregates in *htp-1(gk174)*, with 95% of the aggregates moving from 10 to 130 nm/s (Figure 6Biii). The distance covered was also reduced, as demonstrated by arc values ranging from 9° up to 137° (Figure 6Biv; Mann-Whitney test, $p<0.05$). In *him-19(jf6)* mutants, the number of SUN-1 fusion/splitting events was wild type (Figure 2A and Table S1), whereas the time without exchange increased, with 38% of SUN-1 aggregates coalescing for less than 1 min and 21% for more than 3 min (Figure 2B and Table S2).

Two hours after γ-irradiation, the average number of SUN-1 aggregates reached wild-type levels in 2-d-old *him-19(jf6)* worms (Table 1); however, the number of SUN-1 aggregates was significantly reduced (Mann-Whitney test, $p<0.05$). The displacement tracks of SUN-1::GFP in 2-d-old irradiated *him-19(jf6)* worms recapitulated the polarized conformation of the chromatin (Figure 6Bi' and ii'; Video S13). The distribution of the projected speed of SUN-1::GFP aggregates was shifted towards the higher speed after irradiation and became more Maxwellian-shaped. Nevertheless, long tails were absent from the distribution (Figure 6Biii'). The projected speed of SUN-1 aggregates was reduced in aged irradiated *him-19(jf6)* compared to wild type (Mann-Whitney test, $p<0.05$). In contrast, irradiation-induced SUN-1::GFP aggregates in *him-19(jf6)* moved similar to those in wild-type worms in terms of the distance traveled (Figure 6Biv'; Mann-Whitney test, $p>0.05$), whereas the number of exchanges

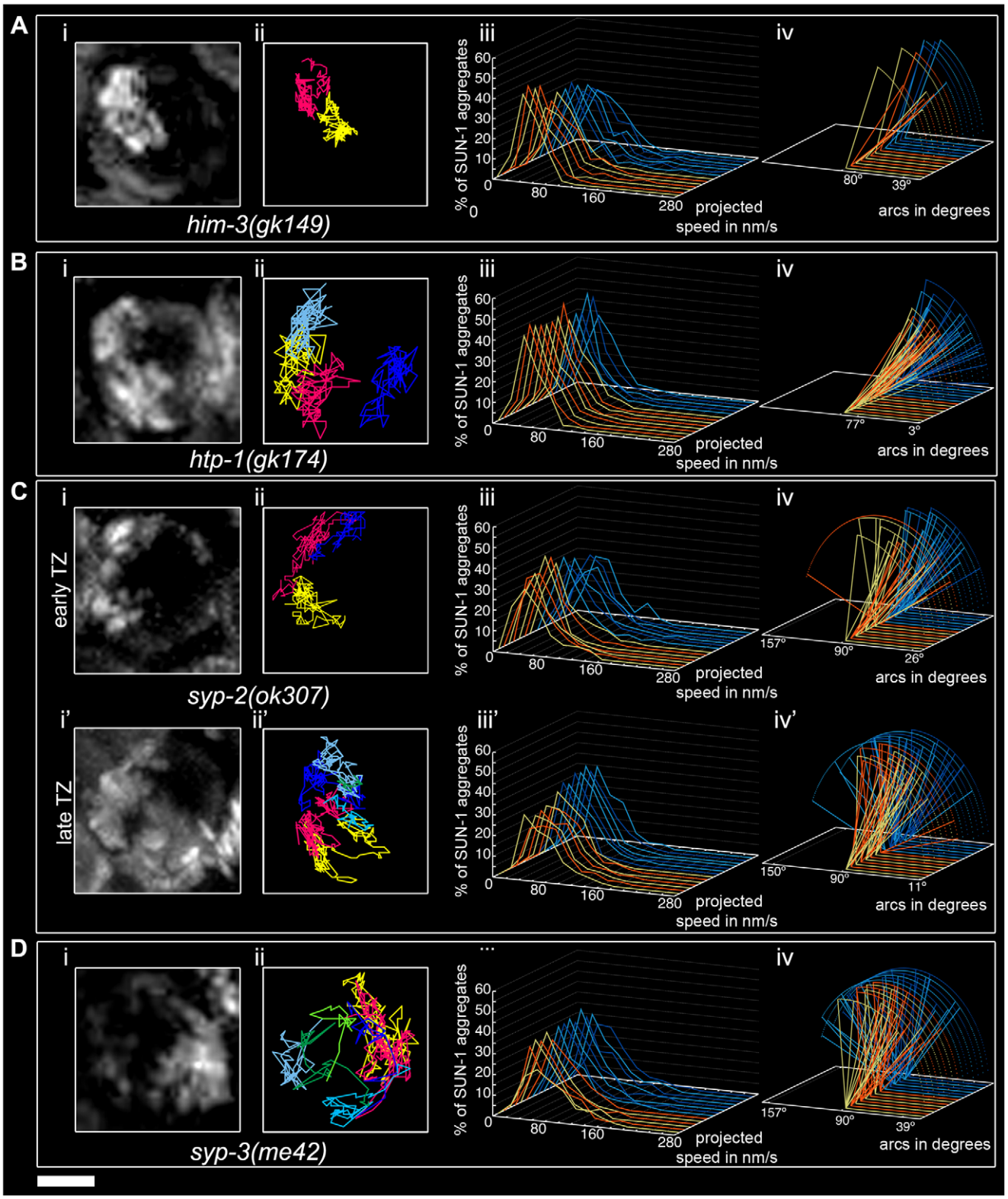

Figure 4. Impact of SC components on the dynamics of SUN-1 aggregates. *him-3(gk149)* (A), *htp-1(gk174)* (B), *syp-2(ok307)* (C), and *syp-3(me42)* (D), with projection of cumulative movement (i), displacement tracks (ii), and distribution of the projected speed (iii). Arcs represent traveled distance (iv). Blue lines represent values from the first movie, orange lines from the second. (C) *syp-2(ok307)* (i), (ii), (iii), and (iv) from the distal part of the extended TZ and i', ii', iii', and iv' from the proximal part. See Table 1 for number of nuclei analyzed. Scale bar: 2 μm.
doi:10.1371/journal.pgen.1001219.g004

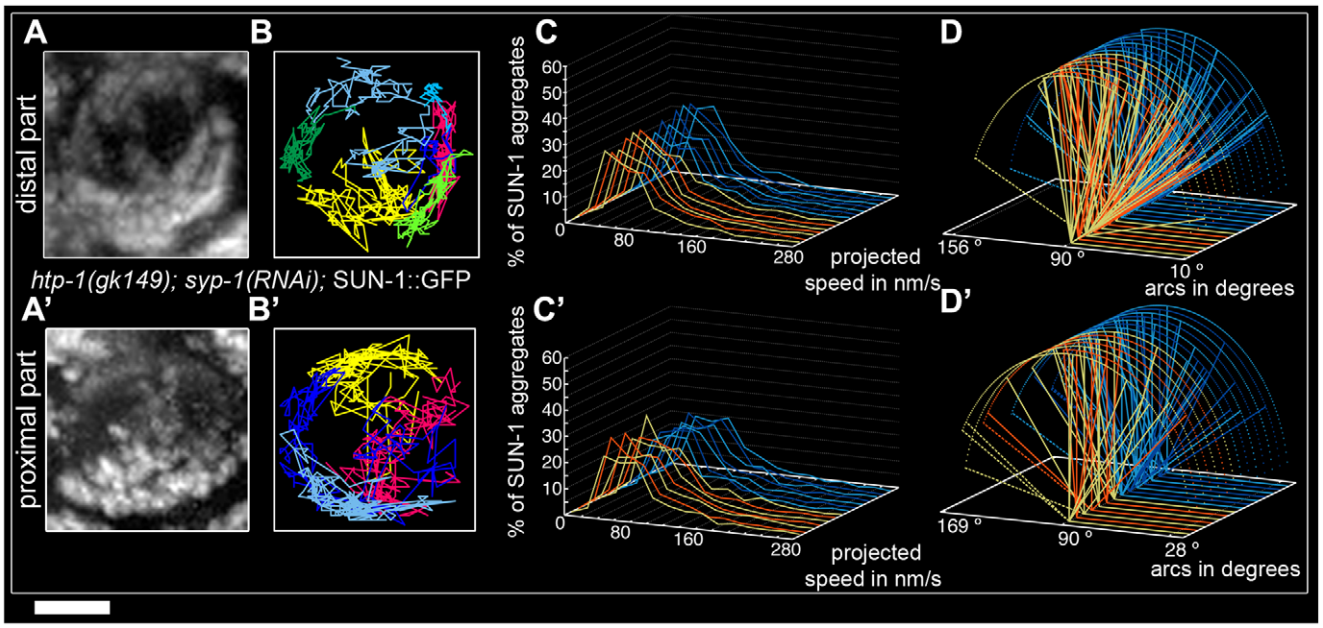

Figure 5. Restrained movement of SUN-1 aggregates in *htp-1(gk174)* is due to precocious synapsis. Projection of the cumulative movement of SUN-1::GFP in *htp-1(gk174)*; *syp-1(RNAi)* (A, A'), displacement tracks (B, B'), distribution of the projected speed (C, C'), and arcs (D, D'). Blue lines represent values from the first movie; orange lines values from the second. (A, B, C, D) from distal TZ, (A', B', C', D') from proximal zone where SUN-1 aggregates move. See Table 1 for number of nuclei analyzed. Scale bar: 2 μm.
doi:10.1371/journal.pgen.1001219.g005

was significantly reduced. The class of 1–5 fusion/splitting events represented more than 50% of nuclei, and the exchange was abrogated for a representative number of nuclei (Figure 2A and Table S1). The frequency of these exchanges was reduced compared to wild type (Figure 2B and Table S2), and there was no significant increase compared to nonirradiated *him-19(jf6)* worms.

We conclude that γ-irradiation restored the formation of SUN-1 aggregates to wild-type levels with respect to their numbers and distances traveled, whereas the dynamics of SUN-1 aggregates remained impaired both in terms of the distribution of the projected speed and the number and frequency of exchanges.

To ensure that γ-irradiation had no side effects, we irradiated 2-d-old worms solely expressing SUN-1::GFP and performed the same analysis. The appearance of the displacement tracks of SUN-1::GFP aggregates was circular in 12 of the 24 nuclei analyzed whereas the other ones recapitulated the crescent shape of the chromatin (Figure 6Ci and 6Cii; Video S14). The distribution of the projected speed of SUN-1::GFP aggregates was shifted markedly towards lower values, with only 3% long tails (>160 nm/s) (Figure 6Ciii; Mann-Whitney test, $p<0.05$). Nonetheless, after γ-irradiation, SUN-1::GFP aggregates move faster in wild-type worms than in irradiated *him-19(jf6)* (Mann-Whitney test, $p<0.05$). In addition, the maximum number of SUN-1 aggregates was reduced (Table 1; Mann-Whitney test, $p<0.05$) compared to nonirradiated wild type. γ-irradiation also reduced the distance traveled by SUN-1 aggregates; arc values ranged between 19° and 128° (Figure 6Civ; Mann-Whitney test, $p<0.05$). γ-irradiation had no impact on the number of SUN-1::GFP fusion/splitting events (Figure 2A and Table S1). However, it significantly increased the time without exchanges (Figure 2B and Table S2). FISH analysis with a probe specific for chromosome V revealed that pairing was affected after γ-irradiation (Figure S6A and S6B). To ascertain whether the decrease in the speed distribution might be due to an SC defect, we stained for SYP-1 in nonirradiated and irradiated wild-type worms. No gross irregularities in SYP-1 polymerization were evident 2 h after γ-irradiation (Figure S6C, Text S2).

γ-irradiation clearly had an impact on the dynamics of SUN-1 aggregates in wild-type gonads. Nonetheless, the behavior of restored SUN-1 aggregates in irradiated *him-19(jf6)* mutants adopted a more wild-type-like behavior compared to the sparse aggregates in non-irradiated *him-19(jf6)* gonads.

In *cra-1(tm2144)* mutants, SUN-1 aggregates were movement competent (Video S15), and their displacement tracks adopted a rather circular form (19 out of 22), like in *htp-1(gk174); syp-1(RNAi)* (Figure 6Di and 6Dii). Likewise, in *cra-1(tm2144)* chromatin loosely clustered following a short stretch of nuclei with strong chromatin polarization (Figure S5). The number of SUN-1 aggregates was similar to that of wild type (Table 1; Mann-Whitney test, $p>0.05$). However, the distribution of the projected speeds of SUN-1 aggregates increased towards higher speeds (12% long tails) (Figure 6Diii; (Mann-Whitney test, $p<0.05$). This was also the case for the distance traveled, with arcs ranging from 15° up to 173° (Figure 6Div; Mann-Whitney test, $p<0.05$). Except for the class of 1–5 fusion/splitting events, which was significantly reduced compared to wild type, the number of SUN-1 fusion/splitting events was similar to that of wild type in the *cra-1(tm2144)* background (Figure 2A and Table S1). The frequency of SUN-1 aggregate exchanges was unaffected in *cra-1(tm2144)* (Figure 2B and Table S2).

In *cra-1(tm2144)*, the kinetics of SUN-1 aggregates were increased (speed and distance traveled) compared to wild type, whereas the number and frequency of fusion/splitting events was unaffected.

Impairment of meiotic regulators showed that DSBs could be involved in the formation of functional SUN-1 aggregates, and that γ-irradiation nonetheless had some impact on SUN-1 aggregate movement. Improper orchestration of the meiotic program disturbed SUN-1 aggregate dynamics.

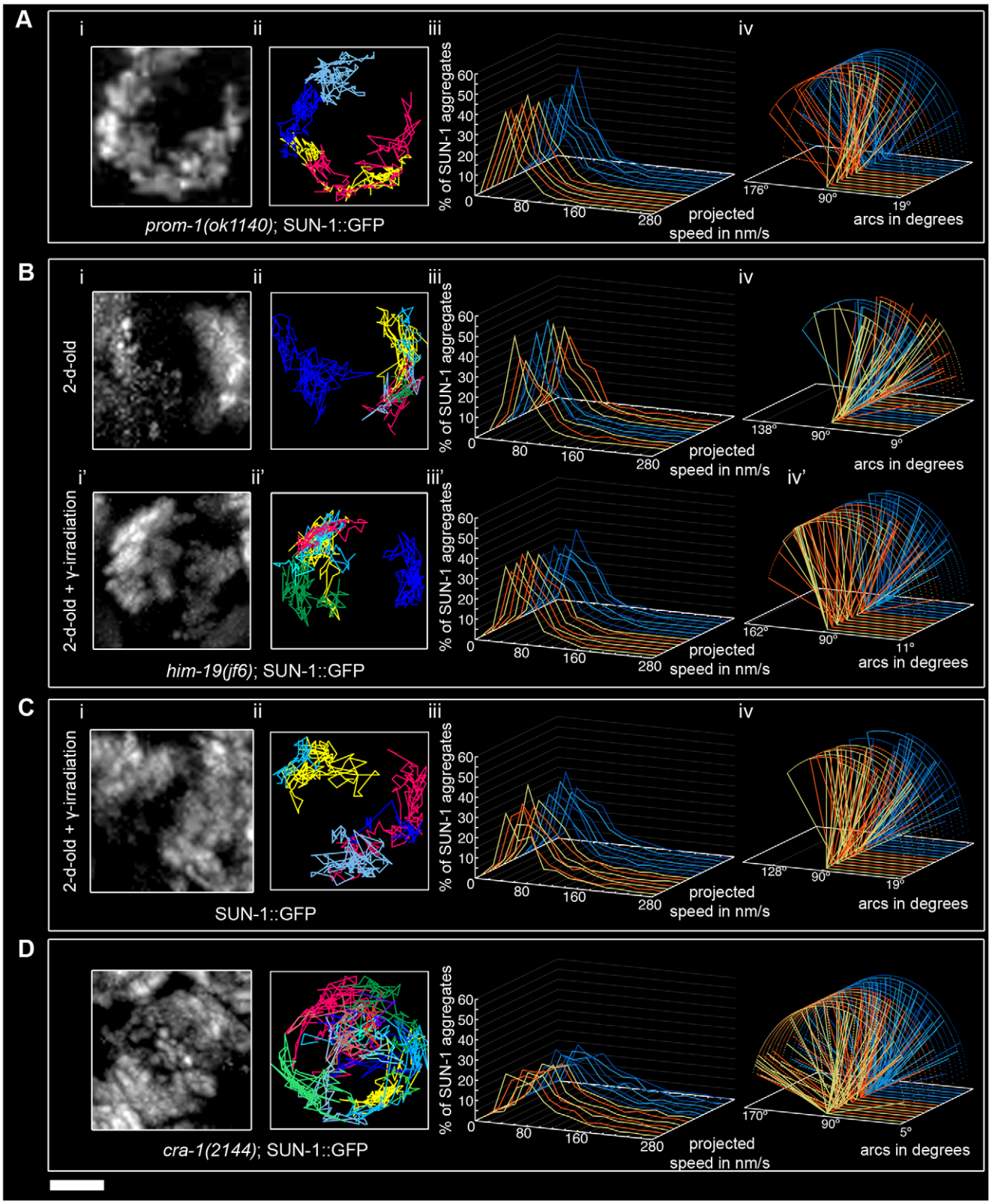

Figure 6. Influence of meiotic regulators on dynamics of SUN-1 aggregates. *prom-1(ok1140)* (A), *him-19(jf6)* (B), irradiated wild type (C), and *cra-1(tm2144)* (D), showing projection of the cumulative movement of SUN-1::GFP aggregates (i), displacement tracks (ii), distribution of the projected speed (iii), and arcs representing travelled distances (iv). Blue lines represent values from the first movie, orange lines from the second. See Table 1 for number of nuclei analyzed. Scale bar: 2 μm.
doi:10.1371/journal.pgen.1001219.g006

DSBs are required for wild-type SUN-1 aggregate behavior

In order to test whether recombination impacts SUN-1 aggregate dynamics, we followed SUN-1 movement in the *spo-11(me44)* mutant (Video S16).

The average number of SUN-1 aggregates was significantly reduced (3.0±0.6, SD, n = 18, Table 1) compared to wild type. Surprisingly, the appearance of SUN-1 displacement tracks was circular in 9 out of the 18 nuclei analyzed (Figure 7Ai and 7Aii). The distribution of the projected speed of SUN-1 aggregates in *spo-11(me44)* showed only 5% long tails (Figure 7Aiii), and was reduced in terms of speed and distance traveled (Mann-Whitney test, $p<0.05$) (Figure 7Aiv). In *spo-11(me44)*, the number and frequency of exchanges (Figure 2A and 2B, Tables S1 and S2) were wild type.

Next we tested whether introduction of artificial DSBs by γ-irradiation in *spo-11(me44)* (Video S17) could restore the properties of SUN-1 aggregates to wild-type values. The average number of SUN-1 aggregates (3.6±0.6, SD, n = 23, Table 1) in *spo-11(me44)* mutants increased to wild-type levels after irradiation. The displacement tracks were circular in 11 of the 23 nuclei analyzed (Figure 7Bi and 7Bii). The distribution of the projected speed of SUN-1 aggregates displayed 3% of long tails, like wild type 2 hours after irradiation, but SUN-1 aggregates tended to move faster (Mann-Whitney test, $p<0.05$). γ-irradiation had no impact on the distance traveled (Figure 7Biv, Mann-Whitney test, $p>0.05$). The frequency of exchanges was significantly reduced when compared to wild type (Figure 2B, Table S2), but no effect could be detected in the number of SUN-1 aggregates exchanged (Figure 2A, Table S1). The properties of SUN-1 aggregates in *spo-11(me44)* after irradiation were close to wild-type values after irradiation.

Intrigued by the fact that less SUN-1 aggregates can be found in *spo-11(me44)*, we compared the ratio of foci and patches in the gonad of both irradiated and non-irradiated wild type and *spo-11(me44)* worms. We found a significant increase in the number of foci in *spo-11(me44)* compared to wild type (Figure 7C, Fisher's exact test, $p<0.05$). The ratio of foci to patches was significantly reduced after irradiation (Figure 7C, Fisher's exact test, $p<0.05$) with an increase in the fraction of patches for wild type and *spo-11(me44)*.

All together, these results confirm that formation of DSBs is necessary for the generation of wild-type numbers of SUN-1 aggregates and patches. The appearance of circular tracks in *spo-11(me44)* confirms loose chromatin clustering in *spo-11(me44)* (not shown).

Discussion

During early meiotic prophase, SUN-1 forms movement-competent aggregates that can be categorized into two classes: foci and patches. Foci most likely represent single chromosome end attachments, whereas patches harbor multiple chromosome ends in a local cluster, reminiscent of the chromosomal bouquet [28]. These aggregates fuse and disperse, with an average number of four aggregates during leptotene/zygotene, and cover distances on the order of half a circle after projecting movement into two dimensions. The movement of SUN-1 aggregates anchored in the inner nuclear membrane is able to induce outward directed protrusion of the chromatin and, thus, of the nuclear envelope, as in budding yeast [7] and maize [9].

Formation of functional SUN-1 aggregates

Wild-type numbers of SUN-1 aggregates require HIM-3, a component of the lateral elements of the SC. The sole movement-competent aggregate in the *him-3(gk149)* mutant colocalizes with the X chromosome [28]. The "autosomal SUN-1 aggregates" are, therefore, missing. Lateral elements of the SC are possibly required for their formation; alternatively, they may affect their stability. The fact that formation of attachment plaques at the nuclear periphery is independent of the lateral element of the SC in rat testis [41] provides support for the latter explanation. The reduced mobility of the SUN-1 aggregate in *him-3(gk149)* could be explained by the ability of the lateral element of the SC to rigidify the chromosomes, thereby supporting resolution of chromatin entanglements that otherwise might slow down movement.

Formation of functional SUN-1 aggregates also requires a functional SUN-domain, enabling the movement of SUN-1 aggregates. We showed that disruption of the SUN/KASH bridge abrogated the movement of SUN-1 aggregates, leading to nonhomologous synapsis in SUN-1(G311V)::GFP. The movement of SUN-1 aggregates, thus, exerted an inhibitory action on synapsis with the wrong partners. In addition, SUN/KASH-mediated movement exerted a positive effect on synapsis by mixing chromosomes in the nucleus, thereby positively reinforcing homologous synapsis. The movement of SUN-1 aggregates also elicited the polarized appearance of the chromatin, which required more than one aggregate to be moving, as exemplified in *him-3(gk149)*, where chromatin did not cluster.

Do SUN-1 patches solely reflect chromosome end shuffling as the driving force for pairing?

Chromosome ends move along the inner surface of the nuclear envelope and come together in areas where patches of SUN-1 are seen. At the same time, SC polymerization is present, implying that once parental partner chromosomes have met, they engage in synapsis [37]. At this point, successful synapsis did not lead to dissolution of the aggregate. There was no difference in terms of the number of SUN-1 aggregates during the progression of leptotene/zygotene (as assessed by dividing this stage into three substages); instead, the average number of SUN-1 aggregates fluctuated at around four.

We propose that duplets/multiplets of chromosome ends are linked to SUN-1 patches. These duplets/multiplets of chromosome ends attached to SUN-1 patches continue to move and meet other SUN-1 patches or foci. While the newly met SUN-1 aggregates coalesce, homology is assessed; how homology is assessed is still an open question. Chromosome ends are then shuffled through patches of SUN-1, and when the right partner is met, synapsis can take place. The shuffling of chromosome ends through the patches continues until all of the chromosomes have found their homolog. This process is dynamic, as most SUN-1 aggregates coalesce for less than 1 min. The shuffling of the chromosome ends during SUN-1 aggregate coalescence is, thus, one of the driving forces for homology search (Figure 8A and 8B). This allows homologous chromosome ends to meet and nonhomologous chromosomes to separate.

Chromosome ends coalescing in SUN-1 patches might not solely reflect shuffling chromosome ends but also interactions caused by recombination repair intermediates. Indeed, in *spo-11* fewer patches are formed than in wild type and introduction of DSBs significantly increases the formation of patches. These two processes (assessing homology) and ongoing repair of DSBs (up to the strand invasion step) might be the source of the long tails observed in the speed distribution of SUN-1 aggregates (see below). In addition interlocked chromosomes could contribute to the long tails.

Formation of high-speed SUN-1 aggregates

During the leptotene/zygotene stage, SUN-1 aggregates in *C. elegans* moved more slowly and did not accelerate abruptly,

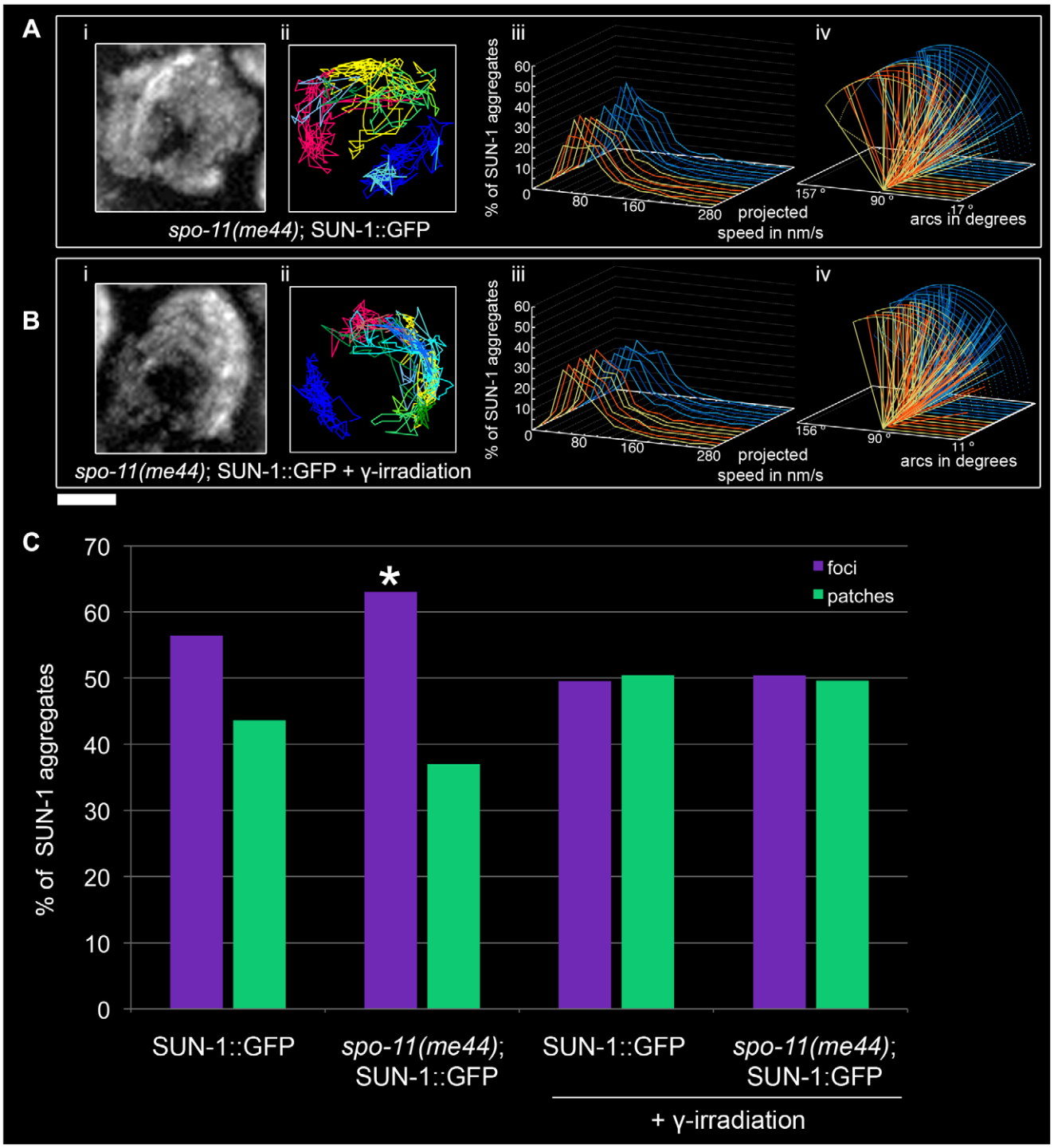

Figure 7. Effect of DSB formation on SUN-1 aggregate dynamics. *spo-11(me44)* (A), 2-d-old *spo-11(me44)* (B) 2 hours after irradiation with projection of cumulative movement (i), displacement tracks (ii), and distribution of the projected speed (iii). Arcs represent traveled distance (iv). Blue lines represent values from the first movie, orange lines from the second. See Table 1 for number of nuclei analyzed. (C) Distribution of SUN-1 foci and patches formed in wild type, *spo-11(me44)*, 2-d-old wild type 2 hours after irradiation and 2-d-old *spo-11(me44)* 2 hours after irradiation. >400 SUN-1 aggregates counted per genotype. Scale bar: 2 μm.
doi:10.1371/journal.pgen.1001219.g007

similar to what was reported for telomere ends in budding yeast and maize [6,7,9]. Nonetheless, SUN-1 aggregates reached relatively high speeds (>160 nm/s), as demonstrated by the long tails in the distribution of the projected speed of SUN-1 aggregates.

Two nonexclusive explanations could account for the formation of the long tails in the projected speed distribution of SUN-1 aggregates: first, "a model of tension" [29], where assessment of homology (Figure 8A and 8B), a nascent repair intermediate (Figure 8C) or chromosome entanglements (Figure 8D) leads to the

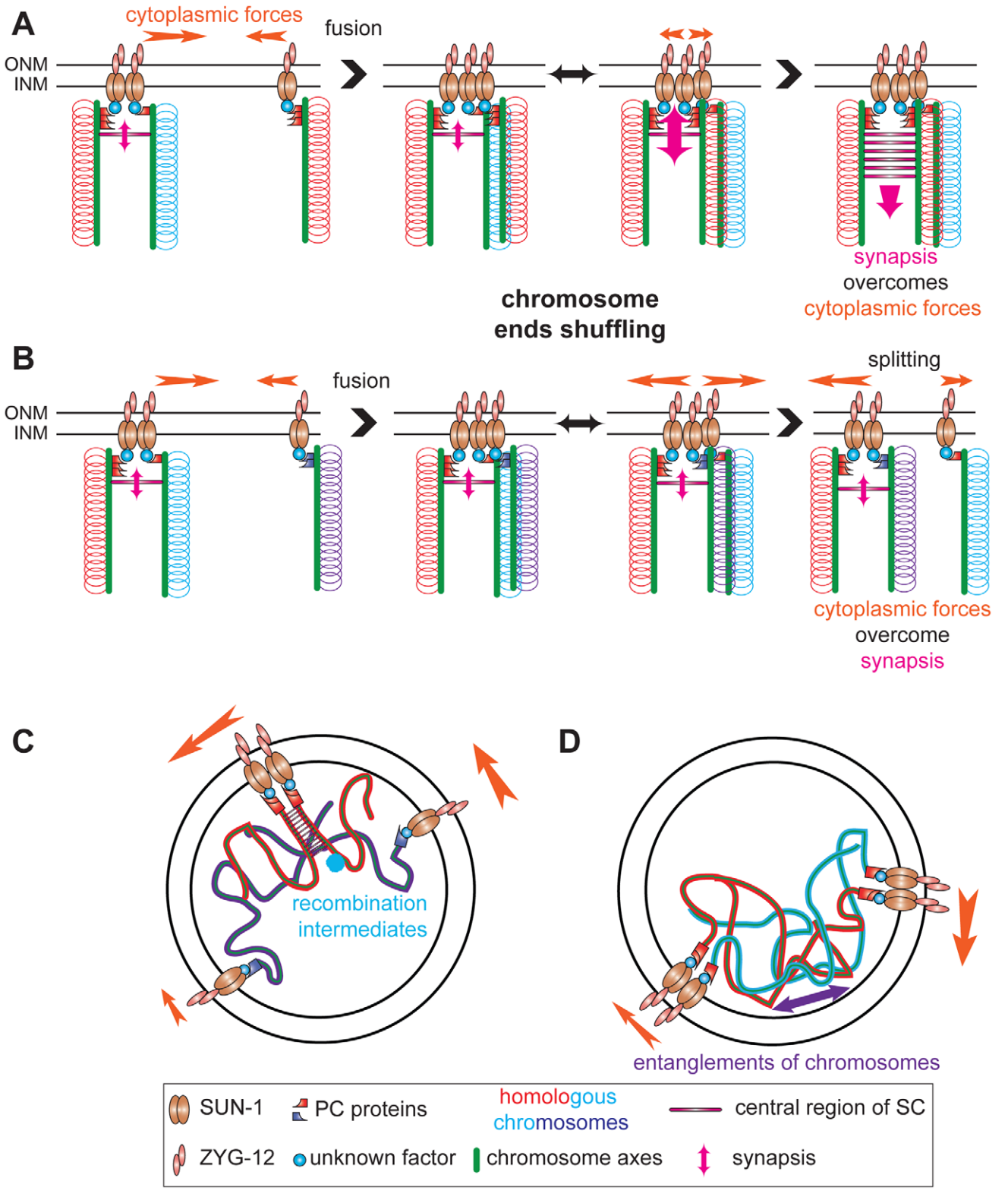

Figure 8. Establishment of synapsis and formation of high speed via shuffling of chromosome ends through SUN-1 patches. Chromosome axes (green lines) support binding of PC proteins (red or violet shapes) that connect chromosome ends (red, blue, and violet loops) to SUN-1 (brown ellipses), directly or indirectly, (unknown factor, blue circle). ZYG-12 (pink ellipses) and SUN-1 bridge chromosomes to cytoplasmic forces (orange arrow) to move chromosome ends. (A) SUN-1 patch containing two nonhomologous chromosome ends (red and blue loops) fuses with SUN-1 focus carrying a single chromosome end, a homolog (red loops). After fusion, chromosome ends will be shuffled inside the newly formed SUN-1 patch. When the homologous chromosome is found, synapsis overcomes the cytoplasmic forces and synapsis can be established. (B) The same scenario is depicted, except that ends of nonhomologous chromosomes are in the SUN-1 aggregate (violet loops). After fusion, chromosome ends will be shuffled. However, as the cytoplasmic forces overcome the attempt to synapse, one SUN-1 focus will be driven out of the patch. This tension-

generated splitting event is one of the factors leading to the formation of high speed in the distribution of SUN-1 aggregates. Our data support other factors as sources for the high speed aggregates: recombination intermediates (C) and chromosomes entanglements (D).
doi:10.1371/journal.pgen.1001219.g008

formation of tension between chromosome ends. These interactions are counteracted by cytoplasmic forces (generation of tension). When cytoplasmic forces overcome these interactions, the two chromosome ends are disjoined (loss of accumulated tension), leading to an increase in the speed distribution of SUN-1 aggregates. Absence of DSBs significantly reduces the formation of long tails. Indeed other factors, such as chromosome interlocks, could contribute to the formation of the tension. Recently, the repair protein *mlh-1* in *S. macrospora* had been assigned a critical role in resolution of interlocks [42]. When SYP-1 is depleted in *htp-1*, long tails reappear in the speed distribution despite their absence in *htp-1*, and fewer DSBs are made, as previously observed in *htp-1*;*syp-2* [21]. This suggests that entanglements can also contribute to the generation of tensions.

A second explanation for the formation of high speed could be that a patch containing paired homologs could move faster than a patch of nonpaired homologs. In the mutant SUN-1(S12E), pairing is fairly effective in the proximal part of the TZ [28]. The distribution of the projected speed of SUN-1 aggregates in this area was significantly shifted towards higher speeds (16% of long tails), supporting the idea that patches containing paired homologs could move faster (see Text S1, Videos S18 and S19, and Figures S7, S8, and S9). This is in contradiction with our finding that SUN-1 dynamics remained unchanged during the leptotene/zygotene stage despite processing of pairing. In fact, paired homologs in patches cannot account for the shift towards higher speeds, because we showed that patches (paired or unpaired homologs) and foci (most likely single chromosome ends) were both able to reach high speeds (Text S1). Patches are only faster than foci in the middle segment of the speed distribution. Addressing this paradox will require live imaging of the tagged end of a single chromosome.

Exit of the polarized conformation

It has been shown that an unpaired chromosome keeps chromatin loosely clustered once stable strand invasion is established [43]. Similarly, we found that in *htp-1*; *syp-1*, chromatin was also loosely clustered concomitant with circular displacement tracks. Circular displacement tracks are likewise found in *cra-1* where partial synapsis is coupled with accumulation of DSB intermediates [34]. The fact that in *htp-1*; *syp-2* DSBs do not accumulate [21] could be an explanation why circular tracks were less frequent than in *cra-1*. Previously, we proposed that exit from polarized chromatin requires a certain recombination intermediate and/or full synapsis [28]. Loose chromatin clustering in *spo-11*, together with circular displacement tracks, could be explained by the absence of the particular recombination intermediate required to dissolve chromosomal attachment plaques.

Chromosome end-led prophase movement alone is not sufficient for successful pairing

The absence of SUN-1 aggregates in *chk-2(me64)* confirms that this gene plays an indispensible role in pairing [28]. The triggers to activate CHK-2 are unknown, but DSBs could be one such trigger, as shown by the analyses of SUN-1 aggregates in aged *him-19(jf6)* irradiated worms [28]. In the present study, γ-irradiation significantly rescued some aspects of the behavior of SUN-1 aggregates in aged *him-19(jf6)*.

Despite their different roles during meiosis, *htp-1* and *prom-1* mutants display nonhomologous synapsis [20,21,32]. Deletion of either of these two proteins results in different phenotypes (precocious synapsis or delayed progression of meiosis). These mutants highlight the necessity of coordinating sub-events right after meiotic entry for the generation of functional SUN-1 aggregates. In both mutants, the speed distributions of SUN-1 aggregates lacked long tails; perhaps when chromosomes non-homologously synapse, the tension-generating process cannot take place (assessment of pairing). The maximum number of aggregates was five in both cases, because when aggregates coalesce into a patch, chromosome ends could not be shuffled, because synapsis had already taken place. The two mutants were also similar in terms of the number of fusion/splitting events and of periodicity of coalescence time. The analysis of these two mutants strongly suggests that effective pairing of homologs requires more than just chromosome end movement. Other prophase I events are also necessary for successful pairing.

In this study, we showed that instead of single chromosome ends looking for their homologous partner, duplets or multiplets and single chromosome ends were brought together in groups (patches) during the leptotene/zygotene stage by SUN-1 aggregate movement. Chromosome ends shuffled through these patches in search of the correct partner. Simultaneous in vivo imaging of specific chromosome ends and SUN-1 aggregates should be the next step to substantiate our finding. Second, these patches might represent ongoing repair of DSBs. Deciphering the regulation of synapsis initiation while chromosome ends are being shuffled in a tightly regulated process is one of the challenges for the future.

Materials and Methods

Nematode strains, strain construction, and culture conditions

All *C. elegans* strains were cultured using standard techniques [44]. The following *C. elegans* strains were used: N2 Bristol, *sun-1(ok1282)*; *sun-1::GFP* [28], *sun-1(ok1282)*/nT1[*let-?qIs51*]; *sun-1::GFP(G311V)* [28], *chk-2(me64)/unc-51(e369) rol-9(sc148)*; *sun-1::GFP* [28], *syp-2(ok307)*/nT1[qIs51]; *sun-1::GFP* [28], *him-3(gk149)*/nT1[*let-?qIs51*]; *sun-1::GFP* [28], *htp-1(gk174)*/nT1[*let-?qIs51*]; *sun-1::GFP* [28] *him-19(jf6)*; *sun-1::GFP* [33], *syp-3(me42)/* hT2[*bli-4(e937)let-?(q782)qIs48*]; *sun-1::GFP*, *prom-1(ok1140)*; *sun-1::GFP*, *cra-1(tm2144)*/hT2(GFP); *sun-1::GFP*, *spo-11(me44)/* nT1[*unc-?(n754) let-? qIs50*]; *sun-1::GFP* [45].

Nematode strains were provided by the *Caenorhabditis Genetics Center*, which is funded by the NIH National Center for Research Resources (NCRR).

him-19(jf6); *sun-1::GFP* and *sun-1(ok1282)*; *sun-1::GFP* worms were γ-irradiated with a dose of 50 Gy for 10 sec using a ^{137}Cs source and the time lapse microscopy was recorded 2 hrs after irradiation. *syp-1(RNAi)* was done as described in [46].

Time-lapse microscopy

For time lapse acquisitions, adult hermaphrodites preselected at the L4 stage 16 hrs before were mounted in a drop of 10 mM Levamisol on a 2% agarose pad and covered with a coverslip. For *him-19(jf6)*, worms were preselected 2 days before irradiation. The coverslip was sealed with melted Vaseline. Images were acquired at room temperature every 5 sec over a 15 min time period as stacks of optical sections at 1 µm intervals using a Deltavision deconvolution microscopy system (Applied Precision, Inc, 1040 12th Avenue, Northwest Issaquah, Washington 98027, USA)

under the following conditions: FITC channel, 32%ND, bin 1×1, exposure time 200 msec, objective 60x. To assay the effect of Levamisole on the worms, worms were mounted as described above in a drop of Levamisole or M9 and then the hatch rate of the filmed worms evaluated under the two conditions. No significant decrease of the hatch rate was observed (Levamisol hatch rate: 93% (>500 eggs laid), M9 hatch rate: 96% (>200 eggs laid), Fisher's exact test: $p>0.05$).

Maximum intensity projection was done using Softworx software (Applied Precision, Inc, 1040 12th Avenue, Northwest Issaquah, Washington 98027, USA) and the collection of files saved. The collection of pictures was opened with Metamorph Offline (Molecular Devices, 402 Boot Rd., Downingtown, PA 19335, USA) and saved as stack files. To support the plotting process, the background of the stack pictures was removed using Autoquant X2 (AutoQuant Imaging, Troy, NY, USA) and the slices realigned using the first slice as a reference.

Image analysis

With the help of Metamorph Offline, the positions of SUN-1 aggregates were manually followed. When two aggregates split, instead of starting to record two new tracks, tracking of the larger aggregate was continued. Then movement of the second aggregate was recorded. Subsequently positions of SUN-1 aggregates were plotted using Gnuplot software (Thomas Williams, Colin Kelley et al. 2004, http://www.gnuplot.info). Frequency and number of fusion/splitting events were computed using the number of aggregates as a function of time. Automated plotting of the movement of SUN-1 aggregates was done using Image J (NIH, http://rsbweb.nih.gov/ij/) and the plug-in MTrack2 (author: Nico Stuurman, http://valelab.ucsf.edu/people/p-stuurman.htm) (see Figure S9).

Computations and statistics

The speed of the object between two successive data points was calculated as the distance covered divided by the time required to cover the distance. Arcs were computed as described in Figure S3. Three-dimensional reconstruction of SUN-1 aggregate movement was done using the relationship $x^2+y^2+z^2=r^2$, where x, y, z are the coordinates of a point situated on a sphere of radius r. The z-coordinates were computed from the x- and y-coordinates of the nuclei viewed from the top as follows: $z=\sqrt{(r^2-x^2-y^2)}$, and when $x^2+y^2>r^2$, the previous z-coordinate was used. Statistical analysis was done using the software R (R Development Core Team, http://www.R-project.org).

Supporting Information

Figure S1 Background movement during time-lapse microscopy and definition of Maxwellian-shaped distribution. (A) Worms were killed in sodium azide and analyzed. Each line corresponds to the distribution of the projected speed of SUN-1::GFP aggregates in wild-type (blue), *him-3(gk149)* (yellow), and *htp-1(gk174)* (red) backgrounds. The corresponding cumulative projections of moving SUN-1::GFP aggregates are shown. (B) Left, a normal distribution, which is symmetric around the mean value. Right, a Maxwellian distribution with tails in the distribution (in red).
Found at: doi:10.1371/journal.pgen.1001219.s001 (0.89 MB TIF)

Figure S2 Arc computation. Distances *a* and *b* were calculated from the most extreme positions of the tracks (orange in A [SUN-1::GFP], red in A' [SUN-1(G311V)::GFP]). Distance *c* was calculated using the Pythagoras theorem (B, B'). *c* was circumscribed on a circle with the radius of the average size of a nucleus. Angle β (pink) was calculated using the cosine law (C, C'). When the distance *c* was greater than the radius *r* (D), the value of *r* was increased so that *c* could be circumscribed and the line for this arc is shown as a dotted line (e.g., Figure 4D). Description of the tracks by expressing the sum of their total length is misleading, because this does not reflect how far the tracks reach. For example, small oscillations, as in SUN-1(G311V), add up to large distances traveled, although the aggregates have not moved far. Arcs have the advantage of allowing for comparisons between different genotypes (compare C and C').
Found at: doi:10.1371/journal.pgen.1001219.s002 (0.20 MB TIF)

Figure S3 Lack of patterns for the traveled distance of SUN-1::GFP aggregates in nuclei located at different positions in the TZ. Box plot of the arc values for subregions in TZ (distal, central, and proximal parts of TZ). Red box plot, first movie; blue box plot, second movie. Green line represents the median value in the distribution of the arc; extremities of the whiskers are minima and maxima; bottom of the box, first quartile; top of the box, last quartile of the distribution of the arcs.
Found at: doi:10.1371/journal.pgen.1001219.s003 (0.27 MB TIF)

Figure S4 Lateral elements are required for proper loading of PC proteins. Localization of the PC protein ZIM-3 in *him-3(gk149)* and *htp-1(gk174)*. Immunostaining of ZIM-3 (red) and SUN-1::GFP (green); DAPI (blue).
Found at: doi:10.1371/journal.pgen.1001219.s004 (1.96 MB TIF)

Figure S5 SUN-1 aggregates are present in nuclei with loose clustering of the chromatin. Immunostaining of SUN-1 in wild type, *htp-1(gk174)*; *syp-1(RNAi)* and *cra-1(tm2144)*. White arrows indicate nuclei with loose clustering of the chromatin.
Found at: doi:10.1371/journal.pgen.1001219.s005 (3.82 MB TIF)

Figure S6 An excess of DSBs affected pairing but not SC polymerization. Dissected gonads of aged irradiated and nonirradiated worms were divided into seven zones of equal length (A), and the pairing of homologs was assessed by FISH with a probe for 5S rDNA (on chromosome V). (B) Pairing in nonirradiated 3-d-old wild-type gonads (dark blue) and three-d-old wild-type gonads 24 h after irradiation (light blue). The histogram shows at least two gonads with or without irradiation. Asterisks highlight the differences that are significant (Fisher's exact test, $p<0.05$). (C) SYP-1 polymerization in wild-type worms without irradiation (upper part) and γ-irradiated wild-type worms 2 h after irradiation (lower part).
Found at: doi:10.1371/journal.pgen.1001219.s006 (3.05 MB TIF)

Figure S7 Effect of SUN-1 phosphorylation on aggregate dynamics. Projection of the cumulative movement of SUN-1(S12E)::GFP (A, A'), displacement tracks (B, B'), distribution of the projected speed (C, C'), and arcs (D, D'). Blue lines represent values from the first movie; orange lines values from the second. (A, B, C, D) from distal TZ, (A', B', C', D') from proximal TZ. See Figure S8 for number of nuclei analyzed. Scale bar: 2 μm.
Found at: doi:10.1371/journal.pgen.1001219.s007 (1.46 MB TIF)

Figure S8 Dynamics of SUN-1(S12E)::GFP aggregates. (A) Numbers of aggregates in the regions proximal to the mitotic zone. The variations indicated correspond to the standard deviation. (B) Number of SUN-1 fusion/splitting events grouped into classes. (C) Quantification of the coalescence time (*t*) grouped into classes ($t<1$ min, 1 min$\leq t<3$ min, and $t\geq 3$ min). (D) Fisher's exact test to assess the difference between wild type and SUN-1(S12E)::GFP for the values 'number of fusion/splitting events'. (E) Fisher's exact to assess the difference between wild type and SUN-1(S12E)::GFP for the values 'time-window of SUN-1 aggregate coalescence'.

Found at: doi:10.1371/journal.pgen.1001219.s008 (0.47 MB TIF)

Figure S9 Correlation between speed and size of SUN-1 aggregates. (A) A deconvolved image was converted to a binary image using a threshold and then initial segmentation restored using a watershed transform (i). Aggregates $<2.15\ \mu m^2$ were defined as foci, aggregates $>2.15\ \mu m^2$ as patches. Output image (yellow) overlaid with the starting picture (i, right panel). Collection of background-subtracted movies treated the same manner (ii). Correlation factor $=-0.017$ for size of foci and their speed. Correlation factor $=-0.016$ for size of patches and their speed. No correlation was found in either case. (B) CDF of the foci (red) and patches (green). Differences in distribution of the projected speed of SUN-1 foci and patches are highlighted by the subtraction of the CDF of the foci to the CDF of the patches (blue). SUN-1 patches in the range of 15–120 nm/s moved faster than SUN-1 foci.
Found at: doi:10.1371/journal.pgen.1001219.s009 (0.92 MB TIF)

Table S1 Fisher's exact test to assess the difference between wild type and all other genotypes tested for the values 'number of fusion/splitting events'. Significant p-values ($p<0.05$) are highlighted in bold.
Found at: doi:10.1371/journal.pgen.1001219.s010 (0.06 MB DOC)

Table S2 Fisher's exact to assess the difference between wild type and all other genotypes tested for the values' time-window of SUN-1 aggregate coalescence'. Significant p-values ($p<0.05$) are highlighted in bold.
Found at: doi:10.1371/journal.pgen.1001219.s011 (0.05 MB DOC)

Text S1 Supplemental results.
Found at: doi:10.1371/journal.pgen.1001219.s012 (0.04 MB DOC)

Text S2 Supplemental methods.
Found at: doi:10.1371/journal.pgen.1001219.s013 (0.03 MB DOC)

Video S1 Time lapse series of SUN-1::GFP with counterstaining of the chromatin using Hoechst 33342. The first inset shows the merging of SUN-1::GFP (green) and the chromatin (blue). The second inset shows the chromatin and the third inset SUN-1::GFP. Scale bar: 2 μm.
Found at: doi:10.1371/journal.pgen.1001219.s014 (1.16 MB MOV)

Video S2 Time lapse series of SUN-1::GFP in the *sun-1(ok1282)* background. The three insets show three enlarged independent nuclei. Scale bar: 2 μm.
Found at: doi:10.1371/journal.pgen.1001219.s015 (0.76 MB MOV)

Video S3 Time lapse series of SUN-1(G311V)::GFP in the *sun-1(ok1282)* background. The three insets show three enlarged independent nuclei. Scale bar: 2 μm.
Found at: doi:10.1371/journal.pgen.1001219.s016 (0.84 MB MOV)

Video S4 Time lapse series of SUN-1::GFP in the *him-3(gk149)* background. The three insets show three enlarged independent nuclei. Scale bar: 2 μm.
Found at: doi:10.1371/journal.pgen.1001219.s017 (0.56 MB MOV)

Video S5 Time lapse series of SUN-1::GFP in the *htp-1(gk174)* background. The three insets show three enlarged independent nuclei. Scale bar: 2 μm.
Found at: doi:10.1371/journal.pgen.1001219.s018 (0.26 MB MOV)

Video S6 Time lapse series of SUN-1::GFP in the *syp-2(ok307)* background; distal part of the TZ. The three insets show three enlarged independent nuclei. Scale bar: 2 μm.
Found at: doi:10.1371/journal.pgen.1001219.s019 (0.55 MB MOV)

Video S7 Time lapse series of SUN-1::GFP in the *syp-2(ok307)* background; proximal part of the TZ. The three insets show three enlarged independent nuclei. Scale bar: 2 μm.
Found at: doi:10.1371/journal.pgen.1001219.s020 (0.55 MB MOV)

Video S8 Time lapse series of SUN-1::GFP in the *syp-3(me42)* background. The three insets show three enlarged independent nuclei. Scale bar: 2 μm.
Found at: doi:10.1371/journal.pgen.1001219.s021 (0.55 MB MOV)

Video S9 Time lapse series of SUN-1::GFP in the *htp-1(gk174)*; *syp-1(RNAi)* background in the distal part of the zone with SUN-1 aggregates. The three insets show three enlarged independent nuclei. Scale bar: 2 μm.
Found at: doi:10.1371/journal.pgen.1001219.s022 (0.87 MB MOV)

Video S10 Time lapse series of SUN-1::GFP in the *htp-1(gk174)*; *syp-1(RNAi)* background in the proximal part of the zone with SUN-1 aggregates. The three insets show three enlarged independent nuclei. Scale bar: 2 μm.
Found at: doi:10.1371/journal.pgen.1001219.s023 (0.84 MB MOV)

Video S11 Time lapse series of SUN-1::GFP in the *prom-1(ok1140)* background. The three insets show three enlarged independent nuclei. Scale bar: 2 μm.
Found at: doi:10.1371/journal.pgen.1001219.s024 (0.84 MB MOV)

Video S12 Time lapse series of SUN-1::GFP in the *him-19(jf6)* background; non-irradiated 2-d-old hermaphrodites. Scale bar: 2 μm.
Found at: doi:10.1371/journal.pgen.1001219.s025 (0.96 MB MOV)

Video S13 Time lapse series of SUN-1::GFP in the *him-19(jf6)* background; irradiated 2-d-old hermaphrodites. The three insets show three enlarged independent nuclei. Scale bar: 2 μm.
Found at: doi:10.1371/journal.pgen.1001219.s026 (0.84 MB MOV)

Video S14 Time lapse series of SUN-1::GFP in the *sun-1(ok1282)* background; irradiated 2-d-old hermaphrodites. The three insets show three enlarged independent nuclei. Scale bar: 2 μm.
Found at: doi:10.1371/journal.pgen.1001219.s027 (0.84 MB MOV)

Video S15 Time lapse series of SUN-1::GFP in the *cra-1(tm2144)* background. The three insets show three enlarged independent nuclei. Scale bar: 2 μm.
Found at: doi:10.1371/journal.pgen.1001219.s028 (0.98 MB MOV)

Video S16 Time lapse series of SUN-1::GFP in the *spo-11(me44)* background. The three insets show three enlarged independent nuclei. Scale bar: 2 μm.

Found at: doi:10.1371/journal.pgen.1001219.s029 (0.84 MB MOV)

Video S17 Time lapse series of SUN-1::GFP in the *spo-11(me44)* background; irradiated 2-d-old hermaphrodites. The three insets show three enlarged independent nuclei. Scale bar: 2 μm.
Found at: doi:10.1371/journal.pgen.1001219.s030 (0.84 MB MOV)

Video S18 Time lapse series of SUN-1(S12E)::GFP in the *sun-1(ok1282)* background in the distal part of the prolonged TZ. The three insets show three enlarged independent nuclei. Scale bar: 2 μm.
Found at: doi:10.1371/journal.pgen.1001219.s031 (0.98 MB MOV)

Video S19 Time lapse series of SUN-1(S12E)::GFP in the *sun-1(ok1282)* background in the proximal part of the prolonged TZ. The three insets show three enlarged independent nuclei. Scale bar: 2 μm.
Found at: doi:10.1371/journal.pgen.1001219.s032 (0.98 MB MOV)

Acknowledgments

We thank Christian Pflügl for technical support. We are grateful to Peter Carlton, Arndt von Haeseler, Maria Siomos, and Josef Loidl for suggestions. We thank Anne Villeneuve, Monique Zetka, Monica Colaiacovo, Enrique Martinez-Perez, and the *Caenorhabditis Genetics Center* for strains and reagents.

Author Contributions

Conceived and designed the experiments: AB AP AW YG VJ. Performed the experiments: AB AP AW TM CW JG AF. Analyzed the data: AB FK PP VJ. Contributed reagents/materials/analysis tools: YG. Wrote the paper: AB VJ.

References

1. Petronczki M, Siomos M, Nasmyth K (2003) Un menage a quatre: the molecular biology of chromosome segregation in meiosis. Cell 112: 423–440.
2. Scherthan H (2001) A bouquet makes ends meet. Nat Rev Mol Cell Biol 2: 621–627.
3. Chikashige Y, Haraguchi T, Hiraoka Y (2007) Another way to move chromosomes. Chromosoma 116: 497–505.
4. Fridkin A, Penkner A, Jantsch V, Gruenbaum Y (2008) SUN-domain and KASH-domain proteins during development, meiosis and disease. Cell Mol Life Sci 66: 1518–1533.
5. Hiraoka Y, Dernburg AF (2009) The SUN rises on meiotic chromosome dynamics. Dev Cell 17: 598–605.
6. Conrad MN, Lee CY, Chao G, Shinohara M, Kosaka H, et al. (2008) Rapid telomere movement in meiotic prophase is promoted by NDJ1, MPS3, and CSM4 and is modulated by recombination. Cell 133: 1175–1187.
7. Koszul R, Kim KP, Prentiss M, Kleckner N, Kameoka S (2008) Meiotic chromosomes move by linkage to dynamic actin cables with transduction of force through the nuclear envelope. Cell 133: 1188–1201.
8. Chikashige Y, Tsutsumi C, Yamane M, Okamasa K, Haraguchi T, et al. (2006) Meiotic proteins bqt1 and bqt2 tether telomeres to form the bouquet arrangement of chromosomes. Cell 125: 59–69.
9. Sheehan M, Pawlowski W (2009) Live imaging of rapid chromosome movements in meiotic prophase I in maize. Proc Natl Acad Sci USA 106: 20989–20994.
10. Scherthan H, Wang H, Adelfalk C, White EJ, Cowan C, et al. (2007) Chromosome mobility during meiotic prophase in Saccharomyces cerevisiae. Proc Natl Acad Sci U S A 104: 16934–16939.
11. Trelles-Sticken E, Dresser ME, Scherthan H (2000) Meiotic telomere protein Ndj1p is required for meiosis-specific telomere distribution, bouquet formation and efficient homologue pairing. J Cell Biol 151: 95–106.
12. Wanat JJ, Kim KP, Koszul R, Zanders S, Weiner B, et al. (2008) Csm4, in collaboration with Ndj1, mediates telomere-led chromosome dynamics and recombination during yeast meiosis. PLoS Genet 4: e1000188. doi:10.1371/journal.pgen.1000188.
13. Kosaka H, Shinohara M, Shinohara A (2008) Csm4-dependent telomere movement on nuclear envelope promotes meiotic recombination. PLoS Genet 4: e1000196. doi:10.1371/journal.pgen.1000196.
14. Conrad MN, Lee CY, Wilkerson JL, Dresser ME (2007) MPS3 mediates meiotic bouquet formation in Saccharomyces cerevisiae. Proc Natl Acad Sci U S A 104: 8863–8868.
15. Conrad MN, Dominguez AM, Dresser ME (1997) Ndj1p, a meiotic telomere protein required for normal chromosome synapsis and segregation in yeast. Science 276: 1252–1255.
16. Wu HY, Burgess SM (2006) Two distinct surveillance mechanisms monitor meiotic chromosome metabolism in budding yeast. Curr Biol 16: 2473–2479.
17. Dernburg AF, McDonald K, Moulder G, Barstead R, Dresser M, et al. (1998) Meiotic recombination in C. elegans initiates by a conserved mechanism and is dispensable for homologous chromosome synapsis. Cell 94: 387–398.
18. Colaiacovo MP (2006) The many facets of SC function during C. elegans meiosis. Chromosoma 115: 195–211.
19. Smolikov S, Schild-Prüfert K, Colaiácovo MP (2009) A yeast two-hybrid screen for SYP-3 interactors identifies SYP-4, a component required for synaptonemal complex assembly and chiasma formation in Caenorhabditis elegans meiosis. PLoS Genet 5: e1000669. doi:10.1371/journal.pgen.1000669.
20. Couteau F, Zetka M (2005) HTP-1 coordinates synaptonemal complex assembly with homolog alignment during meiosis in C. elegans. Genes Dev 19: 2744–2756.
21. Martinez-Perez E, Villeneuve AM (2005) HTP-1-dependent constraints coordinate homolog pairing and synapsis and promote chiasma formation during C. elegans meiosis. Genes Dev 19: 2727–2743.
22. McKim KS, Howell AM, Rose AM (1988) The effects of translocations on recombination frequency in Caenorhabditis elegans. Genetics 120: 987–1001.
23. Rosenbluth RE, Baillie DL (1981) The genetic analysis of a reciprocal translocation, eT1(III; V), in Caenorhabditis elegans. Genetics 99: 415–428.
24. MacQueen AJ, Phillips CM, Bhalla N, Weiser P, Villeneuve AM, et al. (2005) Chromosome sites play dual roles to establish homologous synapsis during meiosis in C. elegans. Cell 123: 1037–1050.
25. Phillips CM, Wong C, Bhalla N, Carlton PM, Weiser P, et al. (2005) HIM-8 binds to the X chromosome pairing center and mediates chromosome-specific meiotic synapsis. Cell 123: 1051–1063.
26. Phillips CM, Dernburg AF (2006) A Family of Zinc-Finger Proteins Is Required for Chromosome-Specific Pairing and Synapsis during Meiosis in C. elegans. Dev Cell 11: 817–829.
27. Phillips C, Meng X, Zhang L, Chretien J, Urnov F, et al. (2009) Identification of chromosome sequence motifs that mediate meiotic pairing and synapsis in C. elegans. Nat Cell Biol 11: 934–942.
28. Penkner A, Fridkin A, Gloggnitzer J, Baudrimont A, Machacek T, et al. (2009) Meiotic Chromosome Homology Search Involves Modifications of the Nuclear Envelope Protein Matefin/SUN-1. Cell 139: 920–933.
29. Sato A, Isaac B, Phillips C, Rillo R, Carlton P, et al. (2009) Cytoskeletal Forces Span the Nuclear Envelope to Coordinate Meiotic Chromosome Pairing and Synapsis. Cell 139: 907–919.
30. Penkner A, Tang L, Novatchkova M, Ladurner M, Fridkin A, et al. (2007) The nuclear envelope protein Matefin/SUN-1 is required for homologous pairing in C. elegans meiosis. Dev Cell 12: 873–885.
31. MacQueen A, Villeneuve A (2001) Nuclear reorganization and homologous chromosome pairing during meiotic prophase require C. elegans chk-2. Genes Dev 15: 1674–1687.
32. Jantsch V, Tang L, Pasierbek P, Penkner A, Nayak S, et al. (2007) Caenorhabditis elegans prom-1 is required for meiotic prophase progression and homologous chromosome pairing. Mol Biol Cell 18: 4911–4920.
33. Tang L, Machacek T, Mamnun YM, Penkner A, Gloggnitzer J, et al. (2010) Mutations in C. elegans him-19 show meiotic defects that worsen with age. MBC 21: 885–896.
34. Smolikov S, Schild-Prüfert K, Colaiácovo MP (2008) CRA-1 uncovers a double-strand break-dependent pathway promoting the assembly of central region proteins on chromosome axes during C. elegans meiosis. PLoS Genet 4: e1000088. doi:10.1371/journal.pgen.1000088.
35. Hubbard EJA, Greenstein D (2005) Introduction to the germ line. WormBook: the online review of C elegans biology. pp 1–4.
36. Malone CJ, Misner L, Le Bot N, Tsai MC, Campbell JM, et al. (2003) The C. elegans hook protein, ZYG-12, mediates the essential attachment between the centrosome and nucleus. Cell 115: 825–836.
37. MacQueen AJ, Colaiácovo MP, McDonald K, Villeneuve AM (2002) Synapsis-dependent and -independent mechanisms stabilize homolog pairing during meiotic prophase in C. elegans. Genes Dev 16: 2428–2442.
38. Colaiácovo MP, MacQueen AJ, Martinez-Perez E, McDonald K, Adamo A, et al. (2003) Synaptonemal complex assembly in C. elegans is dispensable for loading strand-exchange proteins but critical for proper completion of recombination. Dev Cell 5: 463–474.
39. Smolikov S, Eizinger A, Hurlburt A, Rogers E, Villeneuve AM, et al. (2007) Synapsis-defective mutants reveal a correlation between chromosome conformation and the mode of double-strand break repair during Caenorhabditis elegans meiosis. Genetics 176: 2027–2033.
40. Couteau F, Nabeshima K, Villeneuve A, Zetka M (2004) A component of C. elegans meiotic chromosome axes at the interface of homolog alignment, synapsis, nuclear reorganization, and recombination. Curr Biol 14: 585–592.

41. Schmitt J, Benavente R, Hodzic D, Hoog C, Stewart CL, et al. (2007) Transmembrane protein Sun2 is involved in tethering mammalian meiotic telomeres to the nuclear envelope. Proc Natl Acad Sci U S A 104: 7426–7431.
42. Storlazzi A, Gargano S, Ruprich-Robert G, Falque M, David M, et al. (2010) Recombination proteins mediate meiotic spatial chromosome organization and pairing. Cell 141: 94–106.
43. Carlton PM, Farruggio AP, Dernburg AF (2006) A link between meiotic prophase progression and crossover control. PLoS Genet 2: e12. doi:10.1371/journal.pgen.0020012.
44. Brenner S (1974) The genetics of Caenorhabditis elegans. Genetics 77: 71–94.
45. Hayashi M, Chin GM, Villeneuve AM (2007) C. elegans Germ Cells Switch between Distinct Modes of Double-Strand Break Repair During Meiotic Prophase Progression. PLoS Genet 3: e191. doi:10.1371/journal.pgen.0030191.
46. Jantsch V, Pasierbek P, Mueller MM, Schweizer D, Jantsch M, et al. (2004) Targeted gene knockout reveals a role in meiotic recombination for ZHP-3, a Zip3-related protein in Caenorhabditis elegans. Mol Cell Biol 24: 7998–8006.

Developmental Cell
Article

Polo Kinases Establish Links between Meiotic Chromosomes and Cytoskeletal Forces Essential for Homolog Pairing

Sara Labella,[1] Alexander Woglar,[2] Verena Jantsch,[2] and Monique Zetka[1,*]
[1]Department of Biology, McGill University, 1205 avenue Docteur Penfield, Montreal, Quebec H2A 1B1, Canada
[2]Department of Chromosome Biology, Max F. Perutz Laboratories, University of Vienna, Dr. Bohr-Gasse 1, A-1030 Vienna, Austria
*Correspondence: monique.zetka@mcgill.ca
DOI 10.1016/j.devcel.2011.07.011

SUMMARY

During meiosis, chromosomes must find and align with their homologous partners. SUN and KASH-domain protein pairs play a conserved role by establishing transient linkages between chromosome ends and cytoskeletal forces across the intact nuclear envelope (NE). In *C. elegans*, a pairing center (PC) on each chromosome mediates homolog pairing and linkage to the microtubule network. We report that the polo kinases PLK-1 and PLK-2 are targeted to the PC by ZIM/HIM-8-pairing proteins. Loss of *plk-2* inhibits chromosome pairing and licenses synapsis between nonhomologous chromosomes, indicating that PLK-2 is required for PC-mediated interhomolog interactions. *plk-2* is also required for meiosis-specific phosphorylation of SUN-1 and establishment of dynamic SUN/KASH (SUN-1/ZYG-12) modules that promote homolog pairing. Our results provide key insights into the regulation of homolog pairing and reveal that targeting of polo-like kinases to the NE by meiotic chromosomes establishes the conserved linkages to cytoskeletal forces needed for homology assessment.

INTRODUCTION

The accurate segregation of chromosomes during meiosis depends on earlier events that first match homologous chromosomes, a process that in most organisms is then followed by synapsis (synaptonemal complex [SC] formation), and the establishment of physical linkages between homologs (crossovers) as products of recombination (Page and Hawley, 2004). During meiotic chromosome pairing, homologous chromosomes must find and recognize each other within the three-dimensional nuclear space and align along their lengths (Zickler, 2006). Intimately associated with this process is the polymerization of the SC between homologs to stabilize early pairing and to promote crossing over; however, SC polymerization is not dependent on DNA homology and occurs readily between nonhomologous chromosomes, indicating that its initiation must be regulated (Colaiácovo, 2006). Studies from a number of organisms have now revealed a conserved role for cytoskeletal forces in driving meiotic chromosome movement within the nucleus to promote homology assessment and prevent promiscuous synapsis, and to resolve chromosome entanglements during chromosome pairing (Alsheimer, 2009; Hiraoka and Dernburg, 2009; Koszul and Kleckner, 2009).

How are forces originating in the cytoplasm transferred to meiotic chromosomes within nuclei? At the onset of meiotic prophase, chromosome end(s) stably associate with the inner *n*uclear *e*nvelope (NE); in most organisms telomeres associate with the inner NE and cluster to form a meiotic "bouquet" (Scherthan, 2001), while in *C. elegans p*airing *c*enters (PCs) located near one end of each chromosome establish an association with the NE (Phillips and Dernburg, 2006). The tethering of meiotic chromosome ends is widely associated with the formation of an electron-dense attachment plate on the nucleoplasmic face where the chromosome end attaches to the inner NE, and the connection of this plate to the cytoplasm through filament bundles that transverse the NE (Scherthan, 2007). SUN-domain proteins are a widely conserved family of eukaryotic proteins that span the inner NE and interact through their C-terminal SUN domains with the KASH domain of transmembrane proteins that span the outer NE and interact with cytoskeletal components (Tzur et al., 2006). Cytological evidence from studies of meiosis in widely diverse species collectively supports a model in which SUN/KASH-domain protein modules associate with tethered chromosome ends to span the NE and transfer forces generated in the cytoplasm to chromosomes within the nucleus during chromosome pairing (Alsheimer, 2009; Hiraoka and Dernburg, 2009).

In the soma, SUN-domain proteins appear immobile within the NE (Lu et al., 2008) and interact with multiple KASH partners to anchor the nucleus to the cytoskeleton during essential processes like nuclear migration and positioning (Fridkin et al., 2009). In contrast, SUN-KASH modules during meiosis appear to be highly mobile within the NE and aggregate in the vicinity of chromosome ends; fission yeast Sad1-Kms1 complexes relocalize with NE-associated telomeres during telomere clustering (Chikashige et al., 2007), mammalian Sun1 aggregates at telomere attachment sites (Ding et al., 2007), and *C. elegans* SUN-1 and its KASH-domain partner ZYG-12 first transiently concentrate at the sites of PC association with the NE and then coalesce to form the dynamic patches diagnostic of the chromosome-pairing and -sorting processes (Penkner et al., 2009; Sato et al., 2009). Disruption of these integral NE proteins

in these systems results in homolog-pairing defects during meiosis, indicating an essential and conserved role for NE protein dynamics and the resulting transmission of cytoskeletal forces to chromosomes during this process (Alsheimer, 2009; Hiraoka and Dernburg, 2009). An outstanding question is how the NE-spanning connections between chromosomes and the cytoskeletal network are established at the onset of meiosis to produce chromosome movement. In *C. elegans*, the serine/threonine kinase *chk-2* is required for the initiation of multiple early meiotic processes, including two events that have been implicated in the formation of the linkages to the cytoskeletal forces: the association of the autosomal PC-binding proteins (ZIMs) with PCs (Phillips and Dernburg, 2006; Sato et al., 2009); and meiosis-specific phosphorylation of the N terminus of SUN-1 required for SUN-1/ZYG-12 patch formation (Penkner et al., 2009).

During mitosis in yeast and animal cells, key events in the formation of cytoskeletal structures are regulated by Polo kinase (Plk1 in vertebrates, PLK-1 in *C. elegans*, Polo in *Drosophila*, Cdc5 in *S. cerevisiae*), the most conserved member of the *P*olo-*l*ike family of Ser/Thr *k*inases (Plks). Plks are distinguished by the presence of a carboxyl terminal *P*olo *b*ox *d*omain (PBD) that mediates subcellular localization through binding to phosphorylated targets (Archambault and Glover, 2009). Polo kinase progressively localizes to multiple subcellular structures where it regulates key cell division events, including centrosome maturation, microtubule-kinetochore attachments, and contractile ring assembly (Petronczki et al., 2008). While budding and fission yeast each have a single Plk most related to vertebrate Plk1, the increased complexity of metazoans is accompanied by the appearance of additional Plks whose roles in cell division are less understood: Plk2, 3, 4, and 5 in vertebrates; PLK-2, 3, 4 in *C. elegans*; and PLK4 in *Drosophila*. In addition to its functions in mitotic cell division, the single budding yeast homolog of Polo kinase (Cdc5) also functions in crossover formation and pachytene exit during meiosis (Sourirajan and Lichten, 2008), raising the possibility that Plks may have important functions in the complex events of meiosis that have not been revealed by vertebrate cell line studies. While Plk1 shares most homology with Plk2, the function of the latter remains elusive, despite the fact that it is widely conserved in vertebrates and some metazoans; human Plk2 has been implicated in the S-phase checkpoint (Matthew et al., 2007), and *C. elegans* PLK-2 functions redundantly with PLK-1 in regulating embryonic polarity (Nishi et al., 2008). Our study reveals a previously unsuspected role for PLK-2 or any other Plk in meiotic chromosome pairing and the concomitant changes in the NE that have been shown to be an essential component of the process.

RESULTS

Meiotic Prophase Functions for *C. elegans* Polo-like Kinases

We isolated a severe loss of function in the *C. elegans* polo-like kinase 2 that resulted in meiotic chromosome missegregation (see Figures S1 and S2 available online). *plk-2(vv44)* is a missense C-T mutation that results in a P197L amino acid substitution at a highly conserved residue within the activation loop of the kinase domain of the predicted protein (Figure S1A). *plk-2(vv44)* behaves recessively with respect to embryonic lethality and X chromosome nondisjunction, and fails to complement two preexisting deletion null alleles, confirming that it corresponds to a loss-of-function mutation in *plk-2*: *ok1936* (deleting nucleotides 12–1043 of the genomic sequence and followed by a 16 base pair insertion) and *tm1395* (predicted to remove the PBD). While *plk-2(vv44)* homozygotes segregate 80% dead embryos and 30% male progeny among the survivors as a consequence of autosomal and X chromosome nondisjunction, both deletion mutants exhibit a less severe phenotype: *plk-2(ok1936)* mutants segregate 48% dead embryos and 7% male progeny, while *plk-2(tm1395)* homozygotes segregate 54% dead embryos and 7% male progeny. Examination of DAPI-stained diakinesis nuclei (the last stage of oocyte meiotic prophase) revealed a similar phenotypic pattern (Figure S2A); while the nuclei of WT oocytes invariably contain 6 bivalents representing the 12 chromosomes joined by a chiasma, such nuclei were never observed in *plk-2(vv44)* mutants. Instead, over 90% of the nuclei showed 10–12 DAPI-stained bodies, indicating a severe defect in chiasma formation. In contrast, six bivalents were observed in 15% of the germlines of *plk-2(ok1936)* deletion mutants, and over 70% of the nuclei exhibited seven to nine DAPI-stained bodies, a comparatively modest reduction in chiasma formation. Since the *plk-2(vv44)* mutation does not affect the PBD of the protein, and *plk-2* is redundant with *plk-1* for functions in the establishment of embryonic polarity (Nishi et al., 2008), we considered the possibility that the severity of the *plk-2(vv44)* mutant phenotype was a consequence of PLK-2^{vv44} interfering with redundant PLK-1 activity required for chiasma formation. While we could detect no mitotic defects in *plk-2* mutants, PLK-1 is required for mitosis, and its loss results in embryonic lethality and defects in mitotic chromosome structure and segregation (Chase et al., 2000; data not shown). In the germline these defects are transmitted through meiosis and preclude the accurate scoring of diakinesis figures. However, depletion of *plk-2(vv44)* by *plk-2(RNAi)* or by placing in *trans* with the deletion allele *ok1936* results in a significant restoration of chiasma formation (Figure S2A); in the latter case 5% of the nuclei show six bivalents, and 40% of the nuclei show seven to nine DAPI-stained bodies. The observations that mutants lacking any PLK-2 are able to form more bivalents than PLK-2^{vv44}-expressing mutants and that removal of mutant PLK-2^{vv44} by RNAi mitigates the mutant phenotype are most simply explained by PLK-2^{vv44} binding through its intact PBD to PLK-2 targets and interfering with redundant PLK-1 activity by blocking access to the target protein(s). Despite the severe loss-of-function phenotype of *plk-2(vv44)* mutants, PLK-2^{vv44} retains kinase activity in vitro (Figure S1B), suggesting that *vv44* affects the ability of the mutant kinase to recognize physiological targets and/or to efficiently phosphorylate them in vivo.

Meiotic Chromosome PCs Localize PLK-2 to the NE

The syncytial germline of *C. elegans* follows a spatiotemporal progression through meiotic prophase easily visualized in three-dimensionally preserved DAPI-stained gonads. Nuclei proliferate mitotically in the distal germline, and following meiotic S phase enter into the leptotene-zygotene stage of meiotic prophase (also known as the transition zone) where they reorganize to asymmetrically cluster their chromosomes, a process

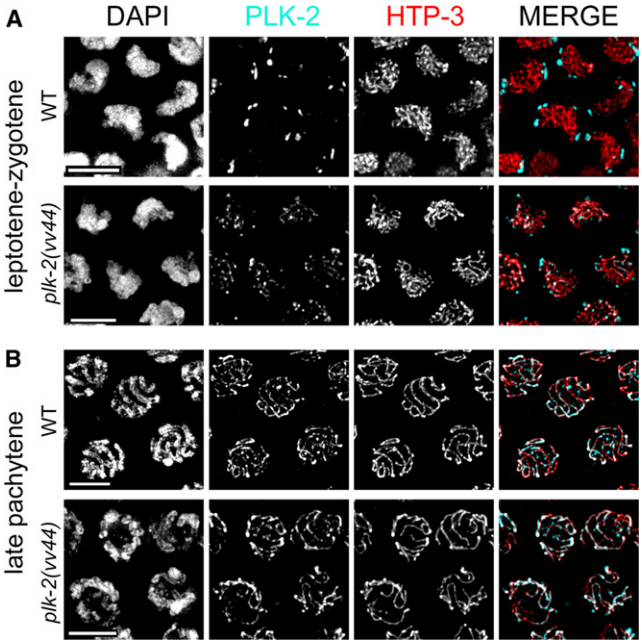

Figure 1. Chromosome-Associated PLK-2 Localizes to Patches at the Nuclear Periphery and to Synapsed Chromosomes

Nuclei from wild-type and *plk-2* mutant germlines at the indicated stages stained with PLK-2 (cyan) and HTP-3 (red).

(A) In wild-types, PLK-2 first localizes to four to five chromosome-associated patches at the nuclear periphery. PLK-2 localization in *plk-2(vv44)* mutants is similar; however, large patches do not form, and instead, numerous small chromosome-associated foci are evident at the nuclear periphery.

(B) At pachytene, PLK-2 localizes to synapsed chromosome axes in both controls and *plk-2* mutants. Scale bars, 5 μm. See also Figure S1.

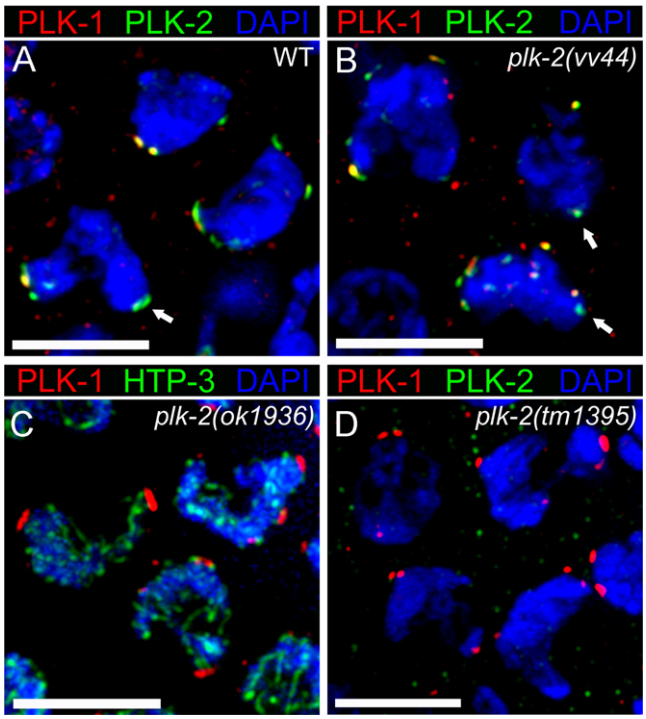

Figure 2. PLK-1 Partially Colocalizes with PLK-2

Transition zone nuclei from wild-type and *plk-2* mutant germlines stained with PLK-1 (red) and (A, B, and D) PLK-2 (green) or (C) HTP-3 (green).

(A and B) PLK-1 colocalizes with PLK-2 to the nuclear periphery in some NE-associated patches but is undetectable in others (arrows).

(C and D) In the absence of PLK-2, bright PLK-1 signals can be detected at four to five NE-associated patches; however, little PLK-1 can be detected on the synapsing chromosomes, in comparison to PLK-2 (compare to Figure S4). Scale bars, 5 μm. See also Figure S2.

intimately linked to the chromosome pairing occurring at this stage (Dernburg et al., 1998). Since the protein interactions mediated by the PBD of polo–like kinases target and spatially restrict their activity in cellular processes, we determined the localization of PLK-2 to investigate its function in meiotic events. In the mitotically dividing nuclei of the distal region of the germline, PLK-2 is first detectable at the centrosomes (data not shown). However, upon entry into meiotic prophase, PLK-2 then localizes to approximately three to five chromosome-associated aggregates at the nuclear periphery of leptotene-zygotene nuclei; these aggregates disappear as synapsis initiates, and PLK-2 then colocalizes with the synapsed chromosomes of pachytene nuclei (Figure 1). We also investigated the localization of PLK-1 in wild-type and *plk-2* mutant germlines, and in all cases PLK-1 can be detected at the nuclear periphery, similar to the pattern observed for PLK-2 (Figure 2; for antibody specificity see Figures S2B and S2C). While the majority of the PLK-1 signal is found in the PLK-2-marked aggregates associated with the NE, PLK-2 aggregates without detectable PLK-1 colocalization are observable in both WT and *plk-2(vv44)* mutants (Figures 2A and 2B, arrows). In deletion mutants lacking PLK-2, PLK-1 still localizes to the NE-associated aggregates, indicating that PLK-2 activity is not required for PLK-1 recruitment (Figures 2C and 2D). Given that the PBDs of mammalian Plk1 and Plk2 display some limited overlap in target recognition (van de Weerdt et al., 2008), these results are consistent with the interpretation that PLK-1 and PLK-2 bind to the same target at the NE but that PLK-2 has a higher affinity for the target and can interfere with PLK-1 access.

The PLK-2-defined aggregates observed at the nuclear periphery of early-stage meiotic prophase nuclei are highly reminiscent of the localization of *C. elegans* proteins participating in the linkages that span the NE to connect the PC-bearing chromosome ends to the force-generating cytoskeletal machinery that drives meiotic chromosome movements. These include the outer NE component ZYG-12 and the inner NE component SUN-1 in association with the PC ends of the chromosomes. The PC of each chromosome recruits one of a family of four paralogous C2H2 Zn-finger DNA-binding proteins (HIM-8, ZIM-1, ZIM-2, ZIM-3), which are required for homolog pairing and synapsis. However, these proteins are unlikely to be the sole basis for homolog recognition since two members of the family bind to the PCs of more than one chromosome pair (Phillips and Dernburg, 2006; Phillips et al., 2005, 2009). Furthermore, PC proteins appear to be dispensable for mediating the association of the PC with the NE since the X chromosome PC still interacts with the NE in the absence of HIM-8 (Phillips et al., 2005). In fact, PLK-2 colocalizes with ZYG-12, SUN-1, and HIM-8 and ZIM-3 into the NE-associated patches implicated in the chromosome homology search process (Figure 3), and we could detect

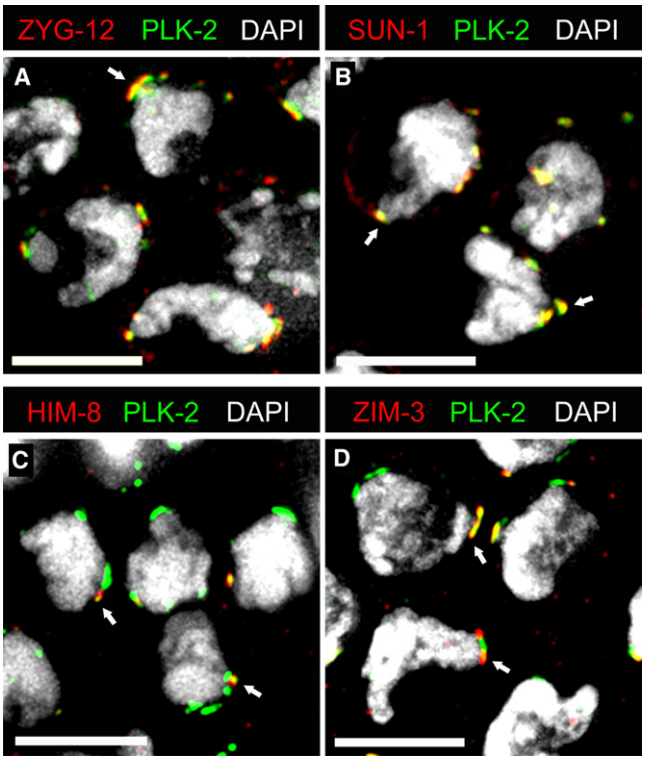

Figure 3. PLK-2 Colocalizes with the NE Bridge that Connects PCs with Cytoskeletal Forces

Transition zone nuclei stained with PLK-2 (green) and (A and B) the NE components ZYG-12 or SUN-1 (red) and (C and D) the PC components HIM-8 and ZIM-3 (red).

(A) PLK-2 and ZYG-12 colocalize into an NE patch (arrow).

(B) PLK-2 colocalizes with SUN-1 into the NE-associated patches (arrows).

(C and D) PLK-2 colocalizes with the PC proteins HIM-8 (marking the X chromosome PC) and ZIM-3 (marking the PCs of chromosomes I and IV) into NE patches; remaining PLK-2 signals presumably mark the PCs of chromosomes II, III, and V. Scale bars, 5 μm.

a similar pattern of PLK-1 localization in the absence of PLK-2 (Figure S2D).

To investigate if PLK-2 association with NE patches was dependent on localization to the PC, we first examined its localization in the absence of any of the PC-associated proteins. Loss of any individual member of the ZIM/HIM-8 family results in loss of pairing and synapsis of the affected chromosome throughout meiotic prophase (Phillips and Dernburg, 2006; Phillips et al., 2005). *him-8* mutant germlines in which *zim-1,2,3* were depleted by RNAi exhibited the 12 univalents in diakinesis oocytes (the last stage of meiotic prophase) predicted to appear in the event of loss of all PC-protein-mediated homolog pairing (data not shown). In leptotene-zygotene nuclei depleted for the ZIM/HIM-8 family, the localization of PLK-2 to patches at the nuclear periphery is lost, indicating that PLK-2 recruitment to PCs is ZIM/HIM-8 dependent (Figure 4). Instead, PLK-2 localizes to the single SYP-1-marked nuclear aggregate that typically forms in mutants in which chromosome axes fail to localize SC components (Colaiácovo, 2006) (Figure 4A and Figure S3). At pachytene PLK-2 colocalizes with SYP-1 between the nonhomologously synapsed chromosomes, indicating that its recruitment to the SC is independent of *zim/him-8* family functions; this localization may reflect additional functions for PLK-2, consistent with the involvement of budding yeast Cdc5 in crossover formation (Sourirajan and Lichten, 2008). Consistent with the interpretation that the ZIM/HIM-8 family is required for PLK-2 localization, PLK-2 is not detectable at the nuclear periphery of early prophase nuclei in the absence of two factors required for ZIM recruitment to PCs (data not shown): HTP-3, an axis component required for meiotic chromosome morphogenesis (Goodyer et al., 2008), and *chk-2*, a serine/threonine kinase required in *C. elegans* for the initiation of homolog pairing (but not axis assembly; MacQueen and Villeneuve [2001]). We next considered if localization of the ZIM/HIM-8 proteins to PCs is sufficient to recruit PLK-2. We examined PLK-2 localization to the X chromosome PC in *him-8(me4)* missense mutants in which X chromosome pairing and synapsis are abrogated, but the mutant protein retains an intact C-terminal DNA-binding domain and localizes to the X chromosome PC (Phillips et al., 2005). We could detect no colocalization of PLK-2 with HIM-8^{me4} (Figure 4B, compare to Figure 3C), indicating that neither the localization of HIM-8 to the PC nor the association of the PC with the NE is sufficient for PLK-2 recruitment. Furthermore, two lines of evidence indicate that *plk-2* is not required for the PC-NE interaction per se: the X chromosome PC continues to associate with the NE in *him-8(me4)* in the absence of PLK-2; and similarly, ZIM-3-marked PCs are localized to the NE in *plk-2(vv44)* mutants (Figures 4B and 4C).

PLK-2 Coordinates Pairing with Synapsis

In comparison to wild-types, *plk-2* mutants show fewer polarized nuclei corresponding to the leptotene-zygotene stage and numerous partially polarized nuclei into early pachytene stages (defined by synapsis between chromosomes), indicating a defect in the progression of the early events of meiotic prophase (data not shown). In *plk-2(vv44)* mutant germlines, PLK-2^{vv44} also localizes to the nuclear periphery and to the SC. Furthermore, meiotic chromosome morphogenesis as defined by the recruitment of axis components like HTP-3 (Figure 1) and concentration of ZIM-3 at the PCs is intact (Figure 4C), suggesting that the chromosome are properly assembled for meiotic processes. However, few large PLK-2-marked patches are observed at the NE in *plk-2* mutants, and instead, the protein localizes to numerous smaller aggregates/foci, some of whose size is consistent with the signal expected from individual tethered chromosomes (<1.1 μm; Penkner et al., 2009 and data not shown). The dynamics of chromosome pairing can be assayed by *f*luorescence *i*n situ *h*ybridization (FISH) to single-copy loci-like PCs, while SC polymerization can be monitored as the appearance of stretches of central region components like SYP-1 between DAPI-stained DNA tracts or coincident with chromosome axis components like HIM-3 or HTP-3. Analysis of the homologous association of chromosomes V and X in *plk-2(vv44)* mutant germlines revealed a severe defect in chromosome pairing throughout meiotic prophase (Figure 5A). Despite this pairing defect, however, nuclei showed robust SYP-1 stretches between paired DAPI-stained tracts and were commonly found associated with unpaired HIM-8-marked X chromosomes (Figures 5B and 5C). The length and number of the SYP-1 tracts observed in *plk-2(vv44)* pachytene nuclei are

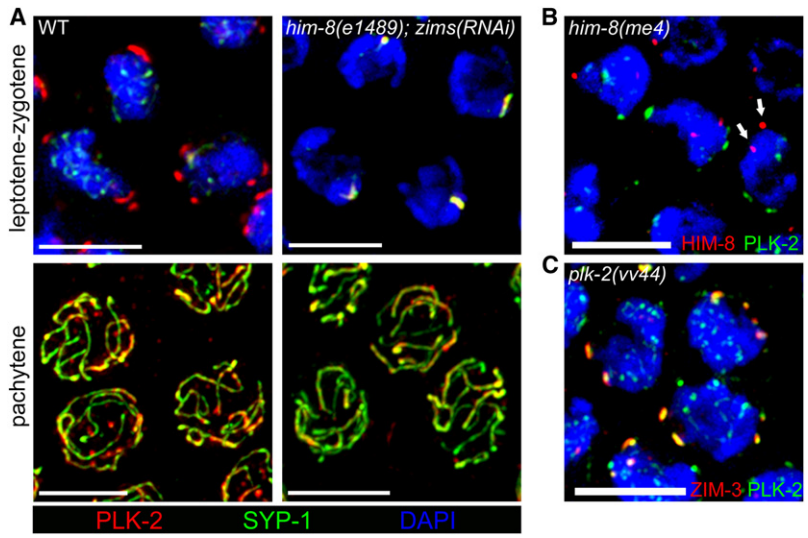

Figure 4. PC Proteins Are Required for PLK-2 Recruitment at the PC and Synapsis Initiation

(A) Nuclei at the indicated stages of meiotic prophase stained with PLK-2 (red) and the synapsis marker SYP-1 (green) in controls and in germlines depleted for the ZIM/HIM-8 family of PC proteins. In the absence of the PC proteins, SYP-1 localizes into a single aggregate with PLK-2, and no SYP-1 or PLK-2 is detectable in association with the chromosomes at leptotene-zygotene. At pachytene, PLK-2 colocalizes with SYP-1 on nonhomologously synapsed chromosomes.

(B) Leptotene-zygotene nuclei from *him-8(me4)* mutants stained with PLK-2 (green) and HIM-8 (red). HIM-8^{me4} at the X chromosome PC localizes to the nuclear periphery but fails to colocalize with PLK-2 (arrows).

(C) Leptotene-zygotene nuclei of *plk-2(vv44)* mutants stained with PLK-2 (green) and ZIM-3 (red). ZIM-3 localizes to the nuclear periphery and colocalizes with PLK-2. In *plk-2(vv44)* mutants, PLK-2-marked patches are small (see Figure 3D for WT), reflecting defects in NE dynamics and PC clustering in the mutant. Scale bars, 5 μm. See also Figure S3.

similar to those found in wild-type nuclei (Figure 5 and Figure S4; data not shown), collectively suggesting that the synapsis observed in *plk-2* mutants is nonhomologous rather than autosynapsis or the consequence of loading of SC components onto individual axes. Since extensive SYP-1 could be detected on chromosomes in polarized nuclei in which chromosome pairing is still taking place (Figure S4A), we examined the possibility that precocious loading of SC components in *plk-2* mutants interferes with homolog pairing and patch formation. In *syp-1(me17)* mutant germlines in which synapsis was prevented by mutation of an essential SC component (Colaiácovo et al., 2003; MacQueen et al., 2002), PLK-2 still localizes to the nuclear periphery (Figure S4C), indicating that its localization to the PC is synapsis independent. Furthermore, in the absence of synapsis, homologous chromosome pairing was reduced to the levels observed in the premeiotic region, indicating that the pairing defect is not the consequence of the precocious synapsis observed in *plk-2(vv44)* mutants. Given that *plk-2(vv44)* mutants are unable to pair homologous PCs but are competent for SC assembly, these results collectively demonstrate that PLK-2-mediated processes are required for both synapsis-independent pairing between PCs and the repression of SC polymerization between nonhomologous chromosomes.

Loss of PLK-2 Function Disrupts Formation of NE Bridge Complex Patches Required for Chromosome Pairing

A failure to coordinate appropriate levels of homolog pairing with synapsis has also been associated with defects in the NE components SUN-1 and ZYG-12 (Penkner et al., 2007, 2009; Sato et al., 2009). Since PCs and PLK-2 colocalized with SUN-1/ZYG-12 patches at early prophase, we next examined the localization of these proteins in *plk-2(vv44)* mutant nuclei undergoing meiotic chromosome pairing. SUN-1 is required for the localization of ZYG-12 to the NE, which in turn interacts through its N terminus with cytoplasmic dynein and the microtubule network (Malone et al., 2003). During meiosis, these cytoskeletal forces are thought to bring together variable numbers of NE-associated PCs (Penkner et al., 2007) to form dynamic SUN-1/ZYG-12 patches in which homology is assessed, and nonhomologous chromosomes are separated to prevent synapsis between them (Penkner et al., 2007, 2009; Sato et al., 2009). A point mutation in *sun-1(jf18)* resulting in a G311V substitution in the protein does not affect SUN-1 localization to the NE of meiotic prophase nuclei but produces defects in chromosome pairing and promiscuous synapsis (Penkner et al., 2007). Expression of SUN-1(G311V) results in the formation of PC-associated SUN-1 foci, but no SUN-1/ZYG-12 patches; these SUN-1 foci show severe defects in movement within the NE, demonstrating that SUN-1/ZYG-12-mediated movement of the PC ends of chromosomes is required to promote homolog pairing and negatively regulate synapsis (Penkner et al., 2009). To determine if PLK-2 functions through the SUN-1 pathway, we examined SUN-1 and ZYG-12 localization in early prophase nuclei of *plk-2(vv44)* mutants (Figure 6). Both NE components were dispersed within the NE and failed to localize into the PC-associated patches observed in wild-type nuclei undergoing chromosome pairing. Moreover, SUN-1 also failed to localize into the PC-associated foci observed in *sun-1(jf18)* mutants (Penkner et al., 2009), indicating that PLK-2 is required at an earlier step in which SUN-1 aggregates in the vicinity of the PC ends of chromosomes to form detectable foci. Since the precocious synapsis observed in *plk-2* mutants could potentially interfere with focus or patch formation, SUN-1 localization was examined in *plk-2(vv44)* mutants in which synapsis is blocked by mutation of *syp-2* (Figure S5A). SUN-1 foci/patch formation was not restored in these asynaptic early prophase nuclei, suggesting that the nonhomologous synapsis observed in *plk-2(vv44)* mutants is a downstream consequence of the failure to form PC-associated SUN-1 foci. Consequently, we conclude that PLK-2 activity is required at two sequential steps relating to NE dynamics during meiotic chromosome pairing: first, its activity is required to form the PC-associated SUN-1 foci; and second, to promote the aggregation of these foci into the patches required for the homolog-pairing process.

PLK-2 at PCs Is Required for Phosphorylation of SUN-1 at Serine 12

Since PLK-2 colocalized with SUN-1 foci/patches, we next considered the possibility that PLK-2 localization to the PCs and NE reflected a requirement for *plk-2* in processes that modulate SUN-1 behavior following PC association with the NE. The N terminus of SUN-1 extends into the nucleus and is phosphorylated at multiple serine residues at the onset of meiosis; the SUN-1 phosphoepitopes S8-Pi, S12-Pi, and S24-Pi can be detected in leptotene-zygotene nuclei where they highlight SUN-1 foci and patches, appear dispersed in the NE upon pachytene entry, and eventually disappear (Penkner et al., 2009). These modifications affect SUN-1 dynamics, aggregate dissolution and crossing over by defining the time window of chromosome movement, and require the activity of the *chk-2* kinase (Penkner et al., 2009). In *plk-2(vv44)* transition zone nuclei, anti-S8-Pi and anti-S24-Pi highlight uniformly dispersed SUN-1 within the NE (Figure S6), consistent with the observation that *plk-2* mutants failed to form SUN-1 foci or patches. In the case of anti-S12-Pi, however, no nuclear SUN-1 signal could be detected in meiotic nuclei above background levels in *plk-2(vv44)* mutants, despite the fact that we could detect nuclear signals from mitotic nuclei and the SUN-1 foci that form in *sun-1(jf18)* mutants (Figure 7A and Figure S7A). A similar loss of S12-Pi staining was observed in the meiotic nuclei of *him-8; zim-1,2,3(RNAi)* germlines that fail to localize PLK-2 to the PC, indicating that it is the PC-associated pool of PLK-2 that is required for acquisition of this modification (Figure 7A). In the absence of PLK-2, S12-Pi appears in a PLK-1-dependent manner and colocalizes with PLK-1 into patches at the NE, indicating that the two polo kinases can function redundantly in this process (Figure S7). We next considered the possibility that PLK-2 directly phosphorylates SUN-1 at serine 12, and could detect PLK-2 in SUN-1-containing complexes (Figure 6G). However, full-length PLK-2 and SUN-1 did not interact in yeast two-hybrid assays (Figure S5B), and HA-tagged PLK-2 with in vitro kinase activity failed to phosphorylate HA-tagged SUN-1 expressed in yeast or GFP-tagged SUN-1 expressed in worms in vitro (data not shown). These results could reflect a requirement for PC-mediated PLK-2 activation that cannot be reconstituted in vitro or that SUN-1 is indirectly phosphorylated following PLK-2-mediated processes. The observation that expression of a phospho-mimetic at S12 (SUN-1(S12E)::GFP) in the absence of any endogenous SUN-1 (Penkner et al., 2009) does not rescue the defects in SUN-1 foci or patch formation in *plk-2(vv44)* mutants (data not shown) is consistent with the latter possibility and suggests that S12 phosphorylation is not sufficient for meiotic chromosome-pairing processes in the absence of PLK-2 function. Our results also suggest that S12 is not a direct target of CHK-2, since CHK-2 is active in *plk-2* mutants as evidenced by the acquisition of S8-Pi and S24-Pi; however, it remains possible that PLK-2-mediated activation of CHK-2 is required for S12 phosphorylation.

DISCUSSION

PLK-2 Is Required for Meiosis-Specific SUN-1 Aggregation and Homologous Chromosome Pairing

SUN-domain proteins show profound changes in localization in the inner NE depending on the cell type and developmental context (Hiraoka and Dernburg, 2009); in the nematode germline SUN-1 is uniformly distributed throughout the NE in mitotically cycling cells but becomes transiently enriched at sites of chromosome attachment to the NE as cells enter meiotic prophase (Penkner et al., 2007). Our study reveals that a critical event in initiating the dramatic changes in NE organization associated with early meiosis is the targeting of PLK-2 activity to the NE. At the onset of meiotic prophase, PLK-2 localizes to the PCs, and several lines of evidence indicate that PLK-2 is required for modifications at the NE that result in the assembly of SUN-1/ZYG-12 patches that link meiotic chromosomes to cytoplasmic dynein and microtubule-mediated forces during homolog pairing (Malone et al., 2003; Sato et al., 2009; Baudrimont et al., 2010). First, SUN-1 fails to redistribute within the NE at the onset of meiosis in *plk-2* mutants in which the PC ends are associated with the NE, indicating that PLK-2 is required for both the initial formation of PC-associated SUN-1 foci and their assembly into larger SUN-1/ZYG-12 patches. Second, no phosphorylation of serine 12 of SUN-1 can be detected in the meiotic nuclei of *plk-2* mutants, a modification correlated with SUN-1/ZYG-12 patch formation (Penkner et al., 2009; this study). Finally, loss of *plk-2* and the failure to appropriately reorganize the NE result in a spectrum of meiotic defects similar to those described for patch-defective mutants of *sun-1* and *zyg-12* (Penkner et al., 2007; Sato et al., 2009). Consequently, our results demonstrate that PLK-2 is required to initiate events essential for homologous chromosome pairing; the modification of SUN-1 and the formation of SUN-1/ZYG-12 patches in which variable numbers of chromosomes are brought together for homology assessment and sorting (Figure 7B). This process can first spatially reduce the homology search from three dimensions (the entire volume of the nucleus) to two dimensions in a restricted area (NE-associated PCs in a patch), consistent with the appearance of severe defects in PC pairing observed in *plk-2* and *sun-1/zyg-12* mutants defective in patch formation. Second, the cytoskeletal forces that are established through this connection also participate in regulating synapsis within the patches since in mutants defective in patch formation, but competent for synapsis, SC components load precociously between nonhomologous chromosomes (Penkner et al., 2007; Sato et al., 2009; this study). Once initiated, SC formation is highly processive (Colaiácovo, 2006), and the precocious appearance of the SC in these backgrounds may result from spurious synapsis initiation between any two closely positioned chromosome segments. In the wild-type situation, such events would be suppressed by patch-mediated movements and synapsis initiation limited to homologously paired chromosomes (likely at the PCs). Consequently, the SC would appear earlier in patch mutants relative to wild-types in which SC initiation is regulated by patch-directed movements. These data are consistent with the model that chromosome movements generated through patch formation function to separate nonhomologous chromosomes to prevent synapsis and to reintroduce them into the pool of unpaired candidates (Baudrimont et al., 2010).

ZIM/HIM-8 PC Proteins Target PLK-2 to the NE

Our results demonstrate that it is the PC-targeted pool of PLK-2 that is required for initiating the meiosis-specific changes in the NE associated with chromosome pairing. First, the failure to

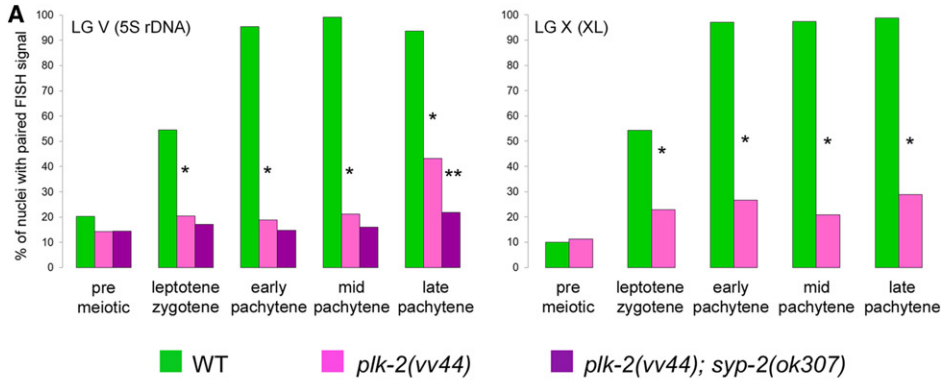

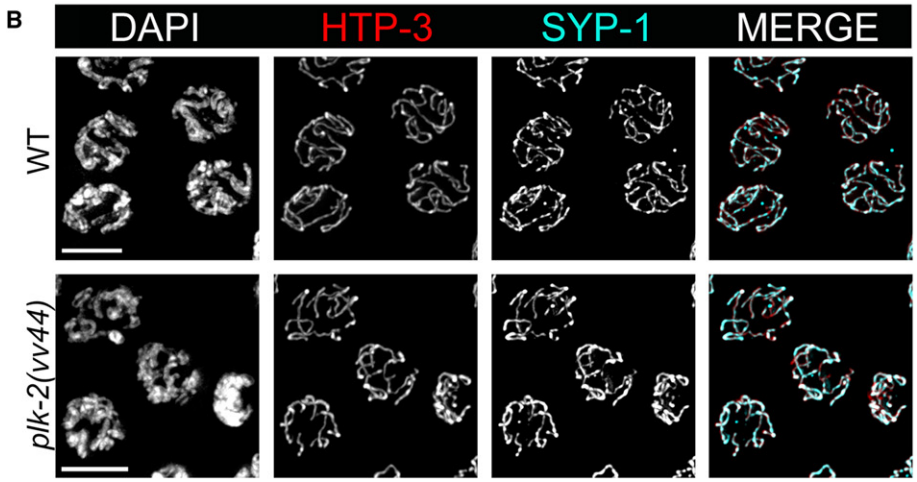

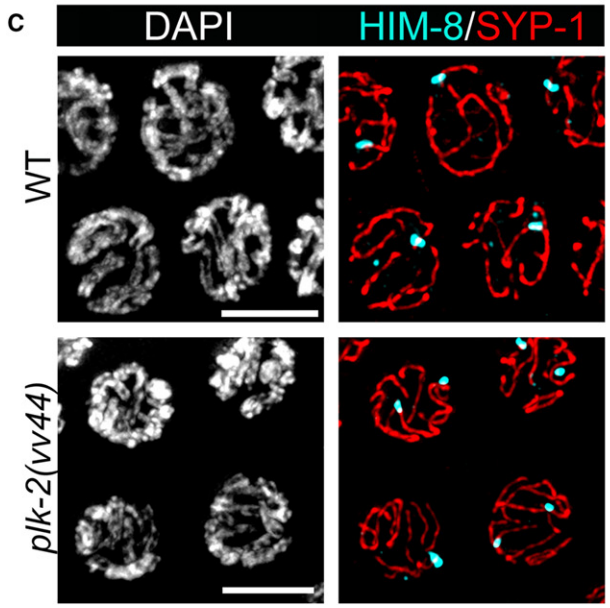

Figure 5. Loss of PLK-2 Function Abrogates Pairing and Licenses Nonhomologous Synapsis

(A) Pairing of chromosome V and X PC regions was assessed by FISH in wild-types, *plk-2* mutants, and *plk-2; syp-2* mutants by dividing the germline into five zones as indicated. One asterisk (*) indicates values different from wild-type controls, while two asterisks (**) indicate values different from *plk-2* mutants at $p < 0.0001$.

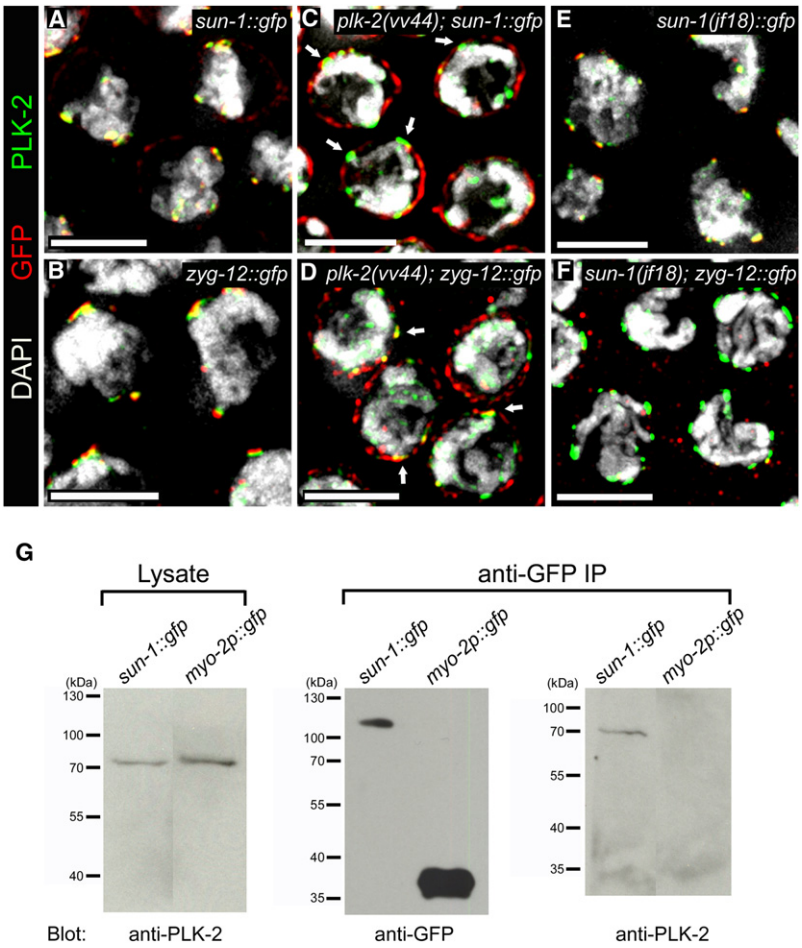

Figure 6. PLK-2 Is Required for SUN-1/ZYG-12 Patch Formation and Coimmunoprecipitates with SUN-1

Leptotene-zygotene nuclei from germlines expressing the indicated GFP fusion protein stained with GFP (red) and PLK-2 (green).

(A and B) PLK-2 colocalizes with SUN-1 and ZYG-12 into patches at the nuclear periphery.

(C and D) In *plk-2(vv44)* mutants, SUN-1 and ZYG-12 appear uniformly distributed within the NE, while PLK-2 appears in small foci at the NE that colocalize with the NE components (arrows). Stretches of PLK-2 not at the nuclear periphery correspond to PLK-2 localization to the precociously formed SC in *plk-2(vv44)* mutants (compare to Figure S4A).

(E) PLK-2 colocalizes with SUN-1^{jf18} into small foci at the nuclear periphery.

(F) In *sun-1(jf18)* mutants little ZYG-12 is detectable at the NE above background levels, but PLK-2 localizes to foci at the nuclear periphery. Scale bars, 5 μm.

(G) Western blot analysis of whole-worm extracts and immunoprecipitates (IP) from *sun-1::gfp*; *sun-1(ok1282); spe-26(hc138)* (*sun-1::gfp*) and *sun-1(ok1282)*/nT1*(qIs51)(myo-2p::gfp)* strains. About 15% of "input" extracts probed with anti-PLK-2 detects a band of the predicted molecular weight for PLK-2 (72.1 kDa). SUN-1::GFP and PLK-2 can be detected in anti-GFP immunoprecipitates probed with anti-GFP and anti-PLK-2, respectively. PLK-2 cannot be detected in anti-GFP immunoprecipitates from whole-worm lysates derived from the *qIs51*-bearing control strain expressing soluble GFP. See also Figure S5.

recruit PLK-2 to PCs in germlines depleted for the ZIM/HIM-8 family is accompanied by a loss of SUN-1 phosphorylation at S12. Second, in *him-8(me4)* mutants, the loss of PLK-2 recruitment to the X PC correlates with the inability of the X chromosomes to associate with SUN-1/ZYG-12 patches (Sato et al., 2009). An outstanding question is how PLK-2 activity at the PC culminates in aggregation of SUN-1 in the vicinity of the chromosome end (SUN-1 foci) and in SUN-1/ZYG-12 patch formation. Studies of meiosis in other organisms have found that the divergent N-terminal tails of SUN-domain proteins can interact with chromosome ends through meiotically expressed species-specific adaptor molecules: Bqt1/2 in *S. pombe*, Ndj1 in *S. cerevisiae*, and possibly the ZIM/HIM-8 family in *C. elegans* (Hiraoka and Dernburg, 2009). Since PLK-2 can be detected in SUN-1-containing complexes and is required for phosphorylation at S12, one possibility is that PLK-2 at the NE directly phosphorylates SUN-1, leading to meiosis-specific changes in its behavior. The N terminus of SUN-1 contains a Plk1 core consensus PBD-binding motif S-[pS/pT]-[P/X] (Elia et al., 2003) that includes a previously identified phosphoepitope (Penkner et al., 2009); however, the observation that S12 is phosphorylated in germlines expressing the unphosphorylatable T36A substitution at this site suggests that PLK-2 is not recruited by this phosphomotif (A.W. and V.J., unpublished data). This interpretation is also consistent with our failure to detect a direct physical interaction between SUN-1 and PLK-2 by yeast two-hybrid or in vitro kinase assays (data not shown). Polo-like kinases also typically phosphorylate the protein to which they are targeted (Petronczki et al., 2008), and the observation that PLK-2 recruitment to the PC is dependent on ZIM/HIM-8 localization suggests that PLK-2 may directly bind and target the PC-bound ZIM/HIM8 proteins, leading to indirect phosphorylation of SUN-1. The *him-8(me4)* mutation results in the replacement of a conserved serine found in all the ZIMs with a unphosphorylatable residue (S85F). While this substitution does not affect HIM-8^{me4} localization to the X chromosome PC, it results in a failure to recruit PLK-2, raising the possibility that phosphorylation at this site may be required for PLK-2 recruitment to all PCs through PBD binding. Although the region surrounding HIM-8 (S85) does not conform to the Plk1 core consensus PBD-binding motif, the PBDs of mammalian Plk1 and Plk2

(B) Wild-type and *plk-2(vv4)* pachytene nuclei stained with the axial component HTP-3 (red). Despite the loss of pairing in *plk-2* mutants, colocalization of HTP-3 and SYP-1 (cyan) reveals extensive synapsis.

(C) Wild-type and *plk-2(vv44)* mutant pachytene nuclei stained with the X chromosome PC component HIM-8 (cyan) and SYP-1 (red). Scale bars, 5 μm. See also Figure S4.

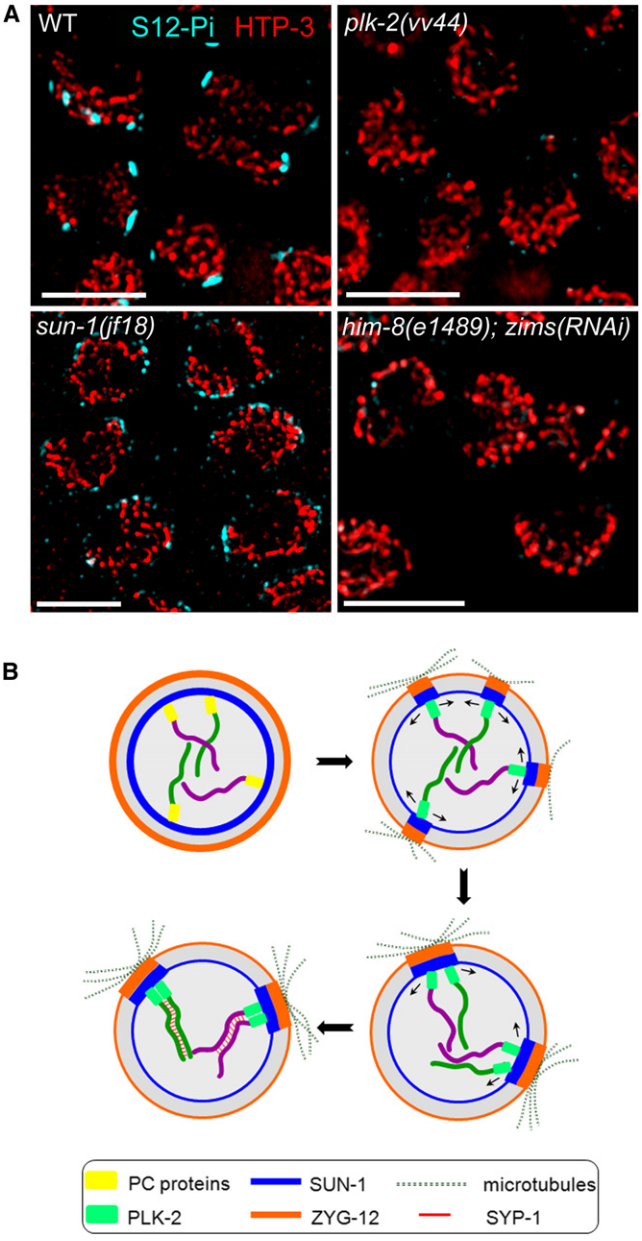

Figure 7. PLK-2 Is Required for SUN-1 Phosphorylation at Serine 12

(A) Leptotene-zygotene nuclei of the indicated genotype stained with phospho-specific S12-Pi of SUN-1 (cyan) and HTP-3 (red) (Experimental Procedures). In wild-types, the S12-Pi pool of SUN-1 localizes to NE-associated patches; localization in *sun-1(jf18)* mutants is reduced to foci in association with PCs (Penkner et al., 2009). No S12-Pi staining above background levels could be detected in *plk-2(vv44)* or *him-8(e1489); zims(RNAi)* mutant germlines, indicating that PLK-2 and the HIM-8 family are required for acquisition of the phosphoepitope. Scale bars, 5 μm.

(B) Proposed model for PLK-2 functions in meiotic chromosome pairing. At the onset of meiosis, chromosome ends associated with the PCs attach to the NE. PLK-2 and, to a lesser extent, PLK-1 (not shown) are recruited to the PCs by the HIM-8/ZIM family of PC proteins in a CHK-2-dependent manner (not shown). PLK-2 at the PC is required for the local concentration of SUN-1 and its phosphorylation at S12. SUN-1 through its linkage with its KASH-domain partner ZYG-12 links the chromosome ends to cytoskeletal forces. Chromosome movement through these linkages brings variable numbers of chromosomes into larger SUN-1/ZYG-12 patches in which homology between pairs of chromosomes is assessed. Nonhomologous chromosomes are separated while homologous chromosomes initiate synapsis at the PC. See also Figures S6 and S7.

show only limited overlap in target recognition (van de Weerdt et al., 2008), and the Plk2 consensus-binding motif has not been defined. Furthermore, Plk1 has been shown to bind phosphomotifs on target proteins distinct from the consensus (Elia et al., 2003), and the yeast Polo kinase Cdc5 can also bind to unphosphorylated targets via PBD sites distinct from the phosphoepitope-binding site (Chen and Weinreich, 2010), revealing that target recognition by Polo kinases can be mediated by non-canonical-binding interactions.

Previous studies have demonstrated that the CHK-2 kinase is also required for phosphorylation of the N terminus of SUN-1 and SUN-1/ZYG-12 patch formation (Penkner et al., 2009); however, we favor for several reasons the model that the major role of CHK-2 in the process is in the assembly of a PC competent for PLK-2 binding. PLK-2 recruitment to the PC is dependent on prior binding of ZIM/HIM-8, and since CHK-2 mutants fail to localize ZIMs and PLK-2 to PCs (Phillips and Dernburg, 2006; this study), a likely scenario is that CHK-2 activity is required for ZIM binding to the PCs, followed by PLK-2 recruitment. Furthermore, loss of PLK-2 abrogates SUN-1/ZYG-12 patch formation despite the fact that CHK-2 is active in *plk-2* mutants as evidenced by ZIM/HIM-8 loading to PCs, the acquisition of SUN-1 S8-Pi/S24-Pi, and the initiation of *chk-2*-dependent processes like meiotic recombination initiation. However, it remains possible that CHK-2 is also required for at a later step in generating the PLK-2-recruiting phosphoepitope following HIM-8/ZIM binding at the PC.

In summary, we favor the model that ZIM/HIM-8 concentrated at the PCs function as chromosome-NE adaptors that are activated by PLK-2 phosphorylation to stably associate with the N terminus of SUN-1, leading to SUN-1 phosphorylation and patch formation. Since SUN-1 is an integral membrane component and is dispersed throughout the inner NE premeiotically, an elegant attribute of this mechanism is that delivery of PLK-2 to the NE via the PC generates localized changes to the NE in the vicinity of the chromosome end, culminating in the transmission of cytoskeletal forces through SUN-1/ZYG-12 to the chromosomes.

The PC as a Functional Reiteration of Centromeres

The centromeres of diverse organisms, including a number of plant species, yeasts, and *Drosophila*, have pairing activity during meiosis that can include heterologous and homologous interactions (Stewart and Dawson, 2008), similar to the interactions between NE-associated PCs. Although *C. elegans* chromosomes contain no localized centromeres, the transient connections established between PCs and the cytoplasmic microtubule network during meiosis functionally mimic canonical kinetochore assembly and microtubule capture during mitosis: specialized chromosome sequences assemble a protein interface that can recruit microtubule-based forces to generate chromosome movement. Like centromeres (Przewloka and Glover, 2009), PCs consist of repetitive DNA sequence motifs (Phillips et al., 2009), are epigenetically modified (Gu and Fire, 2010), and assemble a multiprotein complex that we show in this study mediates assembly of the NE-spanning mechanism

that links chromosomes to forces generated in the cytoplasm. During mitosis, Polo kinase localizes to mitotic kinetochores where it is required for the formation of the kinetochore microtubules that link the chromosomes to spindle forces (Sumara et al., 2004), and *plk-2* function at PCs resembles a reiteration of this Polo kinase role that has been adapted to link chromosomes to microtubule-based forces through the NE during meiosis. Although further studies will be necessary to determine if Polo-like kinases perform similar functions during telomere attachment and clustering in other organisms, our work in *C. elegans* provides a framework to link meiotic chromosome structure with the changes in NE dynamics required to establish chromosome movement during meiotic pairing.

EXPERIMENTAL PROCEDURES

Genetics

The wild-type Bristol N2 strain has been used as control, and all the *C. elegans* strains have been cultured under standard conditions (Brenner, 1974). The *plk-2(vv44)* mutant was isolated in an EMS-based (ethane methyl sulfonate) noncomplementation screen for chromosome missegregation using the deficiency *hDf6* (Couteau et al., 2004). Mutant strains were obtained from the Caenorhabditis Genetics Center (University of Minnesota, St. Paul, MN) and *C. elegans* Gene Knockout Consortium. The following mutations were used in this study (LG, linkage group): LG I, *htp-3(tm3655)*, *plk-2(ok1936)*, *plk-2(tm1395)*; LG IV, *him-3(gk149)*, *him-8(e1489)*, *him-8(me4)*; and LG V, *syp-1(me17)*, *syp-2(ok307)*, *sun-1(jf18)*.

Antibody Production and Testing

Anti-PLK-2 and anti-PLK-1 antibodies were generated (GenScript Corporation, Piscataway, NJ) using N-terminal synthetic peptides corresponding to the first 16 and 20 amino acids, respectively, and purified by immunoaffinity chromatography with activated supports (Affi-Gel 10; Bio-Rad), according to manufacturer's instructions. PLK-2 antibody specificity was verified by a failure to detect the protein by immunofluorescence in *plk-2(tm1395)* and *plk-2(ok1936)* deletion mutants (Figure 2D, Figures S2B and S2C), and on western blot analysis of extracts derived from these strains (data not shown). PLK-1 levels at PCs are low in wild-type germlines (Figure 2A), thereby complicating detection of their loss in *plk-1(RNAi)* germlines; therefore, PLK-1 antibody specificity was verified by loss of the PLK-1 signal at centrosomes in the mitotic region (Figure S2B). The specificity of the SUN-1 phosphoepitope-specific antibodies S8 and S12 was confirmed by loss of immunofluorescence in the germlines of strains carrying chromosomally integrated insertions expressing unphosphorylatable SUN-1(S8A)::GFP and SUN-1(S12A)::GFP in the absence of endogenous SUN-1 (Penkner et al., 2009); in the case of the S24 antibody, no signal could be detected in individuals carrying an extrachromosomal array expressing SUN-1(S8,12,24,43,58,62A)::GFP in the absence of endogenous SUN-1 (data not shown).

RNA Interference

RNA interference experiments were performed as described previously (Fire et al., 1998). dsRNA was generated using PCR amplification of the most conserved region of *zim-1,2* and *3* using the primers CAGCAAGGAGTT GTGTTGGA and TGTGGTTTGATGGGAGTTGA, followed by in vitro transcription with T7 RNA polymerase (Ambion). At 15 hr post-L4, young hermaphrodites were injected and processed for cytological analyses 48 hr postinjection; efficacy of the RNAi was monitored by the appearance of 12 univalents in the diakinesis nuclei of injected worms.

FISH and Immunostaining

FISH analysis was performed as described in Couteau et al. (2004), using identical probes specific for the 5S rDNA locus on chromosome V and left end of chromosome X. Immunofluorescence analyses were performed as described in Martinez-Perez and Villeneuve (2005), with the following modifications: gonads from staged adult hermaphrodites (20–22 hr post-L4) were dissected in PBS and blocked in 1% BSA in PBST. Primary antibodies were used at the following dilutions: guinea pig α-SYP-1, 1:800 (MacQueen et al., 2002); α-HTP-3, 1:500; α-ZIM-3, 1:100 (Penkner et al., 2009); α-HIM-8, 1:100 (Phillips et al., 2005); α-SUN-1, 1:300 (Penkner et al., 2009); α-SUN-1 Ser8-Pi, 1:700 (Penkner et al., 2009); α-SUN-1 Ser12-Pi, 1:1300 (Penkner et al., 2009); α-SUN-1 Ser24-Pi, 1:100 (Penkner et al., 2009); rabbit α-HTP-3, 1:200; α-PLK-1, 1:50; α-PLK-2, 1:5; α-Ce-lamin, 1:200 (Liu et al., 2000); and mouse α-GFP, 1:200 (Abcam). The following day, after washing with PBST, secondary antibodies were added: Alexa Fluor 488 goat α-guinea pig and α-rabbit (1:1000; Molecular Probes); Alexa Fluor 555 goat α-rabbit and α-guinea pig (1:1000; Molecular Probes); and Cy3 donkey α-mouse (1:1000; Jackson ImmunoResearch). Slides were mounted in anti-fading agent (VECTASHIELD; Vector Laboratories) containing 1 μg/μl of DAPI.

Immunoprecipitation

Worms were sonicated (5 × 30 s; 28% output) in 1× homogenization buffer (15 mM HEPES [pH 7.6]; 10 mM KCl; 1.5 mM $MgCl_2$; 70 mM NaCl; 0.1 nM EDTA; 0.5 mM EGTA; 1 mM DTT; 44 mM Sucrose; 0,1% Triton X-100; 1 mM PMSF; 1× protease inhibiter cocktail; Roche; 50 mM NaF; 0.1 mM Na_3VO_4; 60 mM β -glycerophosphate). The GFP trap (ChromoTek) was used to immunoprecipitate SUN-1::GFP. Beads were washed once with homogenization buffer and two times with washing buffer (10 mM Tris [pH 7.5]; 175 mM NaCl; 0.5 mM EDTA; 1 mM PMSF; 1× protease inhibitor cocktail; Roche). Strains used: *sun-1::gfp*; *sun-1(ok1282); spe-26(hc138)* (Penkner et al., 2009), and *sun-1(ok1282)/nT1(qIs51)*. Antibodies were anti-PLK-2 (this study; 1:100) and anti-GFP (Roche; mouse, 1:2500).

Image Acquisition and Time Course Analysis of Pairing

Images were acquired and processed using a DeltaVision Image Restoration System (Applied Precision). Data were collected as a series of 15–25 optical sections in increments of 0.2 μm under standard parameters with the softWoRx 3.0 software (Applied Precision). For quantitative analysis of pairing, data for three wild-type and mutant gonads were collected and divided into five equal-sized zones (45–50 μm in length) from the first mitotic nuclei to the last pachytene nuclei. FISH signals were scored by examination of a nucleus through its volume and were considered paired if the distance between the signals was ≤0.7 μm (MacQueen and Villeneuve, 2001). Data for each zone of the gonads were pooled together, giving a total number of nuclei with paired/unpaired signals, and the significance of the pairing levels was tested by Fisher's exact test (two-tailed p value and 95% confidence intervals), using InStat3 software (GraphPad).

SUPPLEMENTAL INFORMATION

Supplemental Information includes Supplemental Experimental Procedures and seven figures and can be found with this article online at doi:10.1016/j.devcel.2011.07.011.

ACKNOWLEDGMENTS

The authors would like to thank Damien D'Amours and the members of the laboratory of Richard Roy for technical assistance and helpful discussions; Florence Couteau for comments on the manuscript; the Caenorhabditis Genetics Center, International *C. elegans* Gene Knockout Consortium, Yuji Kohara, and Sanger Center for strains and clones; and Yosef Gruenbaum, Anne Villeneuve, and Abby Dernburg for antibodies. This work was supported by FWF Grant P-21107 to V.J., an ÖAW scholarship to A.W., and Canadian Institutes of Health Research (CIHR) Grant 86684 to M.Z.

Received: March 11, 2011
Revised: June 9, 2011
Accepted: July 21, 2011
Published online: October 20, 2011

REFERENCES

Alsheimer, M. (2009). The dance floor of meiosis: evolutionary conservation of nuclear envelope attachment and dynamics of meiotic telomeres. Genome Dyn. *5*, 81–93.

Archambault, V., and Glover, D.M. (2009). Polo-like kinases: conservation and divergence in their functions and regulation. Nat. Rev. Mol. Cell Biol. *10*, 265–275.

Baudrimont, A., Penkner, A., Woglar, A., Machacek, T., Wegrostek, C., Gloggnitzer, J., Fridkin, A., Klein, F., Gruenbaum, Y., Pasierbek, P., and Jantsch, V. (2010). Leptotene/zygotene chromosome movement via the SUN/KASH protein bridge in *Caenorhabditis elegans*. PLoS Genet. *6*, e1001219.

Brenner, S. (1974). The genetics of *Caenorhabditis elegans*. Genetics *77*, 71–94.

Chase, D., Serafinas, C., Ashcroft, N., Kosinski, M., Longo, D., Ferris, D.K., and Golden, A. (2000). The polo-like kinase PLK-1 is required for nuclear envelope breakdown and the completion of meiosis in *Caenorhabditis elegans*. Genesis *26*, 26–41.

Chen, Y.C., and Weinreich, M. (2010). Dbf4 regulates the Cdc5 Polo-like kinase through a distinct non-canonical binding interaction. J. Biol. Chem. *285*, 41244–41254.

Chikashige, Y., Haraguchi, T., and Hiraoka, Y. (2007). Another way to move chromosomes. Chromosoma *116*, 497–505.

Colaiácovo, M.P. (2006). The many facets of SC function during *C. elegans* meiosis. Chromosoma *115*, 195–211.

Colaiácovo, M.P., MacQueen, A.J., Martinez-Perez, E., McDonald, K., Adamo, A., La Volpe, A., and Villeneuve, A.M. (2003). Synaptonemal complex assembly in *C. elegans* is dispensable for loading strand-exchange proteins but critical for proper completion of recombination. Dev. Cell *5*, 463–474.

Couteau, F., Nabeshima, K., Villeneuve, A., and Zetka, M. (2004). A component of *C. elegans* meiotic chromosome axes at the interface of homolog alignment, synapsis, nuclear reorganization, and recombination. Curr. Biol. *14*, 585–592.

Dernburg, A.F., McDonald, K., Moulder, G., Barstead, R., Dresser, M., and Villeneuve, A.M. (1998). Meiotic recombination in *C. elegans* initiates by a conserved mechanism and is dispensable for homologous chromosome synapsis. Cell *94*, 387–398.

Ding, X., Xu, R., Yu, J., Xu, T., Zhuang, Y., and Han, M. (2007). SUN1 is required for telomere attachment to nuclear envelope and gametogenesis in mice. Dev. Cell *12*, 863–872.

Elia, A.E., Cantley, L.C., and Yaffe, M.B. (2003). Proteomic screen finds pSer/pThr-binding domain localizing Plk1 to mitotic substrates. Science *299*, 1228–1231.

Fire, A., Xu, S., Montgomery, M.K., Kostas, S.A., Driver, S.E., and Mello, C.C. (1998). Potent and specific genetic interference by double-stranded RNA in *Caenorhabditis elegans*. Nature *391*, 806–811.

Fridkin, A., Penkner, A., Jantsch, V., and Gruenbaum, Y. (2009). SUN-domain and KASH-domain proteins during development, meiosis and disease. Cell. Mol. Life Sci. *66*, 1518–1533.

Goodyer, W., Kaitna, S., Couteau, F., Ward, J.D., Boulton, S.J., and Zetka, M. (2008). HTP-3 links DSB formation with homolog pairing and crossing over during *C. elegans* meiosis. Dev. Cell *14*, 263–274.

Gu, S.G., and Fire, A. (2010). Partitioning the *C. elegans* genome by nucleosome modification, occupancy, and positioning. Chromosoma *119*, 73–87.

Hiraoka, Y., and Dernburg, A.F. (2009). The SUN rises on meiotic chromosome dynamics. Dev. Cell *17*, 598–605.

Koszul, R., and Kleckner, N. (2009). Dynamic chromosome movements during meiosis: a way to eliminate unwanted connections? Trends Cell Biol. *19*, 716–724.

Liu, J., Rolef Ben-Shahar, T., Riemer, D., Treinin, M., Spann, P., Weber, K., Fire, A., and Gruenbaum, Y. (2000). Essential roles for *Caenorhabditis elegans* lamin gene in nuclear organization, cell cycle progression, and spatial organization of nuclear pore complexes. Mol. Biol. Cell *11*, 3937–3947.

Lu, W., Gotzmann, J., Sironi, L., Jaeger, V.M., Schneider, M., Lüke, Y., Uhlén, M., Szigyarto, C.A., Brachner, A., Ellenberg, J., et al. (2008). Sun1 forms immobile macromolecular assemblies at the nuclear envelope. Biochim. Biophys. Acta *1783*, 2415–2426.

MacQueen, A.J., and Villeneuve, A.M. (2001). Nuclear reorganization and homologous chromosome pairing during meiotic prophase require *C. elegans* chk-2. Genes Dev. *15*, 1674–1687.

MacQueen, A.J., Colaiácovo, M.P., McDonald, K., and Villeneuve, A.M. (2002). Synapsis-dependent and -independent mechanisms stabilize homolog pairing during meiotic prophase in *C. elegans*. Genes Dev. *16*, 2428–2442.

Malone, C.J., Misner, L., Le Bot, N., Tsai, M.C., Campbell, J.M., Ahringer, J., and White, J.G. (2003). The *C. elegans* hook protein, ZYG-12, mediates the essential attachment between the centrosome and nucleus. Cell *115*, 825–836.

Martinez-Perez, E., and Villeneuve, A.M. (2005). HTP-1-dependent constraints coordinate homolog pairing and synapsis and promote chiasma formation during *C. elegans* meiosis. Genes Dev. *19*, 2727–2743.

Matthew, E.M., Yen, T.J., Dicker, D.T., Dorsey, J.F., Yang, W., Navaraj, A., and El-Deiry, W.S. (2007). Replication stress, defective S-phase checkpoint and increased death in Plk2-deficient human cancer cells. Cell Cycle *6*, 2571–2578.

Nishi, Y., Rogers, E., Robertson, S.M., and Lin, R. (2008). Polo kinases regulate *C. elegans* embryonic polarity via binding to DYRK2-primed MEX-5 and MEX-6. Development *135*, 687–697.

Page, S.L., and Hawley, R.S. (2004). The genetics and molecular biology of the synaptonemal complex. Annu. Rev. Cell Dev. Biol. *20*, 525–558.

Penkner, A., Tang, L., Novatchkova, M., Ladurner, M., Fridkin, A., Gruenbaum, Y., Schweizer, D., Loidl, J., and Jantsch, V. (2007). The nuclear envelope protein Matefin/SUN-1 is required for homologous pairing in *C. elegans* meiosis. Dev. Cell *12*, 873–885.

Penkner, A.M., Fridkin, A., Gloggnitzer, J., Baudrimont, A., Machacek, T., Woglar, A., Csaszar, E., Pasierbek, P., Ammerer, G., Gruenbaum, Y., and Jantsch, V. (2009). Meiotic chromosome homology search involves modifications of the nuclear envelope protein Matefin/SUN-1. Cell *139*, 920–933.

Petronczki, M., Lénárt, P., and Peters, J.M. (2008). Polo on the Rise-from Mitotic Entry to Cytokinesis with Plk1. Dev. Cell *14*, 646–659.

Phillips, C.M., and Dernburg, A.F. (2006). A family of zinc-finger proteins is required for chromosome-specific pairing and synapsis during meiosis in *C. elegans*. Dev. Cell *11*, 817–829.

Phillips, C.M., Wong, C., Bhalla, N., Carlton, P.M., Weiser, P., Meneely, P.M., and Dernburg, A.F. (2005). HIM-8 binds to the X chromosome pairing center and mediates chromosome-specific meiotic synapsis. Cell *123*, 1051–1063.

Phillips, C.M., Meng, X., Zhang, L., Chretien, J.H., Urnov, F.D., and Dernburg, A.F. (2009). Identification of chromosome sequence motifs that mediate meiotic pairing and synapsis in *C. elegans*. Nat. Cell Biol. *11*, 934–942.

Przewloka, M.R., and Glover, D.M. (2009). The kinetochore and the centromere: a working long distance relationship. Annu. Rev. Genet. *43*, 439–465.

Sato, A., Isaac, B., Phillips, C.M., Rillo, R., Carlton, P.M., Wynne, D.J., Kasad, R.A., and Dernburg, A.F. (2009). Cytoskeletal forces span the nuclear envelope to coordinate meiotic chromosome pairing and synapsis. Cell *139*, 907–919.

Scherthan, H. (2001). A bouquet makes ends meet. Nat. Rev. Mol. Cell Biol. *2*, 621–627.

Scherthan, H. (2007). Telomere attachment and clustering during meiosis. Cell. Mol. Life Sci. *64*, 117–124.

Sourirajan, A., and Lichten, M. (2008). Polo-like kinase Cdc5 drives exit from pachytene during budding yeast meiosis. Genes Dev. *22*, 2627–2632.

Stewart, M.N., and Dawson, D.S. (2008). Changing partners: moving from non-homologous to homologous centromere pairing in meiosis. Trends Genet. *24*, 564–573.

Sumara, I., Giménez-Abián, J.F., Gerlich, D., Hirota, T., Kraft, C., de la Torre, C., Ellenberg, J., and Peters, J.M. (2004). Roles of polo-like kinase 1 in the assembly of functional mitotic spindles. Curr. Biol. *14*, 1712–1722.

Tzur, Y.B., Wilson, K.L., and Gruenbaum, Y. (2006). SUN-domain proteins: 'Velcro' that links the nucleoskeleton to the cytoskeleton. Nat. Rev. Mol. Cell Biol. *7*, 782–788.

van de Weerdt, B.C., Littler, D.R., Klompmaker, R., Huseinovic, A., Fish, A., Perrakis, A., and Medema, R.H. (2008). Polo-box domains confer target specificity to the Polo-like kinase family. Biochim. Biophys. Acta *1783*, 1015–1022.

Zickler, D. (2006). From early homologue recognition to synaptonemal complex formation. Chromosoma *115*, 158–174.

OPEN ACCESS Freely available online

PLoS one

A New Thermosensitive *smc-3* Allele Reveals Involvement of Cohesin in Homologous Recombination in *C. elegans*

Antoine Baudrimont[1], Alexandra Penkner[1], Alexander Woglar[1], Yasmine M. Mamnun[1], Margot Hulek[1], Cathrin Struck[2], Ralf Schnabel[2], Josef Loidl[1], Verena Jantsch[1]*

1 Max F. Perutz Laboratories, Department of Chromosome Biology, University of Vienna, Vienna, Austria, **2** Department of Genetics, Technical University of Braunschweig, Braunschweig, Germany

Abstract

The cohesin complex is required for the cohesion of sister chromatids and for correct segregation during mitosis and meiosis. Crossover recombination, together with cohesion, is essential for the disjunction of homologous chromosomes during the first meiotic division. Cohesin has been implicated in facilitating recombinational repair of DNA lesions via the sister chromatid. Here, we made use of a new temperature-sensitive mutation in the *Caenorhabditis elegans* SMC-3 protein to study the role of cohesin in the repair of DNA double-strand breaks (DSBs) and hence in meiotic crossing over. We report that attenuation of cohesin was associated with extensive SPO-11–dependent chromosome fragmentation, which is representative of unrepaired DSBs. We also found that attenuated cohesin likely increased the number of DSBs and eliminated the need of MRE-11 and RAD-50 for DSB formation in *C. elegans*, which suggests a role for the MRN complex in making cohesin-loaded chromatin susceptible to meiotic DSBs. Notably, in spite of largely intact sister chromatid cohesion, backup DSB repair via the sister chromatid was mostly impaired. We also found that weakened cohesins affected mitotic repair of DSBs by homologous recombination, whereas NHEJ repair was not affected. Our data suggest that recombinational DNA repair makes higher demands on cohesins than does chromosome segregation.

Citation: Baudrimont A, Penkner A, Woglar A, Mamnun YM, Hulek M, et al. (2011) A New Thermosensitive *smc-3* Allele Reveals Involvement of Cohesin in Homologous Recombination in *C. elegans*. PLoS ONE 6(9): e24799. doi:10.1371/journal.pone.0024799

Editor: Michael Polymenis, Texas A&M University, United States of America

Received June 14, 2011; **Accepted** August 17, 2011; **Published** September 21, 2011

Funding: This work was supported by the Austrian Science Fund FWF grant P21338-B03. The funders had no role in study design, data collection and analysis, decision to publish, or preparation of the manuscript.

Competing Interests: The authors have declared that no competing interests exist.

* E-mail: verena.jantsch@univie.ac.at

Introduction

The cohesin complex contains members of the highly conserved structural maintenance of chromosomes (SMC) protein family [1]. SMC proteins are involved in DNA condensation, cohesion, and repair. During mitosis, replicated sister chromatids are held together by cohesins in metaphase; this cohesion permits the bipolar orientation of the spindle kinetochores, allowing microtubules to separate the sister chromatids into the two daughter cells (for review see [2]). During meiosis, chromosomes face a new challenge: separation of the homologs during meiosis I to halve the ploidy of the cell. During metaphase I, cohesion supports the co-orientation of the kinetochores of bivalents (pairs of homologous chromosomes) [3]. This co-orientation leads to the separation of homologous chromosomes in anaphase I. Coordinated separation of homologous chromosomes and sister chromatids during meiosis I and II, respectively, is achieved by the two-step loss of cohesin from the arms and the centromeric regions [4].

Cohesin is a tetrameric complex composed of two SMC subunits, Smc1p (the worm homolog would be HIM-1) and Smc3p, and two non-SMC subunits, such as Scc1p and Scc3p in yeast [5]. SMC subunits bear nucleotide-binding domains (NBDs) at the amino and carboxy termini of linked long coiled-coil domains separated by a hinge domain. Each SMC protein folds on itself and forms a central region (coiled coil) with the hinge domain and the two NBDs at either end. Smc1p and Smc3p dimerize via the hinge domain, and the non-SMC subunits bind to the NBDs of the two SMCs. This ring is closed by the non-SMC subunit Scc1p, a member of the α-kleisin family [6]. Scc1 belongs to the mitotic specific cohesin complex, whereas during meiosis, cohesin complexes include the meiosis-specific kleisin Rec8 [1].

Homologs of the cohesin proteins have been identified in *C. elegans* [7,8,9,10,11]. In *C. elegans*, homozygous *smc-1* and *smc-3* deletion mutants cease their development at larval stages L1–L2, suggesting a maternal rescue of cohesins during the first stage of embryonic development [12]. Moreover, depletion of SMC-1 and SMC-3 by RNAi results in embryonic lethality with complete penetrance [9].

Cohesins delineate the axes of meiotic prophase chromosomes. These axes become the lateral elements of the synaptonemal complex (SC) [13]. In addition to the meiotic cohesin complex (SMC-1, SMC-3, REC-8, and SCC-3), *C. elegans* lateral elements contain HIM-3 and HTP-1, 2, and 3, which are related to budding yeast Hop1 [14,15,16] HTP-3 is required to load cohesins onto chromosomes during meiosis [7]. Additionally, HTP-3 is involved in the formation of DSBs [17].

Unlike in yeast, synapsis (i.e., the connection of axial elements by transversal filaments) is independent of the formation of DSBs in *C. elegans* [18]. However, as in other organisms, repair of DSBs

entailing chiasmata takes place in the context of the SC [19]. Repair of DSBs requires the MRN complex to generate 5′ to 3′ resected DNA overhangs [20]. This resection is necessary to allow loading of the strand invasion protein RAD-51. As in yeast, in worms, the MRN complex is also needed for the formation of DSBs [21,22]. However, under conditions of weakened REC-8 function, DSBs can be formed in the absence of RAD-50 or MRE-11 [23], which are components of the MRN complex. In meiosis, effective repair depends on the availability of a homologous chromosome as the template, because repair via the sister is inhibited by HIM-3, a constraint that is lost in late pachytene.

C. elegans hermaphrodite gonads are organized in a spatial gradient form distal to proximal representing consecutive stages of meiotic prophase I (leptotene/zygotene (transition zone, TZ), pachytene, diplotene, diakinesis) that follow the most distally positioned proliferative mitotic zone [13]. In leptotene, chromosomes condense and engage in the homolog search. During the zygotene stage, the SC starts to polymerize between paired homologs. After successful repair of the DSBs via the homolog in pachytene the chromosomes condense upon entry into diplotene and reach maximal condensation in diakinesis. In diakinesis the paired homologs (6 bivalents in *C. elegans*) are physically linked by one crossover.

Here, we report the isolation of a new thermosensitive *smc-3* allele with distinct reduced viability at the restrictive temperature (25°C). Our analysis revealed that *smc-3* mutant worms formed organized gonads, but they were defective in meiotic repair, with highly fragmented chromatin at diakinesis. We found significantly reduced cohesin complexes associated with chromatin and show that the homolog search process started with wild-type kinetics but because of defective synapsis, pairing could not be stabilized. Reduced amounts of cohesins rendered the chromatin more susceptible to meiotic DSB formation. We analyzed the repair defect observed in *smc-3* during meiosis by epistasis analysis. We also show that mitotic repair was impaired as soon as it relied on homologous recombination. Our results demonstrate the essential role of cohesin in mitosis and meiosis separate from its role in cohesion, the latter requires less cohesins than the repair of DSBs.

Results

t2553: a new temperature-sensitive allele of the cohesin subunit *smc-3*

t2553 was isolated as a temperature-sensitive maternal effect lethal mutant. Mapping and complementation tests confirmed *t2553* as a new allele of *C. elegans smc-3*. Sequencing of the locus revealed a point mutation (a C-to-T transition) in the coding sequence of *smc-3* at position 3241, resulting in a leucine (L)-to-phenylalanine (F) amino acid change at position 1081. The L1081F mutation resides in a coiled-coil region in proximity to the C-terminal ATPase domain (Figure 1A). Alignment of SMC-3 proteins from various phyla revealed that this leucine is widely conserved (Figure 1B).

smc-3 mutants displayed a reduced brood size compared to wild type when grown at 16°C (Table 1). A total of 89±3% of the *smc-3* embryos hatched (wild type: 98±3%), and 4±2% of the viable offspring were males (wild type: 0%). Both the reduced brood size and the documented Him (*h*igh *i*ncidence of *m*ales) phenotype are consistent with a chromosome segregation failure and a putative meiotic defect in *smc-3* mutants. Shifting L1 larvae to 25°C for approximately 55 h reduced the brood size even further (Table 1) with a high embryonic lethality (hatch rate: *smc-3*, 2±2%; wild type: 98±3%). No obvious growth or morphological defects were observed in the surviving progeny. This particular *smc-3* allele therefore allowed us to analyze the role of SMC-3 in meiotic chromosome behavior.

Repair of programmed DSBs impaired in *smc-3*

Chromatin masses that varied in numbers and size could be seen instead of the normal six DAPI-stained bodies in *smc-3* diakinesis (Figure 2Ai). The numerous small chromatin structures in diakinesis nuclei of *smc-3* hermaphrodites were indicative of DNA fragmentation, which is also observed in DNA repair–deficient mutants [10]. Depleting the SPO-11 endonuclease in *smc-3* mutants suppressed the formation of chromatin fragments in diakinesis (Figure 2Aii, bottom). In 49 diakinesis nuclei of *spo-11;smc-3* double mutants, 12 DAPI-positive structures could be seen on average (standard deviation [SD]: 0.2). Smaller chromatin fragments were completely absent. We therefore conclude that the fragmentation observed at diakinesis in *smc-3* mutants originated from defective meiotic crossing over resulting from SPO-11–induced DSBs.

Requirement of the MRN complex for DBS formation bypassed in *smc-3* mutants

In *C. elegans*, MRE-11 is required for both formation and repair of DSBs [21,22]. In the double mutant *smc-3;mre-11*, we would therefore expect 12 univalents, as was seen in the *smc-3;spo-11*

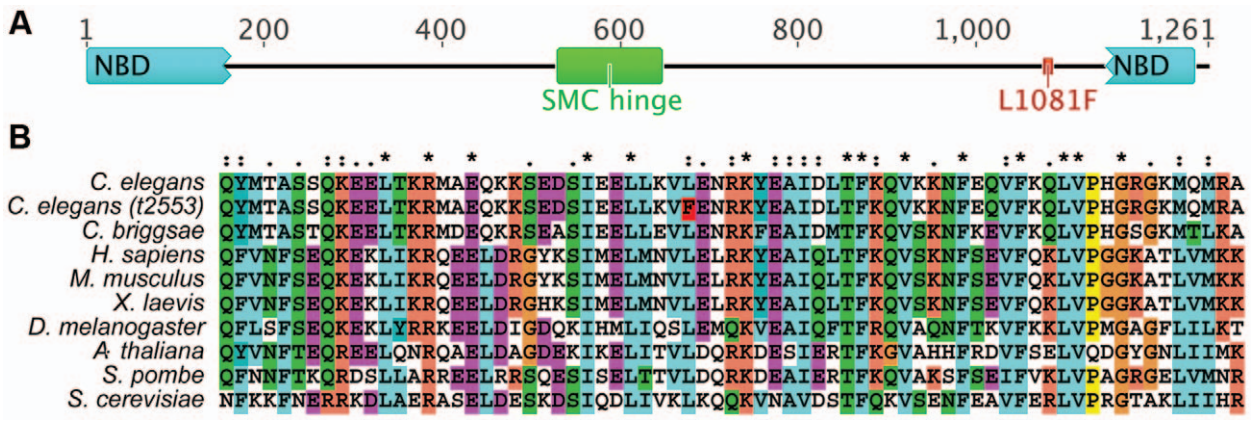

Figure 1. The new allele *smc-3 (t2553).* (A) Domain organization of *C. elegans* SMC-3 highlighting the position of the L1081F amino acid change; domain organizations predicted by CDART [45]. (B) Alignment of SMC-3 sequences for the indicated organisms highlights conservation of the mutated leucine (highlighted in red in *t2553*).
doi:10.1371/journal.pone.0024799.g001

Table 1. Brood size and hatch rates

	16°C		25°C	
	brood size	**hatch rate**	**brood size**	**hatch rate**
wild type	258±25 eggs[a]	98±1%	187±20 eggs[a]	98±2%
smc-3	188±38 eggs[a,b]	89±3%[a,b]	81±21 eggs[a,b]	2±2%[a,b]

[a]Student's *t*-test, $p<0.05$ comparing genotypes at 16°C and 25°C.
[b]Student's *t*-test, $p<0.05$ comparing *smc-3* to the wild type at respective temperature.
Brood size and hatch rate of wild-type and *smc-3* mutant worms at 16°C and 25°C (mean±SD). Progeny of seven worms were scored.
doi:10.1371/journal.pone.0024799.t001

double mutant. However, we observed massive fragmentation at diakinesis (Figure 2Aiii, bottom).

Because both the *smc-3* single mutant and the *smc-3;mre-11* double mutant displayed repair defects, we sought to quantify the fragmentation observed at diakinesis. To avoid artifacts generated by projections of pictures, this quantification was done on picture stacks measuring the volume and the "sphericity" of the DAPI structures (see Materials and Methods). In contrast to the wild type, where 3.7±1.8 (mean±SD) DAPI structures represented connected bivalents (Figure 2Ai, top and 2B, $n=15$ diakinesis), quantification showed that chromosome fragments (3.7±2.9, $n=14$ diakinesis) and "chromatin masses" (5.8±2.5 SD, n = 14 diakinesis) were the most prevalent classes of DAPI structures in *smc-3* mutants (Figure 2B).

Using this method, we detected an overall number of 10.9±0.9 ($n=18$ diakinesis) DAPI structures and on average 7.4±2.2 ($n=18$

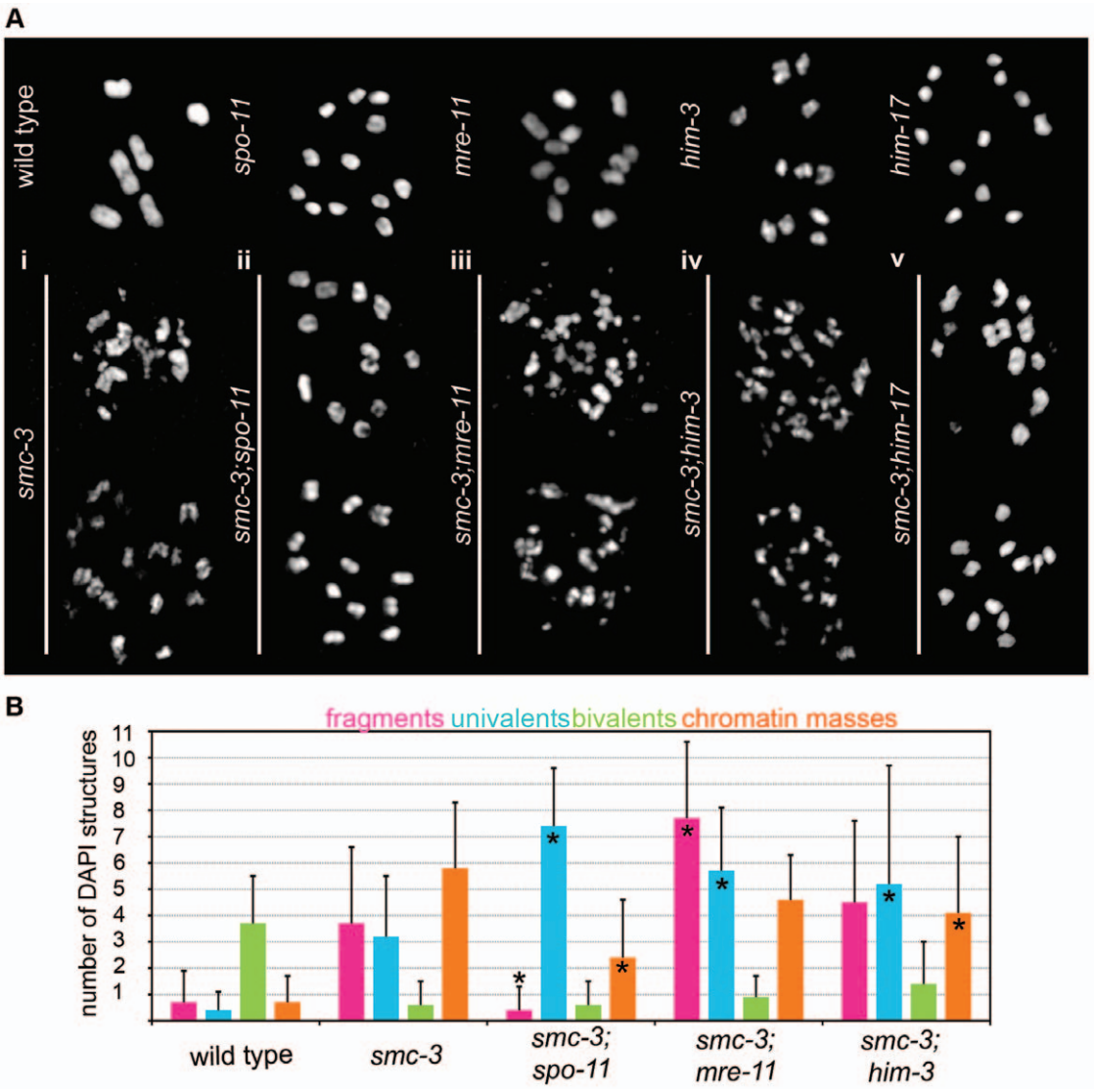

Figure 2. Fragmentation at diakinesis resulting from defective DSBs repair. (A) Representative DAPI structures found at diakinesis in: (i) top: wild type, bottom: *smc-3*; (ii) top: *spo-11*, bottom: *smc-3; spo-11*; (iii) top: *mre-11*, bottom: *smc-3;mre-11;* (iv) top: *him-3*, bottom: *smc-3;him-3*; and (v) top: *him-17*, bottom: *smc-3;him-17*. (B) Quantification of DNA fragmentation at last diakinesis. Classes (fragments, univalents, bivalents, and DNA masses) were defined by the volume (v) and the "sphericity" (s) of the DAPI structures at the last diakinesis before the spermatheca (see Materials and Methods). Single star indicates significant differences ($p<0.05$, Student's *t*-test) for fragments, univalents, bivalents, and masses between double mutants and the *smc-3* single mutant. Error bars represent SD.
doi:10.1371/journal.pone.0024799.g002

diakinesis) univalents (Figure 2B) in *smc-3;spo-11* double mutants. Quantification confirmed that fragmentation was increased in *smc-3;mre-11* compared to *smc-3* worms (Figure 2B). In *smc-3;mre-11* worms, the number of fragments and univalents was significantly increased compared to the *smc-3* single mutant (Student's *t*-test, $p<0.05$). The *smc-3;rad-50* double mutant likewise displayed an increase in fragmentation (unpublished data).

These results indicate that the MRN complex was dispensable for the formation of DSBs in *smc-3* mutants.

Fewer cohesin complexes on *smc-3* chromosomes not associated with defective cohesion

We compared loading of SMC-3 onto chromosome axes in *C. elegans smc-3* and wild-type worms. In wild-type worms, SMC-3 delineated the chromosome axes, whereas in *smc-3*, only short and weakened stretches were observed (Figure 3A). The reduced amounts of SMC-3 could result either from reduced loading or reduced stability of the complex; notably, we did not see a gradual decrease in the SMC-3 signal during meiotic progression. To discriminate between these two possibilities, we examined the abundance of REC-8 in squashed nuclei with stringent sarkosyl washes. (Figure 3B). We reasoned that the addition of detergent should not further decrease the REC-8 signal if cohesin loading was already reduced in the mutant. However, the addition of detergent led to a strong reduction in REC-8 levels in *smc-3* mutants (Figure 3B), suggesting that the point mutation in the coiled-coil domain impaired the stability of the cohesin complex on chromatin. However, this assay cannot judge on the amount of cohesin loaded in the mutant.

To test the validity of the detergent assay, we also probed for HTP-3. Proper loading of the cohesin complex requires efficient HTP-3 loading [7]. The detergent washes did not remove HTP-3 from either wild-type or *smc-3* mutant squashed nuclei. (Figure 3C), confirming the validity of the approach. Furthermore, we subjected *syp-2* squashed nuclei to the same assays (REC-8 and HTP-3 staining with and without sarkosyl). Deletion of SYP-2, a central element component of the SC, results in unsynapsed chromosomes [19]. We did not observe a decrease in REC-8 or HTP-3 signals after washing *syp-2* mutants with sarkosyl (Figure S1B). This reinforces the specificity of the assay, because a lack of synapsis could not account for the decrease in REC-8 loading that we observed after washing with sarkosyl. Similarly, no defects in SMC-3 loading were detectable after depletion of SYP-2 (Figure S1A).

Altogether, these results reinforce the idea that the L1081F mutation in *smc-3* leads to unstable chromatin-associated cohesin complexes entailing a reduced amount of cohesin complexes on chromatin. The presence of 12 univalents instead of 24 sister

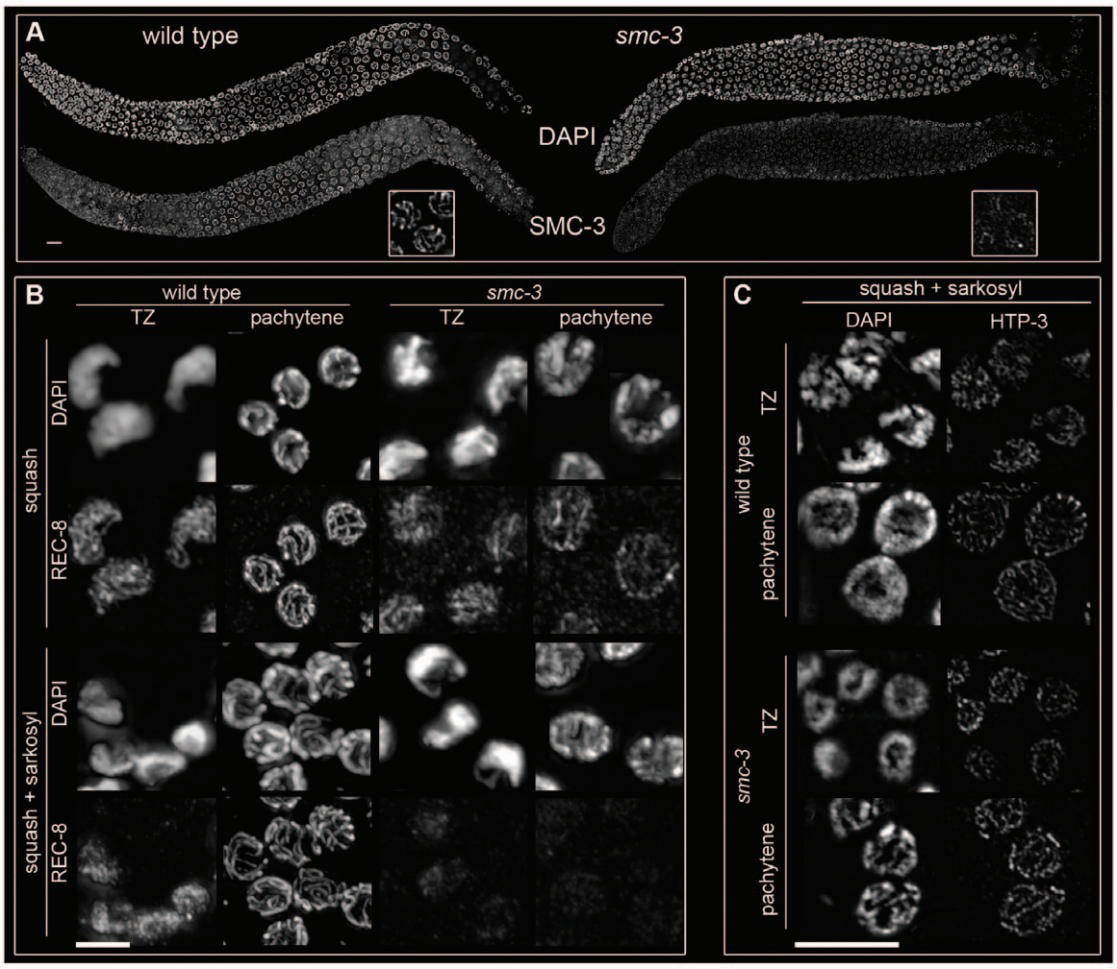

Figure 3. Chromosomes axes are impaired in *smc-3*. (A) Immunostaining of SMC-3 in wild-type and *smc-3* worms. (B) Squashed nuclei untreated and washed with sarkosyl in wild-type and *smc-3* worms in the TZ and pachytene stained with anti-REC-8 antibody. (C) Squashed nuclei washed with sarkosyl stained with anti-HTP-3 in wild-type and *smc-3* worms in TZ and pachytene. Bar: 10 μm.
doi:10.1371/journal.pone.0024799.g003

chromatids in *spo-11;smc-3* diakinesis (Figure 2Aii, bottom) suggests intact cohesion with this particular allele.

To test this assumption, cohesin loading was further reduced by RNAi-mediated depletion of the cohesin subunit REC-8. Indeed, diakinesis nuclei of *spo-11;smc-3;rec-8(RNAi)* triple mutants always showed more than 20 signals (in all 26 diakinesis nuclei scored from eight independent gonads), consistent with the expected 24 isolated sister chromatids in cohesion-deficient mutants (Figure S2). *spo-11;rec-8(RNAi)* control worms also displayed more than 20 DAPI-positive structures (unpublished data). The reduced amount of cohesins appeared to be sufficient for the establishment of cohesion but insufficient for DSB repair in *smc-3*. Additionally, when pairing of the pairing center (PC) protein HIM-8 was assayed, more than two HIM-8 signals were detected in the mitotic zone of *smc-3* gonads only rarely, indicating that cohesion in most cells is effective (Figure S3). In contrast, during the meiotic time course homologous associations were unstable which can be explained by the failure to establish a proper SC (text S1 and Figures S4 and 5). However homologous pairing prior to SC formation was normal in the mutant.

smc-3 mutants deficient in early steps of meiotic DSB repair

To study meiotic DNA repair, we stained nuclei for the strand-invasion protein RAD-51 [24]. Gonads were divided into six zones of equal lengths, and the number of RAD-51 foci were counted per nucleus. In wild-type worms, RAD-51 foci were observed from early pachytene until mid-pachytene (Figure 4A, left) with a

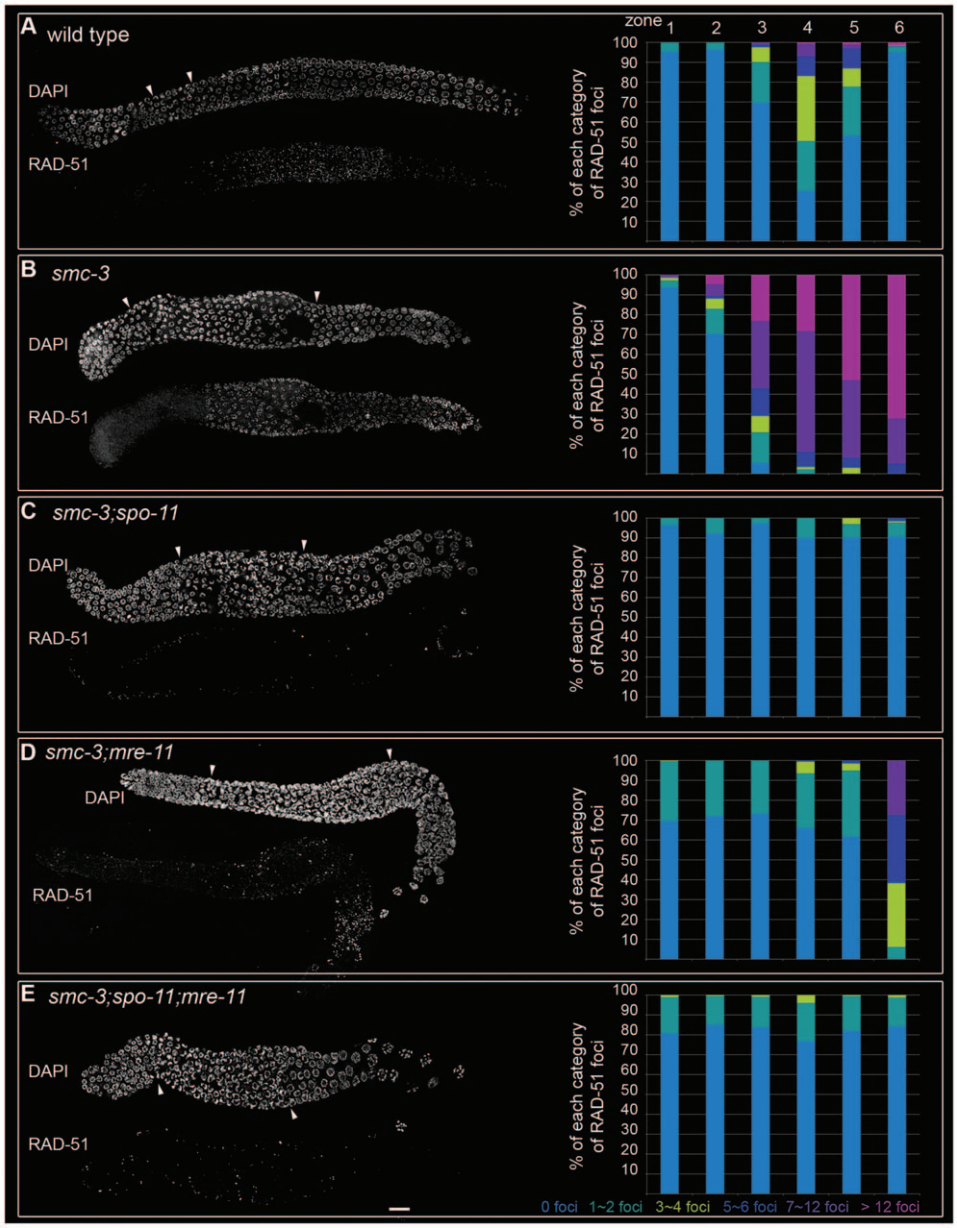

Figure 4. *smc-3* mutants are defective in repair of meiotic DSBs. Left, immunostaining of RAD-51. Right, quantification of RAD-51 foci in wild-type (A), *smc-3 (tm2553)* (B), *smc-3;spo-11* (C), *smc-3;mre-11* (D). and *smc-3;spo-11; mre-11* (E) worms. Gonads were divided into six zones of equal length for quantification. Arrowheads indicate the zone with clustered chromatin. Bar: 10 μm.
doi:10.1371/journal.pone.0024799.g004

maximum number of 7–12 RAD-51 foci in zone 4 (Figure 4A, right). In *smc-3* mutants, the first RAD-51 signals were seen earlier (Figure 4B, left). The number of RAD-51 foci rose from entry into meiosis (zone 2) until late pachytene (zone 6) and continued to accumulate (>12 foci in 70% of nuclei in zone 6; Figure 4B, right), in fact the frequency of foci increased faster in *smc-3*. Few RAD-51 foci could be detected at diakinesis (unpublished data). These data suggest that early steps of HR require functional cohesins and that more DSBs may be formed in *smc-3* mutants.

Next, we wanted to confirm that RAD-51 foci accumulation was SPO-11 dependent. Depletion of SPO-11 in *smc-3* decreased RAD-51 signals (Figure 4C, left). Indeed, in the double mutant *smc-3;spo-11*, a maximum of one or two RAD-51 foci could be observed during the time course (Figure 4C, right). When we scored loading of RAD-51 foci in *smc-3;mre-11* double mutants (Figure 4D, left), we found that until late pachytene (before zone 6), only the class of nuclei with one or two RAD-51 foci was observed. Strikingly, in late pachytene, a significant increase in the number of RAD-51 foci for all classes was found, with a maximum of about 7–12 foci (Figure 4D, right). *smc-3;rad-50(ok197)* double mutants displayed the same phenotype (unpublished data).

We next tested whether this appearance of RAD-51 foci in *smc-3;mre-11* mutants in late pachytene depended on breaks introduced by SPO-11. In the triple mutant *smc-3;spo-11;mre-11*, the number of nuclei with 1–2 RAD-51 foci was significantly decreased compared to *smc-3;mre-11* mutants (Fisher's exact test per class and per zone, $p<0.05$). Remarkably, we did not observe an increase in the number of RAD-51 foci during the time course (Figure 4E, right), confirming that the appearance of excess RAD-51 foci in *smc-3;mre-11* mutants was due to breaks introduced by SPO-11. Furthermore, in *smc-3;spo-11;mre-11* mutants, chromosome fragmentation at diakinesis was absent (Figure S6).

The results of our analysis confirm previous reports (using different components of the protein complexes involved) that the MRN complex is required to restrain the inhibitory action of cohesins on DSB induction [23]. In addition, weakened cohesion led to an increased number of detectable RAD-51 foci, likely due to more DSB induction, suggesting that intact chromosome axes restrain the action of the DSB break machinery.

Repair via the sister chromatid is impaired in *smc-3*

Next, we tested the effectiveness of DSB repair via the sister chromatid. HIM-3 is a major constituent of the lateral element of the SC and exerts an inhibitory effect on meiotic DSB repair via the sister chromatid [14,15]. Fragmentation at diakinesis was still present in the double mutant *smc-3;him-3* (Figure 2Aiv, bottom), suggesting that repair via the sister chromatid was not taking place efficiently. Quantification of the DAPI signals revealed a shift to "univalents" from "chromatin masses" (Student's *t*-test, $p<0.05$) suggesting that some repair might still be taking place (Figure 2B). Therefore, we concluded that despite effective sister chromatid cohesion in *smc-3* mutants, repair of DSBs via the sister chromatid was impaired.

Can weakened cohesion lead to reversion of DSB-refractory chromatin?

The dramatic fragmentation at diakinesis in *smc-3* mutants could reflect a defect in the repair of DSBs, result from an open chromatin conformation that is more permissive to formation of DSBs, or both. The early accumulation of RAD-51 in *smc-3* lends support to the second argument. Previously, it was shown that a mutation in the condensing component DYP-28 could "re-open" chromatin during DSB-refractory chromatin states in *him-17* mutants [25]. Therefore, we compared our *smc-3* mutant to *dpy-28* worms with respect to DSB induction in the DSB compromised mutant *him-17*. Depleting HIM-17 in *smc-3* resulted in diakinesis similar to that seen in *smc-3;spo-11* double mutants, with mostly univalents and reduced fragmentation (Figure 2Av, bottom). This suggests that in contrast to compromised condensin complexes, weakened cohesion could not reverse a failure to induce DSBs in *him-17* mutants.

smc-3 mutation affects mitotic HR but not NHEJ repair

C. elegans genetics is a powerful tool that can be used to separately study two different mitotic repair pathways (Figure 5A). Early embryos repair DSBs by homologous recombination (HR), whereas late-stage embryos repair via the nonhomologous end joining (NHEJ) repair pathway [26]. In addition, repair of DSBs via HR takes place in the primordial germ cells Z2 and Z3 during larval development of the worm (Figure 5A).

Irradiation of late-stage embryos allowed us to test the proficiency of the NHEJ repair pathway using a dose of 60 Gy. *lig-4* mutants, which are defective in the NHEJ repair pathway, slowed down their development when irradiated with 60 Gy as late-stage embryos: all of the worms were still at the L4 stage 66 h after irradiation (Figure 5B). This was in contrast to wild-type worms and *smc-3* mutants, in which only 19% and 24%, respectively, of arrested worms were at the L4 stage 66 h after irradiation (Figure 5B). We therefore concluded that *smc-3* mutants were proficient in the somatic NHEJ repair pathway.

To assess the proficiency of the HR occurring in Z2 and Z3 cells, gonads of adult wild-type and *smc-3* worms that were irradiated (60 Gy) as late-stage embryos were released. DAPI-stained *smc-3* gonads were disorganized, and some showed a lack of meiotic entry (absence of a transition zone) and lacked mature sperm, supporting the idea that mitotic HR repair was also defective (Figure 5, inset) Surprisingly, cells with nuclei of different sizes, indicative of chromosomal nondisjunction, were absent, reinforcing the idea that a reduced amount of cohesin was sufficient for proper segregation of mitotic chromosomes.

DNA damage checkpoint is operating in *smc-3*

Intrigued by the large number of nuclei with more than 12 RAD-51 foci in the last zone of *smc-3* gonads (Figure 4B, left), we first assayed apoptosis in *smc-3* mutants. Acridine orange staining revealed that apoptosis was significantly increased in *smc-3* worms, with 7.8 ± 2.1 (mean$\pm$SD) apoptotic corpses ($n=36$ gonads), compared to wild-type worms, with 3.7 ± 1.3 apoptotic corpses ($n=31$ gonads).

We next asked whether the DNA damage checkpoint was properly activated. Triggering the checkpoint in the mitotic compartment leads to enlargement of nuclei [27]; therefore, we fixed and DAPI stained gonads and then counted nuclei with increased diameters within the first 50 µms from the distal tip of the gonad. In *mrt-2* mutants, which are deficient in DNA damage signaling [28], there was only a slight increase in nuclei diameter 8 h after 60 Gy irradiation (0 Gy: 3.03 ± 0.3 µm [mean$\pm$ SD; $n=25$ nuclei], 60 Gy: 3.5 ± 0.3 µm [$n=23$ nuclei]) compared to wild type (0 Gy: 3.03 ± 0.3 µm [$n=28$ nuclei], 60 Gy: 5.7 ± 0.9 µm [$n=30$ nuclei]). The average size of *mrt-2* nuclei plus the SD was used to define the threshold of checkpoint activation. The analysis revealed that even without irradiation challenge (0 Gy), a significant number of cells in the mitotic portion of *smc-3* gonads had activated the DNA damage checkpoint (Figure 6A), whereas no activation of the checkpoint was observed in wild-type or *mrt-2* worms. We cannot exclude the possibility that the increased number of enlarged nuclei in *smc-3* mutants before irradiation might also be triggered by the activation of the mitotic spindle

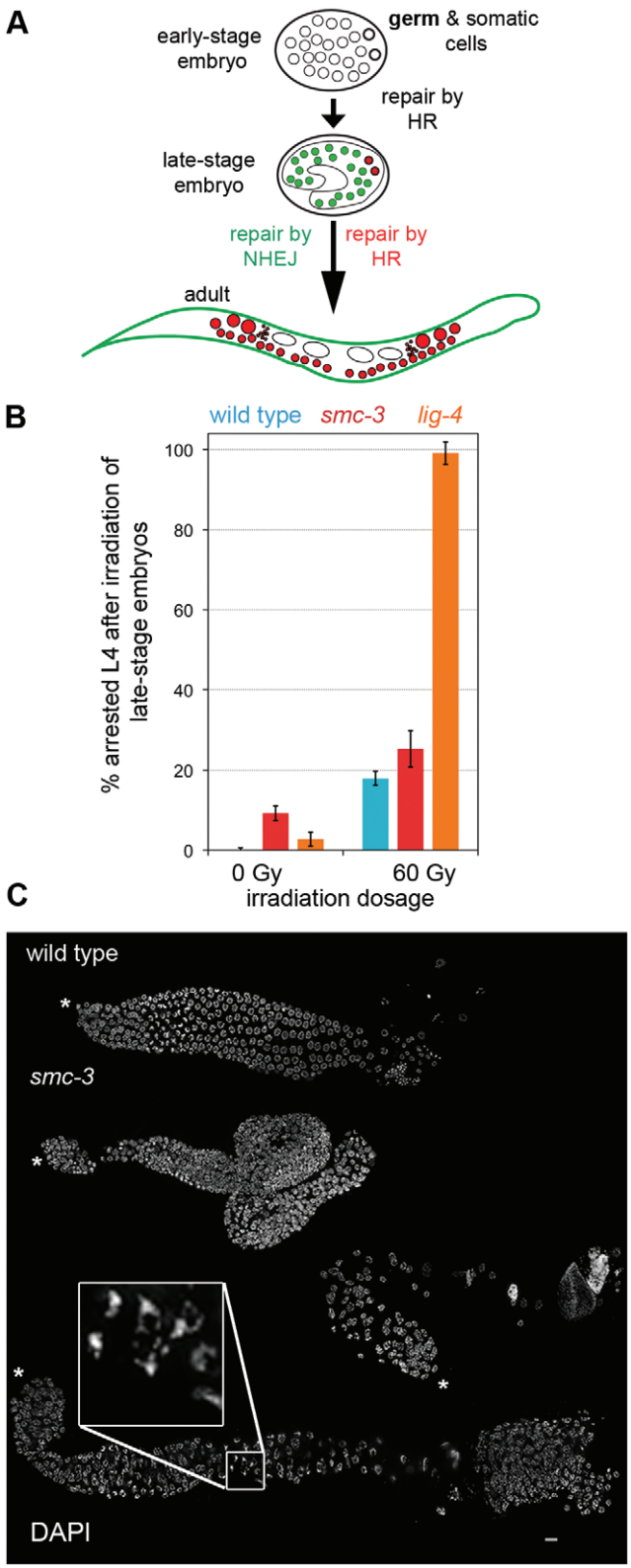

Figure 5. The *t2553* allele impairs mitotic HR repair but not NHEJ repair. (A) Schematic drawing of an embryo with germ (bold circle) and somatic cells (circle). Green color highlights cells repairing DSBs by NHEJ; red cells repair via HR. In the adult, small red circles represent spermatozoa and open ovals represent embryos. (B) Percentage of arrested L4 66 h after 60 Gy irradiation of late-stage embryos with the indicated genotypes. Error bars represent standard error of the mean (SEM). (C) DAPI staining of wild-type and *smc-3* gonads released from worms irradiated (60 Gy) as late-stage embryos. Stars mark the distal tip of the gonad. Bar: 10 μm.
doi:10.1371/journal.pone.0024799.g005

checkpoint due to a slight cohesion or chromosome alignment defect. Moreover, 8 h after irradiation, the proportion of cells activating the DNA damage checkpoint in *smc-3* mutants was even larger than in wild type (Figure 6A). Therefore, the DNA damage checkpoint was properly activated in *smc-3* worms.

To test if the DNA damage checkpoint was also properly activated during the development of the worms, we performed the L1 assay as described in [29]. *C. elegans* develops through four larval stages (L1–L4). Worms deficient for the DNA damage checkpoint do rarely survive to the adult stage upon irradiation. Irradiation with 60 Gy had almost no impact on the development of *smc-3* worms into adults, the same as for wild-type worms; however, only 20% of *mrt-2* worms reached the adult stage (Figure 6B). This supports our conclusion that during worm development, the DNA damage checkpoint was properly activated in *smc-3* worms.

Discussion

We isolated a conditional partial loss-of-function mutant of the cohesin component SMC-3 and showed that a reduction in cohesin molecules mainly impaired repair of DSBs in mitosis and meiosis. The mutation (L1081F) in the newly identified thermo-sensitive allele *smc-3(t2553)* resides in the coiled-coil region close to the NBDs. In human Hela cells, Smc1 is phosphorylated in the coiled-coil region (serines 957 and 966) after induction of DSBs in an ATM-dependent manner [30,31]. Two similar sites of phosphorylation (serines 1067 and 1083) are found in the coiled-coil region close to the NBDs of Smc3. Recently, phosphorylation of Smc3 at serine 1083 was shown to take place in response to DNA damage in Hela cells [32]. In the *t2553* allele, the mutation L1081F might interfere with phosphorylation of SMC-3 upon DNA damage signaling, in addition to the overall reduction in stably DNA bound cohesin molecules that could contribute to the observed DNA repair defects.

From our analysis, it appears that the mutation introduced in the *t2553* allele (L1081F) led to reduced stability of the cohesin complexes on chromosome arms during meiosis, as shown by a weaker SMC-3 signal in immunofluorescence assays. In addition, the cohesin component REC-8 could be expelled from chromatin by detergent treatment of the *smc-3* mutant. This suggests that stable association of cohesin with chromatin was reduced, but sister chromatid cohesion remained robust. Indeed, *smc-3* mutants formed organized gonads at the restrictive temperature (25°C) and segregation defects were only rarely detectable in the mitotic zone in *smc-3* gonads. In addition, in *smc-3;spo-11* worms, 12 DAPI structures were observed at diakinesis, whereas 24 DAPI structures were observed after REC-8 RNAi treatment in this double mutant. This *smc-3* mutant, which lacks a major subunit of the cohesin complex, demonstrates that even a considerable reduction in the number of cohesin molecules on chromatin does not notably affect cohesion in either mitosis or meiosis in *C. elegans*. This is in agreement with a recent report that reducing functional cohesin rings by 87% does not notably affect cohesion in yeast [33].

Nevertheless, this *smc-3* mutant displays defects in meiotic and radiation-induced mitotic DSB repair. It is known that cohesion supports DSB repair, presumably by connecting the damaged site to the sister template in mitosis [34], and cohesin complexes are recruited to DSB-flanking regions extending up to several kilobases

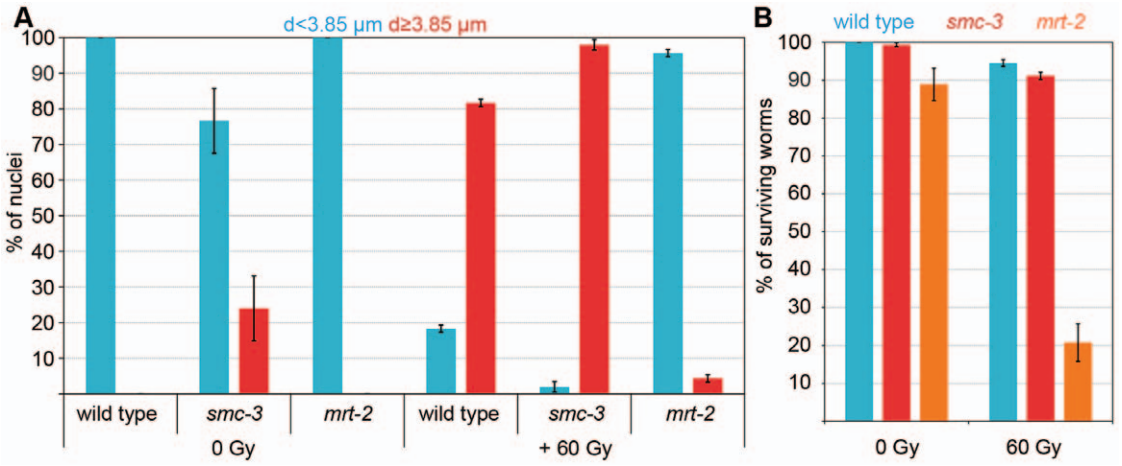

Figure 6. DNA damage checkpoints are working in *smc-3*. Proportion of nuclei with "normal" (<3.85 µm) or "double" (≥3.85 µm) diameters before and 8 h after 60 Gy irradiation (more than 200 nuclei assayed in five different gonads per genotype for the indicated genotypes (N2, *smc-3*, and *mrt-2*). Error bars represent SEM. (B) Percentage of surviving worms 48 h after 60 Gy irradiation. Error bars represent SEM. More than 500 L1s were scored per genotype.
doi:10.1371/journal.pone.0024799.g006

[34]. The reduced amount of stably chromatin-bound cohesin complexes in the *smc-3* mutant could explain the sensitivity to DNA damage that we observed during mitosis. Indeed, a sufficient amount of cohesin might not be established at the site of the DSBs.

It has been proposed that cohesins inhibit repair via the homologous chromosome [35]. In fact, holding sister chromatids together in meiosis might be unproductive when DSB-carrying DNA strands should detach from their sisters in order to undergo recombination with the homolog [36]. Therefore, in meiosis, the requirement for cohesin might be different, and might rather be required to create the platform for lateral element assembly as the backbone of the synaptonemal complex [5,10,37]. The dramatic increase in RAD-51 signals and their persistence until later stages of meiotic prophase I in *smc-3* argue for a defect in DSB repair downstream of the loading of RAD-51. We found that weakened SMC-3 did not allow DSB formation in the absence of HIM-17, but did in the absence of MRE-11/RAD-50. Therefore, the role of cohesion in supporting DSB generation is distinct from that of HIM-17, which confers competence for meiotic DSB formation by methylation of histone H3 [38]. This demonstrates that the MRN complex and HIM-17 act in different pathways upstream of SPO-11.

In the double mutant *smc-3;mre-11*, we observed pachytene chromosome fragmentation and increased RAD-51 foci as hallmarks of DSBs. In the absence of MRE-11 or RAD-50, DSBs are not observed [21,23]. It should be noted that the dependence on *rad-50* for DSB formation is also partially abrogated in *htp-1* and *him-3* mutants, both of which are defective in functions connected to axial elements [23]. These mutants are most likely altered in composition or organization of chromosome axes, thereby making the requirement for the MRN complex dispensable for DSB formation. Weakened SMC-3 suspends the requirement for MRE-11 (or MRN) for DSB formation, as does weakened REC-8. Because both SMC-3 and REC-8 are components of meiotic cohesin, it is likely that weakening the cohesin complex as a whole promotes the generation of DSBs by SPO-11. It is conceivable that the chromosome axis structure interferes with the access or activity of SPO-11 and that this obstacle is locally and/or temporally released by the activity of MRN. This could represent yet another layer in the control of meiotic recombination. Notably, we observed increased RAD-51 signals right after meiotic entry, suggesting that weakened cohesion augments DSB induction.

Smc3 is required for the complete activation of damage signaling to checkpoints upon introduction of artificial DSBs in human cells [32] involving the cohesin complex in the activation of the DNA damage checkpoint. We can state with certainty that the NHEJ repair pathway in mitotic divisions still takes place in the weakened cohesion mutant *smc-3*. Although repair of meiotic lesions was impaired in worms with the *t2553* allele, we found that the few cohesion molecules left were nonetheless able to activate DNA damage checkpoints effectively.

To summarize, this work reinforces the idea that effective repair of DSBs during mitosis and meiosis is more vulnerable to loss of cohesin complexes compared to proper chromosome segregation. It also confirms that, even for holocentric chromosomes, few cohesin complexes are required for proper segregation. Furthermore, the newly isolated temperature-sensitive *smc-3* allele represents a new tool with which to study the effects of weakened cohesion in worms.

Materials and Methods

Nematode strains, strain construction and culture conditions

All *C. elegans* strains were cultured using standard techniques (Brenner, 1974). The following *C. elegans* strains were used: N2 Bristol, GE4345 *smc-3(t2553)* AV276 *syp-2(ok307)* [19], AV106 *spo-11(ok79)* [18], AV112 *mre-11(ok179)* [21], VC418 *him-3(gk149)* [15], VC255 *him-17(ok424)* [38], CB5348 *mrt-2(e2663)* [28]. Nematode strains were provided by the *Caenorhabditis Genetics Center*, which is funded by the NIH National Center for Research Resources (NCRR).

Cytological preparation of gonads and immunostaining

Hermaphrodite gonads were dissected and fixed as described in [39]. For chromatin staining, the preparations were mounted in Vectashield anti-fade (Vector Laboratories Inc., Burlingame, CA) containing 2 µg/ml 4′6-diamidino-2-phenylindole (DAPI). For immunostaining, gonads were blocked in 3% BSA/1x PBS for 20 min. Primary antibodies were applied overnight at 4°C. Antibodies were diluted in 1x PBS/0.01% sodium azide as

follows: anti-SUN-1 Ser8-Pi [40] 1:700, anti-HIM-8 [41] 1:500, anti-ZIM-3 [42] 1:100, anti-RAD-51 [24] 1:300, anti-SYP-1 [43] 1:200, anti-HTP-3 [17] 1:500, anti-SMC-3 [44] 1:10. After 3 washes in 1x PBST (1x PBS, 0.1% Tween-20), secondary antibodies were applied for 2 h at RT. After washes in PBST, samples were mounted.

Fluorescence *in situ* hybridization (FISH)

The PCR-amplified 5S rDNA was used as a probe for the right arm of chromosome V. The 5S rDNA was labeled by PCR with digoxigenin-11-dUTP. FISH was performed as described in [10]. Hybridized digoxigenin-labeled probes were detected with FITC-conjugated anti-digoxigenin antibodies (1:100). Slides were mounted in Vectashield/DAPI.

Microscopy and evaluation

A Zeiss Axioskop epifluorescence microscope was used and images were recorded with a cooled CCD camera (Photometrics Ltd., Tucson, AZ). Evaluation of cytological phenotypes was performed in animals shifted to 25°C at the L1 stage for 66 hours. 3D stacks of images were taken (MetaVue software, Universal Imaging Co., Downingtown, PA), deconvolved (AutoDeblur software, AutoQuant Imaging Inc., Troy, NY) and projected (Helicon Focus software http://helicon.com.ua/heliconfocus/). Artificial coloring and merging were undertaken with Adobe Photoshop 7.0 software (Adobe Systems Incorporated).

RNA interference of *rec-8*

Double stranded RNA was produced by *in vitro* transcription and injected after [10].

Mitotic repair assay

Ten young adult worms for each genotype (wild type, *smc-3*, *mrt-2*) were allowed to lay eggs at the restrictive (25°C) for 2 h. Next, hermaphrodites were removed from the plates and after 3∼4 h at 25°C the eggs were γ-irradiated with a dose of 60 Gy using a ^{137}Cs source. Synchrony of the late-stage embryo at the bean stage was controlled before irradiation. Worms were kept at the restrictive temperature for 66 hours and then the number of arrested worms was scored. The L1 assay was performed as described in [29].

Quantification of DNA fragmentation

Stack pictures from diakinesis were deconvolved (AutoDeblur software, AutoQuant Imaging Inc., Troy, NY). Volumes were quantified with the 3D Object Counter plugin using ImageJ. Classes were defined by the volume (v) and the sphericity (s) of the DAPI structures at the last diakinesis before the spermatheca. Sphericity, as a measure of the roundness of an object, is the ratio of the surface area of a sphere (with the same volume as the given object) to the surface area of the object. Using this method bivalents and univalents could be identified (bivalents: $v = 3.0 \pm 1.1\ \mu m^3$ (mean±SD), $s = 0.65 \pm 0.07$ (mean±SD), $n = 15$ diakinesis; univalents: $v = 1.2 \pm 0.4\ \mu m^3$, $s = 0.80 \pm 0.06$, SD, $n = 16$ diakinesis). DAPI structures with a larger volume than the defined volume of bivalents or with a volume in the range of bivalents but with different sphericity than bivalents were classified as "chromatin masses". DAPI structures with a smaller volume than a univalent or with a volume of a univalent but different sphericity were defined as fragments. 3-dimensional projections of deconvolved pictures and counted volumes are provided for each genotype (Video S1, S2, S3, S4, S5 and S6).

Supporting Information

Figure S1 Lack of synapsis cannot account for a decrease in immunostaining after washing with sarkosyl. A. Immunostaining of SMC-3 in *syp-2* mutant worms. B. *syp-2* squashed nuclei untreated and washed with sarkosyl stained with anti-REC-8 in TZ and pachytene. C. *syp-2* squashed nuclei washed with sarkosyl stained with anit-HTP-3 in TZ and pachytene. Bar: 10 μm.
(TIFF)

Figure S2 Meiotic cohesion is effective in *smc-3*. Representative diakinesis of indicated genotypes (wild type, *spo-11*, *smc-3*, *smc-3;spo-11*, *smc-3;spo-11;rec-8*(RNAi).
(TIFF)

Figure S3 Rare mitotic defects in *smc-3* mutants worms. Time course of HIM-8 pairing in wild type and *smc-3* revealed the presence of 3 foci in the mitotic zone of *smc-3* on rare occasions.
(TIFF)

Figure S4 Proper loading of the PC protein ZIM-3 in *smc-3* but defective synapsis. A. Immunostaining of the pairing center protein ZIM-3 in wild type and *smc-3* (DAPI blue). B. Immunostaining of SUN-1S8Pi in wild type and *smc-3;* (DAPI blue). C. Time course for pairing of HIM-8 in wild type and *smc-3*. Gonads were subdivided into 6 zones of equal lengths. D. Time course for pairing with the 5S rDNA FISH probe (chromosome V) in wild type and *smc-3*. Gonads were subdivided into 6 zones of equal lengths. E. Immunostaining of SYP-1 in wild type and *smc-3*; pachytene nuclei enlarged in the inset; bar 10 μm.
(TIFF)

Figure S5 HIM-3 loading is strongly reduced in *smc-3*. Immunostaining of HIM-3 (red) in wild type and *smc-3*; bar 10 μm.
(TIFF)

Figure S6 Absence of fragmentation in the triple mutant *smc-3;spo-11;mre-11*. A. Representative diakinesis of the indicated genotypes (wild type, *smc-3*, *smc-3;mre-11*, *smc-3;mre-11;spo-11*). Bar 5 μm. B. Quantification of DAPI structures at diakinesis in *smc-3;spo-11;mre-11*.
(TIFF)

Video S1 3-dimensional projection of deconvolved stack pictures (left) and colored surface of the DAPI structures (right) in wild type.
(AVI)

Video S2 3-dimensional projection of deconvolved stack pictures (left) and colored surface of the DAPI structures (right) in *smc-3*.
(AVI)

Video S3 3-dimensional projection of deconvolved stack pictures (left) and colored surface of the DAPI structures (right) in *smc-3; spo-11*.
(AVI)

Video S4 3-dimensional projection of deconvolved stack pictures (left) and colored surface of the DAPI structures (right) in *smc-3; mre-11*.
(AVI)

Video S5 3-dimensional projection of deconvolved stack pictures (left) and colored surface of the DAPI structures (right) in *smc-3; him-3*.
(AVI)

Video S6 3-dimensional projection of deconvolved stack pictures (left) and colored surface of the DAPI structures (right) in *smc-3; him-17*. (AVI)

Text S1
(DOC)

Acknowledgments

We thank Christian Pflügl for technical assistance. We are grateful to Raymond Chan, Abby Dernburg, Adriana La Volpe, Monique Zetka, Anne Villeneuve and the Caenorhabditis Genetics Center for antibodies and strains. We thank Alexander Schleiffer, Enrique Martinez-Perez and Anton Gartner for discussion.

Author Contributions

Conceived and designed the experiments: AB AP YM RS JL VJ AW. Performed the experiments: AB AP YM MH CS AW. Analyzed the data: AB AP VJ AW. Contributed reagents/materials/analysis tools: RS. Wrote the paper: AB VJ.

References

1. Wood AJ, Severson AF, Meyer BJ (2010) Condensin and cohesin complexity: the expanding repertoire of functions. Nat Rev Genet 11: 391–404.
2. Marston AL, Amon A (2004) Meiosis: cell-cycle controls shuffle and deal. Nat Rev Mol Cell Biol. pp 983–997.
3. Monje-Casas F, Prabhu VR, Lee BH, Boselli M, Amon A (2007) Kinetochore orientation during meiosis is controlled by Aurora B and the monopolin complex. Cell. pp 477–490.
4. Kitajima TS, Kawashima SA, Watanabe Y (2004) The conserved kinetochore protein shugoshin protects centromeric cohesion during meiosis. Nature. pp 510–517.
5. Nasmyth K, Haering CH (2009) Cohesin: its roles and mechanisms. Annu Rev Genet 43: 525–558.
6. Haering CH, Löwe J, Hochwagen A, Nasmyth K (2002) Molecular architecture of SMC proteins and the yeast cohesin complex. Mol Cell. pp 773–788.
7. Severson AF, Ling L, van Zuylen V, Meyer BJ (2009) The axial element protein HTP-3 promotes cohesin loading and meiotic axis assembly in C. elegans to implement the meiotic program of chromosome segregation. Genes Dev. pp 1763–1778.
8. Chan RC, Chan A, Jeon M, Wu TF, Pasqualone D, et al. (2003) Chromosome cohesion is regulated by a clock gene paralogue TIM-1. Nature. pp 1002–1009.
9. Mito Y, Sugimoto A, Yamamoto M (2003) Distinct developmental function of two Caenorhabditis elegans homologs of the cohesin subunit Scc1/Rad21. Mol Biol Cell. pp 2399–2409.
10. Pasierbek P, Jantsch M, Melcher M, Schleiffer A, Schweizer D, et al. (2001) A Caenorhabditis elegans cohesion protein with functions in meiotic chromosome pairing and disjunction. Genes Dev. pp 1349–1360.
11. Pasierbek P, Födermayr M, Jantsch V, Jantsch M, Schweizer D, et al. (2003) The Caenorhabditis elegans SCC-3 homologue is required for meiotic synapsis and for proper chromosome disjunction in mitosis and meiosis. Exp Cell Res. pp 245–255.
12. Mclellan J, O'neil N, Tarailo S, Stoepel J, Bryan J, et al. (2009) Synthetic lethal genetic interactions that decrease somatic cell proliferation in Caenorhabditis elegans identify the alternative RFC CTF18 as a candidate cancer drug target. Mol Biol Cell. pp 5306–5313.
13. Colaiácovo MP (2006) The many facets of SC function during C. elegans meiosis. Chromosoma. pp 195–211.
14. Zetka MC, Kawasaki I, Strome S, Müller F (1999) Synapsis and chiasma formation in Caenorhabditis elegans require HIM-3, a meiotic chromosome core component that functions in chromosome segregation. Genes Dev. pp 2258–2270.
15. Couteau F, Nabeshima K, Villeneuve A, Zetka M (2004) A component of C. elegans meiotic chromosome axes at the interface of homolog alignment, synapsis, nuclear reorganization, and recombination. Curr Biol. pp 585–592.
16. Couteau F, Zetka M (2005) HTP-1 coordinates synaptonemal complex assembly with homolog alignment during meiosis in C. elegans. Genes Dev. pp 2744–2756.
17. Goodyer W, Kaitna S, Couteau F, Ward JD, Boulton SJ, et al. (2008) HTP-3 Links DSB Formation with Homolog Pairing and Crossing Over during C. elegans Meiosis. Dev Cell. pp 263–274.
18. Dernburg AF, McDonald K, Moulder G, Barstead R, Dresser M, et al. (1998) Meiotic recombination in C. elegans initiates by a conserved mechanism and is dispensable for homologous chromosome synapsis. Cell. pp 387–398.
19. Colaiácovo MP, MacQueen AJ, Martinez-Perez E, McDonald K, Adamo A, et al. (2003) Synaptonemal complex assembly in C. elegans is dispensable for loading strand-exchange proteins but critical for proper completion of recombination. Dev Cell. pp 463–474.
20. Gerton JL, Hawley RS (2005) Homologous chromosome interactions in meiosis: diversity amidst conservation. Nat Rev Genet. pp 477–487.
21. Chin GM, Villeneuve AM (2001) C. elegans mre-11 is required for meiotic recombination and DNA repair but is dispensable for the meiotic G(2) DNA damage checkpoint. Genes Dev. pp 522–534.
22. Rinaldo C, Bazzicalupo P, Ederle S, Hilliard M, La Volpe A (2002) Roles for Caenorhabditis elegans rad-51 in meiosis and in resistance to ionizing radiation during development. Genetics. pp 471–479.
23. Hayashi M, Chin G, Villeneuve A (2007) C. elegans Germ Cells Switch between Distinct Modes of Double-Strand Break Repair During Meiotic Prophase Progression. PLoS Genet. pp e191.
24. Alpi A, Pasierbek P, Gartner A, Loidl J (2003) Genetic and cytological characterization of the recombination protein RAD-51 in Caenorhabditis elegans. Chromosoma. pp 6–16.
25. Tsai CJ, Mets DG, Albrecht MR, Nix P, Chan A, et al. (2008) Meiotic crossover number and distribution are regulated by a dosage compensation protein that resembles a condensin subunit. Genes Dev. pp 194–211.
26. Clejan I, Boerckel J, Ahmed S (2006) Developmental modulation of nonhomologous end joining in Caenorhabditis elegans. Genetics 173: 1301–1317.
27. Gartner A, MacQueen A, Villeneuve AM (2004) Methods for analyzing checkpoint responses in Caenorhabditis elegans. Methods Mol Biol 280: 257–274.
28. Gartner A, Milstein S, Ahmed S, Hodgkin J, Hengartner M (2000) A conserved checkpoint pathway mediates DNA damage–induced apoptosis and cell cycle arrest in C. elegans. Mol Cell 5: 435–443.
29. Bailly AP, Freeman A, Hall J, Déclais A-C, Alpi A, et al. (2010) The Caenorhabditis elegans homolog of Gen1/Yen1 resolvases links DNA damage signaling to DNA double-strand break repair. PLoS Genet 6: e1001025.
30. Kim S-T, Xu B, Kastan MB (2002) Involvement of the cohesin protein, Smc1, in Atm-dependent and independent responses to DNA damage. Genes & Development. pp 560–570.
31. Yazdi PT, Wang Y, Zhao S, Patel N, Lee EY, et al. (2002) SMC1 is a downstream effector in the ATM/NBS1 branch of the human S-phase checkpoint. Genes Dev 16: 571–582.
32. Watrin E, Peters J-M (2009) The cohesin complex is required for the DNA damage-induced G2/M checkpoint in mammalian cells. EMBO J. pp 2625–2635.
33. Heidinger-Pauli JM, Mert O, Davenport C, Guacci V, Koshland D (2010) Systematic reduction of cohesin differentially affects chromosome segregation, condensation, and DNA repair. Curr Biol. pp 957–963.
34. Unal E, Arbel-Eden A, Sattler U, Shroff R, Lichten M, et al. (2004) DNA damage response pathway uses histone modification to assemble a double-strand break-specific cohesin domain. Mol Cell. pp 991–1002.
35. Covo S, Westmoreland JW, Gordenin DA, Resnick MA (2010) Cohesin Is Limiting for the Suppression of DNA Damage-Induced Recombination between Homologous Chromosomes. PLoS Genet. e1001006 p.
36. Kim KP, Weiner BM, Zhang L, Jordan A, Dekker J, et al. (2010) Sister cohesion and structural axis components mediate homolog bias of meiotic recombination. Cell 143: 924–937.
37. Klein F, Mahr P, Galova M, Buonomo SB, Michaelis C, et al. (1999) A central role for cohesins in sister chromatid cohesion, formation of axial elements, and recombination during yeast meiosis. Cell 98: 91–103.
38. Reddy KC, Villeneuve AM (2004) C. elegans HIM-17 links chromatin modification and competence for initiation of meiotic recombination. Cell. pp 439–452.
39. Martinez-Perez E, Villeneuve AM (2005) HTP-1-dependent constraints coordinate homolog pairing and synapsis and promote chiasma formation during C. elegans meiosis. Genes Dev. pp 2727–2743.
40. Penkner A, Fridkin A, Gloggnitzer J, Baudrimont A, Machacek T, et al. (2009) Meiotic Chromosome Homology Search Involves Modifications of the Nuclear Envelope Protein Matefin/SUN-1. Cell 139: 920–933.
41. Phillips CM, Wong C, Bhalla N, Carlton PM, Weiser P, et al. (2005) HIM-8 binds to the X chromosome pairing center and mediates chromosome-specific meiotic synapsis. Cell. pp 1051–1063.
42. Tang L, Machacek T, Mamnun YM, Penkner A, Gloggnitzer J, et al. (2010) Mutations in Caenorhabditis elegans him-19 show meiotic defects that worsen with age. Mol Biol Cell. pp 885–896.
43. MacQueen AJ, Colaiácovo MP, McDonald K, Villeneuve AM (2002) Synapsis-dependent and -independent mechanisms stabilize homolog pairing during meiotic prophase in C. elegans. Genes Dev. pp 2428–2442.
44. Howe M, McDonald KL, Albertson DG, Meyer BJ (2001) HIM-10 is required for kinetochore structure and function on Caenorhabditis elegans holocentric chromosomes. The Journal of Cell Biology 153: 1227–1238.
45. Geer LY, Domrachev M, Lipman DJ, Bryant SH (2002) CDART: protein homology by domain architecture. Genome Res 12: 1619–1623.

Transgene-mediated cosuppression and RNA interference enhance germ-line apoptosis in *Caenorhabditis elegans*

Adele Adamo[a], Alexander Woglar[b], Nicola Silva[a,1], Alexandra Penkner[b], Verena Jantsch[b], and Adriana La Volpe[a,2]

[a]Consiglio Nazionale delle Ricerche-Institute of Genetics and Biophysics "A. Buzzati-Traverso," 80131 Naples, Italy; and [b]Department of Chromosome Biology, Max F. Perutz Laboratories, University of Vienna, A-1030 Vienna, Austria

Edited by Iva Greenwald, Columbia University, New York, NY, and approved January 20, 2012 (received for review May 12, 2011)

Introduction of multiple copies of a germ-line–expressed gene elicits silencing of the corresponding endogenous gene during *Caenorhabditis elegans* oogenesis; this process is referred to as germ-line cosuppression. Transformed plasmids assemble into extrachromosomal arrays resembling extra minichromosomes with repetitive structures. Loss of the transgene extrachromosomal array leads to reversion of the silencing phenomenon. Cosuppression and RNAi depend upon some of the same genes. In the *C. elegans* germ line, about half the cells undergo a physiological programmed cell death that shares most genetic requirements with somatic apoptosis. In addition, apoptosis is stimulated by DNA damage and synaptic failure mediated through different apoptotic checkpoints. We found that both germ-line cosuppression and RNAi of germ-line–expressed genes enhance apoptosis during *C. elegans* oogenesis. In contrast, apoptosis is not enhanced by extrachromosomal arrays carrying genes not driven by germ-line–specific promoters that thus do not elicit transgene-mediated cosuppression/silencing. Similarly, introduction of doubled-stranded RNA that shares no homology with endogenous genes has no effect on apoptosis. "Silencing-induced apoptosis" is dependent upon *sir-2.1* and *cep-1* (the worm p53 ortholog), and is accompanied by a rise in RAD-51 foci, a marker for ongoing DNA repair, indicating induction of DNA double-strand breaks. This finding suggests that the DNA damage-response pathway is involved. RNAi and cosuppression have been postulated as defense mechanisms against genomic intruders. We speculate that the mechanism here described may trigger the elimination of germ cells that have undergone viral infection or transposon activation.

genome-preservation | gametogenesis | meiosis

The ability of double-stranded RNA (dsRNA) to inhibit expression of homologous genes, a process known as RNAi, was discovered over a decade ago in *Caenorhabditis elegans* (1) and proved to be a widespread phenomenon shared by many phyla. To induce interference, dsRNAs must be processed into siRNAs by the Dicer protein and amplified by RNA-directed RNA polymerase, thereby generating secondary siRNAs. Subsequent assembly of RNA-induced silencing complexes governs degradation of the corresponding endogenous mRNAs. A related phenomenon, cosuppression, had first been discovered in plants and fungi (2) and a few years later in *C. elegans*. Cosuppression protects the *C. elegans* germ-line genome from invasion by repetitive sequences, transposons, viruses, and exogenous transgenes (3, 4). The introduction of multiple copies of a homologous germ-line–specific transgene leads to silencing of both the exogenous sequences and the endogenous genomic copy of the corresponding gene. In the following decade, genes involved in both phenomena were identified. Many of the genes and mechanisms discovered are also involved in the endogenous/physiological RNAi-mediated regulation of gene expression (5–10).

RNAi and transgene-mediated cosuppression phenocopy the depletion phenotypes of the corresponding genes. RNAi has thus become a powerful reverse-genetic technique for gene depletion. The efficiency of RNAi has led to its use in genomic screening, and, being able to maintain a cosuppressed line for several generations and introduce extrachromosomal arrays in different genetic backgrounds by crosses, has furthered our understanding of meiotic pathways.

Although RNAi and transgene-mediated cosuppression share many key players [e.g., *dcr-1* (Dicer) and *rde-2* genes (4)], clear distinctions exist between the two processes. RNAi is not stably inherited for more than a few generations and can affect every cell of the nematode in which the gene is expressed. In contrast, upon introduction of dsDNA carrying a coding sequence under a genuine germ-line promoter, extrachromosomal arrays are formed that can be inherited for several generations despite their non-Mendelian segregation. Because a somatic selectable marker can be coinjected together with the germ-line gene, nematodes carrying the extrachromosomal array can be easily identified and stable cosuppressed transgenic lines selected for. Only germ-line genes can be silenced in this way. Interestingly, upon loss of the extrachromosomal array, silencing is attenuated and gradually lost in the following generations (10).

In the *C. elegans* germ line, recombination occurs at the very early stages of meiotic prophase; the endonuclease SPO-11 induces meiotic double-strand breaks (DSBs) (11) and the recombinase RAD-51 is quickly loaded onto processed DSBs, which are rapidly resolved (12). Genome integrity during oogenesis is guarded by checkpoints. At least three checkpoints operate in the different gonad compartments: (*i*) the spindle checkpoint, which acts in the premeiotic compartment and arrests nuclear divisions in the mitotic compartment (13); (*ii*) the pachytene checkpoint, which safeguards chromosome pairing and synapsis (a prerequisite for crossing over) and acts in the transition zone/early pachytene stage (14); and (*iii*) the DNA-damage checkpoint, which preserves genome integrity throughout oogenesis (15). Activation of the latter two checkpoints leads to increased apoptosis immediately after the pachytene stage in *C. elegans*. Massive physiological germ-line cell death takes place in the wild-type germ line and requires all of the conserved apoptotic players, such as the caspase CED-3 (16). Apoptosis further increases once one or both checkpoints are activated (14, 15). Many mutants in meiotic genes involved in chromosome organization and DNA repair display increased apoptosis.

In previous studies of the repair gene *fcd-2*, we used transgene-mediated cosuppression to deplete *fcd-2*. Comparing the

Author contributions: A.A., V.J., and A.L.V. designed research; A.A., A.W., N.S., and A.P. performed research; A.A., V.J., and A.L.V. analyzed data; and V.J. and A.L.V. wrote the paper.

The authors declare no conflict of interest.

This article is a PNAS Direct Submission.

[1]Present address: Medical Research Council-Clinical Sciences Centre, Faculty of Medicine, Imperial College, London W12 0NN, United Kingdom.

[2]To whom correspondence should be addressed. E-mail: adriana.lavolpe@igb.cnr.it.

This article contains supporting information online at www.pnas.org/lookup/suppl/doi:10.1073/pnas.1107390109/-/DCSupplemental.

cosuppressed line with the null mutant (*tm1298*), we observed very similar phenotypes, such as an increase in pachytene RAD-51 foci, indicating a DNA repair problem, and a high incidence of developmental defects (ref. 17 and Table S1). Surprisingly, although the damage-induced apoptosis observed in *fcd-2* mutants is totally suppressed in a *spo-11*–mutant background (where meiotic DSBs are not induced), cell death remains markedly high in *spo-11* worms cosuppressed with the extrachromosomal array of the *fcd-2* gene (present study and Fig. S1*A*). This finding led us to postulate that the ongoing germ-line cosuppression per se enhances apoptosis. Therefore, the objective of our study was study this phenomenon and its genetic requirements.

Results

Does the Presence of an Extrachromosomal Array Lead to Transgene-Induced Apoptosis? To explore a possible relation between germline apoptosis and transgene-mediated cosuppression, we generated two independent cosuppressed lines of a different meiotic gene, *com-1*. Although the *com-1* mutation affects meiotic repair, the loss-of-function mutant of this gene does not display any increase in germ-line apoptosis compared with the wild-type (18) (Fig. 1 *A* and *D*). However, the two independent lines, both of which exhibited cosuppression of *com-1*, displayed more than twice the level of apoptosis compared with the wild-type or the *com-1* mutant (Fig. 1*A*). Importantly, siblings that have lost the transgenic array [easily identified by the lack of the associated selectable marker *rol-6(su1006)*] show an attenuated *com-1* phenotype (Table S2) and an intermediate level of apoptosis at the F1 generation that further decreases in the next generations (Fig. 1*A*). It has been reported that the epigenetic effect of cosuppression is gradually lost over the first two generations, further suggesting a link between the mechanisms of silencing and the induction of apoptosis (10).

Extrachromosomal arrays appear as small distinct chromatin structures with properties of real chromosomes. These structures are passed on to the next generation, although in a non-Mendelian fashion. We wondered whether the presence of an unpaired extrachromosomal array might itself activate the pachytene pairing checkpoint and induce apoptosis (14). To test this idea, we measured the level of apoptosis in nematode lines bearing extrachromosomal arrays that carry the plasmid pRF4*rol-6(su1006)*, which expresses a dominant mutation of the *rol-6* gene in the soma and is used as a selectable marker, or a mixed array containing the mutant *rol-6* coding sequence and the *act-5* gene. Neither of these genes is expressed in the germ line: the *rol-6* gene encodes a cuticle collagen and is required for normal cuticular morphology, and *act-5* is only expressed in microvillous intestinal cells and excretory cells. Therefore, neither of these extrachromosomal arrays is likely to induce transgene-mediated germ-line cosuppression. In both circumstances, we did not observe a significant increase in the physiological levels of apoptosis (Fig. 1*B*).

Extrachromosomal arrays can be integrated into the genome and kept in homozygosis, resulting in gene silencing of both the transgene and the endogenous locus (19). We integrated the *com-1* array by γ-irradiation and out-crossed the integrated line several times. In worms homozygous for the *com-1*–integrated array, the germ-line apoptosis level was still significantly higher than in the wild-type after 10 generations and remained elevated over 50 generations, suggesting that it is the mechanism of gene silencing itself (and not the presence of an unpaired additional chromosome-like structure) that is responsible for apoptosis up-regulation (Fig. 1 *B* and *E*).

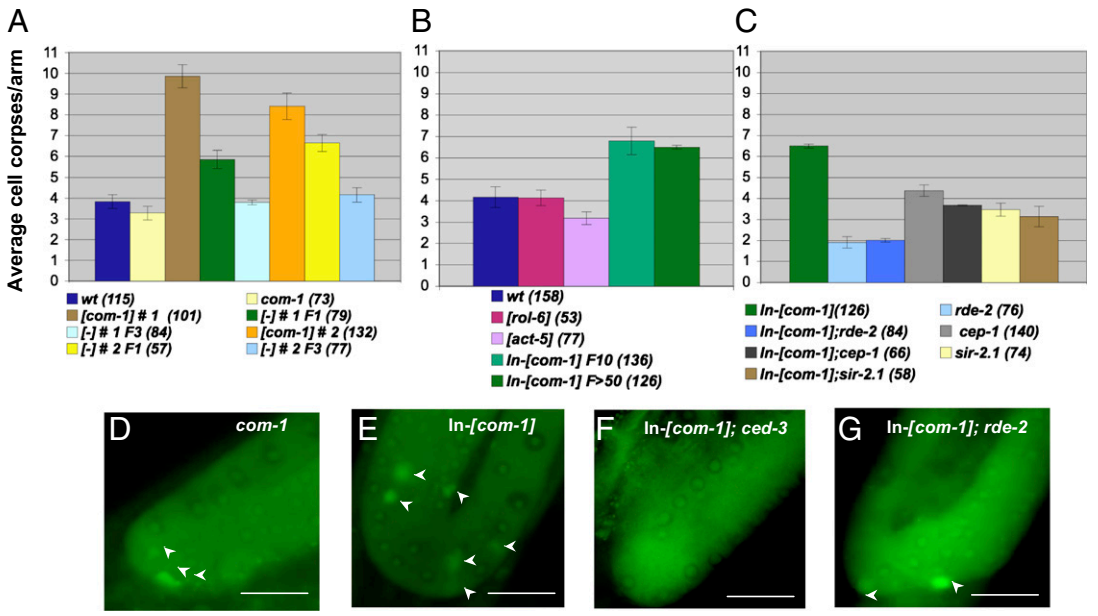

Fig. 1. Transgene-mediated cosuppression of the *com-1* gene induces up-regulation of germ-cell apoptosis. (*A*–*C*) Average apoptosis levels were scored in the indicated genotypes. The *y* axis shows the average number of SYTO12-labeled nuclei per gonadal arm. Genotypes are shown in the color legend at the bottom of each chart. Cosuppressed transgenes are indicated in squared parenthesis. The numbers of gonadal arms analyzed are written as numbers in parenthesis next to the genotype color legend. The two independent *com-1* cosuppressed lines are labeled #1 and #2. Siblings of cosuppressed nematodes that have lost the extrachromosomal arrays and their descendants are indicated as "*[-]* #1" and "*[-]* #2" followed by the generation (F1 or F3). [*rol-6*] Are nematodes carrying the extrachromosomal array somatically expressing the dominant mutation (*su1006*) in the gene *rol-6* as selectable marker. [*act-5*] Are nematodes carrying a mixed extrachromosomal array of the two genes, *rol-6*(*su1006*) and *act-5,* both expressed in the soma. The integrated line is derived from line #2 and indicated as In-*[com-1]*. Error bars correspond to SEMs calculated from at least three independent experiments. (*D*–*G*) SYTO12-stained gonads of the indicated genotype. (Scale bar, 25 μm.)

Genetic Requirements for Cosuppression-Mediated Apoptosis. Silencing-induced cell death is *ced-3*–dependent, because we barely detected any apoptotic corpses in worms stably cosuppressed for *com-1* and lacking the CED-3 caspase (Fig. 1*F*) (one germ-cell corpse from 60 scored gonadal arms compared with one corpse from 64 arms in the *ced-3* mutant alone). Furthermore, when the *com-1*–integrated array was crossed to the *rde-2* mutant (in which cosuppression does not take place) (3, 4), we did not detect any increase in apoptosis compared with the wild-type (Fig. 1 *C* and *G*). All of the *com-1* meiotic phenotypes (i.e., maternal effect lethality and fragmented and decondensed diakinesis chromosomes) were reproduced both in the *ced-3* and in the wild-type, but not in the *rde-2*–mutant background (Table S2).

The experiments shown so far excluded activation of the pairing checkpoint as a cause for the apoptosis enhancement. The other checkpoint responsible for apoptotic induction during pachytene is the DNA-damage checkpoint. We tested whether lack of the CEP-1 protein (the ortholog of p53, an essential player in DNA damage-induced apoptosis) abrogates cosuppression-induced apoptosis (15) by crossing the integrated *com-1* array into a *cep-1*–deficient background. All of the *com-1* meiotic phenotypes (Fig. S2 and Table S2) were reproduced in the *cep-1* mutant. However, enhancement of apoptosis was suppressed in the absence of CEP-1, suggesting that the DNA-damage apoptosis pathway is activated during cosuppression (Fig. 1*C*). It has been suggested that the SIR-2.1 protein (ortholog of the yeast Sir2 deacetylase) acts at the chromatin level and is also involved in damage-dependent apoptosis (20, 21). We found that cosuppression-mediated apoptosis is also abolished in *sir-2.1*–mutant background (Figs. 1*C* and Fig. S1*B*).

Does Silencing of Meiotically Expressed Genes Induce Apoptosis in General? A concern at this point was that both genes used in the cosuppression experiments (i.e., *fcd-2* and *com-1*) are involved in meiotic DNA repair. It is possible that suppression of these genes might somehow induce more DNA damage than those present in the null mutants.

To address this concern, we cosuppressed an ectopically germline–expressed transgene unrelated to DNA repair. We used the strain AZ212 carrying a copy of the *Ppie-1::gfp-his-11* transgene (10). In this strain, the transgene is integrated in a single copy, and therefore it is not silenced and does not induce silencing of the endogenous *his-11* gene. In strain AZ212 the transgene expresses histone H2B fused to the GFP coding sequence under a genuine germ-line promoter (22). The endogenous *his-11* gene is intact, and the GFP-HIS-11–fused protein is expressed only in the germ line being observed in the gonad and during early embryonic divisions. To specifically cosuppress the *gfp-his-11* transgene, we injected a construct carrying the GFP coding sequence (but not the histone sequence) under a different germline promoter, *Prad-51* (23). The resulting cosuppressed line lost meiotic chromosome fluorescence (Fig. 2*A*, *Upper*), and at the same time we observed a net increase in germ-line apoptosis associated with the silencing effect (Fig. 2*B*). As expected, chromosome fluorescence was gradually regained in some individuals in the following generations upon loss of the extrachromosomal array (Fig. 2*A*, *Lower*). Apoptosis also gradually decreases in these worms (Fig. 2*B*). These experiments clearly demonstrate that cosuppression of a meiotically expressed gene unrelated to the DNA repair pathway induces additional germ-cell death events.

Cosuppression Induces RAD-51 Foci in the Absence of Meiotic DSBs. Based on the activation of the DNA damage pathway during cosuppression, we wondered whether the silencing mechanism may cause DNA damage. The recombinase protein RAD-51 binds processed DSBs during meiotic prophase, promoting recombination and crossovers; therefore, increase of RAD-51 foci (detected by immunolocalization) may be an indication of an increase in DSBs (24). We, therefore, quantified and compared the levels of meiotic RAD-51 foci in the strain AZ212 and in the strain AZ212 cosuppressing GFP expression. RAD-51 foci appeared significantly more abundant in the germ line of cosuppressed worms, confirming that cosuppression per se induces DSBs (Fig. 2 *C* and *D* and Table S3). We also observed a discrete number of brightly staining apoptotic nuclei in middle/late pachytene stages of AZ212 worms cosuppressed with the extrachromosomal array of the GFP coding construct. These

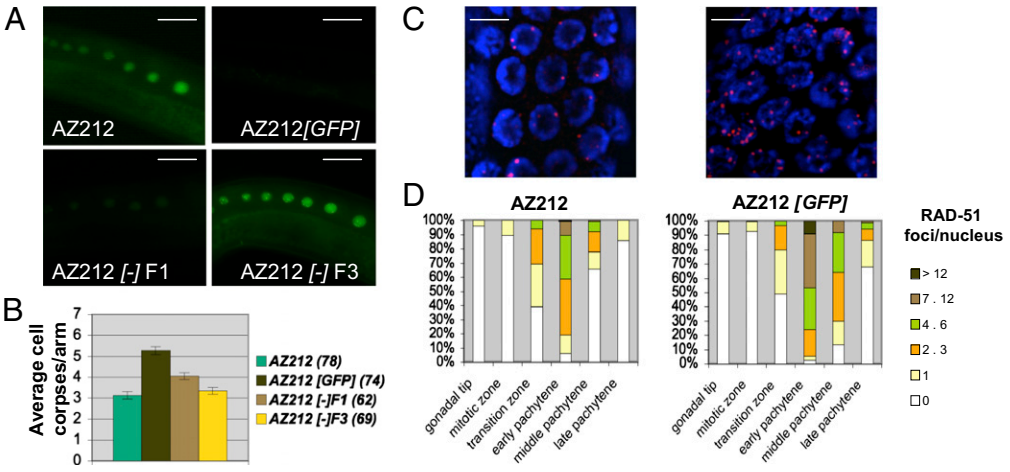

Fig. 2. Cosuppression of a meiotically expressed transgene induces additional germ-cell death events. (*A*) GFP-labeled diakinesis chromosomes in strain AZ212. (Scale bar, 25 μm.) Labeling is lost in worms carrying the extrachromosomal array expressing GFP under the *rad-51* promoter (indicated as AZ212*[GFP]*) and regained after loss of the extrachromosomal array in the following generations (AZ212*[-]* F1 and AZ212*[-]* F3). (*B*) Apoptosis levels in AZ212 and AZ212 *[GFP]*. The *y* axis represents the average number of SYTO12-labeled nuclei present per gonadal arm. Each genotype is indicated in the color legend at the bottom of the chart. Numbers in parenthesis correspond to the number of scored gonadal arms. Error bars correspond to SEM calculated from at least three independent experiments. (*C*) AZ212*[GFP]* show elevation of RAD-51 foci compared with AZ212. (Scale bars, 5 μm.) Representative image of germ lines immunostained with anti-RAD-51 (24) and DNA counterstained with DAPI (blue). (*D*) Histograms represent quantification of RAD-51 foci in germ lines of animals of the indicated genotypes. The *y* axis represents the percentage of nuclei with the indicated number of foci. The *x* axis represents the position (zone) along the germ line. Statistical analysis was carried out using the Student *t* test (Table S3).

brightly staining nuclei may be interpreted as apoptotic nuclei containing fragmented DNA because of the action of the *nuc-1* endonuclease; their number, in fact, is proportional to the apoptotic levels in any strain analyzed so far (17, 24, 25) and absent in the *ced-3* mutant.

We also compared RAD-51 foci in *spo-11*, *fcd-2* double mutants and *spo-11* worms cosuppressed with the extrachromosomal array of the *fcd-2* gene. SPO-11 is the meiotic endonuclease responsible for physiological DSB induction, and is essential for crossover and proper chromosome segregation. Therefore, in the absence of SPO-11, almost no RAD-51 foci are generated and chromosomes do not properly segregate. We again observed a biologically and statistically significant increase in RAD-51 foci in early pachytene stage of cosuppressed worms (Fig. S3 and Table S4).

Does RNAi of Germ-Line–Expressed Genes Have a Similar Effect on Germ-Cell Death? Because the mechanisms of cosuppression and RNAi partially overlap, we performed RNAi by injecting dsRNA homologous to the GFP coding sequence into the AZ212 strain, thus inhibiting expression of the *Ppie-1::gfp-his-11* integrated construct, and then measured germ-cell death. Active ongoing RNAi also enhanced germ-line RAD51 foci and *ced-3*–dependent apoptosis (Fig. 3 *A* and *D*). GFP RNAi induced enhancement of RAD-51 foci also in an AZ212 strain carrying the *ced-3* allele, although brightly staining late pachytene nuclei disappeared because of the absence of apoptosis (Fig. S4 and Table S3). On the other hand, simple injection of GFP-dsRNA into wild-type worms did not elevate apoptosis (Fig. 3*A*). We therefore conclude that an excess of dsRNA per se does not cause apoptosis induction.

To confirm that ongoing RNAi promotes germ-line cell death, we also used an endogenous gene. We reasoned that depletion of SPO-11 (11) should decrease the number of DNA breaks in the germ line; therefore, the *spo-11* gene is an ideal substrate upon which to perform RNAi to test whether RNAi per se can induce germ-cell death. Mothers subjected to RNAi were selected for lethal (aneuploid) progeny and for univalent diakinesis chromosomes. F1 progeny of injected mothers were stained for apoptosis. Only nematodes with a fully penetrant *spo-11* phenotype were analyzed (see *Materials and Methods* and Table S5 for details). Enhancement of cell death was similarly observed in this experiment (Fig. 3*B*). Furthermore, we confirmed that, also in this context, apoptosis was *ced-3*–dependent (only one germ-cell corpse detected from 42 scored gonadal arms), and that SPO-11 dsRNA injection did not enhance apoptosis in the *rde-2* or *cep-1* mutant backgrounds (Fig. 3 *B* and *C*).

Discussion

Evolution may select common genetic components to be shared by different pathways; different input signals make use of such common genetic components to activate functions that are sometimes very different (26). The phenomenon of RNAi is thought to protect the cell from viral infection, and it is related to pathways of gene regulation by small RNAs. In addition, RNAi overlaps in part with the phenomenon of transposon silencing. It is therefore not totally surprising that in the germ line, where genome preservation is crucial for species survival, several layers

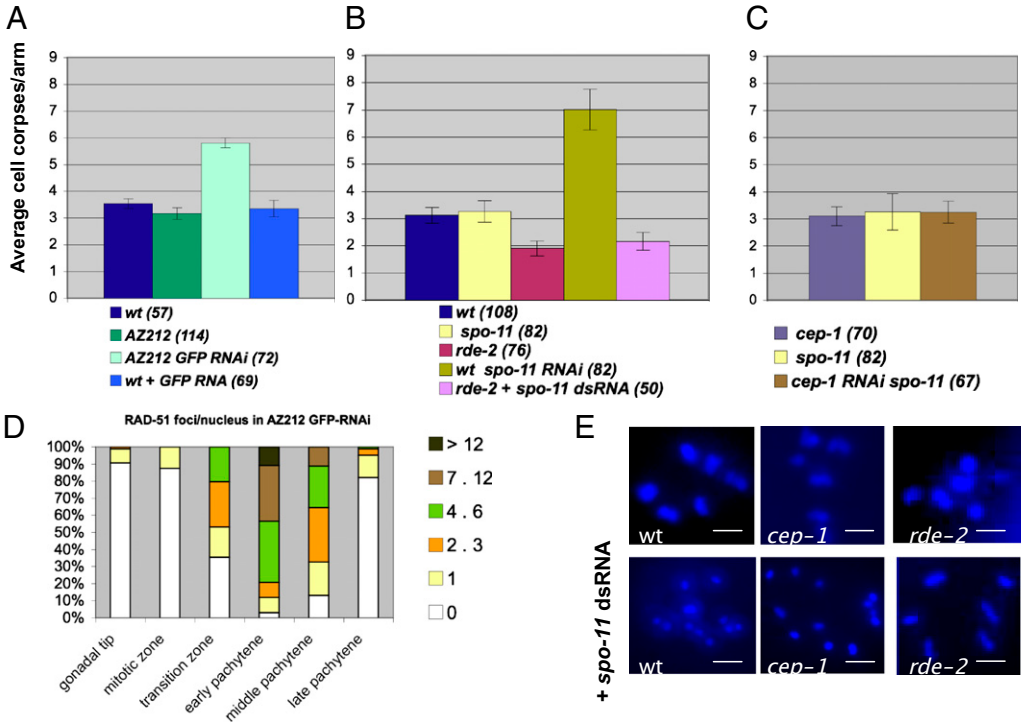

Fig. 3. RNAi of germ-line–expressed genes enhances germ-cell apoptosis. (*A*) GFP RNAi induces apoptosis in the strain AZ212. dsRNA of GFP was injected in the strain AZ212 and in wild-type. (*B*) *spo-11* RNAi elicits apoptosis. dsRNA of *spo-11* was injected in the wild-type and *rde-2* strains. (*C*) Lack of apoptosis enhancement after *spo-11* RNAi in *cep-1* strain. The *y* axis represents the average number of SYTO12-labeled nuclei present per gonadal arm. Each genotype is indicated in the color legend at the bottom of the chart. Numbers in parenthesis correspond to the number of scored gonadal arms. Error bars correspond to SEM calculated from at least three independent experiments. (*D*) GFP RNA interference induces DSBs in the strain AZ212. Histograms represent quantification of RAD-51 foci in germ lines of animals of the indicated genotypes. The *y* axis represents the percentage of nuclei with the indicated number of foci. The *x* axis represents the position (zone) along the germ line. Statistical analysis was carried out using the Student *t* test (Table S3). (*E*) Diakinesis chromosomes of indicated genotypes: wild-type, *cep-1*, *rde-2* nuclei show six bivalents held together by chiasmata. *spo-11* dsRNA injection abrogates chiasmata, and therefore nuclei show 12 univalents in wild-type and *cep-1* strains, but not in the *rde-2* mutant. (Scale bars, 2 μm.)

of responses share the same goal. DNA damage induces cell-cycle arrest and DNA repair, and ultimately culminates in programmed cell death, if the damage persists. Therefore, it is conceivable that transposon mobilization or viral attack, which can seriously alter genomic information, may induce gene silencing and ultimately lead to cell death. In support of this idea, when RNAi was first studied in mammalian cells, it was apparent that the response to a large amount of dsRNA led to IFN-mediated apoptosis (27, 28). This effect might be envisioned as the result of coevolving mechanisms similar to the one described in this work (silencing-dependent germ-line apoptosis).

The results of the experiments described above demonstrate that gene silencing due to cosuppression or RNAi is coupled with enhanced germ-cell death. The presence of an additional meiotically unpaired chromosome per se does not induce higher apoptotic levels unless active silencing is ongoing. Furthermore, neither transgene multicopy arrays nor introduction of dsRNA up-regulates apoptosis in a genetic background in which silencing is blocked, such as in the *rde-2* mutant.

The silencing-mediated apoptosis pathway takes advantage of crucial death regulators also used in the DNA damage-induced apoptotic pathway; in fact, both the CEP-1 (p53) and SIR-2.1 (sirtuin) proteins are required. Although enhancement of apoptosis is abrogated in the *sir-2.1* mutant, SIR-2.1 does not seem to be involved in silencing of the endogenous gene copy per se, because in a *sir-2.1* deletion mutant the *com-1* cosuppressed construct maintains the *com-1*–mutant phenotype, such as embryonic lethality and fragmented and decondensed diakinesis chromosomes (Fig. S2 and Table S2).

When the cosuppressing extrachromosomal array is lost during consecutive chromosome segregation cycles, the somatically expressed selectable marker disappears at the first generation, whereas the effects of the cosuppressed phenotype gradually decrease over more than two generations and the level of apoptosis declines in parallel. It will be interesting to find out whether the apoptosis-triggering signal is linked to sensors at the chromatin level. It is worth noting that the deacetylase sirtuin SIR-2.1, which is known to operate at the chromatin level (21) and to participate in DNA damage-induced apoptosis (20), is required for the increase in germ-cell death during cosuppression. In fact, the yeast *sir2* gene is known to alter the genomic distribution of DSBs (29, 30).

Activation of the DNA-damage apoptosis pathway is accompanied by *spo-11*–independent DSBs induction during cosuppression and RNAi. A significant increase in RAD-51 foci can be observed in the silencing experiments. Silencing-induced apoptosis, but not DSB induction, is *ced-3*–dependent. This observation strongly suggests that increase in DSBs is the cause and not the consequence of apoptosis enhancement. Further investigations will be necessary to identify the pathway leading to this increase in DNA damage.

The observation that DSBs are indeed induced during silencing is consistent with the observation that the phenotypic effects of cosuppression or RNAi of the *spo-11* gene are much less pronounced than RNAi of other genes coding for more abundant meiotic proteins, such as *rad-51* (12) or the *his-11::gfp* transgene. Only a fraction of the dsRNA-injected mothers displayed a fully penetrant *spo-11* phenotype (aneuploid lethal progeny caused by crossover failure) that, in turn, was inherited by only a fraction of the offspring (Table S5). It is known that exogenous induction of DSBs by ionizing radiations (11) is able to rescue the *spo-11* phenotype by promoting crossovers and segregation. The weak penetrance of the *spo-11* RNAi can be explained by the fact that, although depleting SPO-11, the RNAi process also induces DSBs that may similarly suppress in part the *spo-11* phenotype (11). In support of this idea, in a blinded experiment, we observed that apoptotic levels throughout the entire *spo-11 RNAi* F1 population were higher than expected (average of 5.15 SYTO12-positive nuclei per gonadal arm).

We think that the present observations are highly relevant to a comprehensive understanding of how sexual organisms protect their germ line from attacks from viruses and repetitive sequences, not only by neutralizing the invaders, but also by eliminating affected nuclei. Our findings also indicate that particular caution should be used when interpreting depletion phenotypes of germline genes obtained by RNAi and cosuppression.

Materials and Methods

Quantification of Germ-Line Apoptosis. Adult nematodes (24–36 h after larval stage L4) were suspended in M9 solution and stained by incubating with 33 μM SYTO-12 (Molecular Probes) for 1 h 30 min at room temperature in the dark. The worms were then transferred to seeded plates to allow stained bacteria to be purged from the gut. After 30 min, the animals were mounted on 2% agarose pads in 2 mM levamisole. For the time course, germ-line apoptosis were quantified at 12, 24, and 36 h postlarval stage L4 (Fig. S1*C*).

The quantitative analysis was performed using a Leica DM6000 fluorescence microscope, Leica DC 350 FX camera under the control of Leica LAS AF 6000 software. The numbers of gonadal arms scored for each genotype are indicated in the legends to the charts.

Immunostaining. RAD-51 immunostaining was carried out as described by Colaiácovo et al. (24). Quantitative analysis of RAD-51 foci was carried out on *z*-series of images acquired using a Leica DM5000 fluorescence microscope, Leica DC 350 FX camera under the control of Leica LAS AF 6000 software. Optical sections were collected at 0.25-μm increments. An average of 100 nuclei per region per genotype were scored.

RNAi. The dsRNA was injected at a concentration of 500 μg/mL into the gonad (1). Young AZ212 adult hermaphrodites were injected with GFP dsRNA (corresponding to nucleotides 253–697 of GFP coding sequence). Efficiency of interference was controlled by chromosome fluorescence loss.

Young wild-type *cep-1*, and *ced-3* adult hermaphrodites were injected with *spo-11* dsRNA (corresponding to nucleotides 593–1500 of cosmid T05E11). Injected worms (P0) were individually cloned and then transferred to seeded plates every 12 h. The F1 laid 12–48 h after injection were transferred to fresh plates for 24 h and screened for embryonic lethality (Table S5). Only F1 laid by P0 mothers that produced over 90% lethal progeny in the time window corresponding to 60–84 h after injection (12) were further analyzed. Those F1 nematodes that showed the fully penetrant *spo-11* phenotype (F2 embryonic lethality > 92%) were treated with SYTO-12 and checked for apoptosis. Sibling F1 nematodes laid 12–24 h after injection were stained with DAPI and diakinesis chromosomes were analyzed (Fig. 3*E*). We also performed a blind experiment testing the average number of SYTO12-positive nuclei in the entire F1 population (irrespectively of the *spo-11* phenotype).

Young *rde-2* adult hermaphrodites were similarly injected with *spo-11* dsRNA to simulate RNA interference, progeny laid 24–48 h after injection (corresponding to the peak of *spo-11* interference penetrance in wild-type) were treated with SYTO-12 and corpses were scored.

ACKNOWLEDGMENTS. We thank Paolo Bazzicalupo, Maria Ciaramella, Aurora Storlazzi, and John F. Pulitzer for stimulating discussions and useful suggestions, Christian Pflügl for technical help, and the Institute of Genetics and Biophysics for the use of the Integrated Microscopy Facility. The A.L.V. laboratory is funded by Progetto Merit RBNE08YFN3 and Progetto IG11422 Associazione Italiana per la Ricerca sul Cancro; N.S. was recipient of a predoctoral fellowship from the Italian Ministry of University and Research (MIUR) (PhD School Molecular Genetics and Medicine); and V.J. was supported by Austrian Fund for the Promotion of Scientific Research-Project FWF Grant P21338-B03.

1. Fire A, et al. (1998) Potent and specific genetic interference by double-stranded RNA in *Caenorhabditis elegans*. *Nature* 391:806–811.
2. Cogoni C, Macino G (1999) Homology-dependent gene silencing in plants and fungi: A number of variations on the same theme. *Curr Opin Microbiol* 2:657–662.
3. Dernburg AF, Zalevsky J, Colaiácovo MP, Villeneuve AM (2000) Transgene-mediated cosuppression in the *C. elegans* germ line. *Genes Dev* 14:1578–1583.
4. Ketting RF, Plasterk RH (2000) A genetic link between co-suppression and RNA interference in *C. elegans*. *Nature* 404:296–298.
5. Hayes GD, Ruvkun G (2006) Misexpression of the *Caenorhabditis elegans* miRNA let-7 is sufficient to drive developmental programs. *Cold Spring Harb Symp Quant Biol* 71: 21–27.
6. Ruvkun GB (2003-2004) The tiny RNA world. *Harvey Lect* 99:1–21.

7. Ruvkun G (2008) Tiny RNA: Where do we come from? What are we? Where are we going? *Trends Plant Sci* 13:313–316.
8. Sijen T, Plasterk RH (2003) Transposon silencing in the *Caenorhabditis elegans* germ line by natural RNAi. *Nature* 426:310–314.
9. Robert VJ, Vastenhouw NL, Plasterk RH (2004) RNA interference, transposon silencing, and cosuppression in the *Caenorhabditis elegans* germ line: Similarities and differences. *Cold Spring Harb Symp Quant Biol* 69:397–402.
10. Robert VJ, Sijen T, van Wolfswinkel J, Plasterk RH (2005) Chromatin and RNAi factors protect the *C. elegans* germline against repetitive sequences. *Genes Dev* 19:782–787.
11. Dernburg AF, et al. (1998) Meiotic recombination in *C. elegans* initiates by a conserved mechanism and is dispensable for homologous chromosome synapsis. *Cell* 94: 387–398.
12. Rinaldo C, Bazzicalupo P, Ederle S, Hilliard M, La Volpe A (2002) Roles for *Caenorhabditis elegans* rad-51 in meiosis and in resistance to ionizing radiation during development. *Genetics* 160:471–479.
13. Kitagawa R, Rose AM (1999) Components of the spindle-assembly checkpoint are essential in *Caenorhabditis elegans*. *Nat Cell Biol* 1:514–521.
14. Bhalla N, Dernburg AF (2005) A conserved checkpoint monitors meiotic chromosome synapsis in *Caenorhabditis elegans*. *Science* 310:1683–1686.
15. Gartner A, Milstein S, Ahmed S, Hodgkin J, Hengartner MO (2000) A conserved checkpoint pathway mediates DNA damage—Induced apoptosis and cell cycle arrest in *C. elegans*. *Mol Cell* 5:435–443.
16. Gumienny TL, Lambie E, Hartwieg E, Horvitz HR, Hengartner MO (1999) Genetic control of programmed cell death in the *Caenorhabditis elegans* hermaphrodite germline. *Development* 126:1011–1022.
17. Adamo A, et al. (2010) Preventing nonhomologous end joining suppresses DNA repair defects of Fanconi anemia. *Mol Cell* 39:25–35.
18. Penkner A, et al. (2007) A conserved function for a *Caenorhabditis elegans* Com1/Sae2/CtIP protein homolog in meiotic recombination. *EMBO J* 26:5071–5082.
19. Mello C, Fire A (1995) DNA transformation. *Methods Cell Biol* 48:451–482.
20. Greiss S, Hall J, Ahmed S, Gartner A (2008) *C. elegans* SIR-2.1 translocation is linked to a proapoptotic pathway parallel to cep-1/p53 during DNA damage-induced apoptosis. *Genes Dev* 22:2831–2842.
21. Wirth M, et al. (2009) HIS-24 linker histone and SIR-2.1 deacetylase induce H3K27me3 in the *Caenorhabditis elegans* germ line. *Mol Cell Biol* 29:3700–3709.
22. Mello CC, Draper BW, Krause M, Weintraub H, Priess JR (1992) The pie-1 and mex-1 genes and maternal control of blastomere identity in early *C. elegans* embryos. *Cell* 70:163–176.
23. Rinaldo C, Ederle S, Rocco V, La Volpe A (1998) The *Caenorhabditis elegans* RAD51 homolog is transcribed into two alternative mRNAs potentially encoding proteins of different sizes. *Mol Gen Genet* 260:289–294.
24. Colaiácovo MP, et al. (2003) Synaptonemal complex assembly in *C. elegans* is dispensable for loading strand-exchange proteins but critical for proper completion of recombination. *Dev Cell* 5:463–474.
25. Adamo A, et al. (2008) BRC-1 acts in the inter-sister pathway of meiotic double-strand break repair. *EMBO Rep* 9:287–292.
26. Anderson DG, Kowalczykowski SC (1998) Reconstitution of an SOS response pathway: Derepression of transcription in response to DNA breaks. *Cell* 95:975–979.
27. Kumar A, Haque J, Lacoste J, Hiscott J, Williams BR (1994) Double-stranded RNA-dependent protein kinase activates transcription factor NF-kappa B by phosphorylating I kappa B. *Proc Natl Acad Sci USA* 91:6288–6292.
28. Reynolds A, et al. (2006) Induction of the interferon response by siRNA is cell type- and duplex length-dependent. *RNA* 12:988–993.
29. Casper AM, Mieczkowski PA, Gawel M, Petes TD (2008) Low levels of DNA polymerase alpha induce mitotic and meiotic instability in the ribosomal DNA gene cluster of *Saccharomyces cerevisiae*. *PLoS Genet* 4:e1000105.
30. Mieczkowski PA, Dominska M, Buck MJ, Lieb JD, Petes TD (2007) Loss of a histone deacetylase dramatically alters the genomic distribution of Spo11p-catalyzed DNA breaks in *Saccharomyces cerevisiae*. *Proc Natl Acad Sci USA* 104:3955–3960.